UNIVERSITY OF CALIFORNIA
RIVERSIDE

Structural Characterization of Chemically Modified GAG Oligosaccharides through ^{1}H NMR Measurements of the Labile Nitrogen-bound Protons

A Dissertation submitted in partial satisfaction
of the requirements for the degree of

Doctor of Philosophy

in

Chemistry

by

Andrew R. Green

March 2019

Dissertation Committee:
Dr. Cynthia K. Larive, Chairperson
Dr. Ryan R. Julian
Dr. Leonard J. Mueller

The Dissertation of Andrew R. Green is approved:

_____

_____

_____

Committee Chairperson

University of California, Riverside

Acknowledgements

First, I would like to express my sincere gratitude and deep appreciation to Professor Cynthia K. Larive. She expertly guided me through my graduate program at the Chemistry Department at University of California Riverside. Her constructive and logical approach has transformed my scientific way of thinking. Her unwavering enthusiasm for chemistry kept me constantly engaged in my research. Dr. Larive's dedications to science, research, and education together with hardworking attitude will forever be the model of excellence for me.

I'm also deeply grateful to Professor Stephen L. Morgan, Dr. Kevin Drost, Dr. Dan B. Borchardt, and Professor Leonard J. Mueller for their help, encouragement, guidance, and support through my undergraduate and graduate studies. My appreciation for great working environment extends to Corey Griffith, Dr. Meredith Dinges, Dr. Melissa Morgan and other people with whom I was lucky to work with in Larive's lab during my years in graduate school. I'm very grateful to our research group collaborator Dr. Robert Young, former Mueller's lab member, who taught me the basics of molecular dynamics simulations.

A special thanks to my family. Words can't express how grateful I am to my loving wife and best friend Natalie V. Green for all the sacrifices that she has made on my behalf and how supportive she was along the way. Thanks to all other people who helped me and were involved in reaching this hard but important milestone!

Dedication

To my wife Natalie V. Green

ABSTRACT OF THE DISSERTATION

Structural Characterization of Chemically Modified GAG Oligosaccharides through ^{1}H NMR Measurements of the Labile Nitrogen-bound Protons

by

Andrew R. Green

Doctor of Philosophy, Graduate Program in Chemistry
University of California, Riverside, March 2019
Dr. Cynthia K. Larive, Chairperson

Glycosaminoglycans (GAGs) mediate a variety of biological processes through their interactions with proteins. To advance our understanding of these interactions, it is necessary to explore the structural characteristics and physico-chemical properties of GAGs. The major focus of the research presented in this dissertation is the structural analysis of GAG oligosaccharides with emphasis on the chemical modification and isolation of oligosaccharides with unique structures. Reactions for the solvolytic de-*N*-sulfation, chemoselective *N*-acetylation, and reduction of reducing end residues with sodium borohydride were employed to obtain oligosaccharides containing amide and free amine moieties with unique structural elements. The impact of oligosaccharide primary structure on elements of secondary structure in aqueous solution was explored using ^{1}H NMR.

The role of rare, but biologically important 3-*O*-sulfated glucosamine residues in heparan sulfate related oligosaccharides was examined. Possible salt bridge formation was probed through the measurement of amino proton temperature coefficients, amino proton solvent exchange rates, and comparison of the carboxylate and amino group pK_a values of

de-*N*-sulfated Arixtra (dNSA). Reduced amino proton temperature coefficients, accelerated exchange rates measured by exchange spectroscopy (EXSY), and altered pK_a values of amino and carboxylate groups provided evidence that the dNSA 3-*O*-sulfated glucosamine amino group is likely involved in salt bridge with the neighboring 3-*O*-sulfo group and possibly with carboxylate group of the adjacent iduronic acid residue. This hypothesis was supported by the results of molecular dynamics simulations.

The effect of oligosaccharide structure on the solvent exchange behavior of GAG oligosaccharide amide group protons was evaluated through comparison of temperature coefficients, activation energy barriers, and pH titrations of oligosaccharides containing amide groups. A library of 20 oligosaccharides differing in size, glycosidic linkage, saccharide type, and sulfation position and extent, allowed the examination of the effect of charge repulsion by nearby negatively charged sulfate and carboxylate groups on the hydroxyl ions responsible for catalyzing amide proton exchange. This charge repulsion effect calls into question the validity of using exchange rates and activation energies for detection of hydrogen bonds without support from temperature coefficients measured for labile protons.

Table of Contents

List of Figures

List of Tables

CHAPTER ONE

Introduction

The aims of the research presented in this dissertation are the development of new analytical approaches for the structural analysis of glycosaminoglycans (GAGs). Emphasis is placed on the chemical modification and isolation of oligosaccharides with unique structures. Structural elements including the identity of the uronic acid residue, nature of the glycosidic linkage, sulfation position and the nitrogen substitution are all explored. The primary structures of oligosaccharides are elucidated using mass spectrometry (MS) and nuclear magnetic resonance (NMR) spectroscopy and the impacts of unique elements of primary structure, such as glucosamine 3-*O* sulfation, on secondary structure in aqueous solution are determined using NMR.

The analysis of intact GAG polysaccharides can represent a significant challenge due to the structural complexity and microheterogeneity introduced during their non-template driven biosynthesis.[1-4] Characterization and structural studies of these biopolymers proceed through a bottom-up approach that employs depolymerization followed by chromatographic isolation of individual oligosaccharides based on size and charge.[5-11] However, isolation of sufficient quantities of oligosaccharides with rare structural elements is not always feasible, therefore, this work relied on the synthetic modification of several isolated and chemically synthesized oligosaccharides.

Research of the former lab members Dr. Consuelo Beecher and Dr. Derek Langeslay established the foundation for this research. They identified conditions suitable

for detection of labile protons in hydroxyl, amino, and sulfamate groups, and detected persistent intramolecular hydrogen bonds involving sulfamate and hydroxyl groups in synthetic antithrombotic drug Arixtra™. In desire to expand our knowledge of physico-chemical properties of GAGs in aqueous solutions, the objectives of this thesis are outlined below.

Objective 1: Develop and optimize chemical modifications of GAG oligosaccharides. Through the selective chemical modifications of suitable abundantly available precursors, rare elements of biopolymer structure can be introduced via chemical means to enable structural studies of unusual oligosaccharides.

Objective 2: Establish methods for identification of intramolecular salt bridges involving the amino groups of GAG oligosaccharides and determine the structural elements that promote salt bridge formation in aqueous solution.

Objective 3: Evaluate the effect of GAG structure on amide proton exchange rates at physiological pH to gain insights into the hydration, hydrogen bonding, and structural flexibility of GAG oligosaccharides.

Objective 4: Predict and confirm the presence of hydrogen bonds and salt bridges through molecular dynamic simulations of GAG oligosaccharides.

1.1. Glycosaminoglycans

The glycosaminoglycan (GAG) family is comprised of heparin, heparan sulfate, chondroitin sulfate, dermatan sulfate, keratan sulfate, and hyaluronic acid. The GAGs are unbranched and highly anionic polysaccharides. Varying in size, composition, glycosylation linkage, and substitution, GAGs are classified based on their major disaccharide repeat subunits, in which a hexose residue is linked through the glycosidic bond to a hexosamine residue. The generalized representation of disaccharide repeat units of each GAG are shown in Figure 1.1.

1.1.1. Structural variability and complexity. The structures of GAG polysaccharides range from relatively simple to highly complex. For instance, hyaluronic acid, the only GAG that is not biosynthesized as a proteoglycan and is ubiquitously expressed in the extracellular matrix of mammals, is comprised of only β-D-glucuronic acid (GlcA) and *N*-acetylglucosamine (GlcNAc) disaccharide repeat units (Figure 1.1A). Though they are derived from a similar GlcA-GlcNAc backbone linked by (1→4) glycosidic bonds as a result of enzymatic transformations during biosynthesis, heparin and heparan sulfate are more complex, heterogeneous, polydisperse, and highly negatively charged.[3] The uronic acid residue in heparin and heparan sulfate can exist in one of two epimeric forms, β-D-glucuronic acid (GlcA) or α-L-iduronic acid (IdoA), while the nitrogen of the GlcN residue can be *N*-sulfated (GlcNS), *N*-acetylated (GlcNAc), or unsubstituted as the free amine (GlcN) (Figure 1E).[3, 12, 13] Additionally, the uronic acid residues can be 2-*O*-sulfated or unsulfated and glucosamine residues can be 3-*O*- and/or 6-*O*-sulfated.[12, 13]

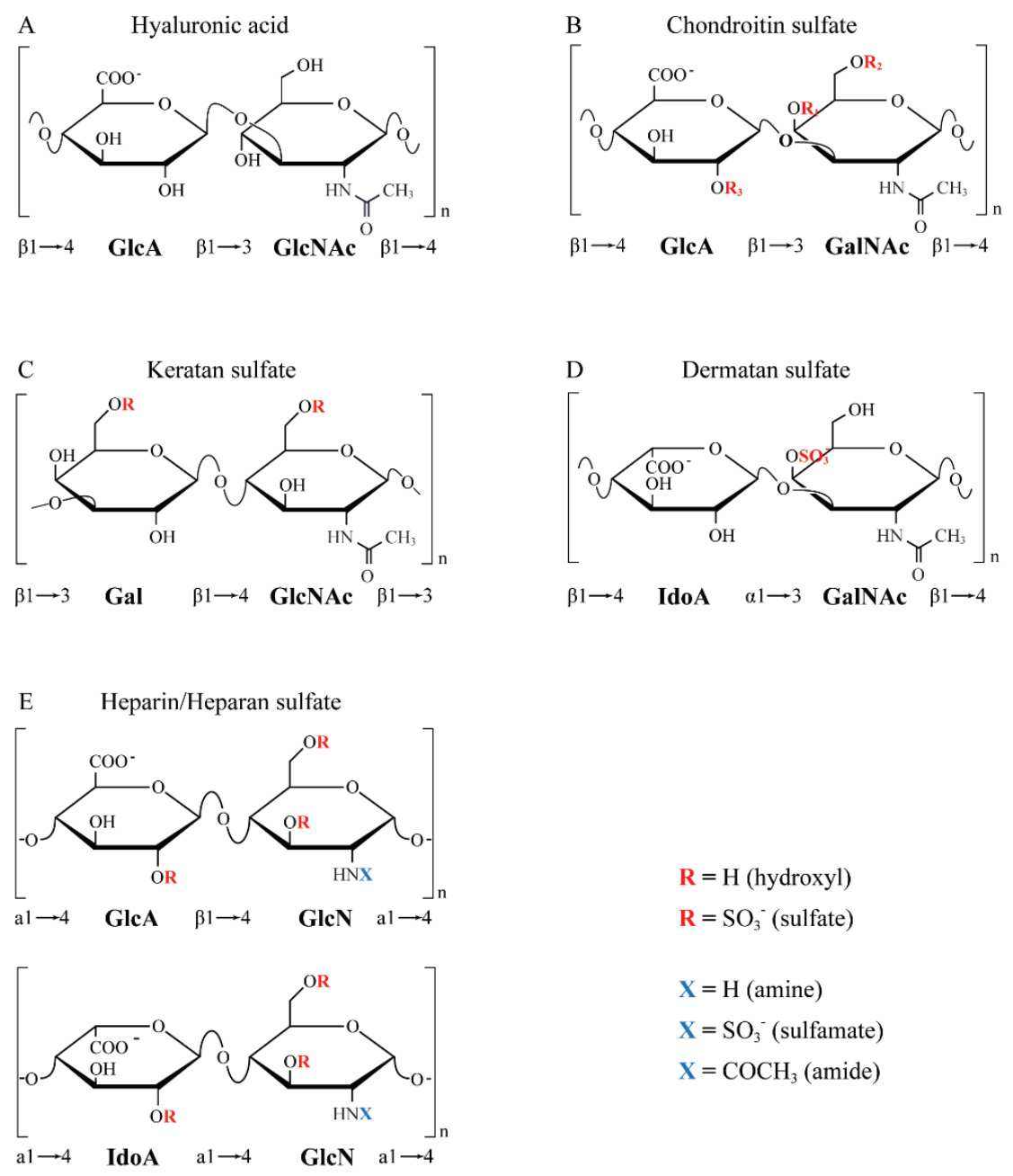

Figure 1.1. Haworth projections of the disaccharide repeat units characterizing the members of the GAG family. (A) Hyaluronic acid is the only unsulfated GAG. (B) Chondroitin sulfate is subclassified based on sulfate positions as chondroitin sulfate A,

chondroitin sulfate C, chondroitin sulfate D, and chondroitin sulfate E. Disaccharides containing 4-*O*-sulfated GalNAc residues are chondroitin sulfate A, 6-*O*-sulfated GalNAc residues are chondroitin sulfate C, 2-*O*-sulfated GlcA and 6-*O*-sulfated GlcNAc residues are chondroitin sulfate D, and 4,6-*O*-sulfated GalNAc residues are chondroitin sulfate E. (C) Keratan sulfate is the only GAG without a uronic acid residue. (D) Dermatan sulfate. (E) Heparin and heparan sulfate.

Table 1.1. Abbreviations of monosaccharides used throughout this dissertation with their corresponding full names.

Abbreviation	Full name
GlcN	glucosamine
GlcNS	*N*-sulfated glucosamine
GlcNS3S	*N*-,3-*O*-disulfated glucosamine
GlcNS6S	*N*-,6-*O*-disulfated glucosamine
GlcNS3S6S	*N*-,3,6-*O*-trisulfated glucosamine
GlcN3S	3-*O*-sulfated glucosamine
GlcN3S6S	3,6-*O*-disulfated glucosamine
GlcNAc	*N*-acetylglucosamine
GlcNAc3S	3-*O*-sulfated *N*-acetylglucosamine
GlcNAc6S	6-*O*-sulfated *N*-acetylglucosamine
Gal	galactose
Gal6S	6-*O*-sulfated galactose
GalNAc	*N*-acetylgalactosamine
GalNAc4S	4-*O*-sulfated *N*-acetylgalactosamine
GalNAc6S	6-*O*-sulfated *N*-acetylgalactosamine
UA	uronic acid
UA2S	2-*O*-sulfated uronic acid
ΔUA	unsaturated uronic acid
ΔUA2S	2-*O*-sulfated unsaturated uronic acid
GlcA	glucuronic acid
GlcA2S	2-*O*-sulfated glucuronic acid
IdoA	iduronic acid
IdoA2S	2-*O*-sulfated iduronic acid

Structurally heparin and heparan sulfate are distinguished from each other based on the content of the major disaccharide repeat units and the ratio of sulfate groups per disaccharide unit (the sulfate/hexosamine ratio). In heparin, the tri-sulfated IdoA2S - GlcNS6S disaccharide comprises over 70% of the polysaccharide and heparin has on average 1.8 - 2.6 sulfate groups per disaccharide unit.[13, 14] In contrast, the major disaccharide repeating unit of heparan sulfate is GlcNAc - GlcA comprising about 40 - 60% of the polymer and a 0.8 - 1.8 sulfate/hexosamine ratio.[12, 13] Additionally, heparan sulfate contains highly sulfated heparin-like regions with other regions where there is a greater structural variability at the disaccharide level.[15] The structural complexity of heparin and heparan sulfate is introduced during biosynthetic chain elongation during which a variety of enzymes act on specific locations of the growing polysaccharide backbone.[3, 16] For instance, the variability of *N*-/*O*-sulfo group substitution is introduced by sulfotransferase enzymes, while inversion of GlcA to IdoA is performed by an epimerase.[3, 17, 18]

Similar non-template driven polysaccharide backbone modifications account for the polydisperse and heterogeneous nature of the chondroitin sulfate, dermatan sulfate, and keratan sulfate polysaccharides. The chondroitin sulfate disaccharide repeat unit is comprised of a GlcA residue linked through a β(1→3) glycosidic bond to *N*-acetylgalactosamine (GalNAc). The GlcA residue can be sulfated at the 2-*O* position and the GalNAc residue can be sulfated at the 4-*O* and 6-*O* positions. The dermatan sulfate polysaccharide resembles chondroitin sulfate, except that uronic acid residue exists exclusively as IdoA. The keratan sulfate structure differs from all other GAGs in that

hexose residue of the disaccharide repeat sequence is a Gal or Gal6S residue linked by a β(1→4) linkage to GlcNAc or GlcNAc6S hexosamine residues.[4] Keratan sulfate is only GAG doesn't containing uronic acid residues.

1.1.2. Significance of GAG structure to physiological processes and interactions with proteins. GAGs are the most abundant heteropolysaccharides in the body and they are important components in many life-essential physiological processes. The unsulfated polysaccharide hyaluronic acid, the only GAG not covalently attached to a protein core, is an important component in maintenance of the elastoviscosity of liquid connective tissues, control of tissue hydration and water transport, numerous receptor-mediated roles in cell detachment, mitosis, migration, tumor development and metastasis, inflammation, and the supramolecular assembly of proteoglycans in the extracellular matrix.[19-22] Hyaluronic acid is widely used in regenerative medicine and cosmetics.[23-26] Chondroitin sulfate and dermatan sulfate are major components of the extracellular matrix and are found in many connective tissues such as bone, cartilage, skin, ligaments and tendons.[27, 28] Chondroitin sulfate and dermatan sulfate can specifically interact with variety of heparin-binding proteins.[29] They are an important components for central nervous system development, wound repair, infection, growth factor signaling, morphogenesis and cell division.[30, 31] Chondroitin sulfate is also well known for its potential function in the treatment of osteoarthritis.[32] Keratan sulfate, originally identified as the major GAG of the cornea, is also found in cartilage and aggrecan.[33] Keratan sulfate is known for its ability to bind and modify proteins including fibromodulin, PRELP, and osteoadherin.[34-36] Heparin and heparan sulfate, interact with a wide variety of proteins and participate in a range of

important biological activities including cell development,[37, 38] proliferation,[39-41] differentiation,[42] adhesion,[3, 43] inflammation, [44-47] angiogenesis,[48] viral[49-51] and microbial infections, [52] and in the pathological conditions of tumor growth. [3, 53-55]

Countless number of interactions between GAGs and proteins mediate diverse physiological effects including hemostasis, lipid transport and absorption, cell growth and migration, and development. Binding to GAGs can immobilize proteins at their sites of production and in the extracellular matrix, regulate enzyme activity, binding of ligands to their receptors, and protect proteins against degradation.[1] While charge is a major component of protein binding, the microheterogeneity of GAGs allows specific recognition of proteins through different structural motifs that include various patterns of uronic acid and glucosamine *O*-sulfation, glucosamine *N*-substitutions (acetyl, sulfo or free amino groups), uronic acid C-5 epimerization (α-L-iduronic acid or β-D-glucuronic acid) etc. These interactions are critically dependent on particular arrangements of saccharides with specific structural elements localized within the polysaccharide chain.

One of the best studied GAG-protein interactions is the binding of heparin to the serine protease inhibitor antithrombin-III which is driven by the interactions of the negatively charged sulfate and carboxyl groups of heparin with the positively charged amino acids of protein. High affinity binding to antithrombin-III, which is critical for triggering downstream coagulation-cascade proteases, requires a pentasaccharide that includes a -GlcA-GlcNS3S6S-IdoA2S- motif as the minimum binding sequence. This pentasaccharide motif is also present in synthetic antithrombotic drug Arixtra™ (Fondaparinux sodium) shown in Figure 1.2. The relatively rare 3-*O*-sulfate modification

in the trisulfated glucosamine residue GlcNS3S6S is found in roughly 5% of heparin disaccharides[56] and is critical for high affinity binding. Removal of this 3-*O*-sulfo group decreases the antithrombin-III binding affinity of an oligosaccharide by 1000-fold.[57] A recent study by Langeslay et al. revealed the involvement of this 3-*O*-sulfo group in a persistent intramolecular hydrogen bond with the adjacent *N*-sulfo proton of GlcNS3S6S in Arixtra™.[58] This hydrogen bond may be correlated with the "kink" observed in the crystal structure of oligosaccharides bound to antithrombin-III.[59, 60] Additional studies of Arixtra™ identified hydrogen bonds involving hydroxyl protons and revealed the flexibility of IdoA2S residue.[61] The specific hydrogen bonds involving IdoA2S residue depend on the presence of the 3-*O*-sulfo group in GlcNS residue, suggesting that IdoA2S residue may contribute to stability of the pentasaccharide secondary structure. Consequently, not only do electrostatic interactions play an important role in GAG-protein interactions, structural elements that promote intramolecular hydrogen bonds may help pre-organize the oligosaccharide secondary structure to facilitate protein binding.

The importance of 3-*O*-sulfated GlcN motifs is not limited to heparin-antithrombin-III binding. Multiple studies suggest that incorporation of 3-*O*-sulfated glucosamine (GlcN3S) residues into the polysaccharide sequence is critical for heparan sulfate activity in many biological processes. For example, the entry of herpes simplex virus type 1[62, 63] into cells begins through the non-specific binding of viral glycoproteins B and C (gB and gC, respectively) to an heparan sulfate proteoglycan polysaccharide chain localized on the cell surface.[64-66] However, this interaction alone is insufficient for cell entry and infection, which requires fusion between the viral envelop and the cell membrane. Specific binding

of the viral glycoprotein D (gD) with a sequence that includes a 3-*O*-sulfated glucosamine residue leads to fusion between the viral envelop and the cell membrane.[64-66] Moreover, the heparan sulfate disaccharides IdoA2S-GlcN3S and IdoA2S-GlcN3S6S are reported to be possible mediators of herpes simplex virus type 1 entry.[67] Besides the interaction with gD,[49, 50] different heparan sulfate oligosaccharides containing GlcN3S or GlcNS3S6S residues are known to bind to a number of important proteins mediating critical biological functions. For example, cyclophilin B (CyPB) binding to a heparan sulfate sequence containing GlcN3S promotes lymphocyte adhesion and migration,[68] while binding of a different oligosaccharide with 3-*O*-sulfated glucosamine residues to stabilin-1 and 2 enhance the clearance of circulating heparin.[69, 70] 3-*O*-sulfated GlcNS3S and GlcNS3S6S residues are also a critical part of the binding motif for FGF and FGF receptors affecting cell growth.[71, 72] Binding specificity may be related to the relative rarity of 3-*O*-sulfated content in heparan sulfate (only 1 - 6%).[73-75] Clearly the heparan sulfate 3-*O*-sulfo group in GlcN3S is biologically important, but it's structural role in heparan sulfate remains unclear. In Chapter 3 the identification of a salt bridge involving the negatively charged GlcN3S 3-*O*-sulfo group with the adjacent positively charged amino is described for the first time. This non-covalent interaction could be an important element of heparan sulfate secondary structure and contribute to its specific interactions with proteins.

1.2. Challenges in structural studies of GAGs: The bottom-up approach

Structural studies and the investigation of the physico-chemical properties of GAGs are complicated by their polydisperse nature in addition to their flexibility in aqueous

solutions. Unlike genomics, proteomics and transcriptomics, the non-template driven chain elongation process of GAG biosynthesis does not allow the use of omics approaches or knowledge bases for their analysis. To overcome problems associated with polysaccharide complexity, the bottom-up approach is widely utilized in GAG studies. This approach initially involves depolymerization of the GAG polysaccharide followed by chromatographic isolation of uniformly fractionated oligosaccharides based on size and charge. Finally, the oligosaccharide is isolated in sufficient quantities for structure elucidation by MS and NMR and ideally, characterization of its biological properties.

1.2.1. Polysaccharide depolymerization. The depolymerization strategy employed usually depends on the final application and the need to obtain oligosaccharides with certain degree of polymerization. Generally, two methods are utilized to depolymerize GAG polysaccharides: 1) enzymatic digestion and 2) chemical depolymerization. In both methods, the specificity and degree of depolymerization can be controlled by selecting appropriate reaction conditions.

1.2.1.1. Enzymatic digestion. One of the greatest advantages of employing enzymes for GAG depolymerization is their ability to cleave glycosidic bonds at only specific locations of the polysaccharides. There are wide variety of enzymes are available to accommodate selective or non-selective GAG depolymerization reactions. For instance, depolymerization of chondroitin sulfate A can be performed by using Chondroitin ABC lyase (Chondroitinase ABC) derived from *Proteus vulgaris* bacteria.[5, 76] This enzyme is nonspecific, cleaving the glycosidic bond between GalNAc and uronic acid residues in chondroitin sulfate A (4-*O*-sulfated), chondroitin sulfate C (6-*O*-sulfated) and

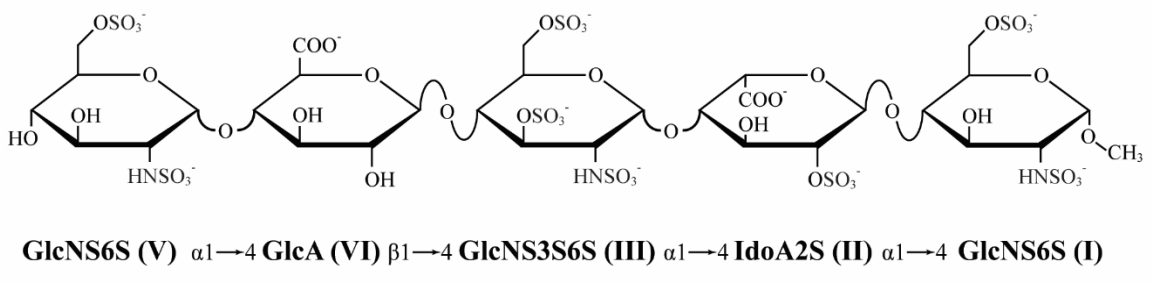

Figure 1.2. Haworth projection of the synthetic antithrombic drug Arixtra™ (Fondaparinux Sodium), a potent inhibitor of activated Factor Xa. The numbering of the oligosaccharide residues in this dissertation is from right to left, in other words, numbering starts at oligosaccharide reducing end residue and terminates at non-reducing end residue.

dermatan sulfate (Figure 1.3.). Enzymatic cleavage of the glycosidic bond introduces a Δ4,5-unsaturated residue at the non-reducing end of the oligosaccharide. This double bond provides a unique analytical handle absorbing UV light at 232 nm and producing a characteristic ^{1}H NMR resonance. The depolymerization reaction can be performed as an exhaustive digestion reducing the polysaccharide to its constituent disaccharide building blocks, or when larger oligosaccharides are desired for structural or protein binding experiments, the degree of depolymerization can be conveniently controlled and stopped at a partial digestion by monitoring the progress of the enzymatic reaction by ^{1}H NMR (Figure 1.4).

1.2.1.2. Chemical depolymerization. A variety of chemical reactions have been developed for GAG depolymerization including oxidative cleavage, β-elimination, and reductive deamination. Oxidative depolymerization proceeds through reaction of the polysaccharide with hydrogen peroxide and the divalent ions copper or iron.[6, 77] The reaction is highly specific to unsubstituted uronic acid (GlcA or IdoA) residues and yields an oxidized fragments of the hexuronic acid. The β-elimination reaction proceeds through the two steps. First, the carbon of the uronic acid carboxylate group reacts with benzyl halide to form an ester. Then treatment with strong base abstracts the proton from the fifth carbon of the uronic acid to form a double bond between fourth and fifth carbons of the uronic acid. Reductive deamination reaction proceeds through treatment of the polysaccharide with nitrous acid below pH 1.5. Cleavage occurs at *N*-unsubstituted GlcN residues to form a 2,5-anhydro-D-mannose residue at the reducing end of depolymerized

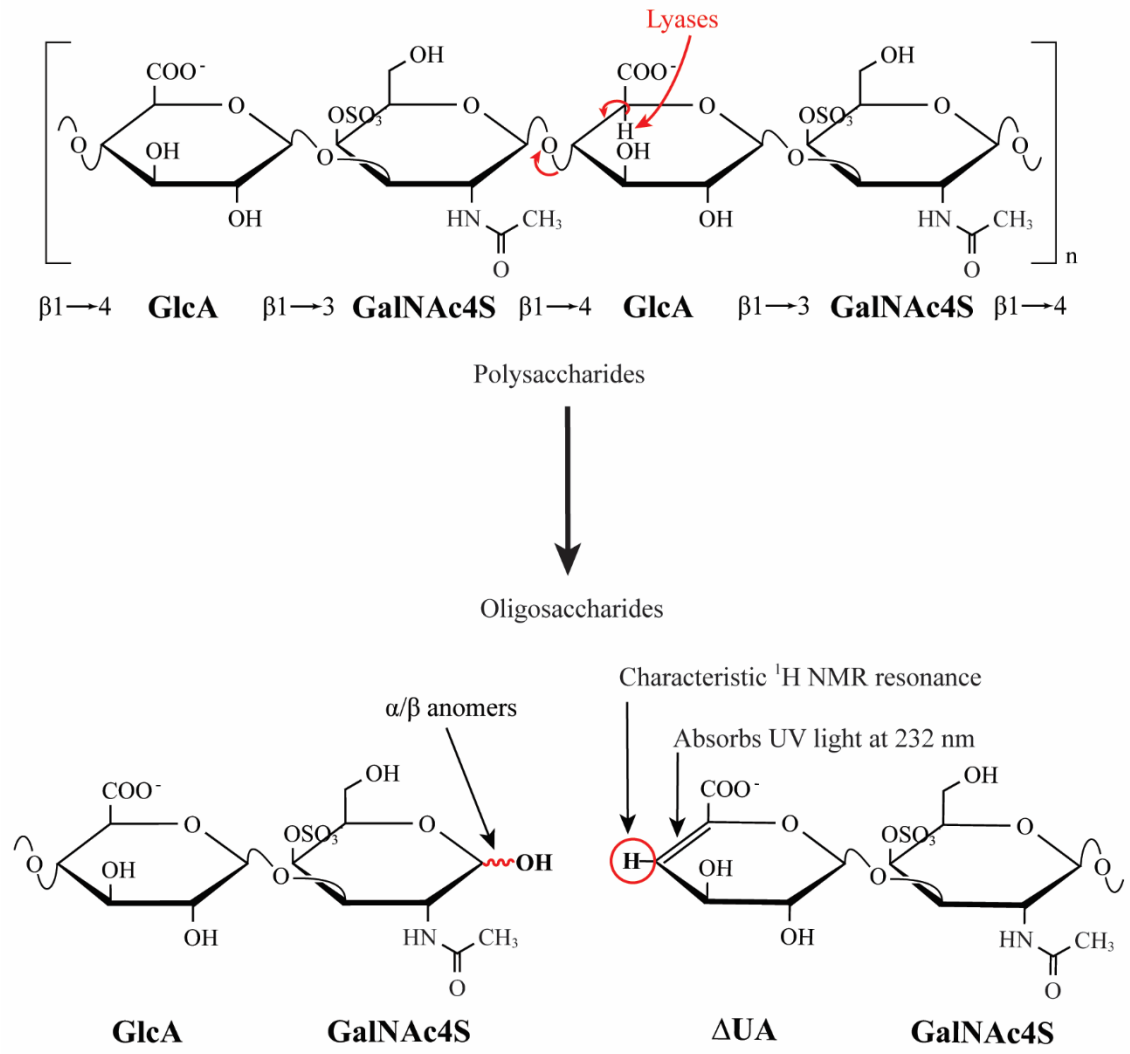

Figure 1.3. Schematic showing the eliminative cleavage of a chondroitin sulfate A polysaccharide by Chondroitinase ABC from *Proteus vulgaris*. The enzyme is not specific to chondroitin sulfate A and also lyses the glycosidic linkage between GalNAc and the uronic acid residues in chondroitin sulfate C and dermatan sulfate. As a result of this cleavage, a double bond is incorporated into the uronic acid residue of the non-reducing end between carbons 4 and 5 (Δ4,5-unsaturated), while the new reducing end GlcNAc residue exists as α/β anomers.

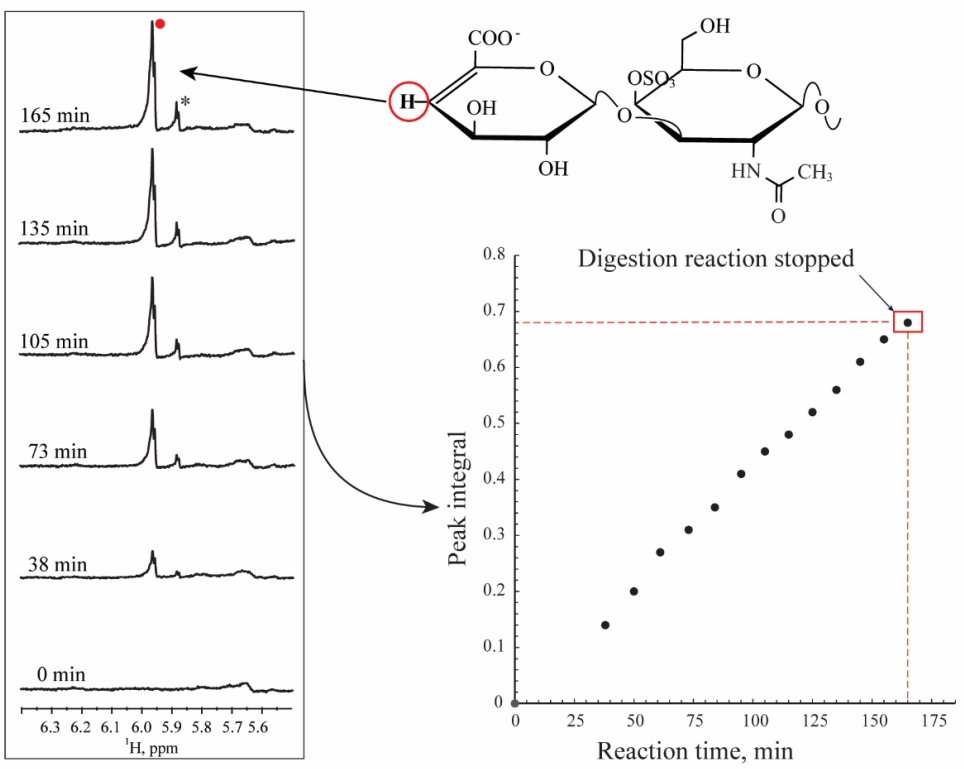

Figure 1.4. Monitoring the partial enzymatic digestion of chondroitin sulfate A by ^{1}H NMR. An aliquot of the digestion mixture containing the chondroitin sulfate A polysaccharide and Chondroitinase ABC was transferred into an NMR tube and placed in the magnet for incubation at 310.2 K. ^{1}H NMR spectra were acquired at intervals during digestion period. The resonance of hydrogen atom bound to fourth carbon of the modified uronic acid residue (H4) has a characteristic chemical shift between 5.8 - 6.0 ppm. As the digestion proceeds, the intensity of the H4 resonance increases. The resonance labeled with a red dot belongs to chondroitin sulfate A oligosaccharides and the resonance labeled with black star belongs to chondroitin sulfate C and/or dermatan sulfate oligosaccharides (Section 1.2.2.2). Plotting the integrated resonance as function of time generates a digestion progress graph.

oligosaccharide. This reaction can also be applied to any GalNAc containing polysaccharide, but requires preliminary de-*N*-acetylation, and yields 2,5-anhydro-D-talose residues at the oligosaccharide reducing end.[78]

1.2.2. Isolation of depolymerized oligosaccharides. Solutions of depolymerized GAGs contain multicomponent mixtures of oligosaccharides. The composition of the mixture can be directly analyzed by mass spectrometry, either through direct infusion or in conjunction with a mass spectrometry-compatible separation.[79-82] However, the investigation of the structure, physico-chemical properties, and biological activities of GAG oligosaccharides demands sufficient quantities (typically milligrams) of pure oligosaccharides and therefore, requires isolation of individual oligosaccharides from the mixture through chromatographic approaches.

1.2.2.1. Size-exclusion chromatography. Size-exclusion chromatography is typically the first step in oligosaccharide separations. The partially depolymerized GAG is loaded onto the chromatographic column and eluted with appropriate mobile phase. The choice of stationary and mobile phases is selected for the particular application and the separation can be performed at the analytical or preparative scale. Size-exclusion chromatography resolves similarly-sized oligosaccharides into separate bands that can be collected for subsequent separation based on charge. Figure 1.5 shows the representative preparative size-exclusion chromatographic profiles obtained for 905 mg of chondroitin sulfate A partially digested with Chondroitinase ABC and 50 mg of hyaluronic acid digested with Hyaluronic acid lyase derived from *Streptomyces hyalurolyticus*.

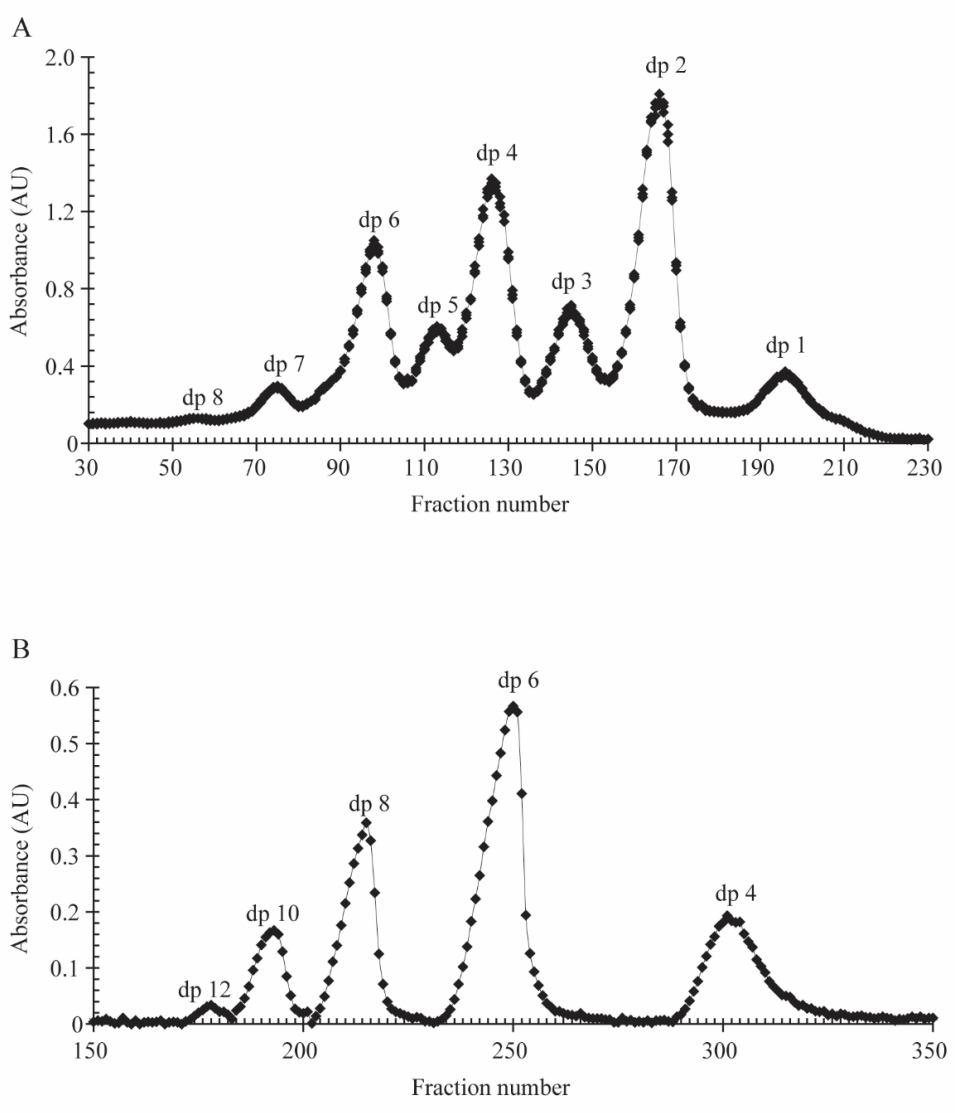

Figure 1.5. Size-exclusion chromatograms of (A) chondroitin sulfate A and (B) hyaluronic acid. Each data point represents individual 4.5 mL or 3.5 mL size-uniform fractions collected for chondroitin sulfate A or hyaluronic acid, respectively. The peak labeling corresponds to oligosaccharide size: mono- (dp 1), di- (dp 2), tri- (dp 3), tetra-(dp 4), penta-(dp 5), hexa-(dp 6), hepta-(dp 7), octa-(dp 8), deca-(dp 10), and dodecasaccharides (dp 12) where dp refers to depolymerization product.

The separations were performed at atmospheric pressure using a preparative size-exclusion chromatography column (3 × 200 cm) packed with Bio-Gel P10 fine gel. Though preparative scale chromatography requires a much longer time (on the order of days) to complete the separation, its advantage over analytical HPLC-size-exclusion chromatography is the capacity of the column to resolve large amounts of material in one separation. For the size-exclusion chromatograms shown in Figure 1.5, the eluent was collected in individual fractions and the progress of the separation monitored offline by measurement of the UV absorbance at 232 nm. Because of the structural differences of the polysaccharides and the specificity of enzymes used in these digestions, the size-exclusion chromatograms reflect structural differences in the depolymerized chondroitin sulfate A and hyaluronic acid. For instance, the digested chondroitin sulfate A contains oligomers comprised of both odd and even numbers of monosaccharides, while the mixture of digested hyaluronic acid contains only even-numbered oligosaccharides with major products consisting of tetra-, hexa-, and octasaccharides. Finally, to remove mobile phase constituents from the isolated oligosaccharides, the pooled size-uniform fractions were lyophilized and desalted using a 1.6 × 70 cm desalting column packed with GE Sephadex G-10 superfine resin and using ultrapure deionized water as the mobile phase. The fractions containing the desalted oligosaccharides were lyophilized and stored at -80 ºC for further analysis.

1.2.2.2. Strong anion-exchange chromatography. The size-uniform fractions isolated by size-exclusion chromatography are heterogeneous mixtures of oligosaccharides with a distribution of structures and charges, therefore, strong anion-exchange-HPLC UV-

Vis chromatography is used for the isolation of pure oligosaccharides derived from GAG digestions. Figure 1.6 shows the strong anion-exchange chromatogram of the chondroitin sulfate A tetrasaccharides fraction isolated by size-exclusion chromatography. Because the chondroitin sulfate A starting material used for this digestion was 70% pure and contains significant amounts of chondroitin sulfate C and dermatan sulfate, the size uniform fractions obtained by size-exclusion chromatography contain oligosaccharides that are variously sulfated and differ in IdoA/GlcA content. The strong anion-exchange separation was performed using a Waters Spherisorb semi-preparative column packed with 5µm silica-based particles with a quaternary ammonium bonded sorbent. Though, semi-preparative columns provide lower resolution and require longer equilibration times compared to analytical columns, this disadvantage is compensated by their capacity to separate larger amounts of material. The eluted strong anion-exchange chromatography peaks are collected over multiple injections, and the fractions containing each oligosaccharide are combined, lyophilized, desalted and lyophilized again for long-term storage at -80 ºC. These purified oligosaccharides are now ready for structure elucidation.

1.3. Structure elucidation

The complete structure elucidation of isolated GAG oligosaccharides is accomplished using two of the most powerful analytical techniques: MS and NMR spectroscopy.

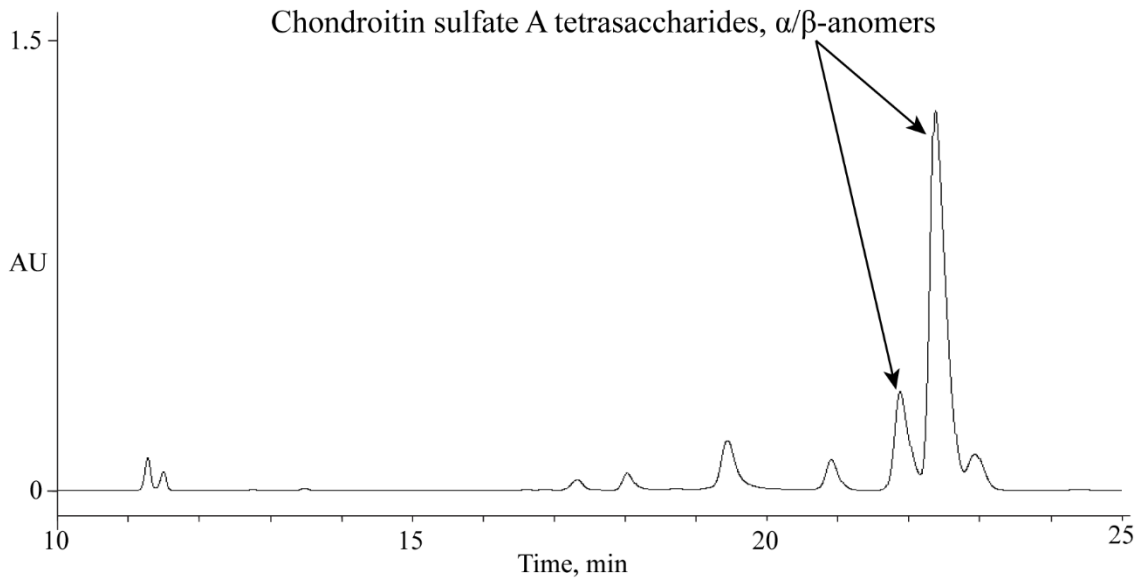

Figure 1.6. Strong anion-exchange -HPLC chromatogram of the pooled chondroitin sulfate A tetrasaccharide fractions obtained by size-exclusion chromatography. Components of the mixture are separated by differences in charge. The chondroitin sulfate A tetrasaccharide α and β anomer peaks are resolved indicating that their mutorotation is slow on the separation time scale. The remaining peaks are due to impurities or minor structural variants present in original chondroitin sulfate A polysaccharide sample.

1.3.1. Mass spectrometry. Destructive in nature but highly sensitive, MS identifies the oligosaccharide composition including molecular weight, extent of sulfation and acetylation and, through fragmentation, can often elucidate the sequence of the monosaccharide residues.[83-85] Electrospray ionization mass spectrometry (ESI-MS) is typically used in negative mode and provides effective ionization of the negatively charged oligosaccharides. However, when direct infusion is used, the ESI mass spectra can be complicated by the presence of sodium or/and potassium adducts and the presence of multicharged molecular ions associated with sulfate loss. While adduct ions can be reduced by thoughtful sample preparation (e.g. careful desalting and use of ammonium buffers[80]) or by incorporating a reversed-phase ion pairing HPLC separation,[86-90] the loss of sulfate during the ionization process is much harder to control. Sulfate loss can be reduced by careful tuning of the ionization and ion-extraction voltage parameters of the ionization source, but complete elimination of sulfate loss is a challenge. In cases where additional structural information is required, tandem mass spectrometry can elucidate the oligosaccharide sequence.[85, 91-93] The ion activation technique electron detachment dissociation along with tandem mass spectrometry is even able to distinguish the uronic acid epimers GlcA and IdoA.[94]

1.3.2. Solution state NMR. NMR spectroscopy is an invaluable analytical tool for the study of GAGs,[95-97] protein-GAG interactions,[98] and oligosaccharide secondary structure.[15, 58, 61, 99-104] NMR is also used in structure elucidation to confirm the structures postulated by mass spectrometry, and is particularly helpful when advanced techniques like electron detachment dissociation are not readily accessible. NMR is non-destructive and

therefore allows full recovery of the precious and limited amounts of sample isolated through the painstaking processes described in Section 1.2. However, NMR struggles with fundamental issues of low sensitivity especially compared with mass spectrometry. This disadvantage can be partially overcome using more concentrated samples, reduced volume NMR tubes, and by performing the measurements at the highest available magnetic field using probes and preamplifiers that are cryogenically cooled to reduce Johnson noise in the detected signals.[105]

One-dimensional (1D) and multi-dimensional (2D, 3D) NMR experiments employing ^{1}H, ^{13}C and ^{15}N are among most successful approaches for the characterization of GAG oligosaccharides.[97, 106-108] Because of the limited dispersion of the ^{1}H NMR resonances of carbohydrates, resonance overlap can make it challenging to assign the NMR spectra of even medium-sized oligosaccharides.[5, 109, 110] The use of higher field magnets and, when feasible, GAG isotopic labeling in cell cultures[97] can improve peak resolution and sensitivity.

The standard arsenal of 2D homonuclear NMR experiments COSY, TOCSY, and ROESY are invaluable for oligosaccharide spectral assignments by connecting ^{1}H resonances through cross peaks that reflect through bond or through space interactions.[111-116] The greater dispersion of [^{1}H,^{13}C] HSQC spectra can make it useful for resonance assignments, and this experiment has even been used to characterize the components of the anticoagulant drug Enoxaparin, a complex mixtures of oligosaccharides produced by the chemical depolymerization of heparin.[106, 107] Indirect detection of the ^{15}N nuclei found in every other monosaccharide residue in GAGs can provide important structural information.

The detection and characterization of the amide groups in hyaluronic acid oligosaccharides up to decamers has been successfully accomplished through [^{1}H,^{15}N] HSQC NMR,[95] in contrast to ^{13}C NMR where only a hyaluronic acid hexamer's internal acetyl groups could be resolved. Major advances in the application of [^{1}H,^{15}N] HSQC for GAG analysis were made by Langeslay et al. and Beecher et al. who identified experimental conditions that minimize the exchange rates of the GAG sulfamate and amine protons. Langeslay et al. also used the [^{1}H,^{15}N] HSQC spectra of Enoxaparin to demonstrate the sensitivity of the sulfamate group ^{1}H and ^{15}N chemical shifts to subtle structure differences.[9]

Much of the work in this dissertation relies on NMR spectroscopy. In Chapter 2, the detailed structure characterization of chemically modified oligosaccharides is presented. In Chapters 3 and 4, NMR is used to study the properties of the labile nitrogen-bound protons of the GAG acetyl and amino groups, and this topic is briefly introduced in the following section.

1.4. The examination of labile protons in the study of GAG secondary structure

Hydrogen bonds and salt bridges play very important roles in many chemical and biochemical processes.[117-119] They are responsible for determining the conformation and complexation of large and small chemical and biochemical molecules and systems. For instance, structure of DNA is crucially dependent on the strength of the hydrogen bonds between the base pairs. Similarly, the strength of the cellulose, a polysaccharide composed of glucose units, is fully dependent on intermolecular hydrogen bonding.[120, 121] Because elements of secondary structure like hydrogen bonds or salt bridges may help stabilize the

conformation of an oligosaccharide in an orientation that facilitates protein binding, the exploration of the intramolecular properties of oligosaccharides in aqueous solution could help advance our understanding of specific GAG-protein interactions.

NMR methods and approaches to study oligosaccharide solution structure and dynamics continue to advance. For instance, the investigation of the dynamics of hyaluronic acid oligosaccharides in aqueous solution through ^{1}H and ^{15}N NMR spectroscopy revealed the absence of amide-carboxylate hydrogen bonds which were previously believed to be responsible for the stiffening of the hyaluronic acid polymer by forming inter-residue hydrogen bonds.[122] This discovery provided a new view on the secondary and tertiary structures of the hyaluronic acid biopolymer in aqueous solution. More recently, Langeslay et al. reported that the 3-*O*-sulfo group of the center GlcNS3S(III) residue in synthetic pentasaccharide Arixtra™ (Figure 1.2) is involved in a hydrogen bond with the nitrogen-bound proton of the adjacent sulfamate group.[58] Beecher et al. complemented these findings by identifying two additional intramolecular hydrogen bonds involving the Arixtra™ hydroxyl protons. Chapter 3 discusses the identification of salt bridge in a model heparan sulfate pentasaccharide involving the 3-*O*-sulfated glucosamine (GlcN3S) amine group and adjacent 3-*O*-sulfo group. In each of these examples, the intermolecular interactions were identified (or in the case of hyaluronic acid disproved) by exploration of the dynamics and chemical exchange properties of labile protons in aqueous solution using NMR spectroscopy.

1.4.1. Chemical exchange and the NMR time scale. In NMR, the term chemical exchange refers to the process by which a nucleus relocates from one chemical

environment to another and is simultaneously replaced by another nucleus maintaining the chemical equilibrium of the system.[123] It should be noted that chemical exchange doesn't perturb chemical equilibrium and is observable only in NMR spectra, providing that the rate of exchange is in the appropriate regime. The NMR chemical shift time scale is defined by the difference in chemical shift in Hz of the nuclei in the two environments. Because this chemical shift difference depends linearly on magnetic field strength, it can be helpful to acquire spectra at more than one magnetic field.

Using simulated spectra, Figure 1.7 shows an example of the effect of chemical exchange between the *cis*- (A) and *trans*- (B) methyl groups of dimethylformamide on the ^{1}H NMR spectrum. In this case, the exchange is governed by first order kinetics and the populations of the exchanging groups are equal, though this need not be the case. The different chemical environments of the *cis*- and *trans*- methyl groups cause their protons to resonate at two different frequencies, ν_A and ν_B, and it is the difference in chemical shift (ν_A - ν_B) that defines the NMR time-scale for this system. Because of the partial double bond character of the amide N-C bond, rotation about this bond is slow enough to be observed in the ^{1}H NMR spectrum. At low temperature, the rate of rotation about the N-C bond is sufficiently slow that during the acquisition of the free induction decay, exchange is not observed and the exchange rate constant, k, is very much less than the difference in chemical shift (ν_A - ν_B). In this slow exchange regime, the *cis*- and *trans*- methyl protons produce narrow resonances at their characteristic frequencies (ν_A and ν_B). Gradual heating increases the rate of rotation and the effects of chemical exchange can be observed in the NMR spectrum as the methyl proton resonances broaden and their chemical shifts move

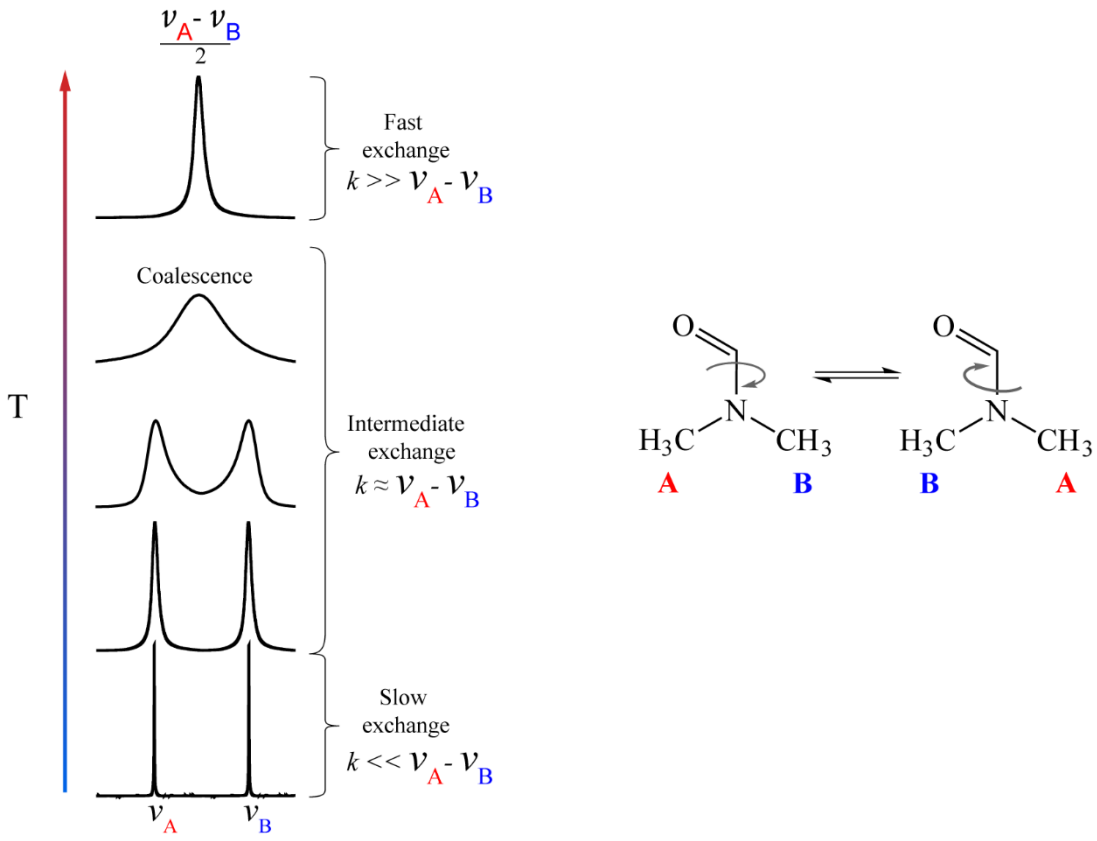

Figure 1.7. The effects of chemical exchange between two equally populated *cis*- and *trans*- dimethylamino groups in the simulated ^{1}H NMR spectra of dimethylformamide. The rate of the rotation of the dimethylamino group about the single bond joining nitrogen and carbon is temperature dependent. As the temperature increases, individual methyl resonances assigned as ν_A and ν_B, become broader and shift toward each other until they coalesce. Chemical exchange rates in the intermediate regime can be determined from the NMR spectral parameters.

environments. Eventually the two resonances coalesce at the average chemical shift, (ν_A + ν_B)/2, and then sharpen as the fast exchange regime is reached. In this fast exchange regime, the rate of exchange is much larger than frequency difference separating two dimethylformamide methyl proton resonances. It is important to note that when the populations of the exchanging protons are much different, as with chemical exchange between the labile protons of a GAG oligosaccharide (~1 mM) and the protons of water (~110 M), the coalescence frequency is the population weighted average and therefore appears essentially at the water resonance frequency.

1.4.2. Chemical exchange and the labile protons of GAGs. The labile GAG protons observable by ^{1}H NMR in aqueous solution include the amide ($NHCOCH_3$), amino (NH_3^+), sulfamate ($NHSO_3^-$), and hydroxyl (OH) protons. Figure 1.8 shows the generalized chemical exchange reaction between an amino sugar residue (R) containing labile protons of different types and the protons of water. The rate of proton exchange is temperature-dependent and hence follows the Eyring-Polanyi equation (Eq. 1.1) which describes the relationship between the chemical exchange rate constant (*k*), temperature (T), and the energy barrier associated with exchange ($\Delta G^{\ddagger}$).

$$k = \frac{k_B \mathrm{T}}{\pi h} e^{\frac{\Delta G^{\ddagger}}{\mathrm{RT}}} \qquad \text{(Eq. 1.1)}$$

Eq. 1.1 indicates that exchange rates are directly proportional to the solution temperature, and consequently slower exchange occurs at reduced temperatures. In aqueous solutions of sugars, it is possible to lower the temperature below the freezing point

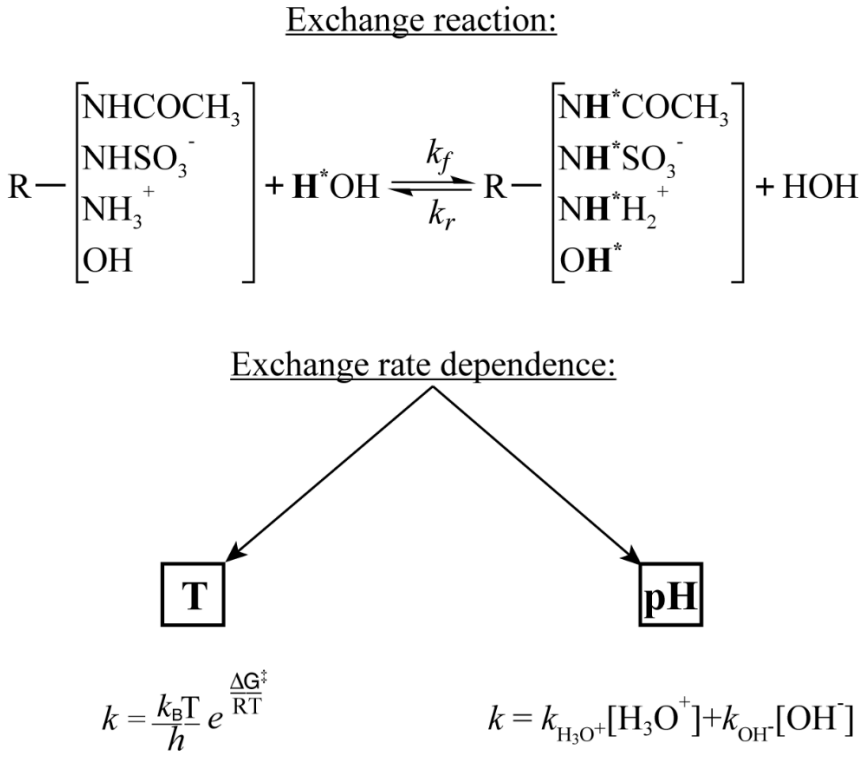

Figure 1.8. Exchange reaction of labile protons with water is temperature and pH dependent. The asterisk in the exchange reaction denotes a proton transferred during the exchange.

of water by adding 10 - 15% of the minimally-perturbing solvent deuteroacetone, which can also serve as the spectrometer lock.[61, 124] The solution pH is another important experimental parameter because the chemical exchange reaction between the labile protons and water is catalyzed by H_3O^+ and OH^- ions. Because exchange process occurs in aqueous solution with a large excess of the water, the proton exchange reaction is governed by the pseudo first-order kinetics as described by Eq. 1.2.[125]

$$k_{obs} = k_{H^+}[H^+] + k_{OH^-}[OH^-] \qquad \text{(Eq. 1.2)}$$

According to Eq. 1.2, the overall rate constant (k_{obs}) of the proton exchange reaction is the sum of two terms, $k_{H_3O^+}[H_3O^+]$ and $k_{OH^-}[OH^-]$, representing the exchange rate of the base and acid catalyzed reactions, respectively. Because the exchange rate constants for the acid ($k_{H_3O^+}$) and base (k_{OH^-}) catalyzed reactions are not equal and depend on the chemical system, the solution pH that produces the slowest exchange is also system dependent.

Among the four GAG functional groups with observable labile protons, the rate of solvent exchange with the amide protons is slowest and their resonances can be easy detected at room temperature over a wide pH range, with an optimum around pH 6.0.[126] The sulfamate protons exchange with solvent more rapidly than amide protons, but slower than the protons of hydroxyl and amine groups. Though, sulfamate protons are detectable at room temperature, the pH range over which they can be detected is much narrower than for amides, with an optimum solution pH between 7.5 and 8.5.[58, 127] Detection of hydroxyl and amine group proton resonances is more challenging and requires temperatures below

0 °C. The optimum pH for detection of hydroxyls is around 7.8 - 8.8 and that for aminos is around 3.2 - 4.2.[61, 124] Furthermore, the optimum pH to detect the labile protons of a particular oligosaccharide depends on factors that including the size and extent of sulfation.

1.4.3. Experimental approaches for studying properties of the labile protons of GAG oligosaccharides by NMR. A variety of NMR approaches originally developed to study hydrogen bonding, salt bridge formation, and proton-solvent exchange in aqueous solutions of peptides and oligonucleotides can also be used to characterize the properties of labile protons in solutions of GAG oligosaccharides.[99, 104, 128-130]

1.4.3.1. Temperature coefficients. Temperature coefficients, $\Delta\delta/\Delta T$, are measured by observing changes in the ^{1}H NMR resonance frequency as a function of temperature, and are one of the most powerful indicators of hydrogen bonds in proteins, peptides, and carbohydrates.[128, 129, 131, 132] The overall effect is that the change in resonance frequency as function of temperature for a labile proton involved in a hydrogen bond will be less than for a proton that does not participate in a hydrogen bond. The value of $\Delta\delta/\Delta T$ is obtained by taking the absolute value of the slope of the line obtained by plotting the chemical shift of the exchangeable proton as function of temperature, and a low temperature coefficient can indicate participation of a proton in a hydrogen bond.[130]

1.4.3.2. Line shape analysis and the quantification of energy barriers associated with exchange. ^{1}H NMR spectra acquired for the determination of temperature coefficients can also provide insights into the kinetics of the exchange of labile protons with water. For the more slowly exchanging protons of the amide and sulfamate groups, the resonance line width measured at half of the peak height is proportional to the exchange rate constant (k).

Resonance line widths measured as function of temperature can be fit using the Eyring-Polanyi equation (Eq. 1.1), allowing the extraction of the energy barrier (or activation energy), $\Delta G^{\ddagger}$, associated with proton exchange as it will be discussed in Chapter 4. Protons with a significantly greater energy barrier compared to other structurally similar protons may be protected from exchange with solvent, for example by participating in an intramolecular hydrogen bond.[58, 133-135]

1.4.3.3. Exchange spectroscopy for the direct measurement of proton exchange rates. Due to limits on how low a temperature can be reached in aqueous solution, the more rapid exchange of the amino and hydroxyl group protons with water precludes the accurate measurement of their exchange rate constants through line shape analysis. Luckily, the faster solvent exchange rates of the amino and hydroxyl protons put them in an exchange regime accessible by 2D exchange spectroscopy (EXSY). EXSY utilizes the NOESY pulse and detects the magnetization transfer between exchanging protons.[115] The intensity of the EXSY cross peaks depends on the exchange rate, mixing time, and the longitudinal (T_1) relaxation times of the exchanging nuclei. Plotting the EXSY cross peak volumes as function of mixing time generates a build-up curve from which exchange rates can be extracted by fitting to the Bloch equation modified to account for contributions of radiation damping to the longitudinal relaxation rate of the hydroxyl and amino protons.[61] Comparison of the exchange rates of similar protons can indicate participation in a hydrogen bond and/or a salt bridge (Chapter 3)

1.5. Conclusions

The purpose of the research presented in this dissertation is the development of new methods and approaches for the structural characterization of GAGs in aqueous solution using NMR. The major focus of the work discussed in Chapter 2 is the preparation of unique GAG structures by enzymatic and chemical modifications. Mechanisms are proposed for the reactions used for modification of saccharides and an example of the process of structure elucidation of modified oligosaccharides by MS and NMR is also presented.

The methods of chemical modification used in this research provided access to heparan sulfate oligosaccharides containing rare, unique, and important 3-*O*-sulfated glucosamine residues. In Chapter 3, temperature coefficients, exchange rates and pKa values for de-*N*-sulfated Arixtra™ are used to evaluate possibility of a salt bridge between the 3-*O*-sulfate and adjacent amino group of the central glucosamine residue.

Chapter 4 explores the amide proton exchange properties of *N*-acetylated residues in GAG oligosaccharides. The dependence on oligosaccharide size, extent of sulfation, position of sulfation, glycosidic linkage, and type of sugar (GalNAc/GlcNAc and IdoA/GlcA) were investigated by employing temperature experiments and pH titrations. The chemically modified *N*-acetylated Arixtra™ and *N*-acetylated GlcN3S facilitated this study and helped discern the effect of charge repulsion of hydroxyl ions by nearby negatively charged groups in the catalysis of amide proton solvent exchange. All experimental findings were further complemented by molecular dynamics simulations

using GLYCAM 06g force fields. Chapter 5 summarizes the work presented in this dissertation and provides an outlook for future research in GAG structural analysis.

1.6. References

1. In *Essentials of Glycobiology*, 2nd; Varki, A.; Cummings, R. D.; Esko, J. D.; Freeze, H. H.; Stanley, P.; Bertozzi, C. R.; Hart, G. W.; Etzler, M. E., Eds. Cold Spring Harbor Laboratory Press: Cold Spring Harbor (NY), **2009**.

2. Sasisekharan, R.; Venkataraman, G., Heparin and heparan sulfate: biosynthesis, structure and function. *Curr. Opin. Chem. Biol.* **2000,** *4* (6), 626-31.

3. Whitelock, J. M.; Iozzo, R. V., Heparan sulfate: a complex polymer charged with biological activity. *Chem. Rev.* **2005,** *105* (7), 2745-64.

4. DeAngelis, P. L., Glycosaminoglycan polysaccharide biosynthesis and production: today and tomorrow. *Appl. Microbiol. Biotechnol.* **2012,** *94* (2), 295-305.

5. Pomin, V. H.; Park, Y.; Huang, R.; Heiss, C.; Sharp, J. S.; Azadi, P.; Prestegard, J. H., Exploiting enzyme specificities in digestions of chondroitin sulfates A and C: production of well-defined hexasaccharides. *Glycobiology* **2012,** *22* (6), 826-38.

6. Jones, C. J.; Beni, S.; Limtiaco, J. F.; Langeslay, D. J.; Larive, C. K., Heparin characterization: challenges and solutions. *Annu. Rev. Anal. Chem. (Palo Alto, Calif.)* **2011,** *4* (1), 439-65.

7. Ziegler, A.; Zaia, J., Size-exclusion chromatography of heparin oligosaccharides at high and low pressure. *J. Chromatogr. B Analyt. Technol. Biomed. Life Sci.* **2006,** *837* (1-2), 76-86.

8. Chuang, W. L.; McAllister, H.; Rabenstein, L., Chromatographic methods for product-profile analysis and isolation of oligosaccharides produced by heparinase-catalyzed depolymerization of heparin. *J. Chromatogr. A* **2001,** *932* (1-2), 65-74.

9. Langeslay, D. J.; Beecher, C. N.; Naggi, A.; Guerrini, M.; Torri, G.; Larive, C. K., Characterizing the microstructure of heparin and heparan sulfate using N-sulfoglucosamine 1H and 15N NMR chemical shift analysis. *Anal. Chem.* **2013,** *85* (2), 1247-55.

10. Deepa, S. S.; Yamada, S.; Fukui, S.; Sugahara, K., Structural determination of novel sulfated octasaccharides isolated from chondroitin sulfate of shark cartilage and their application for characterizing monoclonal antibody epitopes. *Glycobiology* **2007,** *17* (6), 631-45.

11. Pothacharoen, P.; Kalayanamitra, K.; Deepa, S. S.; Fukui, S.; Hattori, T.; Fukushima, N.; Hardingham, T.; Kongtawelert, P.; Sugahara, K., Two related but distinct

chondroitin sulfate mimetope octasaccharide sequences recognized by monoclonal antibody WF6. *J. Biol. Chem.* **2007,** *282* (48), 35232-46.

12. Meneghetti, M. C.; Hughes, A. J.; Rudd, T. R.; Nader, H. B.; Powell, A. K.; Yates, E. A.; Lima, M. A., Heparan sulfate and heparin interactions with proteins. *J. R. Soc. Interface* **2015,** *12* (110), 0589.

13. Rabenstein, D. L., Heparin and heparan sulfate: structure and function. *Nat. Prod. Rep.* **2002,** *19* (3), 312-31.

14. Gatti, G.; Casu, B.; Hamer, G. K.; Perlin, A. S., Studies on the Conformation of Heparin by 1H and 13C NMR Spectroscopy. *Macromolecules* **1979,** *12* (5), 1001-1007.

15. Mazak, K.; Beecher, C. N.; Kraszni, M.; Larive, C. K., The interaction of enoxaparin and fondaparinux with calcium. *Carbohydr. Res.* **2014,** *384*, 13-9.

16. Carlsson, P.; Kjellén, L., Heparin Biosynthesis. In *Heparin - A Century of Progress*, Lever, R.; Mulloy, B.; Page, P. C., Eds. Springer Berlin Heidelberg: Berlin, Heidelberg, **2012**; pp 23-41.

17. Esko, J. D.; Lindahl, U., Molecular diversity of heparan sulfate. *J. Clin. Invest.* **2001,** *108* (2), 169-73.

18. Kreuger, J.; Kjellen, L., Heparan sulfate biosynthesis: regulation and variability. *J Histochem. Cytochem.* **2012,** *60* (12), 898-907.

19. Ghosh, P., The role of hyaluronic acid (hyaluronan) in health and disease: interactions with cells, cartilage and components of synovial fluid. *Clin. Exp. Rheumatol.* **1994,** *12* (1), 75-82.

20. Tzellos, T. G.; Sinopidis, X.; Kyrgidis, A.; Vahtsevanos, K.; Triaridis, S.; Printza, A.; Klagas, I.; Karakiulakis, G.; Papakonstantinou, E., Differential hyaluronan homeostasis and expression of proteoglycans in juvenile and adult human skin. *J. Dermatol. Sci.* **2011,** *61* (1), 69-72.

21. Almond, A., Hyaluronan. *Cell Mol. Life Sci.* **2007,** *64* (13), 1591-6.

22. Papakonstantinou, E.; Roth, M.; Karakiulakis, G., Hyaluronic acid: A key molecule in skin aging. *Dermatoendocrinol.* **2012,** *4* (3), 253-8.

23. Burdick, J. A.; Prestwich, G. D., Hyaluronic acid hydrogels for biomedical applications. *Adv. Mater.* **2011,** *23* (12), H41-56.

24. Highley, C. B.; Prestwich, G. D.; Burdick, J. A., Recent advances in hyaluronic acid hydrogels for biomedical applications. *Curr. Opin. Biotechnol.* **2016,** *40*, 35-40.

25. Juhlin, L., Hyaluronan in skin. *J. Intern. Med.* **1997,** *242* (1), 61-6.

26. Anderegg, U.; Simon, J. C.; Averbeck, M., More than just a filler - the role of hyaluronan for skin homeostasis. *Exp. Dermatol.* **2014,** *23* (5), 295-303.

27. Henrotin, Y.; Mathy, M.; Sanchez, C.; Lambert, C., Chondroitin sulfate in the treatment of osteoarthritis: from in vitro studies to clinical recommendations. *Ther. Adv. Musculoskelet. Dis.* **2010,** *2* (6), 335-48.

28. Zhang, G.; Ezura, Y.; Chervoneva, I.; Robinson, P. S.; Beason, D. P.; Carine, E. T.; Soslowsky, L. J.; Iozzo, R. V.; Birk, D. E., Decorin regulates assembly of collagen fibrils and acquisition of biomechanical properties during tendon development. *J. Cell. Biochem.* **2006,** *98* (6), 1436-49.

29. Sugahara, K.; Mikami, T.; Uyama, T.; Mizuguchi, S.; Nomura, K.; Kitagawa, H., Recent advances in the structural biology of chondroitin sulfate and dermatan sulfate. *Curr. Opin. Struct. Biol.* **2003,** *13* (5), 612-20.

30. Avram, S.; Shaposhnikov, S.; Buiu, C.; Mernea, M., Chondroitin sulfate proteoglycans: structure-function relationship with implication in neural development and brain disorders. *Biomed. Res. Int.* **2014,** *2014*, 642798.

31. Ida, M.; Shuo, T.; Hirano, K.; Tokita, Y.; Nakanishi, K.; Matsui, F.; Aono, S.; Fujita, H.; Fujiwara, Y.; Kaji, T.; Oohira, A., Identification and functions of chondroitin sulfate in the milieu of neural stem cells. *J. Biol. Chem.* **2006,** *281* (9), 5982-91.

32. Bishnoi, M.; Jain, A.; Hurkat, P.; Jain, S. K., Chondroitin sulphate: a focus on osteoarthritis. *Glycoconj. J.* **2016,** *33* (5), 693-705.

33. Funderburgh, J. L., Keratan sulfate biosynthesis. *IUBMB life* **2002,** *54* (4), 187-94.

34. Antonsson, P.; Heinegard, D.; Oldberg, A., Posttranslational modifications of fibromodulin. *J. Biol. Chem.* **1991,** *266* (25), 16859-61.

35. Sommarin, Y.; Wendel, M.; Shen, Z.; Hellman, U.; Heinegard, D., Osteoadherin, a cell-binding keratan sulfate proteoglycan in bone, belongs to the family of leucine-rich repeat proteins of the extracellular matrix. *J. Biol. Chem.* **1998,** *273* (27), 16723-9.

36. Bengtsson, E.; Neame, P. J.; Heinegard, D.; Sommarin, Y., The primary structure of a basic leucine-rich repeat protein, PRELP, found in connective tissues. *J. Biol. Chem.* **1995,** *270* (43), 25639-44.

37. Mitsiadis, T. A.; Salmivirta, M.; Muramatsu, T.; Muramatsu, H.; Rauvala, H.; Lehtonen, E.; Jalkanen, M.; Thesleff, I., Expression of the Heparin-Binding Cytokines, Midkine (Mk) and Hb-Gam (Pleiotrophin) Is Associated with Epithelial-Mesenchymal

Interactions during Fetal Development and Organogenesis. *Development* **1995,** *121* (1), 37-51.

38. Ringvall, M.; Ledin, J.; Holmborn, K.; van Kuppevelt, T.; Ellin, F.; Eriksson, I.; Olofsson, A. M.; Kjellen, L.; Forsberg, E., Defective heparan sulfate biosynthesis and neonatal lethality in mice lacking N-deacetylase/N-sulfotransferase-1. *J. Biol. Chem.* **2000,** *275* (34), 25926-30.

39. Khorana, A. A.; Sahni, A.; Altland, O. D.; Francis, C. W., Heparin inhibition of endothelial cell proliferation and organization is dependent on molecular weight. *Arterioscler. Thromb. Vasc. Biol.* **2003,** *23* (11), 2110-5.

40. Reilly, C. F.; Fritze, L. M.; Rosenberg, R. D., Heparin inhibition of smooth muscle cell proliferation: a cellular site of action. *J. Cell. Physiol.* **1986,** *129* (1), 11-9.

41. Fasciano, S.; Patel, R. C.; Handy, I.; Patel, C. V., Regulation of vascular smooth muscle proliferation by heparin: inhibition of cyclin-dependent kinase 2 activity by p27(kip1). *J. Biol. Chem.* **2005,** *280* (16), 15682-9.

42. Nairn, A. V.; Kinoshita-Toyoda, A.; Toyoda, H.; Xie, J.; Harris, K.; Dalton, S.; Kulik, M.; Pierce, J. M.; Toida, T.; Moremen, K. W.; Linhardt, R. J., Glycomics of proteoglycan biosynthesis in murine embryonic stem cell differentiation. *J. Proteome. Res.* **2007,** *6* (11), 4374-87.

43. Kresse, H.; Schonherr, E., Proteoglycans of the extracellular matrix and growth control. *J. Cell. Physiol.* **2001,** *189* (3), 266-74.

44. Parish, C. R., The role of heparan sulphate in inflammation. *Nat. Rev. Immunol.* **2006,** *6* (9), 633-43.

45. Mousa, S. A., Heparin, low molecular weight heparin, and derivatives in thrombosis, angiogenesis, and inflammation: emerging links. *Semin. Thromb. Hemost.* **2007,** *33* (5), 524-33.

46. Li, J. P.; Vlodavsky, I., Heparin, heparan sulfate and heparanase in inflammatory reactions. *Thromb. Haemost.* **2009,** *102* (5), 823-8.

47. Tyrrell, D. J.; Kilfeather, S.; Page, C. P., Therapeutic Uses of Heparin Beyond Its Traditional Role as an Anticoagulant. *Trends Pharmacol. Sci.* **1995,** *16* (6), 198-204.

48. Folkman, J.; Taylor, S.; Spillberg, C., The role of heparin in angiogenesis. *Ciba Foundation symposium* **1983,** *100*, 132-49.

49. Shukla, D.; Liu, J.; Blaiklock, P.; Shworak, N. W.; Bai, X.; Esko, J. D.; Cohen, G. H.; Eisenberg, R. J.; Rosenberg, R. D.; Spear, P. G., A novel role for 3-O-sulfated heparan sulfate in herpes simplex virus 1 entry. *Cell* **1999,** *99* (1), 13-22.

50. Tiwari, V.; Clement, C.; Xu, D.; Valyi-Nagy, T.; Yue, B. Y.; Liu, J.; Shukla, D., Role for 3-O-sulfated heparan sulfate as the receptor for herpes simplex virus type 1 entry into primary human corneal fibroblasts. *J. Virol.* **2006,** *80* (18), 8970-80.

51. Bartlett, A. H.; Park, P. W., Proteoglycans in host-pathogen interactions: molecular mechanisms and therapeutic implications. *Expert. Rev. Mol. Med.* **2010,** *12*, e5.

52. Garcia, B.; Merayo-Lloves, J.; Martin, C.; Alcalde, I.; Quiros, L. M.; Vazquez, F., Surface Proteoglycans as Mediators in Bacterial Pathogens Infections. *Front. Microbiol.* **2016,** *7*, 220.

53. Raman, R.; Sasisekharan, V.; Sasisekharan, R., Structural insights into biological roles of protein-glycosaminoglycan interactions. *Chem. Biol.* **2005,** *12* (3), 267-77.

54. Sasisekharan, R.; Shriver, Z.; Venkataraman, G.; Narayanasami, U., Roles of heparan-sulphate glycosaminoglycans in cancer. *Nat. Rev. Cancer* **2002,** *2* (7), 521-8.

55. Vlodavsky, I.; Beckhove, P.; Lerner, I.; Pisano, C.; Meirovitz, A.; Ilan, N.; Elkin, M., Significance of heparanase in cancer and inflammation. *Cancer Microenviron.* **2012,** *5* (2), 115-32.

56. Casu, B.; Lindahl, U., Structure and biological interactions of heparin and heparan sulfate. *Adv. Carbohydr. Chem. Biochem.* **2001,** *57*, 159-206.

57. Atha, D. H.; Lormeau, J. C.; Petitou, M.; Rosenberg, R. D.; Choay, J., Contribution of monosaccharide residues in heparin binding to antithrombin III. *Biochemistry* **1985,** *24* (23), 6723-9.

58. Langeslay, D. J.; Young, R. P.; Beni, S.; Beecher, C. N.; Mueller, L. J.; Larive, C. K., Sulfamate proton solvent exchange in heparin oligosaccharides: evidence for a persistent hydrogen bond in the antithrombin-binding pentasaccharide Arixtra. *Glycobiology* **2012,** *22* (9), 1173-82.

59. Johnson, D. J.; Li, W.; Adams, T. E.; Huntington, J. A., Antithrombin-S195A factor Xa-heparin structure reveals the allosteric mechanism of antithrombin activation. *EMBO J* **2006,** *25* (9), 2029-37.

60. Hricovini, M.; Guerrini, M.; Bisio, A.; Torri, G.; Petitou, M.; Casu, B., Conformation of heparin pentasaccharide bound to antithrombin III. *Biochem. J.* **2001,** *359* (Pt 2), 265-72.

61. Beecher, C. N.; Young, R. P.; Langeslay, D. J.; Mueller, L. J.; Larive, C. K., Hydroxyl-proton hydrogen bonding in the heparin oligosaccharide Arixtra in aqueous solution. *J. Phys. Chem. B* **2014,** *118* (2), 482-91.

62. Eisenstein, L. E.; Calio, A. J.; Cunha, B. A., Herpes simplex (HSV-1) aseptic meningitis. *Heart Lung* **2004,** *33* (3), 196-7.

63. Whitley, R. J.; Roizman, B., Herpes simplex virus infections. *Lancet (London, England)* **2001,** *357* (9267), 1513-8.

64. Akhtar, J.; Shukla, D., Viral entry mechanisms: cellular and viral mediators of herpes simplex virus entry. *FEBS J.* **2009,** *276* (24), 7228-36.

65. Spear, P. G., Entry of Alphaherpesviruses into Cells. *Seminars in Virology* **1993,** *4* (3), 167-180.

66. Spear, P. G., Herpes simplex virus: receptors and ligands for cell entry. *Cell. Microbiol.* **2004,** *6* (5), 401-10.

67. Liu, J.; Shriver, Z.; Blaiklock, P.; Yoshida, K.; Sasisekharan, R.; Rosenberg, R. D., Heparan Sulfate d-Glucosaminyl 3-O-Sulfotransferase-3A SulfatesN-Unsubstituted Glucosamine Residues. *J. Biol. Chem.* **1999,** *274* (53), 38155-38162.

68. Vanpouille, C.; Deligny, A.; Delehedde, M.; Denys, A.; Melchior, A.; Lienard, X.; Lyon, M.; Mazurier, J.; Fernig, D. G.; Allain, F., The heparin/heparan sulfate sequence that interacts with cyclophilin B contains a 3-O-sulfated N-unsubstituted glucosamine residue. *J. Biol. Chem.* **2007,** *282* (33), 24416-29.

69. Pempe, E. H.; Xu, Y.; Gopalakrishnan, S.; Liu, J.; Harris, E. N., Probing structural selectivity of synthetic heparin binding to Stabilin protein receptors. *J. Biol. Chem.* **2012,** *287* (25), 20774-83.

70. Borjigin, J.; Deng, J.; Sun, X.; De Jesus, M.; Liu, T.; Wang, M. M., Diurnal pineal 3-O-sulphotransferase 2 expression controlled by beta-adrenergic repression. *J. Biol. Chem.* **2003,** *278* (18), 16315-9.

71. Samson, S. C.; Ferrer, T.; Jou, C. J.; Sachse, F. B.; Shankaran, S. S.; Shaw, R. M.; Chi, N. C.; Tristani-Firouzi, M.; Yost, H. J., 3-OST-7 regulates BMP-dependent cardiac contraction. *PLoS Biol.* **2013,** *11* (12), e1001727.

72. McKeehan, W. L.; Wu, X.; Kan, M., Requirement for anticoagulant heparan sulfate in the fibroblast growth factor receptor complex. *J. Biol. Chem.* **1999,** *274* (31), 21511-4.

73. Marcum, J. A.; Rosenberg, R. D., Heparinlike molecules with anticoagulant activity are synthesized by cultured endothelial cells. *Biochem. Biophys. Res. Commun.* **1985,** *126* (1), 365-72.

74. Pejler, G.; Backstrom, G.; Lindahl, U.; Paulsson, M.; Dziadek, M.; Fujiwara, S.; Timpl, R., Structure and affinity for antithrombin of heparan sulfate chains derived from basement membrane proteoglycans. *J. Biol. Chem.* **1987,** *262* (11), 5036-43.

75. de Agostini, A. I.; Dong, J. C.; de Vantery Arrighi, C.; Ramus, M. A.; Dentand-Quadri, I.; Thalmann, S.; Ventura, P.; Ibecheole, V.; Monge, F.; Fischer, A. M.; HajMohammadi, S.; Shworak, N. W.; Zhang, L.; Zhang, Z.; Linhardt, R. J., Human follicular fluid heparan sulfate contains abundant 3-O-sulfated chains with anticoagulant activity. *J. Biol. Chem.* **2008,** *283* (42), 28115-24.

76. Hamai, A.; Hashimoto, N.; Mochizuki, H.; Kato, F.; Makiguchi, Y.; Horie, K.; Suzuki, S., Two distinct chondroitin sulfate ABC lyases. An endoeliminase yielding tetrasaccharides and an exoeliminase preferentially acting on oligosaccharides. *J. Biol. Chem.* **1997,** *272* (14), 9123-30.

77. Rota, C.; Liverani, L.; Spelta, F.; Mascellani, G.; Tomasi, A.; Iannone, A.; Vismara, E., Free radical generation during chemical depolymerization of heparin. *Anal. Biochem.* **2005,** *344* (2), 193-203.

78. Conrad, H. E., Nitrous acid degradation of glycosaminoglycans. *Curr. Protoc. Mol. Biol.* **2001,** *Chapter 17* (1), Unit17 22A.

79. Camara, J. E.; Satterfield, M. B.; Nelson, B. C., Quantitative determination of disaccharide content in digested unfragmented heparin and low molecular weight heparin by direct-infusion electrospray mass spectrometry. *J. Pharm. Biomed. Anal.* **2007,** *43* (5), 1706-14.

80. Saad, O. M.; Leary, J. A., Compositional analysis and quantification of heparin and heparan sulfate by electrospray ionization ion trap mass spectrometry. *Anal. Chem.* **2003,** *75* (13), 2985-95.

81. Saad, O. M.; Ebel, H.; Uchimura, K.; Rosen, S. D.; Bertozzi, C. R.; Leary, J. A., Compositional profiling of heparin/heparan sulfate using mass spectrometry: assay for specificity of a novel extracellular human endosulfatase. *Glycobiology* **2005,** *15* (8), 818-26.

82. Muresan, A.; Galusca, M.; Seidler, D. G.; Dinca, N.; Zamfir, A. D. In *Structural Analysis of Chondroitin Sulfate Disaccharides by Electrospray Ionization High Capacity Ion Trap Mass Spectrometry*, Dordrecht, Springer Netherlands: Dordrecht, **2008**; pp 85-95.

83. Kailemia, M. J.; Li, L.; Xu, Y.; Liu, J.; Linhardt, R. J.; Amster, I. J., Structurally informative tandem mass spectrometry of highly sulfated natural and chemoenzymatically synthesized heparin and heparan sulfate glycosaminoglycans. *Mol. Cell. Proteomics.* **2013,** *12* (4), 979-90.

84. Lianli, C.; Jonathan, A.; Robert, J. L., Mass Spectrometry for the Analysis of Highly Charged Sulfated Carbohydrates. *Curr. Anal. Chem.* **2005,** *1* (3), 223-240.

85. Zaia, J.; Costello, C. E., Tandem mass spectrometry of sulfated heparin-like glycosaminoglycan oligosaccharides. *Anal. Chem.* **2003,** *75* (10), 2445-55.

86. Jones, C. J.; Beni, S.; Larive, C. K., Understanding the effect of the counterion on the reverse-phase ion-pair high-performance liquid chromatography (RPIP-HPLC) resolution of heparin-related saccharide anomers. *Anal. Chem.* **2011,** *83* (17), 6762-9.

87. Korir, A. K.; Limtiaco, J. F.; Gutierrez, S. M.; Larive, C. K., Ultraperformance ion-pair liquid chromatography coupled to electrospray time-of-flight mass spectrometry for compositional profiling and quantification of heparin and heparan sulfate. *Anal. Chem.* **2008,** *80* (4), 1297-306.

88. Karamanos, N. K.; Vanky, P.; Tzanakakis, G. N.; Tsegenidis, T.; Hjerpe, A., Ion-pair high-performance liquid chromatography for determining disaccharide composition in heparin and heparan sulphate. *J. Chromatogr. A* **1997,** *765* (2), 169-79.

89. Thanawiroon, C.; Linhardt, R. J., Separation of a complex mixture of heparin-derived oligosaccharides using reversed-phase high-performance liquid chromatography. *J. Chromatogr. A* **2003,** *1014* (1-2), 215-23.

90. Thanawiroon, C.; Rice, K. G.; Toida, T.; Linhardt, R. J., Liquid chromatography/mass spectrometry sequencing approach for highly sulfated heparin-derived oligosaccharides. *J. Biol. Chem.* **2004,** *279* (4), 2608-15.

91. Kailemia, M. J.; Li, L.; Ly, M.; Linhardt, R. J.; Amster, I. J., Complete mass spectral characterization of a synthetic ultralow-molecular-weight heparin using collision-induced dissociation. *Anal. Chem.* **2012,** *84* (13), 5475-8.

92. Meissen, J. K.; Sweeney, M. D.; Girardi, M.; Lawrence, R.; Esko, J. D.; Leary, J. A., Differentiation of 3-O-sulfated heparin disaccharide isomers: identification of structural aspects of the heparin CCL2 binding motif. *J. Am. Soc. Mass Spectrom.* **2009,** *20* (4), 652-7.

93. Minamisawa, T.; Suzuki, K.; Hirabayashi, J., Systematic identification of N-acetylheparosan oligosaccharides by tandem mass spectrometric fragmentation. *Rapid Commun. Mass Spectrom. : RCM* **2006,** *20* (2), 267-74.

94. Wolff, J. J.; Chi, L.; Linhardt, R. J.; Amster, I. J., Distinguishing glucuronic from iduronic acid in glycosaminoglycan tetrasaccharides by using electron detachment dissociation. *Anal. Chem.* **2007,** *79* (5), 2015-22.

95. Blundell, C. D.; DeAngelis, P. L.; Day, A. J.; Almond, A., Use of 15N-NMR to resolve molecular details in isotopically-enriched carbohydrates: sequence-specific observations in hyaluronan oligomers up to decasaccharides. *Glycobiology* **2004,** *14* (11), 999-1009.

96. Limtiaco, J. F.; Beni, S.; Jones, C. J.; Langeslay, D. J.; Larive, C. K., The efficient structure elucidation of minor components in heparin digests using microcoil NMR. *Carbohydr. Res.* **2011,** *346* (14), 2244-54.

97. Pomin, V. H.; Sharp, J. S.; Li, X.; Wang, L.; Prestegard, J. H., Characterization of glycosaminoglycans by 15N NMR spectroscopy and in vivo isotopic labeling. *Anal. Chem.* **2010,** *82* (10), 4078-88.

98. Joseph, P. R.; Poluri, K. M.; Sepuru, K. M.; Rajarathnam, K., Characterizing protein-glycosaminoglycan interactions using solution NMR spectroscopy. *Methods Mol. Biol. (Clifton, N.J.)* **2015,** *1229*, 325-33.

99. Battistel, M. D.; Pendrill, R.; Widmalm, G.; Freedberg, D. I., Direct evidence for hydrogen bonding in glycans: a combined NMR and molecular dynamics study. *J. Phys. Chem. B* **2013,** *117* (17), 4860-9.

100. Battistel, M. D.; Shangold, M.; Trinh, L.; Shiloach, J.; Freedberg, D. I., Evidence for helical structure in a tetramer of alpha2-8 sialic acid: unveiling a structural antigen. *J. Am. Chem. Soc.* **2012,** *134* (26), 10717-20.

101. Sattelle, B. M.; Almond, A., Shaping up for structural glycomics: a predictive protocol for oligosaccharide conformational analysis applied to N-linked glycans. *Carbohydr. Res.* **2014,** *383*, 34-42.

102. Almond, A.; Brass, A.; Sheehan, J. K., Oligosaccharides as Model Systems for Understanding Water−Biopolymer Interaction: Hydrated Dynamics of a Hyaluronan Decamer. *J. Phys. Chem. B* **2000,** *104* (23), 5634-5640.

103. Almond, A.; Sheehan, J. K., Predicting the molecular shape of polysaccharides from dynamic interactions with water. *Glycobiology* **2003,** *13* (4), 255-64.

104. Blundell, Charles, D.; Deangelis, Paul, L.; Almond, A., Hyaluronan: the absence of amide–carboxylate hydrogen bonds and the chain conformation in aqueous solution are incompatible with stable secondary and tertiary structure models. *Biochem. J.* **2006,** *396* (3), 487.

105. Kovacs, H.; Moskau, D.; Spraul, M., Cryogenically cooled probes—a leap in NMR technology. *Prog. Nucl. Magn. Reson. Spectrosc.* **2005,** *46* (2), 131-155.

106. Guerrini, M.; Guglieri, S.; Naggi, A.; Sasisekharan, R.; Torri, G., Low molecular weight heparins: structural differentiation by bidimensional nuclear magnetic resonance spectroscopy. *Semin. Thromb. Hemost.* **2007,** *33* (5), 478-87.

107. Guerrini, M.; Naggi, A.; Guglieri, S.; Santarsiero, R.; Torri, G., Complex glycosaminoglycans: profiling substitution patterns by two-dimensional nuclear magnetic resonance spectroscopy. *Anal. Biochem.* **2005,** *337* (1), 35-47.

108. Welti, D.; Rees, D. A.; Welsh, E. J., Solution conformation of glycosaminoglycans: assignment of the 300-MHz 1H-magnetic resonance spectra of chondroitin 4-sulphate, chondroitin 6-sulphate and hyaluronate, and investigation of an alkali-induced conformation change. *Eur. J. Biochem.* **1979,** *94* (2), 505-14.

109. Blossom, D. B.; Kallen, A. J.; Patel, P. R.; Elward, A.; Robinson, L.; Gao, G.; Langer, R.; Perkins, K. M.; Jaeger, J. L.; Kurkjian, K. M.; Jones, M.; Schillie, S. F.; Shehab, N.; Ketterer, D.; Venkataraman, G.; Kishimoto, T. K.; Shriver, Z.; McMahon, A. W.; Austen, K. F.; Kozlowski, S.; Srinivasan, A.; Turabelidze, G.; Gould, C. V.; Arduino, M. J.; Sasisekharan, R., Outbreak of adverse reactions associated with contaminated heparin. *N. Engl. J. Med.* **2008,** *359* (25), 2674-84.

110. Torri, G.; Guerrini, M., Quantitative 2d Nmr Analysis of Glycosaminoglycans. *Nmr Spectroscopy in Pharmaceutical Analysis* **2008**, 407-428.

111. Chuang, W.-L.; Christ, M. D.; Rabenstein, D. L., Determination of the Primary Structures of Heparin- and Heparan Sulfate-Derived Oligosaccharides Using Band-Selective Homonuclear-Decoupled Two-Dimensional 1H NMR Experiments. *Anal. Chem.* **2001,** *73* (10), 2310-2316.

112. Yamada, S.; Yoshida, K.; Sugiura, M.; Sugahara, K., One- and Two-Dimensional 1H-NMR Characterization of Two Series of Sulfated Disaccharides Prepared from Chondroitin Sulfate and Heparan Sulfate/Heparin by Bacterial Eliminase Digestion. *J. Biol. Chem.* **1992,** *112* (4), 440-447.

113. Mascellani, G.; Guerrini, M.; Torri, G.; Liverani, L.; Spelta, F.; Bianchini, P., Characterization of di- and monosulfated, unsaturated heparin disaccharides with terminal N-sulfated 1,6-anhydro-beta-D-glucosamine or N-sulfated 1,6-anhydro-beta-D-mannosamine residues. *Carbohydr. Res.* **2007,** *342* (6), 835-42.

114. Claridge, T. D. W., Chapter 6 - Correlations Through the Chemical Bond I: Homonuclear Shift Correlation. In *High-Resolution NMR Techniques in Organic Chemistry (Third Edition)*, Claridge, T. D. W., Ed. Elsevier: Boston, **2016**; pp 203-241.

115. Claridge, T. D. W., Chapter 9 - Correlations Through Space: The Nuclear Overhauser Effect. In *High-Resolution NMR Techniques in Organic Chemistry (Third Edition)*, Claridge, T. D. W., Ed. Elsevier: Boston, **2016**; pp 315-380.

116. Claridge, T. D. W., Chapter 13 - Structure Elucidation and Spectrum Assignment. In *High-Resolution NMR Techniques in Organic Chemistry (Third Edition)*, Claridge, T. D. W., Ed. Elsevier: Boston, **2016**; pp 499-525.

117. Perrin, C. L.; Nielson, J. B., "Strong" hydrogen bonds in chemistry and biology. *Annu. Rev. Phys. Chem.* **1997,** *48*, 511-44.

118. Strop, P.; Mayo, S. L., Contribution of surface salt bridges to protein stability. *Biochem. J.* **2000,** *39* (6), 1251-5.

119. Bosshard, H. R.; Marti, D. N.; Jelesarov, I., Protein stabilization by salt bridges: concepts, experimental approaches and clarification of some misunderstandings. *J. Mol. Recognit.* **2004,** *17* (1), 1-16.

120. Nishiyama, Y.; Langan, P.; Chanzy, H., Crystal structure and hydrogen-bonding system in cellulose Ibeta from synchrotron X-ray and neutron fiber diffraction. *J. Am. Chem. Soc.* **2002,** *124* (31), 9074-82.

121. Gardner, K. H.; Blackwell, J., The hydrogen bonding in native cellulose. *Biochim. Biophys. Acta* **1974,** *343* (1), 232-7.

122. Blundell, C. D.; Deangelis, P. L.; Almond, A., Hyaluronan: the absence of amide-carboxylate hydrogen bonds and the chain conformation in aqueous solution are incompatible with stable secondary and tertiary structure models. *Biochem. J.* **2006,** *396* (3), 487-98.

123. Bain, A. D., Chemical exchange in NMR. *Prog. Nucl. Magn. Reson. Spectrosc.* **2003,** *43* (3-4), 63-103.

124. Beecher, C. N.; Larive, C. K., (1)H and (15)N NMR Characterization of the Amine Groups of Heparan Sulfate Related Glucosamine Monosaccharides in Aqueous Solution. *Anal. Chem.* **2015,** *87* (13), 6842-8.

125. Englander, S. W.; Kallenbach, N. R., Hydrogen exchange and structural dynamics of proteins and nucleic acids. *Q. Rev. Biophys.* **1983,** *16* (4), 521-655.

126. Blundell, C. D.; Reed, M. A.; Almond, A., Complete assignment of hyaluronan oligosaccharides up to hexasaccharides. *Carbohydr. Res.* **2006,** *341* (17), 2803-15.

127. Langeslay, D. J.; Beni, S.; Larive, C. K., Detection of the 1H and 15N NMR resonances of sulfamate groups in aqueous solution: a new tool for heparin and heparan sulfate characterization. *Anal. Chem.* **2011,** *83* (20), 8006-10.

128. Adams, B.; Lerner, L., Observation of Hydroxyl Protons of Sucrose in Aqueous-Solution - No Evidence for Persistent Intramolecular Hydrogen-Bonds. *J. Am. Chem. Soc.* **1992,** *114* (12), 4827-4829.

129. Baxter, N. J.; Williamson, M. P., Temperature dependence of H-1 chemical shifts in proteins. *J. Biomol. NMR* **1997,** *9* (4), 359-369.

130. Cierpicki, T.; Otlewski, J., Amide proton temperature coefficients as hydrogen bond indicators in proteins. *J. Biomol. NMR* **2001,** *21* (3), 249-261.

131. Kindahl, L.; Sandstrom, C.; Norberg, T.; Kenne, L., H-1 NMR studies of hydroxy protons of Asn- and Ser-linked disaccharides in aqueous solution. *J. Carbohydr. Chem.* **2000,** *19* (9), 1291-1303.

132. Kindahl, L.; Sandstrom, C.; Norberg, T.; Kenne, L., H-1 NMR studies of hydroxy protons of the V[beta-Gal(1 -> 3)-alpha-GalNAc(1 -> O)THPGY glycopeptide. *Carbohydr. Res.* **2001,** *336* (4), 319-323.

133. Olsen, R. A.; Liu, L.; Ghaderi, N.; Johns, A.; Hatcher, M. E.; Mueller, L. J., The amide rotational barriers in picolinamide and nicotinamide: NMR and ab initio studies. *J. Am. Chem. Soc.* **2003,** *125* (33), 10125-32.

134. Frey, P. A., Review: Strong hydrogen bonding in molecules and enzymatic complexes. *Magn. Reson. Chem.* **2001,** *39* (S1), S190-S198.

135. Pimentel, G. C.; Mcclella.Al, Hydrogen Bonding. *Annu. Rev. Phy.s Chem.* **1971,** *22* (1), 347-&.

CHAPTER TWO

Chemical Modifications of GAGs

Acknowledgements: I would like to thank undergraduate student researcher Blake Lockard for his contributions to this research.

Abstract: *In vivo*, the enzymatic modification of heparan sulfate and heparin can introduce rare structural elements, for example 3-*O*-sulfated glucosamine residues. Understanding the way that these unique elements impact GAG structure and biological function are among the great challenges facing the fields of biology and chemistry. For example, the low abundance of these elements in GAG polysaccharides can make it challenging for researchers to obtain pure material from natural sources in the quantities necessary for structural and biological studies. The development of approaches to synthesize or modify GAG oligosaccharides can open up new avenues for the investigation of novel compounds. This chapter discusses methods for the chemical modification of GAG oligosaccharides. The investigations of the physico-chemical properties of the modified oligosaccharides through the properties of labile protons in amino and amide groups are presented in Chapter 3 and 4, respectively. The solvolytic selective de-*N*-sulfation, chemoselective *N*-acetylation, and reduction of oligosaccharides with sodium borohydride were successfully applied. Proposed reaction mechanisms with optimized conditions for unique chemical modifications are presented. The assessment of chemically modified oligosaccharide

structures was accomplished using ESI-MS and ^{1}H NMR, and a detailed example of the structure elucidation process is provided.

2.1. Introduction

The enzymatic or chemical depolymerization of GAGs in conjunction with isolation strategies is an important approach for obtaining oligosaccharides from natural sources. For example, heparin is well known for its role as an anticoagulant in the antithrombotic physiological process, where it binds to the protease inhibitor antithrombin-III.[1-3] Naturally occurring unfractionated heparin (UFH) and its derivative low molecular weight (LMWH) heparin are two widely prescribed pharmaceuticals to treat thrombosis-related medical conditions.[4-7] Although these important drugs provide benefits for human health, both UHF and LMWH heparins can also cause adverse side effects.[8] One of the life-threatening conditions associated with the administration of heparin is heparin-induced thrombocytopenia (HIT), caused by binding large polysaccharide chains to platelet factor 4 (PF4).[9-11] The undesired binding affinity of heparin to PF4 can be minimized by reduction of polysaccharide size.[12] Consequently, LMWH obtained by enzymatic or chemical depolymerization of UFH has significantly reduced affinity to PF4.[12] Unfortunately, the complete elimination of the problems associated with heparins binding to PF4 was not achieved using heparins from natural sources. Furthermore, additional problems with natural heparins arose from difficulties in controlling their purity and structural uniformity due to their size, polydispersity, and heterogeneity. In 2008, these problems were

exasperated by the heparin contamination crisis, caused by the adulteration of UFH with over-sulfated chondroitin sulfate.[13-15]

Advances in synthesis of carbohydrates have offered an alternative way to generate a synthetic version of heparin.[16, 17] In response to problems associated with natural heparins, a fully synthetic version of a biologically active heparin oligosaccharide was prepared and marketed as the pharmaceutical drug Arixtra™. The structure of Arixtra™ mimics heparin's pentasaccharide sequence required for high affinity antithrombin-III binding.[18-20] Lacking long heterogeneous and polydispersed polysaccharide chains, the Arixtra™ pentasaccharide exclusively and selectively binds to antithrombin-III and deactivates factor Xa. The inhibited factor Xa interrupts the blood coagulation cascade and thus inhibits thrombin formation and thrombus development.[19] Importantly, synthetic Arixtra™ completely eliminates problems associated with PF4 binding and HIT development.[21, 22] Furthermore, the synthetic nature and small size of Arixtra™ provides a great advantage in drug quality control. Its structure can be readily elucidated by MS and NMR, which is not the case with UFH and LMWH. As the Arixtra™ example demonstrates, difficulties associated with GAGs from natural sources can be resolved through the development of synthetic analogs of oligosaccharides with desired structural features. Furthermore, the design, synthesis, and chemical modifications of GAGs can be tailored for applications where selective binding is necessary.[23-26]

Specific GAG-protein interactions are heavily reliant on the protein amino acid sequence and conformation as well as the microstructure of the GAG binding region. Therefore, investigation of the physico-chemical properties of GAGs is essential to

advancing our understanding of the structure-function relationship. Beyond the naturally occurring GAG motifs, chemical modifications of GAGs can impart changes in their physico-chemical and biological properties. In this Chapter, methods for the chemical modification of GAG oligosaccharides are discussed for the purpose of providing experimental access to structural elements that are rare in GAGs or are not found in nature. The physico-chemical properties of these modified oligosaccharides were investigated in aqueous solutions using NMR, with results discussed in detail in Chapters 3 and 4. Furthermore, because the modification of oligosaccharides involves chemical reactions, structure elucidation is essential to ascertain whether the modified structure is what was intended. An example highlighting the structure elucidation process for a modified GAG oligosaccharide is presented in this Chapter.

2.2. Experimental Section

2.2.1. Materials and Reagents. Arixtra™ (Fondaparinux sodium), formulated as prefilled syringes for clinical use, was obtained from the University Pharmacy and Department of Pharmacy Administration of Semmelweis University (Budapest, Hungary). Heparin tetrasaccharide (ΔUA2S-GlcNS6S-IdoA2S-GlcNS6S) ammonium salt (Catalog No. HO04) was purchased from Iduron Ltd. (Manchester, UK). Size-uniform fractions of chondroitin sulfate tetra- and hexasaccharides were isolated from a mixture of enzymatically depolymerized chondroitin sulfate A (see details in Sections 4.2.2. - 4.2.5). 3-*O*-sulfated glucosamine (GlcN3S), cation exchange resin Dowex 50WX8 hydrogen form (50-100 mesh), 3-(trimethylsilyl)-1-propanesulfonic acid-d_6 sodium salt (DSS-d_6, 98% D),

35 wt% deuterated hydrochloric acid (DCl, 99% D), and 99.5% acetic anhydride were purchased from Sigma-Aldrich (St. Louis, MO). Methanol HPLC grade, pyridine, 12.1 *N* hydrochloric acid, 50% w/w sodium hydroxide solution, glacial acetic acid, and sodium borohydride were purchased from Thermo Fisher Scientific (Bellefonte, PA). Deuterated acetone (acetone-d_6, 99.9% D), deuterium oxide (D_2O, 99.9% D), 40% w/w sodium deuteroxide (NaOD, 99.5% D), deuterated dimethyl sulfoxide (DMSO-d_6, 99.9% D), and the low temperature methanol standard were purchased from Cambridge Isotope Laboratories (Andover, MA). Ultrapure deionized water (18 MΩ/cm) was prepared using a Simplicity UV water purification system from Millipore (Billerica, MA). The pH meter calibration buffers 2.00, 4.00, 7.00, and 10.00 were purchased from Fisher Scientific (Nazareth, PA). All pH measurements were performed at room temperature using an AB 15 Accumet Basic pH meter and a 9110DJWP double-junction Ag/AgCl micro pH electrode, both from Thermo Scientific (Chelmsford, MA). NMR tubes (NE-H5/3-Br) were purchased from New Era Enterprises (New Era Enterprises Vineland, NJ). Eppendorf 1.5 mL safe-lock tubes were purchased from Eppendorf (Thermo Fisher Scientific). Size-exclusion chromatography resin Sephadex G-10 was purchased from GE Healthcare - Bio Sciences (Pittsburgh, PA).

2.2.2. Chemical modification of GAGs by solvolytic de-*N*-sulfation. The de-*N*-sulfated oligosaccharides were prepared by a selective solvolytic de-*N*-sulfation reaction.[27, 28] All operations were performed in a cold room at 4 °C with materials pre-equilibrated to this temperature. A cation exchange column was prepared by packing Dowex 50 WX8 cation exchange resin into a 1 cc plastic cartridge. The resin was converted to the hydrogen

form with 3 mL of 1M hydrochloric acid followed by conditioning with 3 mL of methanol and 5 mL of deionized water. About 6.0 mg of Arixtra™ sodium salt was dissolved in 200 µL of deionized water and introduced onto the cartridge. The protonated form of Arixtra™ was eluted by washing three times with 1 mL aliquots of deionized water. The effluent was then neutralized with pyridine and freeze dried. The resultant light-brown Arixtra™ pyridinium salt was reconstituted in 400 µL of DMSO-d_6 containing 5% deionized water and incubated at 50°C and 350 rpm for 90 min in Eppendorf ThermoMixer *C* (Thermo Fisher Scientific, Asheville, NC). The reaction was quenched by addition of 400 µL of deionized water followed by pH adjustment to 9.3 with 0.1 M sodium hydroxide. Volatile organic components of the mixture were removed by speed vacuum using Speedvac Savant SC 110 equipped with a refrigerator vapor trap RVT400 (Thermo Fisher Scientific, Asheville, NC) at medium heat for 3 h. The residual solution was diluted with 300 µL of deionized water and speed vacuumed for an additional 3 h and the remaining solution was lyophilized. The sample was purified by dissolving the solid in 400 µL of deionized water and passing it through a 1.6 x 70 cm desalting column packed with Sephadex G-10 superfine resin using deionized degassed water as a mobile phase at a flow rate of 0.15 mL/min. As a result, about 2.7 mg of dNSA sodium salt was recovered as a white powder, a 45% yield. This procedure was repeated to produce a second batch of dNSA with 2.6 mg recovered from the reaction of 5.8 mg of Arixtra™. Similarly, this reaction was used to de-*N*-sulfated 5.0 mg of heparin tetrasaccharide (ΔUA2S-GlcNS6S-IdoA2S-GlcNS6S) yielding 3.8 mg of de-*N*-sulfated heparin tetrasaccharide (dNSt, ΔUA2S-GlcN6S-IdoA2S-GlcN6S), a 76% yield.

2.2.3. Chemical modification of GAGs by chemoselective *N*-acetylation. The *N*-acetylated Arixtra™ was prepared from the previously de-*N*-sulfated Arixtra™ sodium salt. The reaction procedure was developed and optimized starting with approaches elaborated by Danishefsky et al.[29], Naik et al.[30], Roseman et al.[31] and Trombotto et al.[32] About 2.0 mg of dNSA was dissolved in 0.2 mL of 10% acetic acid, the pH of the solution was adjusted to 4.6 with 1M NaOH solution. Aliquots of 1.0 mL of MeOH and 14 µL of 99.5% acetic anhydride were added into the solution. The resultant solution mixture was agitated, followed by overnight incubation at room temperature. The next morning, the mixture was placed into a speed vacuum at medium heat for 3 h to remove volatile components of the mixture. The residual solution after speed vacuum was diluted with 0.1 mL of deionized water and lyophilized. The product was dissolved in 400 µL of deionized water and purified by passing the solution through a 1.6 x 70 cm desalting column packed with Sephadex G-10 superfine resin using deionized degassed water as a mobile phase at a flow rate of 0.15 mL/min. Finally, the collected fractions containing *N*-acetylated Arixtra™ were combined and lyophilized. About 1.8 mg of white dry powder was recovered, a 90% yield. Using the same method was also prepared *N*-acetylated 3-*O*-sulfated glucosamine (GlcNAc3S) from 1.75 mg of 3-*O*-sulfated glucosamine (GlcN3S).

2.2.4. Chemical modification of GAGs by reduction with sodium borohydride. Chondroitin sulfate A tetra- and hexasaccharides were reduced with sodium borohydride. Approximately 77.0 mg of tetrasaccharide (ΔUA-GalNAc4S-GlcA-GalNAc4S) isolated from the enzymatic depolymerization reaction (Sections 1.2.1.1. and 4.2.2.) was dissolved in 1.5 mL of solution containing 1M sodium borohydride in 100 mM sodium hydroxide.

The resultant mixture was incubated overnight in Eppendorf ThermoMixer *C* at 50 °C. The reaction was quenched through the careful and slow addition of 40 µL of glacial acetic acid to avoid excessive effervescence from decomposing borohydride. The excess of borohydride and any reaction by-products were removed by cation exchange chromatography. The column was prepared by packing Dowex 50WX8 cation exchange resin into a 1 cc plastic cartridge and converting it to the hydrogen form with 3 mL of 1M hydrochloric acid followed by conditioning with 3 mL of methanol and 5 mL of deionized water. The sample was introduced onto the cartridge and the tetrasaccharide was eluted by washing three times with 1 mL aliquots of deionized water. The effluent was then neutralized with 1M NaOH solution and lyophilized. The final purification step was performed by dissolving the lyophilized solid in 400 µL of deionized water and passing it through a 1.6 x 70 cm desalting column packed with Sephadex G-10 superfine resin using deionized degassed water as a mobile phase at a flow rate of 0.15 mL/min. The collected fractions containing reduced tetrasaccharide were combined and lyophilized, yielding 64.5 mg of lyophilized product. Similarly, 74.4 mg of an isolated chondroitin sulfate A hexasaccharide (ΔUA-GalNAc4S-GlcA-GalNAc4S-GlcA-GalNAc4S) was reduced by this procedure to yield 68.5 mg of lyophilized product. Additionally, the hyaluronic acid hexasaccharide (ΔUA-GlcNAc-GlcA-GlcNAc-GlcA-GlcNAc) was converted to the alditol by similar reduction reaction with sodium borohydride. 2.0 mg sample of the hyaluronic acid hexasaccharide was dissolved in 0.1 mL of solution containing 1M sodium borohydride in 100 mM sodium hydroxide. However, due to the problems with reduction of non-sulfated hyaluronic acid hexasaccharides leading to oligosaccharide degradation,

all steps of hyaluronic acid hexasaccharide reduction were performed in presence of 10 mM phosphate buffer. After desalting, fractions containing hyaluronic acid hexasaccharides were combined and buffered with 10 mM phosphate followed by lyophilization to yielded 1.7 mg of product. Freeze dried samples then were stored at -80 °C for future use.

2.2.5. Solution preparation and ESI-MS measurements. About 2.7 mg of desalted de-*N*-sulfated Arixtra^{TM} (dNSA) was dissolved in 500 µL of deionized water. An aliquot of 30 µL was transferred into a 1.5 mL Eppendorf safe-lock tube and diluted with 200 µL of solution composed of 30% methanol and 70% water, the remainder of the solution was lyophilized for subsequent NMR experiments. The sample solution was infused into a Micromass/Waters ESI quadrupole time-of-flight (Q-Tof micro) mass spectrometer (Waters Corporation, Millford, MA) at a flow rate of 10 µL/min. Data acquisition was performed using Masslynx 4.1 software and the mass spectrum was obtained in negative mode using the following instrumental parameters: capillary voltage, 3 kV; cone voltage, 25 V; extractor voltage, 1 V; source temperature, 120 °C; desolvation temperature, 275 °C; interscan delay, 0.1 s and m/z range, 150 - 1000.

2.2.6. Solution preparation and NMR measurements.

2.2.6.1. Carbon-bound proton resonance assignments. About 2.6 mg of dNSA was dissolved in 1.5 mL of 10 mM phosphate buffer containing 6 µL of 100 mM DSS-d_6 as a chemical shift reference (0.00 ppm) and freeze dried. To reduce the residual HOD peak, the sample was twice re-dissolved in 300 µL of 99.9% D_2O and freeze dried. The resultant solid was dissolved in 1.5 mL of 99.9% D_2O for NMR measurements. Aliquots of 300 µL

were transferred to three 1.5 mL Eppendorf tubes. The pD was of the solutions were adjusted to 1.77, 6.67, and 11.27 with 10 mM and 100 mM solutions of NaOD and DCl (prepared from concentrated solutions by dilution with appropriate volume of D_2O). Solution pD values were calculated from pH meter readings measured in deuterated solvents (pH^*) using Eq. 3.2[33, 34] ($pD = pH^* + 0.4$). The pD-adjusted solutions were transferred to NE-H5/3-Br NMR tubes and ^1H, ^1H-^1H COSY, ^1H-^1H TOCSY, and ^1H-^1H ROESY spectra were acquired using a Bruker Avance 600 MHz spectrometer operating at 599.52 MHz and equipped with a BBI probe at 298.2 K. All spectra were acquired using a 90° pulse of 9.10 - 9.27 μs with solvent suppression of the residual HOD resonance provided by presaturation at a power of 59 dB and relaxation delay of 2.0 s. All spectra were referenced to the ^1H resonance of DSS-d_6 (0.00 ppm). One-dimensional ^1H NMR spectra were acquired using a spectral window of 6361 Hz and 112 scans coadded into 42,014 complex points. These spectra were processed in 65,536 points using an exponential multiplication window function and 0.4 Hz line broadening. Phase-sensitive two-dimensional COSY, TOCSY, and ROESY spectra were acquired in States-TPPI with a spectral window of 3597 Hz in both dimensions. COSY spectra were acquired into 2048 complex points using 64 experiments, each with 416 coadded scans. TOCSY spectra were acquired using a mixing time of 120 ms with a 36 μs spinlock pulse at a power of 8.20 dB into 2048 complex points using 56 experiments, each with 416 coadded scans. ROESY spectra were acquired into 2048 complex points using 48 experiments, each with 512 coadded scans. All two-dimensional spectra were zero filled to 4096 × 1024 data points

and apodized using a $\cos^2$ window function. All spectra were analyzed using Bruker TopSpin 3.2 software.

2.2.6.2. Amino proton resonance assignment. The dNSA solution lyophilized after the ESI-MS measurements (Section 2.2.5.) was dissolved in 249 µL of deionized water and 6 µL of 100 mM DSS-d_6 solution added as a chemical shift reference (0.00 ppm). The pH of the solution was adjusted to 3.4 with 0.1 M HCl according to previously identified conditions suitable for amino proton detection.[35] A 45 µL aliquot of acetone-d_6 was added to provide a lock-signal and reduce the freezing point giving a final volume of 300 µL with a solvent composition of 85% H_2O/15% acetone-d_6. The solution was transferred into a NE-H5/3-Br NMR tube and ^{1}H, ^{1}H-^{1}H TOCSY, and ^{1}H-^{1}H COSY spectra were acquired using the Bruker Avance spectrometer operating at 600.01 MHz equipped with a 5 mm TBI probe. All spectra were acquired at 259.1 K using a 90° pulse of 9.65 µs at a power level of -4.00 dB with solvent suppression provided by excitation sculpting. The one-dimensional ^{1}H NMR spectrum was recorded using a spectral window of 7788 Hz and a relaxation delay of 1.5 s with 256 scans coadded into 32,768 complex points. The free induction decay (FID) was zero-filled to 65,536 points and apodized by multiplication with an exponential function equivalent to 0.5 Hz line broadening prior to Fourier transformation. Phase-sensitive COSY and TOCSY spectra were acquired into 2048 complex points over 256 increments using States-TPPI using a 2.0 s relaxation delay and a spectral window of 8389 Hz in both dimensions. The COSY spectrum was recorded by coaddition of 128 scans while 88 scans were coadded for the TOCSY spectrum. The TOCSY spectrum was acquired using a mixing time of 120 ms with a 38 µs spinlock pulse

at a power of 6.77 dB. The COSY and TOCSY spectra were zero-filled to 4096 × 1024 data points and apodized using a $\cos^2$ window function.

2.3. Results and Discussion

In this Chapter, we performed a series of chemical modification of oligosaccharides to provide experimental access to structural elements that are rare in GAGs or are not found in nature. In Chapters 3 and 4 these chemically modified structures will be investigated in aqueous solutions using NMR. Herein we describe chemical modifications of oligosaccharides by solvolytic de-*N*-sulfation, chemoselective *N*-acetylation and reduction of oligosaccharides using the mild reducing agent sodium borohydride. The structures of the resultant chemically modified oligosaccharides are elucidated by MS and NMR, and a detailed example of structure elucidation process is provided for de-*N*-sulfated Arixtra™. Structures of other oligosaccharides were elucidated similarly, and the results are presented in Appendix.

2.3.1. Solvolytic de-*N*-sulfation. The goal of the de-*N*-sulfation reaction is the selective removal of *N*-sulfo groups without incorporation of any other structural modifications, including de-*O*-sulfation or oligosaccharide chain degradation. To perform this task, a reaction initially introduced in 1960 by Inoue et al. for the selective solvolytic *N*-desulfation of intact heparin was adapted.[27] A successful de-*N*-sulfation reaction requires two general considerations. First, the oligosaccharide sodium salt must be completely converted to pyridinium salt. Second, incubation of oligosaccharide pyridinium salt must be in a solution containing the right proportion of water in dimethyl sulfoxide

(DMSO). A solution with too high of water content will result in non-selective loss of sulfo groups from both *N*- and *O*-substituted positions.[36] However, a reaction with water content that is too low will not proceed to completion and the final product will contain partially de-*N*-sulfated oligosaccharides.

To the best of our knowledge, there is no proposed mechanism describing solvolytic de-*N*-sulfation. Figure 2.1 shows a possible reaction mechanism for de-*N*-sulfation by treatment of the Arixtra™ pyridinium salt with DMSO containing 5% of water. The first step of the reaction involves conversion of the Arixtra™ sodium salt to a pyridinium salt, a step that is important for the following reasons. First, pyridinium salts more easily react than inorganic salts and therefore give higher yields of final products.[37] Second, pyridinium ions act as counter ions to sulfate and carboxylate groups. A charge balance is necessary to stabilize negatively charged groups and prevent oligosaccharide from degradation during de-*N*-sulfation reaction.[38] Finally, the solubility of the Arixtra™ pyridinium salt in DMSO is much higher than that of sodium salt.

The first step of the reaction is the conversion of the Arixtra™ sodium salt to the protic form by passing it through an acidified cation exchange column. The resulting solution is neutralized with pyridine and lyophilized to yield the pyridinium salt. Removal of the Arixtra™ *N*-sulfo groups occurs rapidly following dissolution of the pyridinium salt in 95% DMSO/5% H_2O and incubating the reaction mixture at 50 °C.

The de-*N*-sulfation reaction most likely occurs through a S_N2 (bimolecular nucleophilic substitution) mechanism. As depicted in Figure 2.1, a DMSO molecule has two resonance structures. A negatively charged oxygen in one of the two resonance

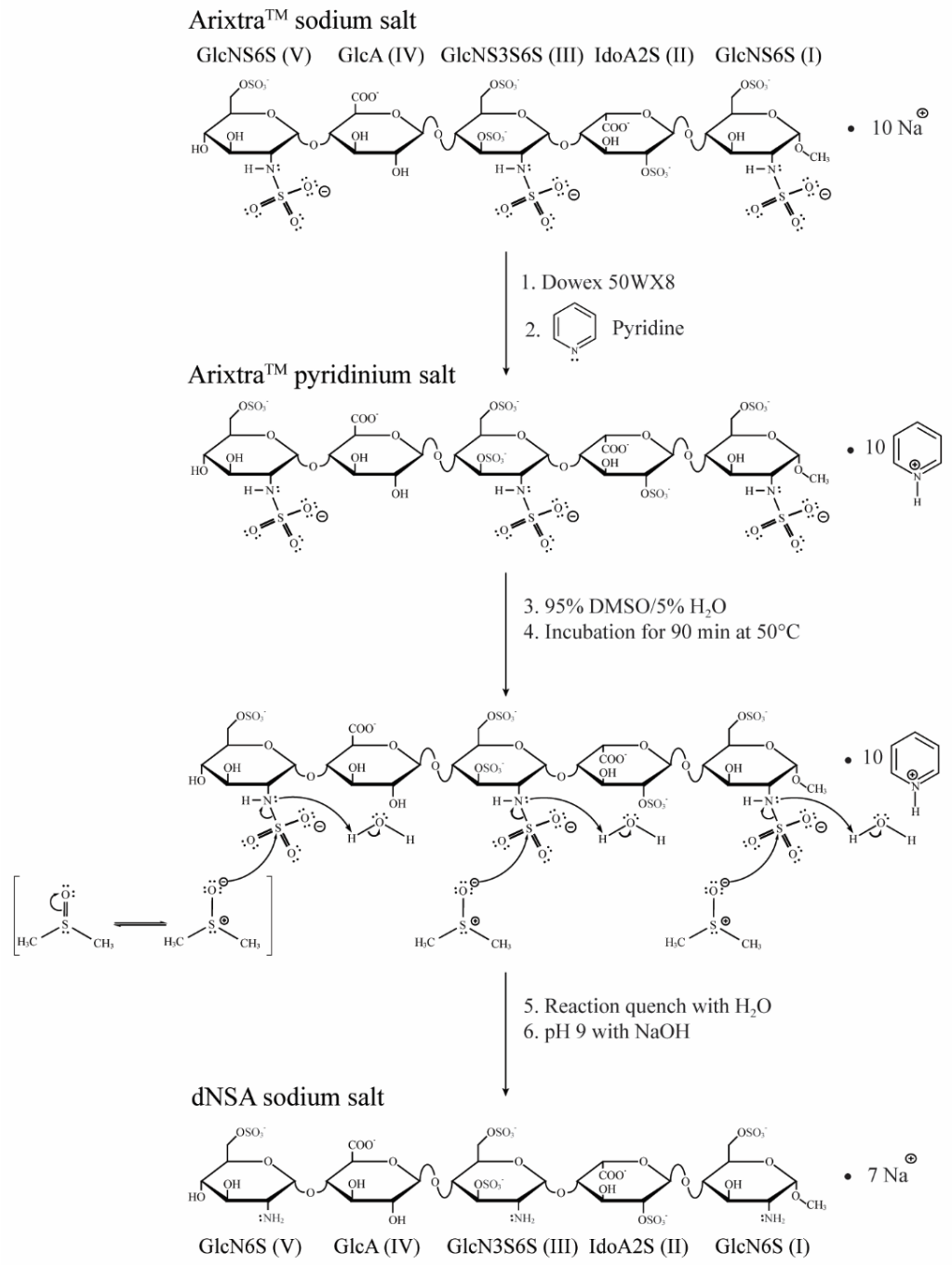

Figure 2.1. Schematic of the S_N2 mechanism proposed for the solvolytic de-*N*-sulfation reaction of Arixtra™.

structures acts as a nucleophile and attacks the partially positively charged sulfur atom of the *N*-sulfo group. The bond connecting the sulfur and nitrogen is broken and the nitrogen atom abstracts a proton from a water molecule. The addition of water into the reaction mixture quenches the reaction because in aqueous solutions, molecules of DMSO form solvation complexes with water molecules[39] and lose their nucleophilic properties. Adjustment to pH 9 with sodium hydroxide deprotonates pyridinium and replaces pyridine by sodium ions as the counterion to negatively charged groups of dNSA. Pyridine than was removed with other volatile compounds by speed vacuuming at medium heat for 3 h.

Visual inspection of the ^{1}H NMR spectra of Arixtra™ and dNSA shown in Figure 2.2A and B, respectively, reveals that the de-*N*-sulfation reaction was successful with essentially 100% yield, converting Arixtra™ to a completely de-*N*-sulfated form. Figure 2.2A shows the spectrum of Arixtra™ before the reaction, with the clearly observable proton resonances of the three *N*-sulfo groups found within the chemical shift region of 5.5 - 6.0 ppm. The doublets of the protons of the sulfamate groups disappear after the reaction, with three new singlets of the amino groups appearing in the region from 8.0 - 8.5 ppm of the dNSA spectrum (Figure 2.2B). To confirm that only de-*N*-sulfation occurred without any additional sulfate losses or side reactions, the successful chemical modification of Arixtra™ by solvolytic de-*N*-sulfation was confirmed through the complete structure elucidation procedure described in following Section 2.3.4. In addition to de-*N*-sulfation of Arixtra™ a de-*N*-sulfated heparin tetrasaccharide was prepared using the same reaction conditions yielding the structure shown in Figure 3.1E of Chapter 3.

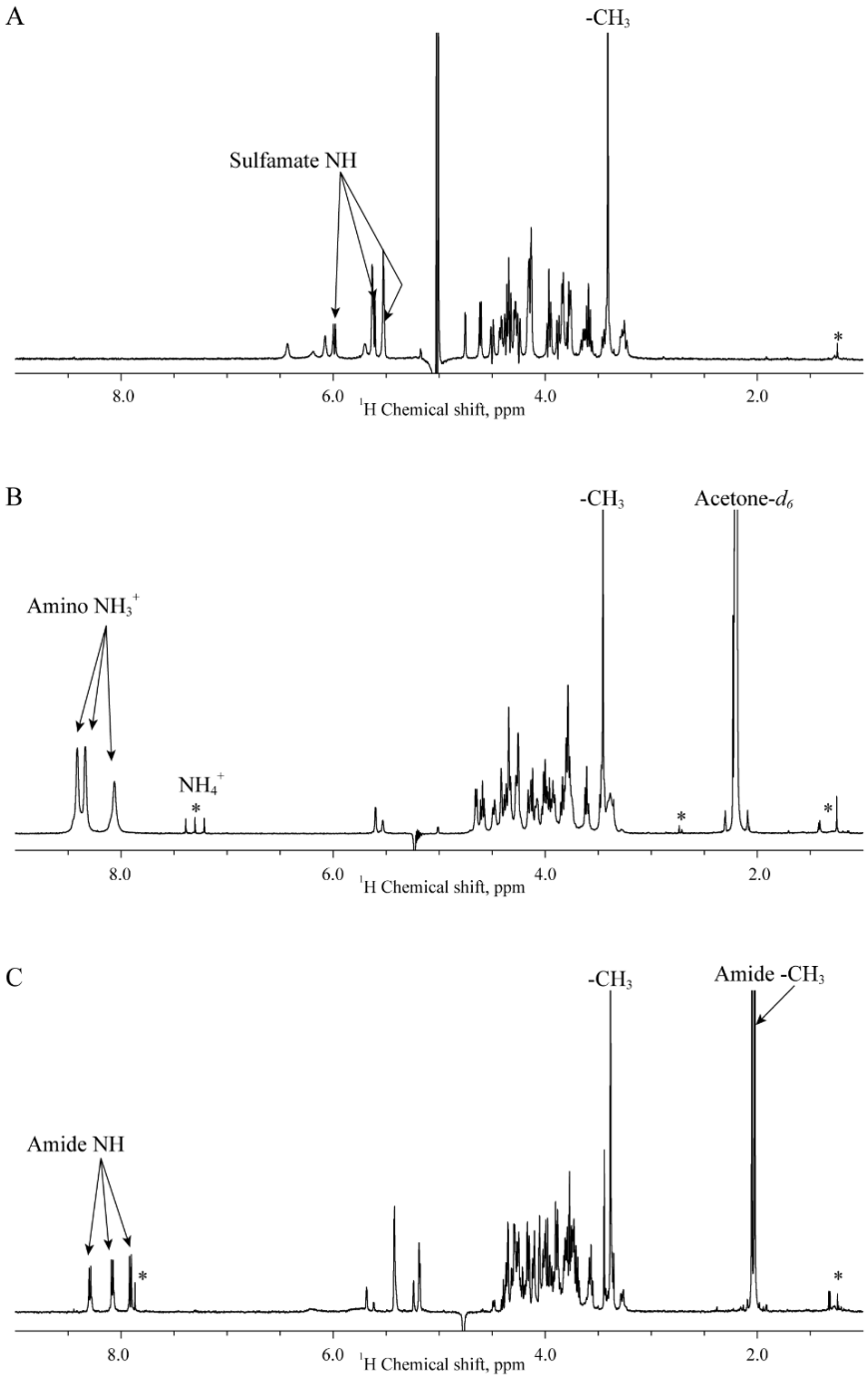

Figure 2.2. ^{1}H NMR spectra of Arixtra^{TM} acquired through the stages of its structural modification. (A) Spectrum of original *N*-sulfated pentasaccharide Arixtra^{TM} acquired at

278.2 K in 90% H_2O/10% D_2O solution at pH 8.14. Doublets of the sulfamate group proton resonances are found in the region 5.5 - 6.0 ppm. (B) Spectrum of de-*N*-sulfated Arixtra™ acquired at 259.1 K in 85% H_2O/15% acetone-d_6 solution at pH 1.54 adjusted before acetone addition. Singlets of the amino group protons resonate downfield in the region 8.0 - 8.5 ppm. (C) Spectrum of *N*-acetylated Arixtra™ acquired at 298.2 K in 90% H_2O/10% D_2O solution with pH 7.4. The amide group doublets are observed in the region 7.8 - 8.2 ppm. Additionally, three characteristic amide group methyl proton singlets were observed around 2.0 ppm. The resonances arising from impurities are indicated by an asterisk.

2.3.2. Chemoselective *N*-acetylation. The de-*N*-sulfated Arixtra™ provided not only an heparan sulfate mimic oligosaccharide containing rare GlcN3S and GlcN3S6S residues (discussed in Chapter 3), it also served as the starting material for the synthesis of a unique *N*-acetylated motif for the investigation of the physico-chemical properties of the labile protons of amide groups (Chapter 4). Herein, a reaction for the chemoselective *N*-acetylation of de-*N*-sulfated Arixtra™ was developed and optimized.[29, 30] The reaction is driven by acetic acid that acts as catalyst for the bonding of acetyl groups to the free amines. An important component of the reaction is the opposite charges of the amino group and acetic acid. Therefore, the deprotonated acetic acid carboxylate and protonated amino promote fast and complete *N*-acetylation. For example, we observed that reactions performed at a solution pH lower than the acetic acid pK_a drastically reduce the yields of *N*-acetylated products (by about 98%).

The proposed reaction mechanism for the *N*-acetylation of dNSA is schematically depicted in Figure 2.3. The reaction is initiated by abstraction of a proton from the positively charged amino group by the deprotonated acetic acid. Simultaneously, the lone pair of the amine group nitrogen forms a bond with the carbonyl carbon of acetic anhydride, which in turn breaks the bond to the adjacent oxygen. The broken bond in acetic acid anhydride leaves the second part of the molecule, deprotonated acetic acid, with a negative charge on the oxygen atom. Extraction of the proton from the amide by the deprotonated acetic acid stabilizes the amide group. Chemoselective *N*-acetylation of oligosaccharides with free amino groups is preferred over other available methods for amine acetylation.[40-44] Reaction is simple and utilizes a green chemistry approach and therefore does not

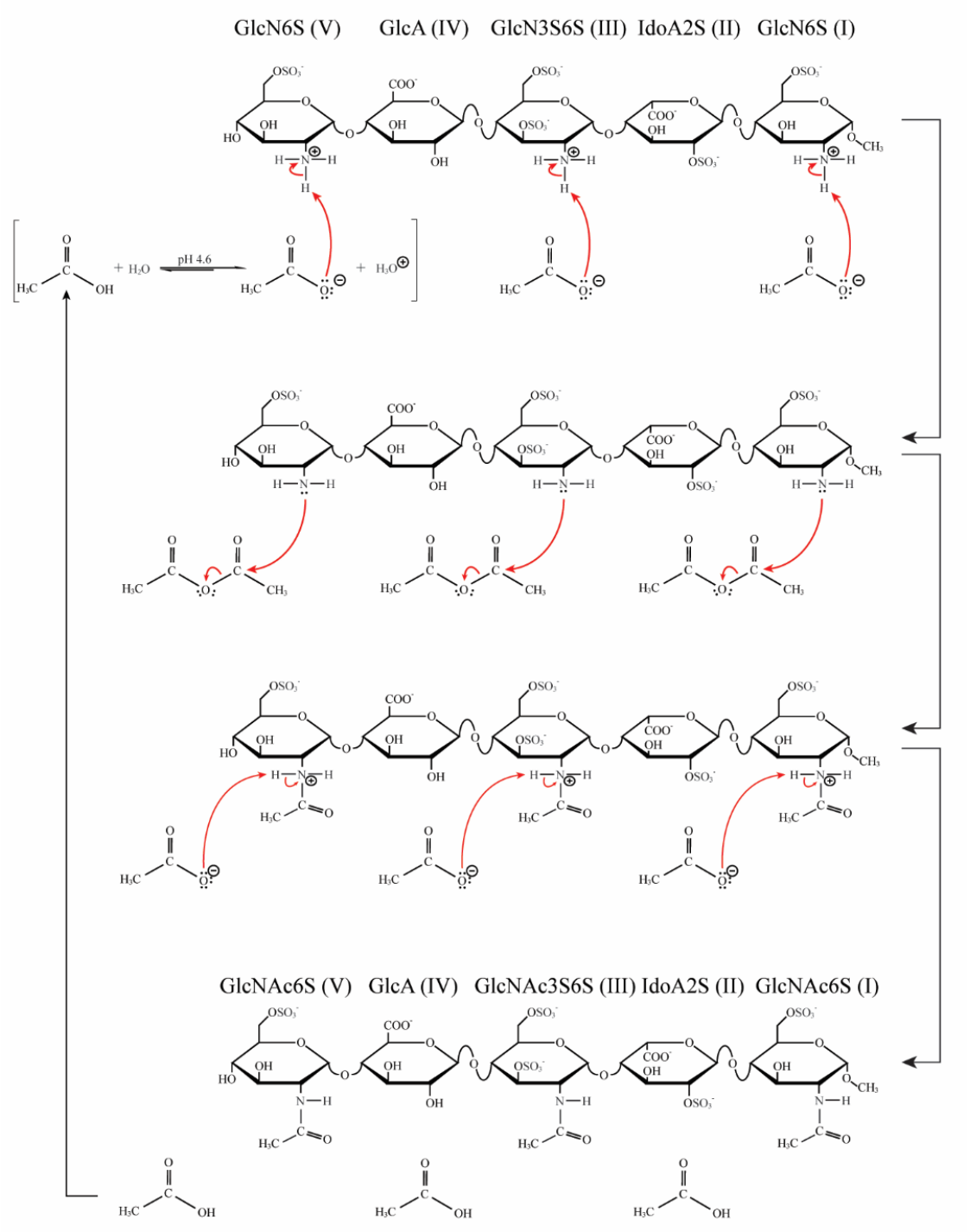

Figure 2.3. Schematic mechanism proposed for the selective *N*-acetylation of dNSA. The reaction is catalyzed by acetic acid.

generate harmful waste. Furthermore, acetic acid, methanol, and unreacted acetic anhydride are volatile compounds and therefore can be easily removed through vaporization, facilitating the isolation of relatively pure end products.

In Figure 2.2B and C show, respectively, the ^{1}H NMR spectra of dNSA and the final product *N*-acetylated Arixtra^{TM} (NAcArixtra). Three amino proton singlets of dNSA appear in the 8.0 - 8.5 ppm in spectrum B. The spectrum recorded after the *N*-acetylation reaction (Figure 2.2C) shows three doublets belonging to the three-amide groups, resonating further upfield in the region 7.8 - 8.2 ppm. In addition, three characteristic singlet resonances of the amide group methyl protons are introduced in spectrum 2.2C around 2.0 ppm. The absence of additional methyl singlets confirms that *O*-acetylation of the hydroxyl groups, a possible side reaction, was avoided.

2.3.3. Reduction with sodium borohydride. The reduction of monosaccharides with sodium borohydride is often applied in studies of polysaccharide structure.[45] The reaction is designed to convert the aldose form of the reducing end monosaccharide to an alditol. Figure 2.4 shows the structure of a representative tetrasaccharide isolated after enzymatic digestion of chondroitin sulfate A with Chondroitinase ABC. In solution, the tetrasaccharide has two anomeric configurations, α and β, due to mutarotation at carbon 1 (C1) of the reducing end residue. The α and β configurations result from cyclization of the acyclic form of the sugar (depicted using a Fisher projection formula) as shown in Figure 2.4. Hemiacetals (depicted with a Haworth projection) are formed through an intramolecular interaction of the hydroxyl group at carbon 5 (C5) with the aldehyde group.

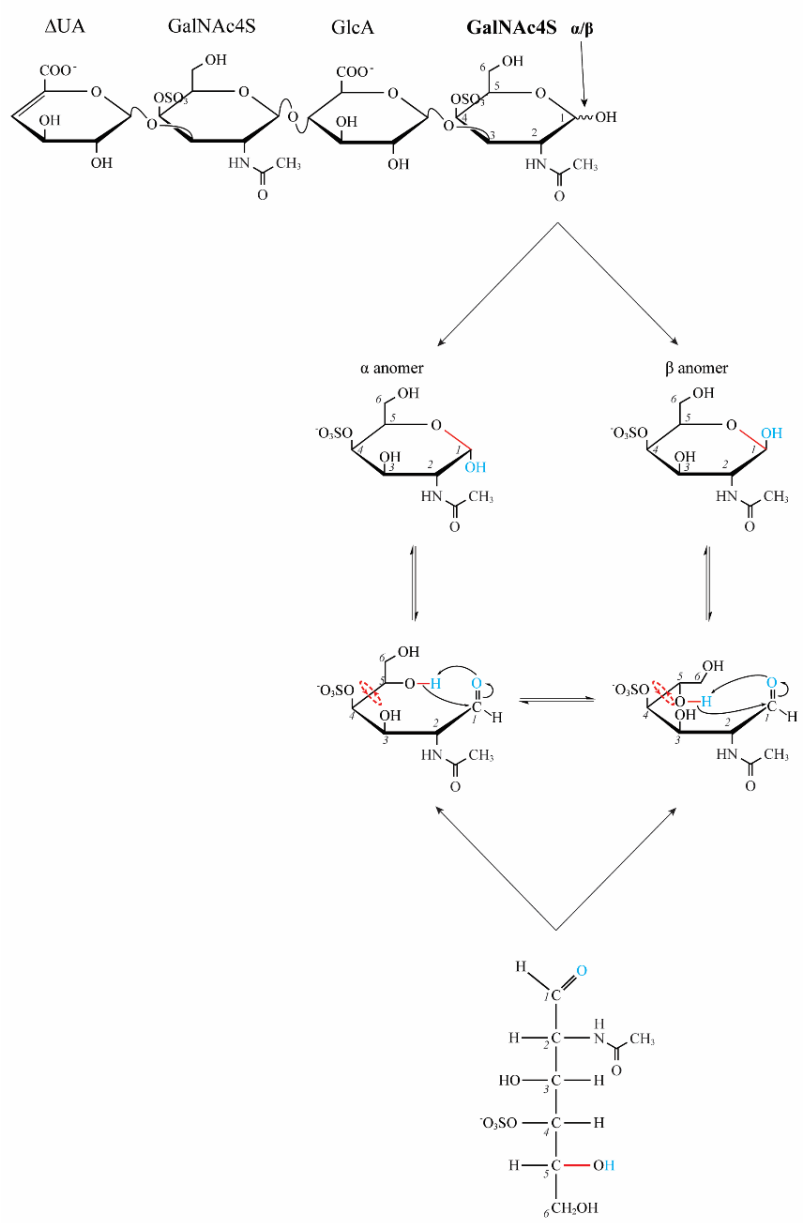

Figure 2.4. Schematic depiction of the cyclization of the reducing end monosaccharide residue of a chondroitin sulfate A tetrasaccharide. The acyclic form of the reducing end sugar is converted to a cyclic form by intramolecular reaction of the -OH group at C5 and the aldehyde group at C1. Red dashed circular arrows show rotation of groups attached to C4. Depending on the position of these groups, either an α or β anomer will be formed.

This cyclization creates a new chirality center at C1, the anomeric carbon. Depending on the position of the group attached to C4 (shown with red dashed arrows), two diastereomers can be formed.

Configurations at C1 are not static, but are in constant dynamic equilibrium in aqueous solution, therefore, both configurations are observed simultaneously in the NMR spectrum. In Figure 2.5, A1 is the NMR spectrum of the 4-*O*-sulfated tetrasaccharide with the sequence given in Figure 2.4. The inset of Figure 2.5 A1 shows the effect of the α and β anomeric carbon configurations on the amide methyl resonances. Though there is a minimal effect on the internal residues, the amide group methyl protons of the reducing end residue resonate at two frequencies, producing partially overlapped singlet resonances. The resonances of the other carbon-bound protons are severely overlapped in the region of the ^{1}H NMR spectrum from 3.6-4.6 ppm complicating the identification of individual resonances. With increasing oligosaccharide size, the ^{1}H NMR spectra become even more complex as observed in Figure 2.5 B1 for the 4-*O*-sulfated chondroitin sulfate hexasaccharide.

One way to improve the quality of an oligosaccharide NMR spectrum is to "lock" the reducing end residue in one configuration by reduction of the aldose to an alditol using sodium borohydride, a relatively mild reducing agent. Under typical conditions, sodium borohydride does not reduce amides and carboxylic acids, which is important for GAGs. Mechanistically, the sodium borohydride reduction reaction proceeds through the two steps schematically depicted in Figure 2.6. In the first step, a nucleophilic hydride ion (H^-) is transferred from borohydride to the electrophilic aldehyde carbon of the aldose forming an

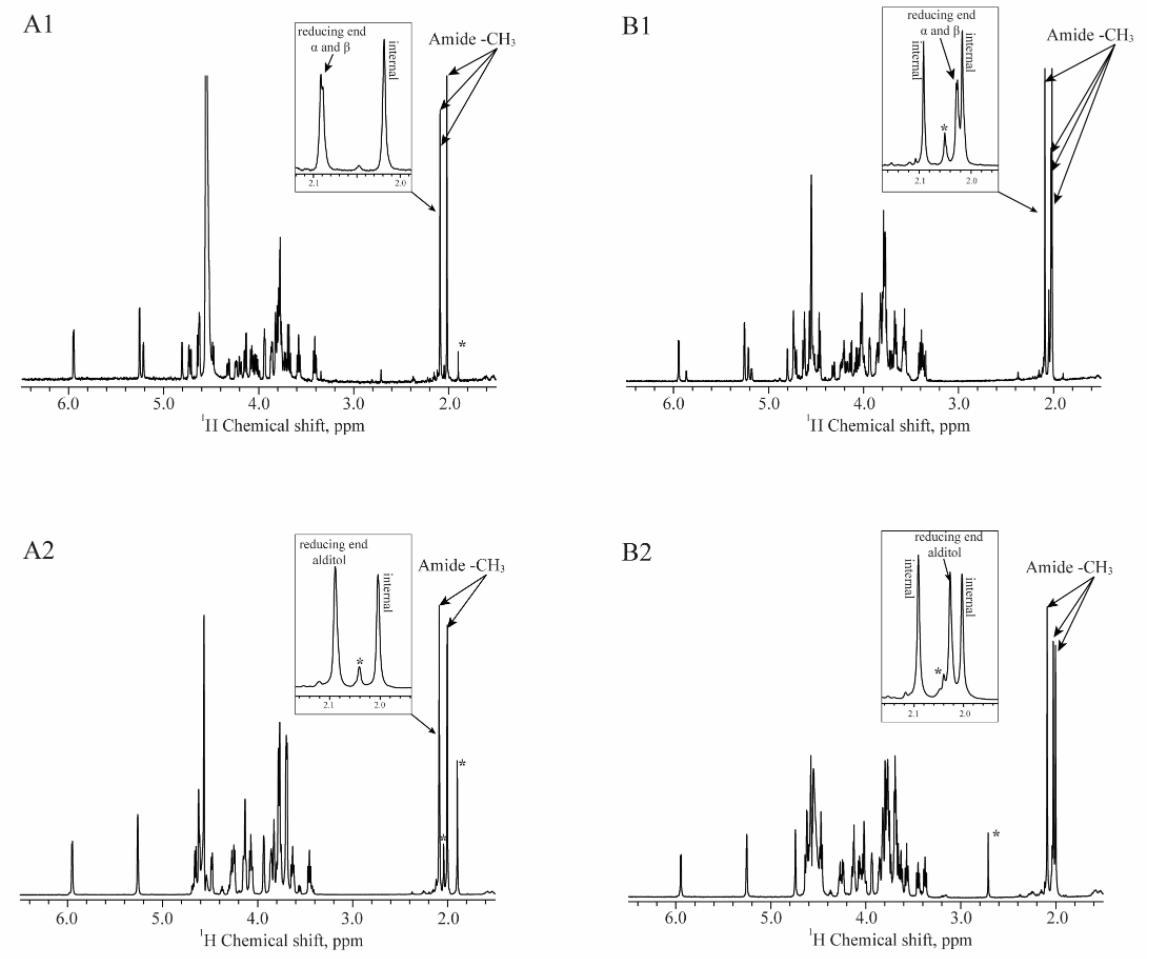

Figure 2.5. ^{1}H NMR spectra of 4-*O*-sulfated chondroitin sulfate oligosaccharides before (A1 and B1) and after (A2 and B2) reduction with sodium borohydride. A1 and A2 are spectra of the tetrasaccharide in Figure 2.4. B1 and B2 are spectra of the hexasaccharide (ΔUA-GalNAc4S-GlcA-GalNAc4S-GlcA-GalNAc4S). Due to mutarotation at the anomeric carbon, in A1 and B1 two sets of chemical shifts are observable in the NMR spectra for the α and β configurations of each oligosaccharide. The insets show the effect of mutarotation and reduction on the resonances of amide group methyl protons. Reduction

of the reducing end monosaccharide converts the α and β aldose configurations to an alditol and only one set of chemical shifts is present in NMR spectra A2 and B2.

*- denotes resonances arising from impurities present in solution

alkoxide salt and borane. Then the basic alkoxide is protonated by acetic acid to form the alcohol. As the ^{1}H NMR spectrum of the reduced 4-*O*-sulfated tetrasaccharide (Figure 2.5, A2) illustrates, elimination of the α and β anomers simplifies the NMR spectrum allowing easier identification of the resonances of each sugar residue. For example, the insets of Figure 2.5 A2 and B2 show that the amide group methyl resonances are converted to a single peak because there is only one possible configuration of the alditol.

Although the sodium borohydride reduction also worked well for the chondroitin sulfate hexasaccharide (Haworth projection shown in Figure 4.1T, Chapter 4), extra care was required for the reduction of oligosaccharides derived from hyaluronic acid. As hyaluronic acid oligosaccharides do not have large sulfo groups capable of stabilizing negative charge, we found the reduced hyaluronic acid oligosaccharides to be less stable. The use of phosphate buffer in the reaction mixture during the reduction reaction and in all post-reaction steps was found to help stabilize the hyaluronic acid oligosaccharides.

2.3.4. Structure elucidation of de-*N*-sulfated Arixtra™. The successful outcome of a chemical reaction can only be reported after elucidation of the complete structure of the product. In this section, the structure elucidation process is illustrated for de-*N*-sulfated Arixtra™. This general approach was applied to all the isolated and chemically modified oligosaccharides used in this dissertation. For those compounds not discussed explicitly in Chapters 2-4, tables with the resonance assignments are provided in the Appendix.

2.3.4.1. Electrospray ionization – mass spectrometry. Electrospray ionization – mass spectrometry (ESI-MS) is commonly used at the initial stages of the oligosaccharide

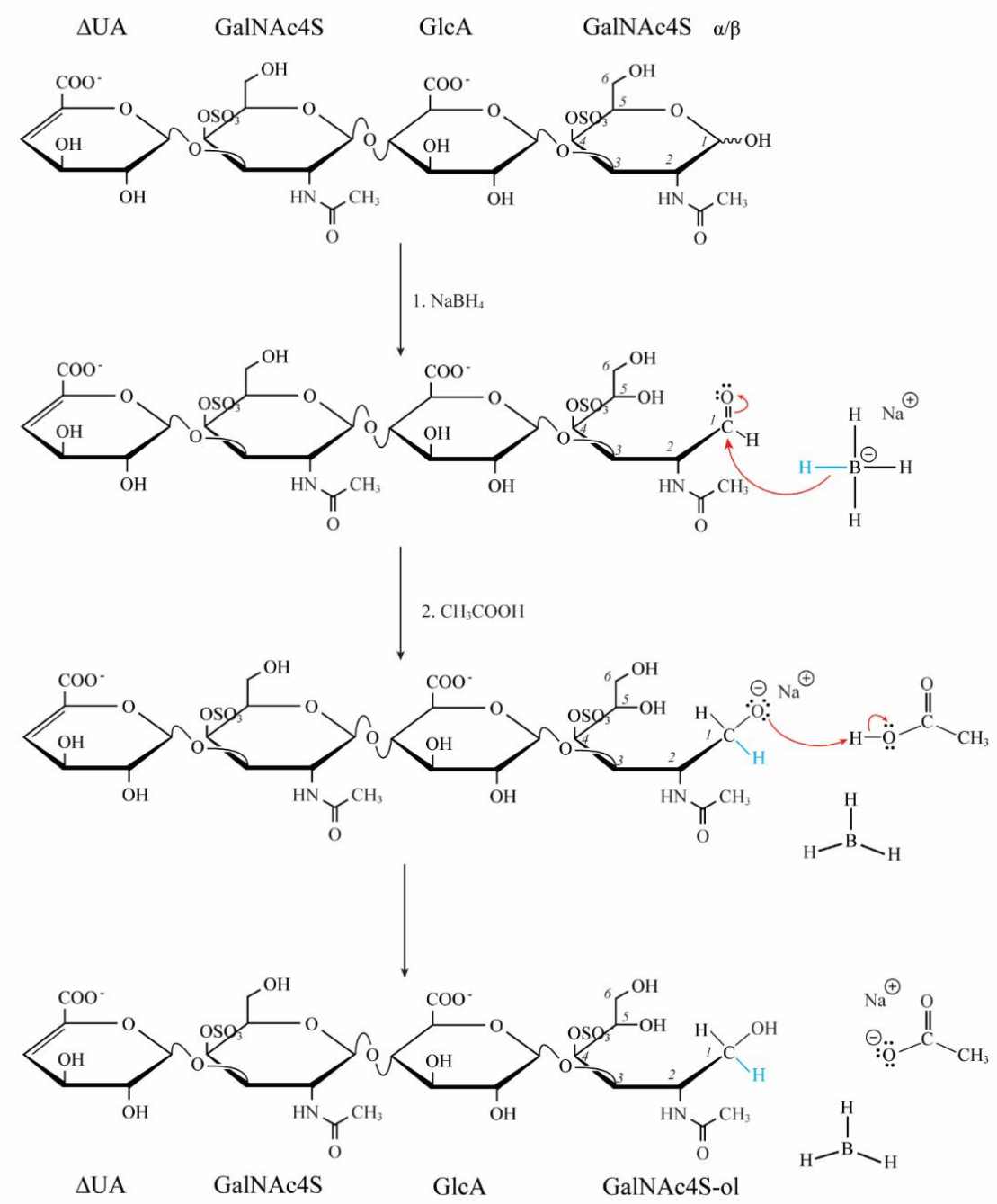

Figure 2.6. Reduction of the chondroitin sulfate A tetrasaccharide with sodium borohydride. The reducing end aldose is converted to alditol form eliminating the α and β anomers.

structure elucidation process. This soft ionization source produces molecular ions with little fragmentation while the MS analyzer produces a spectrum showing ion abundance as a function of mass-to-charge ratio (m/z). The mass spectrum provides rapid determination of the molecular weight, degree of sulfation, and possible acetylation of oligosaccharides.

Figure 2.7 shows the ESI mass spectrum of dNSA with the peak assignments. The calculated expected mass of dNSA is 1267.08 U. The doubly (m/z 632.54), triply (m/z 421.40), and quadruply (m/z 315.84) charged molecular ions were observed, and as expected, the higher charged molecular ions were more prone to sulfate loss (-80 Da). For example, loss of a sulfate group from the triply charged molecular ion corresponds to a m/z difference of 26.66 producing the peak at m/z 394.78. Similarly, m/z 19.99 separates quadruply charged ion peaks with (m/z 295.85) and without (m/z 315.84) sulfate loss. Because dNSA was prepared as the sodium salt and the sample was infused directly into the ESI-MS, molecular ions were also accompanied by sodium adducts. Analysis of the mass spectrum revealed that chemical modification of Arixtra^{TM} did not affect the carbon backbone of pentasaccharide and that only sulfate groups were released during the reaction. ESI-MS results for the de-*N*-sulfated heparin tetrasaccharide (Figure A1) and NAcArixtra (Figure A2) can be found in Appendix.

2.3.4.2. Nuclear magnetic resonance spectroscopy. Though the MS is critical for confirming the basic structure of oligosaccharides, nuclear magnetic resonance (NMR) provides complementary information about oligosaccharide structure and structure-function relationships, physicochemical properties and dynamics. ^{1}H NMR is an essential

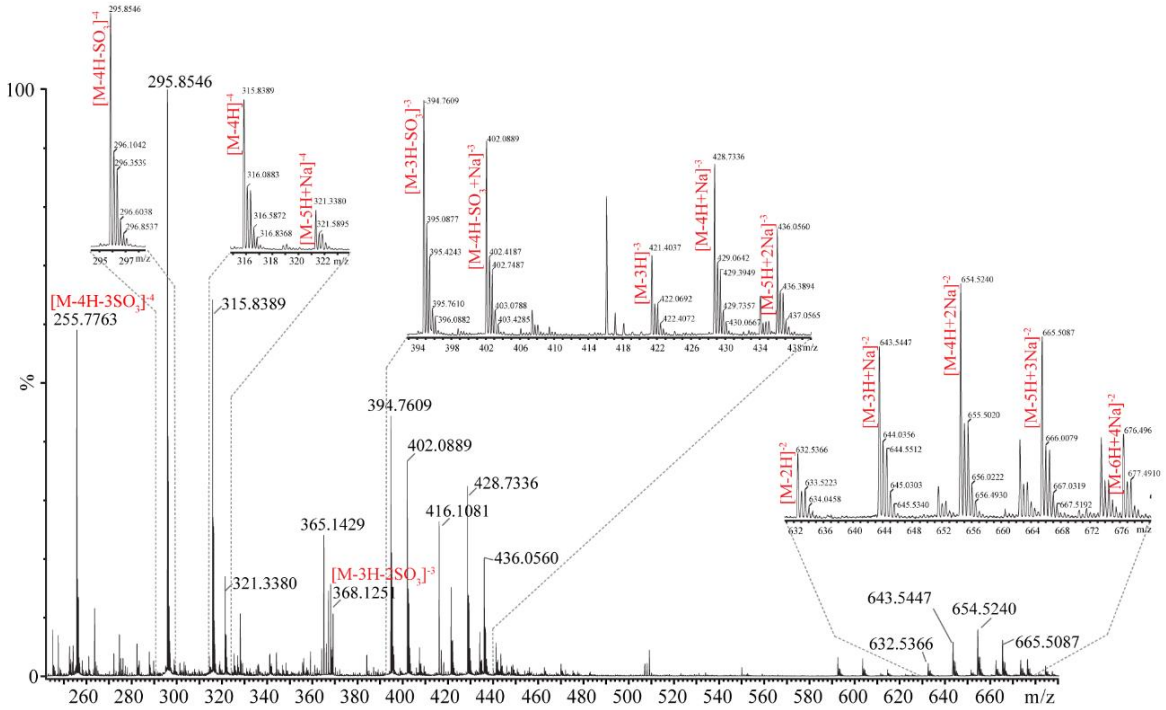

Figure 2.7. Mass spectrum of dNSA obtained using an ESI Q-TOF mass spectrometer operating in negative ionization mode. The loss of sulfate and the presence of sodium adducts is common in analysis of GAG oligosaccharides by ESI-MS. The expected mass of dNSA in 1267.08 U was confirmed by mass spectrometry.

tool for GAG characterization due to its high natural abundance and gyromagnetic ratio, and spin of ½. Furthermore, hydrogen is one of the most abundant elements in GAGs and proton NMR chemical shifts, coupling constants and resonance line widths can report on small changes in GAG structure and conformation, especially at high magnetic fields.

2.3.4.2.1. One-dimensional proton NMR spectra. The process of GAG structure elucidation typically begins with acquisition of the one-dimensional (1D) ^{1}H NMR spectrum of negatively charged GAG oligosaccharides, typically measured in phosphate buffer at neutral pH to ensure that all the carboxylates have been deprotonated and chemical shifts are stable. Additionally, EDTA-d_{16} is often added to remove the line broadening associated with the presence of trace paramagnetic species in solution.[34, 46, 47]

The ^{1}H NMR spectra of GAGs have several common characteristics associated with specific elements of structure. For example, the singlet resonances between 1.8 and 2.2 ppm are characteristic of the *N*-acetyl methyl protons, as observed in Figure 2.3C and Figure 2.5. Most of the protons of the sugar rings resonate in the region between 2.5 and 4.6 ppm. Because of the limited chemical shift dispersion of sugars in this region, the resonances are highly overlapped and resolution of individual resonances is difficult for oligosaccharides of even modest length. Further downfield between about 4.6 and 6.0 ppm, the anomeric proton resonances are better resolved, as are the distinctive peaks of the H4 protons of the unsaturated uronic acid residues (ΔUAs), along with the hydroxyl, and sulfamate group protons. Finally, the most downfield resonances are produced by the protons of amide and amino groups, which typically have chemical shifts between 6.8 ppm and 9.0 ppm. The labile protons of hydroxyl, sulfamate, amide, and amino groups require

special conditions for detection and are not observed in spectra acquired in D_2O due to their exchange with deuterium. The assignment of the dNSA amino protons resonances will be discussed separately in the following sections.

The 1D ^1H NMR spectrum of dNSA (Figure 2.8B) was measured in D_2O solution using phosphate buffer and referenced to zero ppm with a DSS-d_6 internal standard. The spectrum was acquired using the presaturation pulse sequence to suppress the solvent resonance arising from residual protons of HOD.[48] This pulse sequence is composed of only three major pulse components: a long selective pulse to saturate the solvent resonance, a non-selective pulse for excitation and the acquisition of FID. One of the problems with presaturation is that analyte resonances close to the solvent frequency are also attenuated, therefore, care should be used in selection of the presaturation power. Inspection of the ^1H NMR spectrum of dNSA allows one to immediately identify the residual HOD resonance at 4.8 ppm and the methoxy group protons (-OCH_3) at 3.41 ppm. Additionally, the spectrum reveals the resonances of low level impurities (labeled with an *). Although the 600 MHz ^1H NMR spectrum of dNSA contains multiple well-resolved resonances, the spectra still suffer from limited chemical shift dispersion in the region between 2.5 and 4.6 ppm. Consequently, definitive resonance assignments require homonuclear two-dimensional (2D) NMR experiments as described in the following section.[49]

2.3.4.2.2. Homonuclear two-dimensional proton NMR spectroscopy. Fortunately, the overlapped peaks of the 1D spectrum can be readily assigned using a set of 2D homonuclear (^1H-^1H) NMR experiments. Three 2D experiments are generally used for the

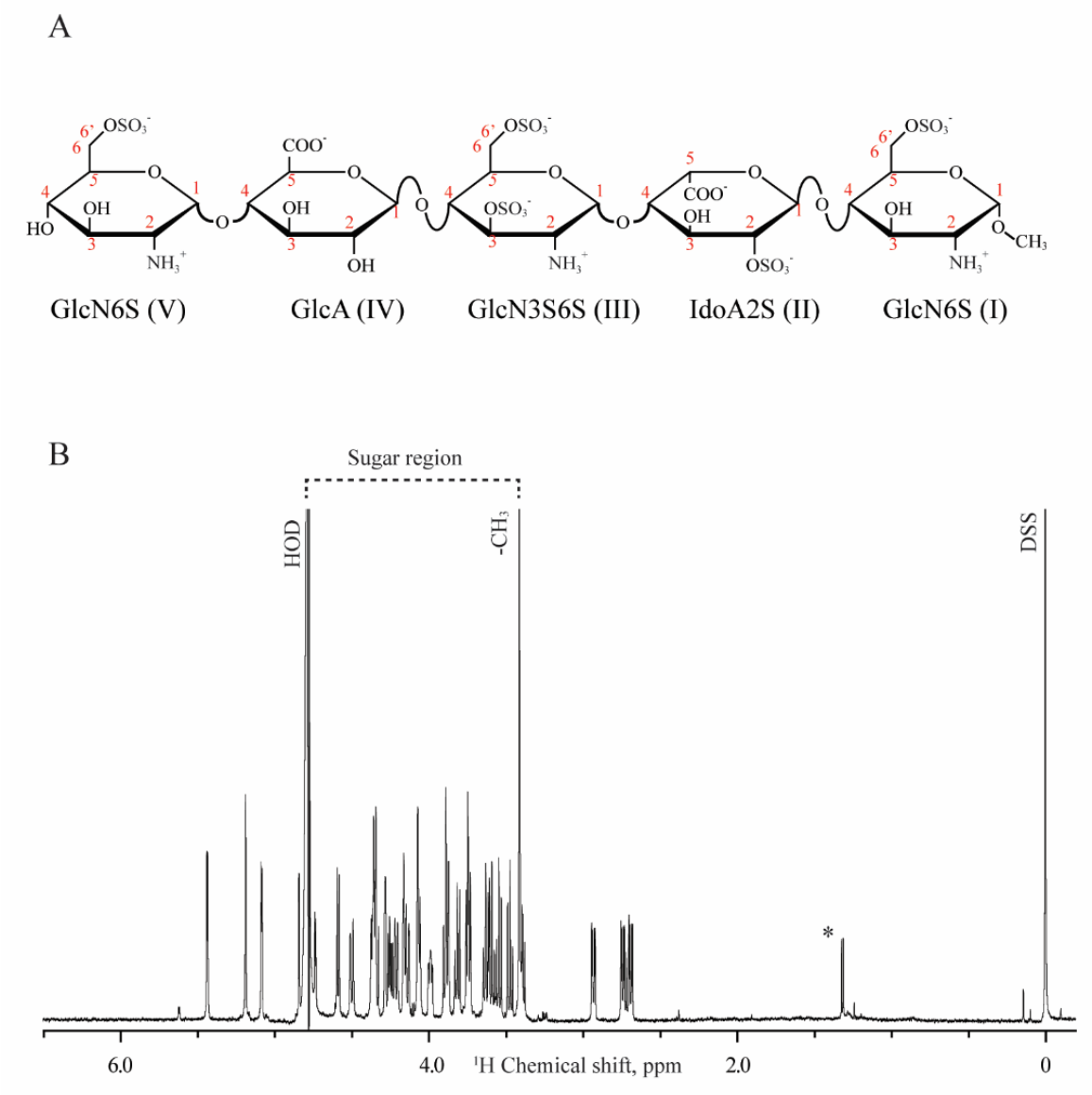

Figure 2.8. (A) The Haworth projection of de-*N*-sulfated Arixtra™ (dNSA) with labeled residues and numbered carbon-bound protons within each residue. For example, the carbon labeled with number 1 in the following sections is referred to as C1, the proton bound to this carbon is referred to as H1, and so on. (B) The ^{1}H NMR spectrum of dNSA acquired in D_2O.

structure elucidation of oligosaccharides: the total correlation spectroscopy (TOCSY), correlation spectroscopy (COSY), and rotating-frame nuclear Overhauser effect spectroscopy (ROESY) experiments.[50-53] Structure elucidation of GAG oligosaccharides by ^{1}H-^{1}H NMR usually begins with acquisition of the TOCSY and COSY spectra. The purpose of these experiments is to identify the individual monosaccharide subunits in the oligosaccharide chain using scalar couplings to provide through-bond connectivity.[54] Finally, dipolar coupling employed in the ROESY experiment completes the structure elucidation process by establishing connectivity across the glycosidic linkage.

Monosaccharides are the major constituents of oligosaccharides linked through a glycosidic bond. Consequently, each monosaccharide represents an individual isolated spin system that can be identified through the cross-peaks of a ^{1}H-^{1}H TOCSY spectrum.[54] The length of the TOCSY mixing time should be sufficient for magnetization transfer from the anomeric proton (H1) to the furthest separated carbon-bound protons (H6) of a monosaccharide ring. In practice, 120 ms allows for transfer of magnetization throughout the spin system. The spin lock pulse length requires calibration and varies for each experiment, though typical values fall in the range of 35 - 45 μs for spectrometers operating at a ^{1}H frequency of 600 MHz.

In the ^{1}H-^{1}H TOCSY spectrum, the diagonal peaks running from the top right to the bottom left corner are the equivalent of the proton spectrum. The off-diagonal cross-peaks correspond to the chemical shifts of the other protons within that spin system. Figure 2.9A shows the TOCSY spectrum of dNSA in which the five spin systems of the individual monosaccharides of the dNSA sequence are identified. Identification of each residue starts

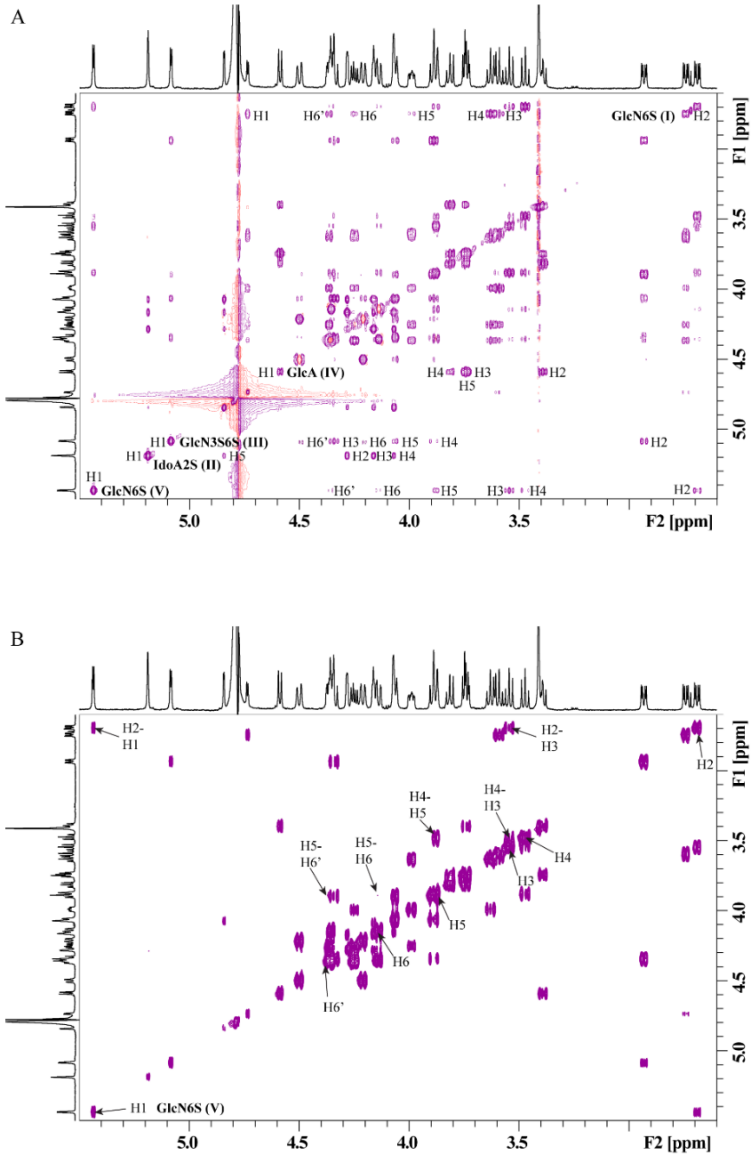

Figure 2.9. (A) ^{1}H-^{1}H TOCSY and (B) ^{1}H-^{1}H COSY spectra of dNSA acquired in D_2O. Five spin systems of dNSA were identified through TOCSY cross-peaks aligned along the F2 dimension. Assignment of the individual resonances of each monosaccharide spin system was performed using the COSY cross-peaks as illustrated for the GlcN6S(V) residue. The one-dimensional ^{1}H NMR spectrum is included along both dimensions of the contour plot.

with recognition of their well-resolved H1 resonances. Then, the cross-peaks are traced to other protons found within the same spin system. Monosaccharides belonging to the uronic acid (GlcA or IdoA2S) and GlcN residues (GlcN6S and GlcN3S6S) can be distinguished from each other based on the number of cross-peaks found in each spin system. For instance, GlcN residues contain 7 cross-peaks that correspond to 7 protons of this spin system. In contrast, GlcA and IdoA2S residues contain only 5 cross-peaks corresponding to 5 carbon-bound protons of their sugar rings.

Once each type of monosaccharide residue has been identified, the structure elucidation process proceeds to determine the chemical shifts of the individual proton resonances found within the same spin system. The ^{1}H-^{1}H COSY experiment allows identification of protons coupled through 3-bonds (typically).[55] Figure 2.9B shows a ^{1}H-^{1}H COSY spectrum acquired in D_2O by using a COSY pulse sequence with presaturation. Similarly to TOCSY, the COSY spectrum contains diagonal peaks running from the top right to the bottom left corners of the spectrum with cross-peaks relating coupled spins. Starting with an H1 chemical shift along the diagonal, the correlations are followed through the cross-peak to the coupled H2, which can then be traced similarly to the H3 cross-peak, and so on. The COSY spectrum shown in Figure 2.9B illustrates the cross-peak correlations for the protons within GlcN6S(V). Similarly, correlated protons are found for the spin systems of the other four monosaccharide residues.

Using the TOCSY and COSY spectra the chemical shifts of all the protons of the dNSA monosaccharide rings were identified. However, complete structure elucidation requires determination of the monosaccharide sequence. This task can be accomplished

through execution of the NMR experiments that provide information about the spatial proximity of protons. The Homonuclear rotating frame Overhauser spectroscopy (^{1}H-^{1}H ROESY) is a good option, especially for medium-sized oligosaccharides like the dNSA pentasaccharide. ROESY is a variation of the nuclear Overhauser effect spectroscopy (NOESY) pulse sequence with both experiments utilizing the nuclear Overhauser effect (NOE), a phenomenon relying on dipolar relaxation of spins localized within about 5 Å.[56] In the NOESY spectrum, the sign of the NOE depends on the product of the spectrometer frequency, ω, and the rotational correlation time, τ_c, which is related to the rate of molecular tumbling in solution.[57] NOEs are positive for small, rapidly tumbling molecules and negative for large, slowly tumbling molecules. The NOE intensity passes through zero when the molecular reorientation lies between these two motional extremes. Because the ROE evolves in the rotating frame of reference, all molecules give rise to positive ROE cross-peaks that are opposite in sign to the diagonal.[56]

In the structure elucidation process, analysis of the ROESY spectrum builds on the assignments made using the TOCSY and COSY spectra. Figure 2.10 shows the ROESY spectrum of dNSA, where the diagonal peaks are shown in pale red and dipolar coupled protons in purple. Because protons coupled through 3 bonds are also close in space, there is some overlap between intramolecular ROESY cross-peaks and those observed in the COSY spectrum. By overlaying the two spectra, the inter-residue ROESY cross-peaks between the H1 and H4 protons across the glycosidic bond can be identified (Figure 2.10) and used to elucidate the oligosaccharide sequence. Table 2.1 provides the assigned chemical shifts of all the carbon-bound protons of dNSA.

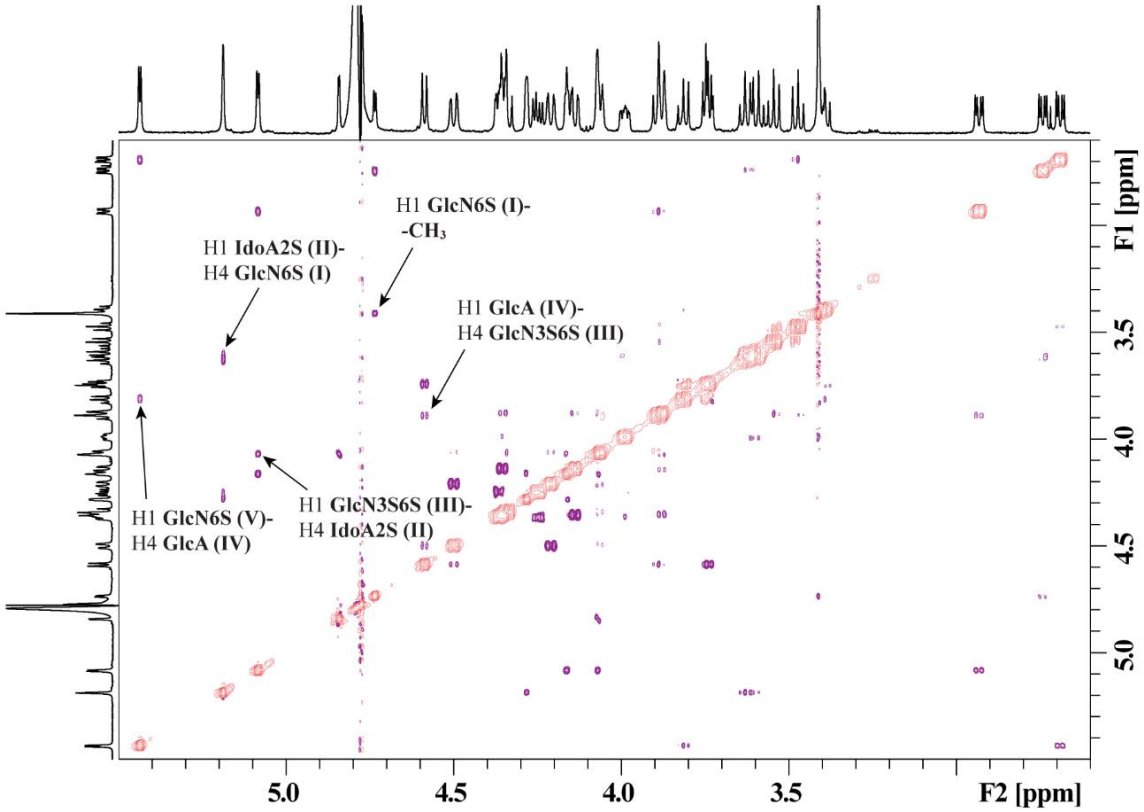

Figure 2.10. The ^{1}H-^{1}H ROESY spectrum of dNSA acquired in D_2O. Cross-peaks in the ROESY spectrum correlate protons coupled through the space within about 5 Å. Identification of the inter-residue cross-peaks between sequential residues GlcN6S(V) H1-H4 GlcA(IV), GlcA(IV) H1-H4 GlcN3S6S(III), GlcN3S6S(III) H1-H4 IdoA2S(II), IdoA2S(II) H1-H4 GlcN6S(I), and GlcN6S(I) H1- CH_3 confirms the sequence and completes the resonance assignment process. The one-dimensional ^{1}H NMR spectrum is included along both dimensions of the contour plot.

Table 2.1. Proton assignments in dNSA. All protons chemical shifts were assigned using 1D spectra, except those labeled with * which were assigned using COSY spectra. Carbon-bound protons are assigned from NMR spectra acquired at 298.2 K in 10 mM phosphate buffer with pD 11.27. Amino proton chemical shifts are assigned from spectra acquired at 259.1K in 85% H_2O/15% acetone-d_6 solution with solution pH 3.4 measured before acetone-d_6 addition.

Residue	Proton	^{1}H Chemical shift, ppm
GlcN6S(I)	1	4.735
	2	2.741
	3	3.59*
	4	3.63*
	5	3.989
	6	4.25*
	6’	4.37*
	-CH_3	3.411
	-NH_3^+	8.393
IdoA2S(II)	1	5.188
	2	4.282
	3	4.16*
	4	4.07*
	5	4.842
GlcN3S6S(III)	1	5.083
	2	2.932
	3	4.34*
	4	3.89*
	5	4.06*
	6	4.21*
	6’	4.499
	-NH_3^+	8.054
GlcA(IV)	1	4.588
	2	3.39*

	3	3.741
	4	3.815
	5	3.74*
GlcN6S(V)	1	5.436
	2	2.689
	3	3.545
	4	3.472
	5	3.88*
	6	4.14*
	6’	4.36*
	$-NH_3^+$	8.336

The resonance assignments of the purchased, isolated and chemically modified mono- and oligosaccharides used in this research were determined using a similar process and are reported in the Appendix.

Unlike carbon-bound protons, the GAG amino, amide, sulfamate, and hydroxyl protons are in dynamic exchange with water. As described in Section 1.4.2. the detection of labile protons by NMR requires the use of solution conditions that minimize the exchange rate. The conditions for detection of the amino proton resonances have been previously reported and involve measurements in low pH aqueous solution at reduced temperature.[35]

The assignment of the amino resonances builds on the assignments of the carbon-bound protons and uses the information contained in the ^{1}H, ^{1}H-^{1}H TOCSY, and ^{1}H-^{1}H COSY spectra. Through the TOCSY spectrum, the spin system to which amino proton belongs can be identified and the COSY spectrum confirms the amino proton scalar-coupling to the adjacent carbon-bound proton H2. Figure 2.11 A and B show the TOCSY (A) and COSY (B) spectra of dNSA acquired in 85% H_2O/15% acetone-d_6 at 259.1K with the 1D ^{1}H NMR spectrum drawn along each dimension of the contour plot. All spectra were acquired using excitation sculpting as the solvent suppression method.[58] Excitation sculpting is preferred over presaturation for measurements of labile protons to avoid saturation of the resonances of interest via exchange with water. In addition, the use presaturation with aqueous solutions can produce baseline distortions in the resulting spectra. In contrast, with excitation sculpting, which utilizes pulsed field gradients and shaped selective pulses, much flatter baselines are obtained.

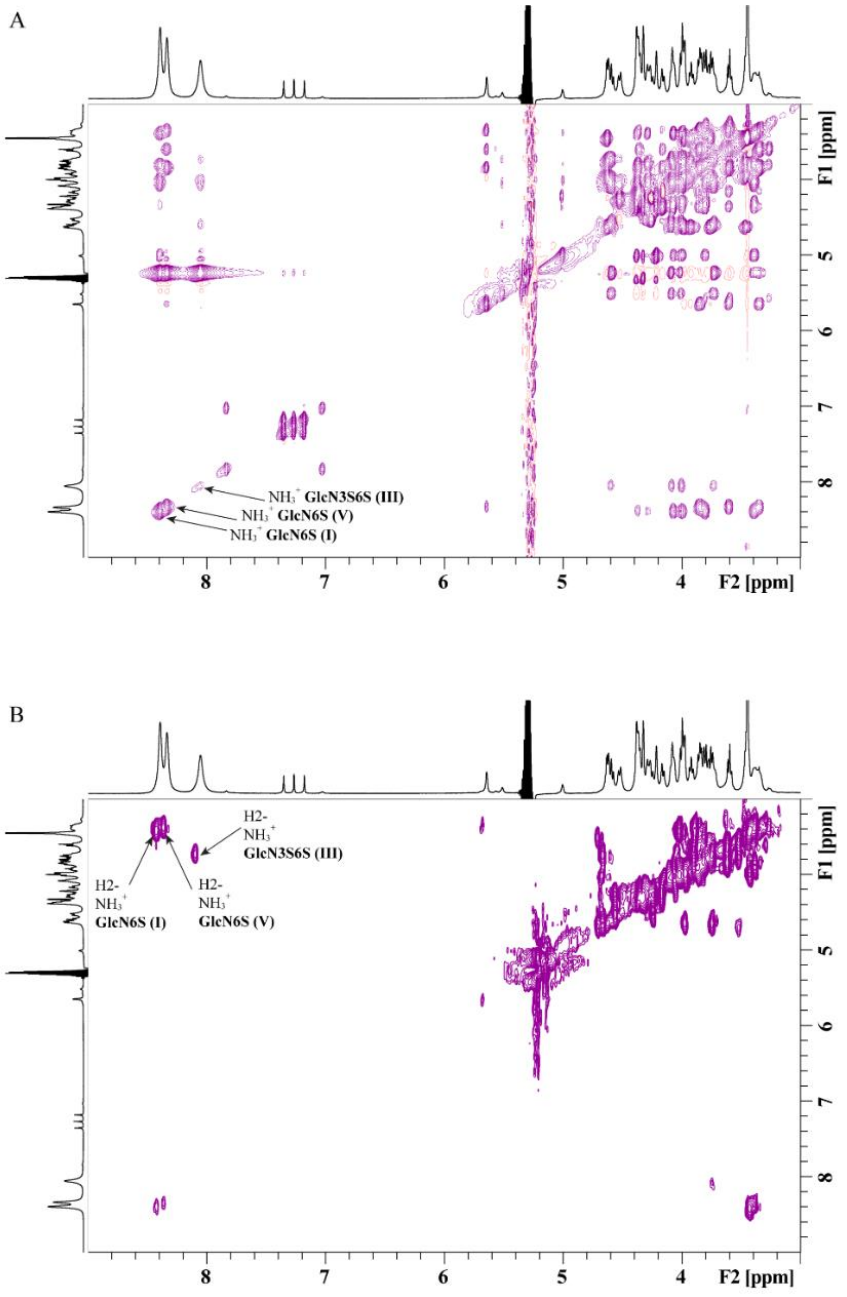

Figure 2.11. Homonuclear (A) TOCSY and (B) COSY spectra of dNSA acquired in 85% H_2O/15% acetone-d_6 at 259.1 K. Through the cross-peak linkages the amino proton resonances were assigned to corresponding glucosamine residues. The one-dimensional ^1H NMR spectrum is included along both dimensions of the contour plot.

The chemical shifts of the amino proton resonances of dNSA are found in the region of the spectrum from 7.9 to 8.5 ppm and are summarized in Table 2.1. At this point, the structure of dNSA is completely elucidated and the carbon- and nitrogen-bound ^{1}H NMR resonances have been assigned. A similar process was used for the resonance assignments of the purchased, isolated and modified mono- and oligosaccharides used in this research and tables containing the resonance assignments for the amino and amide proton resonances of each compound are given in the Appendix.

2.4. Conclusions

In this chapter, to provide access to rare but biologically important elements of structure in GAG polysaccharides, reactions for chemical modification of Arixtra™ and isolated GAG oligosaccharides were developed. Through the solvolytic de-*N*-sulfation of the synthetic Arixtra™ pentasaccharide, the unique structure of de-*N*-sulfated Arixtra™ (dNSA) was obtained mimicking the structure of rare heparan sulfate oligosaccharides containing a 3-*O*-sulfated glucosamine residue. This de-*N*-sulfated Arixtra™ is used in Chapter 3 to study the possibility of salt bridge formation involving the positively charged amino group and the adjacent negatively charged 3-*O*-sulfo group of the GlcN3S6S(III) residue. Furthermore, through the chemoselective *N*-acetylation reaction dNSA was further modified to an *N*-acetylated version of Arixtra™ (NAcArixtra). The comparison of the properties of Arixtra™, dNSA and NAcArixtra in Chapter 3 provides insights into the role of primary structure in stabilizing the hydrogen bonds in Arixtra™ and a salt bridge in dNSA. NAcArixtra was also used in Chapter 4 to investigate the exchange properties of

the amide group protons in aqueous solution at the physiologically important pH 7.4. Importantly, we believe this to be the first report of the preparation and characterization of dNSA and NAcArixtra.

Finally, the reaction of oligosaccharides with sodium borohydride converted the aldose form of the reducing end residue, which exists as α and β anomers to the alditol form simplifying the resulting NMR spectrum. Oligosaccharides derived from chondroitin sulfate A and hyaluronic acid were reduced using this method and the properties of their amide protons are discussed in Chapter 4. Proposed reaction mechanisms for the solvolytic de-*N*-sulfation, chemoselective *N*-acetylation, and reduction with borohydride were presented. Importantly, the structures of all chemically modified oligosaccharides were elucidated using ESI-MS and NMR. A detailed example of the structure elucidation process was provided for dNSA, and tables summarizing the chemical shifts of the purchased, isolated and modified mono- and oligosaccharides are summarized in Chapters 3 and the Appendix.

2.5. References:

1. Olson, S. T., Transient kinetics of heparin-catalyzed protease inactivation by antithrombin III. Linkage of protease-inhibitor-heparin interactions in the reaction with thrombin. *J. Biol. Chem.* **1988,** *263* (4), 1698-708.

2. Rosenberg, R. D., Role of heparin and heparinlike molecules in thrombosis and atherosclerosis. *Fed. Proc.* **1985,** *44* (2), 404-9.

3. Lindahl, U.; Backstrom, G.; Hook, M.; Thunberg, L.; Fransson, L. A.; Linker, A., Structure of the antithrombin-binding site in heparin. *Proc. Natl. Acad. Sci. U S A* **1979,** *76* (7), 3198-202.

4. Geerts, W. H.; Bergqvist, D.; Pineo, G. F.; Heit, J. A.; Samama, C. M.; Lassen, M. R.; Colwell, C. W., Prevention of venous thromboembolism: American College of Chest Physicians Evidence-Based Clinical Practice Guidelines (8th Edition). *Chest* **2008,** *133* (6 Suppl), 381S-453S.

5. Anderson, J. L.; Adams, C. D.; Antman, E. M.; Bridges, C. R.; Califf, R. M.; Casey, D. E., Jr.; Chavey, W. E., 2nd; Fesmire, F. M.; Hochman, J. S.; Levin, T. N.; Lincoff, A. M.; Peterson, E. D.; Theroux, P.; Wenger, N. K.; Wright, R. S.; Smith, S. C., Jr.; Jacobs, A. K.; Adams, C. D.; Anderson, J. L.; Antman, E. M.; Halperin, J. L.; Hunt, S. A.; Krumholz, H. M.; Kushner, F. G.; Lytle, B. W.; Nishimura, R.; Ornato, J. P.; Page, R. L.; Riegel, B.; American College of, C.; American Heart Association Task Force on Practice, G.; American College of Emergency, P.; Society for Cardiovascular, A.; Interventions; Society of Thoracic, S.; American Association of, C.; Pulmonary, R.; Society for Academic Emergency, M., ACC/AHA 2007 guidelines for the management of patients with unstable angina/non-ST-Elevation myocardial infarction: a report of the American College of Cardiology/American Heart Association Task Force on Practice Guidelines (Writing Committee to Revise the 2002 Guidelines for the Management of Patients With Unstable Angina/Non-ST-Elevation Myocardial Infarction) developed in collaboration with the American College of Emergency Physicians, the Society for Cardiovascular Angiography and Interventions, and the Society of Thoracic Surgeons endorsed by the American Association of Cardiovascular and Pulmonary Rehabilitation and the Society for Academic Emergency Medicine. *J. Am. Coll. Cardiol.* **2007,** *50* (7), e1-e157.

6. Krishna, V. N.; Wille, K.; Tolwani, A., Chapter 29 - Anticoagulation for Continuous Renal Replacement Therapy. In *Handbook of Dialysis Therapy (Fifth Edition)*, Nissenson, A. R.; Fine, R. N., Eds. Elsevier: **2017**; pp 380-385.e1.

7. Merli, G. J.; Groce, J. B., Pharmacological and clinical differences between low-molecular-weight heparins: implications for prescribing practice and therapeutic interchange. *P. T.* **2010,** *35* (2), 95-105.

8. Schulman, S.; Beyth, R. J.; Kearon, C.; Levine, M. N., Hemorrhagic complications of anticoagulant and thrombolytic treatment: American College of Chest Physicians Evidence-Based Clinical Practice Guidelines (8th Edition). *Chest* **2008,** *133* (6 Suppl), 257S-298S.

9. Haqqani, O. P.; Iafrati, M. D.; Freedman, J. E., Chapter 7 - Pharmacology of Antithrombotic Drugs. In *Vascular Medicine: A Companion to Braunwald's Heart Disease (Second Edition)*, Creager, M. A.; Beckman, J. A.; Loscalzo, J., Eds. W.B. Saunders: Philadelphia, **2013**; pp 94-109.

10. Amiral, J.; Bridey, F.; Dreyfus, M.; Vissoc, A. M.; Fressinaud, E.; Wolf, M.; Meyer, D., Platelet factor 4 complexed to heparin is the target for antibodies generated in heparin-induced thrombocytopenia. *Thromb. Haemost.* **1992,** *68* (1), 95-6.

11. Hirsh, J.; Raschke, R., Heparin and low-molecular-weight heparin: the Seventh ACCP Conference on Antithrombotic and Thrombolytic Therapy. *Chest* **2004,** *126* (3 Suppl), 188S-203S.

12. Hirsh, J.; Warkentin, T. E.; Shaughnessy, S. G.; Anand, S. S.; Halperin, J. L.; Raschke, R.; Granger, C.; Ohman, E. M.; Dalen, J. E., Heparin and low-molecular-weight heparin: mechanisms of action, pharmacokinetics, dosing, monitoring, efficacy, and safety. *Chest* **2001,** *119* (1 Suppl), 64S-94S.

13. Kishimoto, T. K.; Viswanathan, K.; Ganguly, T.; Elankumaran, S.; Smith, S.; Pelzer, K.; Lansing, J. C.; Sriranganathan, N.; Zhao, G.; Galcheva-Gargova, Z.; Al-Hakim, A.; Bailey, G. S.; Fraser, B.; Roy, S.; Rogers-Cotrone, T.; Buhse, L.; Whary, M.; Fox, J.; Nasr, M.; Dal Pan, G. J.; Shriver, Z.; Langer, R. S.; Venkataraman, G.; Austen, K. F.; Woodcock, J.; Sasisekharan, R., Contaminated heparin associated with adverse clinical events and activation of the contact system. *N. Engl. J. Med.* **2008,** *358* (23), 2457-67.

14. Guerrini, M.; Beccati, D.; Shriver, Z.; Naggi, A.; Viswanathan, K.; Bisio, A.; Capila, I.; Lansing, J. C.; Guglieri, S.; Fraser, B.; Al-Hakim, A.; Gunay, N. S.; Zhang, Z.; Robinson, L.; Buhse, L.; Nasr, M.; Woodcock, J.; Langer, R.; Venkataraman, G.; Linhardt, R. J.; Casu, B.; Torri, G.; Sasisekharan, R., Oversulfated chondroitin sulfate is a contaminant in heparin associated with adverse clinical events. *Nat. Biotechnol.* **2008,** *26* (6), 669-75.

15. Ohnishi, M.; Urry, D. W., Temperature dependence of amide proton chemical shifts: the secondary structures of gramicidin S and valinomycin. *Biochem. Biophys. Res. Commun.* **1969,** *36* (2), 194-202.

16. Linhardt, R. J.; Liu, J., Synthetic heparin. *Curr. Opin. Pharmacol.* **2012,** *12* (2), 217-9.

17. Walenga, J. M.; Jeske, W. P.; Samama, M. M.; Frapaise, F. X.; Bick, R. L.; Fareed, J., Fondaparinux: a synthetic heparin pentasaccharide as a new antithrombotic agent. *Expert. Opin. Investig. Drugs.* **2002,** *11* (3), 397-407.

18. Choay, J.; Petitou, M.; Lormeau, J. C.; Sinay, P.; Casu, B.; Gatti, G., Structure-activity relationship in heparin: a synthetic pentasaccharide with high affinity for antithrombin III and eliciting high anti-factor Xa activity. *Biochem. Biophys. Res. Commun.* **1983,** *116* (2), 492-9.

19. Bauer, K. A.; Hawkins, D. W.; Peters, P. C.; Petitou, M.; Herbert, J. M.; van Boeckel, C. A.; Meuleman, D. G., Fondaparinux, a synthetic pentasaccharide: the first in a new class of antithrombotic agents - the selective factor Xa inhibitors. *Cardiovasc. Drug Rev.* **2002,** *20* (1), 37-52.

20. Thunberg, L.; Backstrom, G.; Lindahl, U., Further characterization of the antithrombin-binding sequence in heparin. *Carbohydr. Res.* **1982,** *100*, 393-410.

21. Weitz, J. I.; Linkins, L. A., Beyond heparin and warfarin: the new generation of anticoagulants. *Expert. Opin. Investig. Drugs* **2007,** *16* (3), 271-82.

22. Corbett, T. L.; Elher, K. S.; Garwood, C. L., Successful use of fondaparinux in a patient with a mechanical heart valve replacement and a history of heparin-induced thrombocytopenia. *J. Thromb. Thrombolysis* **2010,** *30* (3), 375-7.

23. Ferro, V.; Dredge, K.; Liu, L.; Hammond, E.; Bytheway, I.; Li, C.; Johnstone, K.; Karoli, T.; Davis, K.; Copeman, E.; Gautam, A., PI-88 and novel heparan sulfate mimetics inhibit angiogenesis. *Semin. Thromb. Hemost.* **2007,** *33* (5), 557-68.

24. Fairweather, J. K.; Hammond, E.; Johnstone, K. D.; Ferro, V., Synthesis and heparanase inhibitory activity of sulfated mannooligosaccharides related to the antiangiogenic agent PI-88. *Bioorg. Med. Chem.* **2008,** *16* (2), 699-709.

25. Karoli, T.; Liu, L.; Fairweather, J. K.; Hammond, E.; Li, C. P.; Cochran, S.; Bergefall, K.; Trybala, E.; Addison, R. S.; Ferro, V., Synthesis, biological activity, and preliminary pharmacokinetic evaluation of analogues of a phosphosulfomannan angiogenesis inhibitor (PI-88). *J. Med. Chem.* **2005,** *48* (26), 8229-36.

26. Stevenson, J. L.; Choi, S. H.; Varki, A., Differential metastasis inhibition by clinically relevant levels of heparins--correlation with selectin inhibition, not antithrombotic activity. *Clin. Cancer Res.* **2005,** *11* (19 Pt 1), 7003-11.

27. Inoue, Y.; Nagasawa, K., Selective N-desulfation of heparin with dimethyl sulfoxide containing water or methanol. *Carbohydr. Res.* **1976,** *46* (1), 87-95.

28. Nagasawa, K.; Inoue, Y.; Kamata, T., Solvolytic desulfation of glycosaminoglycuronan sulfates with dimethyl sulfoxide containing water or methanol. *Carbohydr. Res.* **1977,** *58* (1), 47-55.

29. Danishefsky, I.; Eiber, H. B.; Carr, J. J., Investigations on the chemistry of heparin. I. Desulfation and acetylation. *Arch. Biochem. Biophys.* **1960,** *90* (1), 114-21.

30. Naik, S.; Bhattacharjya, G.; Talukdar, B.; Patel, Bhisma, K., Chemoselective Acylation of Amines in Aqueous Media. *Eur. J. Org. Chem.* **2004,** *2004* (6), 1254-1260.

31. Roseman, S.; Ludowieg, J., N-Acetylation of the Hexosamines. *J. Am. Chem. Soc.* **1954,** *76* (1), 301-302.

32. Trombotto, S.; Ladaviere, C.; Delolme, F.; Domard, A., Chemical preparation and structural characterization of a homogeneous series of chitin/chitosan oligomers. *Biomacromolecules* **2008,** *9* (7), 1731-8.

33. Glasoe, P. K.; Long, F. A., USE OF GLASS ELECTRODES TO MEASURE ACIDITIES IN DEUTERIUM OXIDE1,2. *J. Phys. Chem.***1960,** *64* (1), 188-190.

34. Mazak, K.; Beecher, C. N.; Kraszni, M.; Larive, C. K., The interaction of enoxaparin and fondaparinux with calcium. *Carbohydr. Res.* **2014,** *384*, 13-9.

35. Beecher, C. N.; Larive, C. K., (1)H and (15)N NMR Characterization of the Amine Groups of Heparan Sulfate Related Glucosamine Monosaccharides in Aqueous Solution. *Anal. Chem.* **2015,** *87* (13), 6842-8.

36. Seto, S. P.; Miller, T.; Temenoff, J. S., Effect of selective heparin desulfation on preservation of bone morphogenetic protein-2 bioactivity after thermal stress. *Bioconjug. Chem.* **2015,** *26* (2), 286-93.

37. Usov, A. I.; Adamyants, K. S.; Miroshnikova, L. I.; Shaposhnikova, A. A.; Kochetkov, N. K., Solvolytic Desulphation of Sulphated Carbohydrates. *Carbohydr. Res.* **1971,** *18* (2), 336-338.

38. Navarro, D. A.; Flores, M. L.; Stortz, C. A., Microwave-assisted desulfation of sulfated polysaccharides. *Carbohydr. Polym.* **2007,** *69* (4), 742-747.

39. Karunakaran, D. J. S. A.; Ganesh, T.; Sylvester, M. M.; Hudge, P.; Kumbharkhane, A. C., Dielectric properties and analysis of H-bonded interaction study in complex systems of binary and ternary mixtures of polyvinyl alcohol with water and DMSO. *Fluid Phase Equilib.* **2014,** *382*, 300-306.

40. Etchison, J. R.; Holland, J. J., A procedure for the rapid, quantitative N-acetylation of amino sugar methyl glycosides. *Anal. Biochem.* **1975,** *66* (1), 87-92.

41. Chen, J. K.; Shen, C. R.; Liu, C. L., N-acetylglucosamine: production and applications. *Mar. Drugs.* **2010,** *8* (9), 2493-516.

42. Kang, Y. J.; Chung, H. A.; Kim, J. J.; Yoon, Y. J., 2-acylpyridazin-3-ones: Novel mild and chemoselective acylating agents for amines. *Synthesis (Stuttg)* **2002,** *2002* (6), 733-738.

43. Mali, S. M.; Bhaisare, R. D.; Gopi, H. N., Thioacids mediated selective and mild N-acylation of amines. *J. Org. Chem.* **2013,** *78* (11), 5550-5.

44. Sonawane, R. B.; Rasal, N. K.; Jagtap, S. V., Nickel-(II)-Catalyzed N-Formylation and N-Acylation of Amines. *Org. Lett.* **2017,** *19* (8), 2078-2081.

45. Nowotny, A., Reduction of Carbohydrates With NaBH4. In *Basic Exercises in Immunochemistry: A Laboratory Manual*, Nowotny, A., Ed. Springer Berlin Heidelberg: Berlin, Heidelberg, **1979**; pp 196-203.

46. McEwen, I., Broadening of 1H NMR signals in the spectra of heparin and OSCS by paramagnetic transition metal ions. The use of EDTA to sharpen the signals. *J. Pharm. Biomed. Anal.* **2010,** *51* (3), 733-5.

47. Rabenstein, D. L.; Robert, J. M.; Peng, J., Multinuclear magnetic resonance studies of the interaction of inorganic cations with heparin. *Carbohydr. Res.* **1995,** *278* (2), 239-56.

48. Hoult, D. I., Solvent Peak Saturation with Single-Phase and Quadrature Fourier Transformation. *J. Magn. Reson.* **1976,** *21* (2), 337-347.

49. Jones, C. J.; Beni, S.; Limtiaco, J. F.; Langeslay, D. J.; Larive, C. K., Heparin characterization: challenges and solutions. *Annu. Rev. Anal. Chem. (Palo Alto Calif)* **2011,** *4*, 439-65.

50. Guerrini, M.; Elli, S.; Gaudesi, D.; Torri, G.; Casu, B.; Mourier, P.; Herman, F.; Boudier, C.; Lorenz, M.; Viskov, C., Effects on molecular conformation and anticoagulant activities of 1,6-anhydrosugars at the reducing terminal of antithrombin-binding octasaccharides isolated from low-molecular-weight heparin enoxaparin. *J. Med. Chem.* **2010,** *53* (22), 8030-40.

51. Guerrini, M.; Beccati, D.; Shriver, Z.; Naggi, A.; Viswanathan, K.; Bisio, A.; Capila, I.; Lansing, J. C.; Guglieri, S.; Fraser, B.; Al-Hakim, A.; Gunay, N. S.; Zhang, Z. Q.; Robinson, L.; Buhse, L.; Nasr, M.; Woodcock, J.; Langer, R.; Venkataraman, G.; Linhardt, R. J.; Casu, B.; Torri, G.; Sasisekharan, R., Oversulfated chondroitin sulfate is a contaminant in heparin associated with adverse clinical events. *Nat. Biotechnol.***2008,** *26* (6), 669-675.

52. Guerrini, M.; Raman, R.; Venkataraman, G.; Torri, G.; Sasisekharan, R.; Casu, B., A novel computational approach to integrate NMR spectroscopy and capillary electrophoresis for structure assignment of heparin and heparan sulfate oligosaccharides. *Glycobiology* **2002,** *12* (11), 713-9.

53. Chuang, W.-L.; Christ, M. D.; Rabenstein, D. L., Determination of the Primary Structures of Heparin- and Heparan Sulfate-Derived Oligosaccharides Using Band-Selective Homonuclear-Decoupled Two-Dimensional 1H NMR Experiments. *Anal. Chem.* **2001,** *73* (10), 2310-2316.

54. Braunschweiler, L.; Ernst, R. R., Coherence Transfer by Isotropic Mixing - Application to Proton Correlation Spectroscopy. *J. Magn. Reson.* **1983,** *53* (3), 521-528.

55. Aue, W. P.; Bartholdi, E.; Ernst, R. R., Two-dimensional spectroscopy. Application to nuclear magnetic resonance. *J. Chem. Phys.* **1976,** *64* (5), 2229-2246.

56. Bothner-By, A. A.; Stephens, R. L.; Lee, J.; Warren, C. D.; Jeanloz, R. W., Structure determination of a tetrasaccharide: transient nuclear Overhauser effects in the rotating frame. *J. Am. Chem. Soc.* **1984,** *106* (3), 811-813.

57. Claridge, T. D. W., Chapter 9 - Correlations Through Space: The Nuclear Overhauser Effect. In *High-Resolution NMR Techniques in Organic Chemistry (Third Edition)*, Claridge, T. D. W., Ed. Elsevier: Boston, **2016**; pp 315-380.

58. Hwang, T. L.; Shaka, A. J., Water Suppression That Works - Excitation Sculpting Using Arbitrary Wave-Forms and Pulsed-Field Gradients. *J. Magn. Reson. Series A* **1995,** *112* (2), 275-279.

CHAPTER THREE

Probing Salt Bridges in GAGs: A Structural Role for 3-*O*-Sulfated Glucosamine in a Model HS Oligosaccharide

Acknowledgements: I would like to thank the following people for their contributions to this project: Dr. Robert Young for teaching me how to perform MD simulations, Dr. Chad Priest and Dr. De-en Jiang for help with charge assignments in dNSA and use of their computer for the 300 ns MD production run, Dr. Leonard Mueller for the Mathematica nonlinear least squares equation incorporating the effects of radiation damping, and Dr. Dan Borchardt and Dr. Alvicler Magalhaes for help with NMR experimental set up and sharing priceless experience in optimization of NMR operations.

Abstract: Although 3-*O*-sulfated glucosamine residues are rare but important elements of heparan sulfate (HS), the functional and structural roles of this residue remain largely unexplored. In this chapter, a model HS oligosaccharide was synthesized by the selective chemical removal of the *N*-sulfo moieties from the Arixtra^{TM} pentasaccharide to produce de-*N*-sulfated Arixtra^{TM} (dNSA). The resultant zwitterionic dNSA can carry up to seven charges simultaneously and provides an excellent substrate to examine the potential for salt bridge formation in HS. Measurement of the amino proton temperature coefficients and exchange rates, in addition to comparison of the carboxylate and amino pK_a values for Arixtra^{TM} and dNSA, provided evidence of salt bridge existence between the positively charged amino group and adjacent negatively charged 3-*O*-sulfo group in the central

glucosamine residue of dNSA. Evidence is also presented that suggests a possible salt bridge with the carboxylate moiety of the 2-*O*-sulfo iduronic acid carboxylate group in its ionized form. The experimental findings were supported by 300 ns molecular dynamics (MD) simulation results.

3.1. Introduction

The glycosaminoglycan (GAG) heparan sulfate (HS) is a linear polysaccharide consisting of 1,4 - linked repeating disaccharide units with alternating α-D-glucosamine (GlcN) and uronic acid residues (β-D-glucuronic acid (GlcA) or α-L-iduronic acid (IdoA)).[1] Structurally, HS is closely related to heparin but is distinguished by the composition of its major repeating disaccharide units and the ratio of sulfate groups per disaccharide unit (sulfate/hexosamine ratio).[1-4] HS has a 0.8 - 1.8 sulfate/hexosamine ratio with GlcA-GlcNAc as the major repeating disaccharide unit comprising 40 - 60% of the polymer length, whereas heparin has 1.8 - 2.6 sulfate groups per disaccharide unit and the tri-sulfated IdoA2S-GlcNS6S comprises over 70% of the polysaccharide.[1-4] Moreover, HS has greater variability with the regions of high and low sulfation.[1, 5] A high degree of microheterogeneity is introduced into the HS structure by various enzyme complexes during biosynthetic polymeric chain elongation.[1, 6-8] As a result, GlcN residues can be *N*-acetylated (GlcNAc) or *N*-sulfated (GlcNS), while β-D-glucuronic acid (GlcA) can be epimerized to α-L-iduronic acid (IdoA). Furthermore, the activity of different classes of sulfotransferases makes HS even more complex and highly negatively charged by the insertion of sulfo groups at carbons 2, 3, and 6.[1, 6-9]

In organisms, HS is covalently attached to multiple core proteins (proteoglycans) and is localized on the cell membranes, in the extracellular matrix, and in secretory vesicles.[1, 6, 10] HS is involved in the regulation of many essential life processes through its interactions with a variety of protein ligands.[2, 6, 9-12] As mentioned in Chapter 1, the polysaccharide chains of the HS proteoglycan localized on the cell surface[13-15] can non-specifically bind to the herpes simplex virus type 1 (HSV-1) viral glycoproteins gB and gC.[16, 17] However, for further entry of HSV-1 into the cell, fusion between the viral envelop and cell membrane is required, which can occur through specific binding of viral glycoprotein gD with a 3-*O*-sulfated glucosamine (GlcN3S) residue confined within the HS polysaccharide chain.[13-15] For instance, HS polysaccharide chains containing disaccharides composed of IdoA2S-GlcN3S and IdoA2S-GlcN3S6S were reported as possible mediators of HSV-1 entry.[18]

Importantly, the glucosamine 3-*O*-sulfo group, which is critical for binding, is generated through the action of 3-*O*-sulfotransferase isoform 3 (3-*OST*-3), which inserts a sulfate at the 3-OH position of a *N*-unsubstituted glucosamine residue linked to a 2-*O*-sulfated iduronic acid (IdoA2S). Multiple studies have reported that incorporation of 3-*O*-sulfo groups in a polysaccharide sequence defines the activity of HS in many biological processes.[19-24]

Because GlcN3S residues are rare elements in HS polysaccharides, their structural role is largely unknown.[24] Nevertheless, there are at least seven isoforms of 3-*O*-sulfotransferase (3-*OST*) complexes, including 3-*OST*-3 mentioned above, responsible for the addition of sulfates to the 3-OH position in glucosamine residues (including *N*-sulfated

glucosamines).[6, 8, 9, 25] Only two of these isoforms are responsible for production of the antithrombin-binding sequence, whereas the remaining five isoforms generate sequences that facilitate ligand binding distinct from the antithrombin-binding motif.[6, 9, 25]

From the best studied heparin-antithrombin complexes, it is known that the high affinity binding of heparin to antithrombin III is driven by a specific sequence of monosaccharide residues and sulfation patterns, including a required 3-*O*-sulfo group localized in the central *N*-sulfo glucosamine residue.[26-28] However, only recent studies of the synthetic pentasaccharide Arixtra™ (fondaparinux sodium) revealed that a central *N*-sulfated glucosamine sulfamate proton ($-NHSO_3^-$) is involved in a hydrogen bond with the adjacent 3-*O*-sulfo group,[29] suggesting that such structural features of the polysaccharide may have an important role in pre-organizing the secondary structure for its interaction with protein ligands.

Given this context, it is of great importance to continue exploring the structure-function relationships of GAGs. In this chapter, the possibility of salt bridge formation between the negatively charged 3-*O*-sulfo group and the positively charged glucosamine amino group is examined. This non-covalent interaction might be important for pre-organizing HS secondary structure for protein recognition. Moreover, understanding the conditions that promote salt bridge formation could provide insights into the role of GlcN3S in HS and in its interactions with proteins, especially as efforts for the in vitro synthesis of novel oligosaccharide structures continue to advance.[30-33]

Previously, a report from our laboratory described an unsuccessful attempt to identify and characterize a possible salt bridge involving the amino group and adjacent 3-

O-sulfo group in the 3-*O*-sulfated glucosamine (GlcN3S) monosaccharide.[34] Nevertheless, this work laid the foundation for the current work. To the best of our knowledge, there have been no other previous studies to probe a salt bridge formation in GAG oligosaccharides. In an attempt to characterize the salt bridge involving the GlcN3S residue, we adapted the idea that the salt bridge can potentially resemble a combination of electrostatic attraction between a negatively charged 3-*O*-sulfo group and a positively charged amino group, on the one hand, and hydrogen bonding involving a 3-*O*-sulfo group oxygen and an amino group hydrogen, on the other. The difficulty of isolating a GlcN3S containing HS oligosaccharide in sufficient quantities for these experiments was overcome by chemical modification of the synthetic antithrombotic drug Arixtra™. The lack of available reference data for salt bridges in GAGs was resolved by comparison with an *N*-sulfated heparin tetrasaccharide, which was chemically modified through a similar reaction as used for the de-*N*-sulfation of Arixtra™. The heparin tetrasaccharide was selected because it has a structure similar to Arixtra™ but is lacking the 3-*O*-sulfo group. Therefore, it provided an excellent reference for the comparison of physico-chemical properties.

In addition to the de-*N*-sulfation of Arixtra™, Arixtra™ was also selectively *N*-acetylated, as described in Chapter 2, converting the sulfamates to amides groups. The molecular stability of Arixtra™ allowed the preparation three structural analogs differing only in the substituents on the glucosamine nitrogen: the original *N*-sulfated Arixtra™, de-*N*-sulfated Arixtra™, and *N*-acetylated Arixtra™. These three structures provide a unique opportunity to investigate and compare the molecular properties of oligosaccharides differing only in their *N*-substituents. Importantly, work in this dissertation lays the

groundwork for many other opportunities offered by these pentasaccharides ranging from structural to biological studies.

3.2. Experimental Section

3.2.1. Materials and Reagents. Heparin tetrasaccharide ammonium salt (Catalog No HO04) was purchased from Iduron Ltd. (Manchester, UK). Arixtra^{TM} (Fondaparinux sodium), formulated as prefilled syringes for clinical use, was obtained from the University Pharmacy and Department of Pharmacy Administration of Semmelweis University (Budapest, Hungary). Cation exchange resin Dowex 50WX8 hydrogen form (50 - 100 mesh), 3-(trimethylsilyl)-1-propanesulfonic acid-d_6 sodium salt (DSS-d_6, 98% D), ACS grade dimethyl sulfoxide (DMSO), and 35 wt% deuterated hydrochloric acid (DCl, 99% D) were purchased from Sigma-Aldrich (St. Louis, MO). Methanol HPLC grade, pyridine, 12.1 *N* hydrochloric acid, and 50% w/w sodium hydroxide solution were purchased from Thermo Fisher Scientific (Bellefonte, PA). The size-exclusion chromatography resin Sephadex G-10 was purchased from GE Healthcare - Bio Sciences (Pittsburgh, PA). Deuterated acetone (acetone-d_6, 99.9% D), deuterium oxide (D_2O, 99.9% D), 40% w/w sodium deuteroxide (NaOD, 99.5% D), and the low temperature methanol standard were purchased from Cambridge Isotope Laboratories (Andover, MA). The pH meter calibration buffers 2.00, 4.00, 7.00, and 10.00 were purchased from Fisher Scientific (Nazareth, PA). Ultrapure deionized water (18 MΩ/cm) was prepared by the Simplicity UV water purification system from Millipore (Billerica, MA). All pH measurements were performed at room temperature using an AB 15 Accumet Basic pH meter and 9110DJWP, a double-

junction Ag/AgCl micro pH electrode, both from Thermo Scientific (Chelmsford, MA). NMR NE-H5/3-Br tubes were purchased from New Era Enterprises (New Era Enterprises Vineland, NJ). Eppendorf 1.5 mL safe-lock tubes were purchased from Eppendorf (Thermo Fisher Scientific).

3.2.2. Preparation of chemically modified oligosaccharides. The de-*N*-sulfated Arixtra™ (dNSA) and de-*N*-sulfated heparin tetrasaccharide (dNSt) were prepared according to the procedure described in Section 2.2.2. Two batches, 2.7 mg and 2.6 mg, of dNSA were prepared from 6.0 mg and 5.8 mg of Arixtra™, respectively. Additionally, 3.8 mg of dNSt was prepared from 5.0 mg of the heparin tetrasaccharide.1.8 mg of *N*-acetylated Arixtra™ (NAcArixtra) was prepared from 2.0 mg of dNSA according to the procedure described in Section 2.2.3.

3.2.3. Solution preparation and NMR measurements

3.2.3.1. Carbon-bound proton resonance assignments. The chemical shift assignments of the carbon-bound protons in dNSA were performed according to procedure described in Section 2.2.6.1. The carbon-bound proton chemical shifts of dNSt were assigned using a similar strategy, with the key difference being that the spectra of dNSt were acquired using a Bruker Avance spectrometer operating at 599.88 MHz and equipped with a 5 mm TBI probe. Chemical shifts assignments for NAcArixtra were performed according to procedure described in Section 4.2.10.1

3.2.3.2. Amino proton resonance assignment. The chemical shift assignments of the amino protons of dNSA were performed according to the procedure described in Section 2.2.6.2. Similarly, spectra of dNSt were acquired using a Bruker Avance spectrometer

operating at 599.88 MHz equipped with a 5 mm TBI probe. The solution pH was adjusted to 1.6 and the spectra were acquired at 259.5 K.

3.2.3.3. Rates of chemical exchange and temperature coefficient measurements. The freeze-dried dNSA sample used for amino proton resonance assignments (Section 2.2.6.2.) was dissolved in 600 µL of deionized water and split equally into two 1.5 mL Eppendorf tubes. At room temperature, the pH of the two samples was adjusted to 1.6 and 4.1 using 10 mM solutions of HCl and NaOH. Next, a 255 µL aliquot of each pH-adjusted solution was diluted with 45 µL of acetone-d_6 and transferred to an NMR tube for temperature and chemical exchange experiments. Due to the challenges of making reproducible pH measurements in unbuffered solutions, pH values are reported to two significant figures. Both the temperature and chemical exchange experiments were performed using a Bruker Avance spectrometer operating at 599.88 MHz and equipped with a 5 mm TBI probe. Similar conditions were applied to the sample of dNSt.

Temperature experiments were performed over the range from 259.5 K to 286.9 K using one-dimensional ^{1}H NMR. Spectra were acquired using a 90° pulse of 9.6 µs at a power level of -4.00 dB with solvent suppression provided by excitation sculpting. A total of 256 scans were coadded into 32,768 complex points for each spectrum. A spectral window of 7788 Hz and a relaxation delay of 1.5 s were used. Free induction decays (FIDs) were zero-filled to 65,536 points and apodized through multiplication by an exponential function equivalent to a 0.5 Hz line broadening prior to Fourier transformation. At least 7 min was allowed for thermal equilibration of the sample. Sample temperatures were calibrated using the external low temperature methanol standard from Cambridge Isotope

Labs (Andover, MA) and calculated using the Van Geet equation.[35] The spectra were referenced to the ^{1}H resonance of DSS-d_6 (0.00 ppm).

Exchange spectroscopy (EXSY) was used to measure the chemical exchange rates of amino protons with water.[34, 36, 37] The EXSY pulse sequence employed utilizes the basic NOESY pulse sequence incorporating excitation sculpting solvent suppression.[38]A total of twelve EXSY spectra were acquired for each solution. For the pH 1.6 sample, the mixing times ranged from 0 to 66 ms in 6 ms increments while for the pH 4.1 sample, the mixing times ranged from 0 to 44 ms in 4 ms increments. EXSY experiments were performed at 259.7 K using a power level of -4.00 dB and a 90° pulse of 9.62 µs. The spectra were recorded using States-TPPI with 2048 complex points and 128 experiments, each with 32 coadded scans. A spectral window of 7184 Hz was used in both dimensions with a 1.5 s relaxation delay. The EXSY spectra were zero-filled into 16,384 complex points in F2 and 4096 complex points in F1 and apodized using a $\cos^2$ window function. Amino proton – water exchange cross-peaks and diagonal amino proton resonances were extracted into one dimensional spectra using TopSpin 3.2, followed by peak fitting and integration in MestReNova-12.0.1.

3.2.3.4. pK_a determination. The pK_a values of the amino and carboxylate groups of dNSA and dNSt were determined in deuterated solution using ^{1}H and ^{1}H-^{1}H TOCSY experiments to follow the chemical shifts of the H2 resonances of the glucosamine residues and the H5 resonances of the uronic acid residues as a function of pD. The calculated pK_a values determined in the deuterated solvent were mathematically adjusted to pK_a equivalents in water.[36, 39, 40]

Five 1.5 mL Eppendorf tubes each containing 300 µL of dNSA or dNSt solution, prepared as described in Sections 2.2.6.1. and 3.2.4.1, respectively, were individually adjusted to the desired pD using 1 mM, 10 mM, and 100 mM solutions of NaOD and DCl prepared from concentrated solutions by dilution with appropriate volumes of D_2O (99.9% D). Aliquots of 280 µL at each pD were transferred to a clean and dry NMR tube for data acquisition. After the spectrum was recorded, the contents of the NMR tube were transferred back to the 1.5 mL Eppendorf tube and adjusted to a new pD value to continue the titration.

1D ^{1}H and TOCSY NMR spectra were acquired at each pD using a Bruker Avance spectrometer operating at 599.52 MHz and equipped with a BBI probe at 298.2 K. All spectra were acquired using a 90° pulse of 8.9 - 9.1 µs with solvent suppression of the residual HOD resonance by presaturation at a power of 59 dB. The resulting spectra were referenced to the ^{1}H resonance of DSS-d_6 (0.00 ppm).

The 1D ^{1}H NMR spectra were acquired using a spectral window of 6361 Hz, a relaxation delay of 2.0 s, and 56 scans coadded into 42,014 complex points. Spectra were zero-filled to 65,536 points and multiplied by an exponential window function equivalent to 0.4 Hz line broadening prior to Fourier transformation.

Phase-sensitive TOCSY spectra were acquired into 2048 complex points over 416 increments using States-TPPI, a 2.0 s relaxation delay, and a spectral window of 3597 Hz in both dimensions. The spectra were recorded by coaddition of 36 scans using a mixing time of 120 ms with a 36 µs spinlock pulse at a power of 8.2 dB. The FIDs were zero-filled to 4096 × 1024 data points and apodized using a $\cos^2$ window function.

The pK_a values of the amino and carboxylate groups in dNSt were determined similarly, using the Bruker Avance spectrometer operating at 599.88 MHz and equipped with a 5 mm TBI probe.

3.2.4. MD simulation parameters. Starting with Arixtra™ in the conformation it adopts when bound to AT-S195A factor Xa,[29, 36, 41] an AmberTools 16 *xleap*[42] module was used to model the dNSA structure and to generate the parameter, topology, and coordinate files for the molecular dynamics simulation using a GLYCAM 06g force field.[43] GlcN residues were prepared by replacement of each of the *N*-sulfo groups with two additional hydrogens. Partial charge adjustments of the nitrogen and hydrogens of the amino groups were performed based on CH_3-NH_3^+ calculated charges using GAUSSIAN B3LYP/6-31G, giving the amino group a +1 charge overall. The AmberTools 16 *xleap* module was used to add four sodium ions (ff99SB parameters) to dNSA to make the system's overall charge neutral (*addions* function) and to construct a cubic water box with each face a distance 12 Å from the solute (2333 TIP3P water molecules were added for dNSA).[42-45]

Minimization, heating, equilibration, and a molecular dynamics simulation production run were performed using NAMD 2.11.[46] To remove possible bad contacts, conjugate-gradient minimization was performed separately in the following order: solute, solvent, and the entire system. Periodic boundary conditions were applied throughout. The particle mesh Ewald algorithm was used to treat long range electrostatic interactions with the grid spacing set to 1 Å.[47] Non-bonded interactions were cut off at 12 Å and a smooth switching function was applied to 10 Å. The VDW and electrostatic 1-4 scaling factors (*SCNB* and *SCEE*, respectively) were set to unity for consistency with the GLYCAM 06g

parameters.[43] The SETTLE algorithm was used to hold rigid hydrogen-oxygen bonds within water molecules.[48] Slow system heating from 0 K to 298 K was performed in 398 ps, including a 100 ps hold at the 298 K using a constant-*NVE* ensemble. The constant-*NPT* ensemble with a pressure of 1 atm and a temperature of 298 K were used for system equilibration and production run. Control over temperature was performed by using the Langevin thermostat with a damping coefficient of 5 ps^{-1}, while control over pressure was performed by using NAMD's Nosé-Hoover Langevin piston method.[46] Trajectory output was saved every 500 fs with a time step of simulation integration in 1 fs. Monitoring of temperature, pressure, and energy, in addition to trajectory visualization, was performed in VMD 1.9.2.[49] The hydrogen-bonding analysis, including a 3.5 Å heavy-atom cutoff distance and a 120° angle cutoff, was performed using the AmberTools 16 *cpptraj* module.[42]

3.3. Results and Discussion

Both the functional and structural roles of the GlcN3S residues of HS are largely unknown,[24] as the challenges of obtaining sufficient amounts of HS or its oligosaccharides in pure form deters research. In this work, a model HS oligosaccharide was prepared by the de-*N*-sulfation of Arixtra™ (Figures 3.1A and B). The resulting dNSA has a partially zwitterionic structure at neutral pH and can potentially carry up to seven negative and three positive charges simultaneously. One and two-dimensional ^{1}H NMR experiments were utilized to probe the presence of a salt bridge involving the negatively charged 3-*O*-sulfo group of GlcN3S with the adjacent positively charged amino group by the measurement of

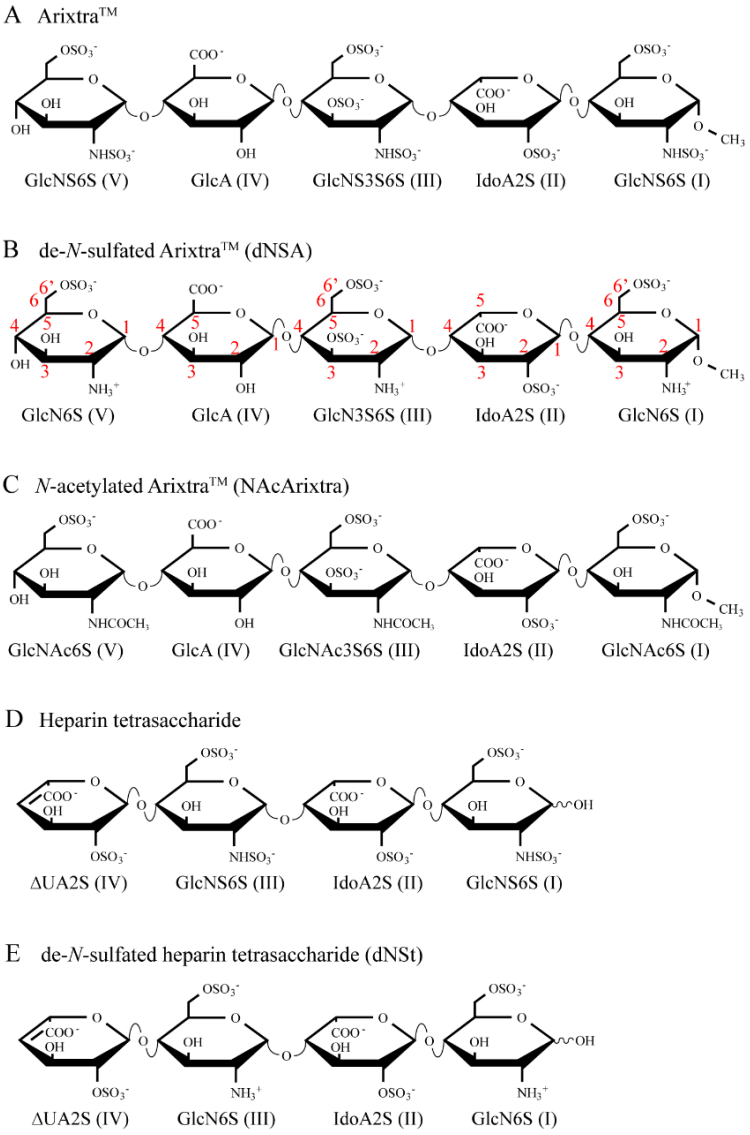

Figure 3.1. Haworth projections of the oligosaccharides: (A) Arixtra™, (B) de-*N*-sulfated Arixtra™ (dNSA), (C) *N*-acetylated Arixtra™ (NAcArixtra), (D) heparin tetrasaccharide, (E) de-*N*-sulfated heparin tetrasaccharide (dNSt). Abbreviated residue names with their relative numbers in an oligosaccharide sequence are shown under each sugar ring. An example of carbon-bound proton numbering order across each residue is shown for dNSA and highlighted in red.

the amino proton temperature coefficients, examination of the chemical exchange properties of the amino groups, and comparison of the pK_a values of the ionizable carboxylate and amino groups. Finally, a complementary 300 ns MD simulation was carried out to provide a molecular perspective of dNSA's structure in aqueous solution.

3.3.1. Chemical shift dependence on *N*-substitution in Arixtra™. Though the focus of current Chapter is the exploration of the properties of de-*N*-sulfated Arixtra™ in solution, he chemical shifts of carbon-bound protons in all three Arixtra™ based pentasaccharides are reported and compared herein (Figure 3.1A, B, and C): *N*-sulfated Arixtra™ (Figure 3.1A), unsubstituted Arixtra™ with free amino groups (Figure 3.1B), and *N*-acetylated Arixtra™ (Figure 3.1C). The unique opportunity, afforded by the chemical modification of Arixtra™ allows us to explore the effect of *N*-substituents on the chemical shifts of the carbon-bound protons. Table 3.1 lists the measured chemical shifts of all the Arixtra™, dNSA, and NAcArixtra protons. The order of proton numbering across each residue is shown in Figure 3.1B. Chemical shifts of overlapped resonances were assigned from COSY spectra and consequently are reported to two decimal places. For easier visualization of the effects of the *N*-substituents on chemical shifts, the data presented in Table 3.1 was transformed into the graph shown in Figure 3.2. In this graph, chemical shifts are plotted along x-axis and protons with corresponding numbers are plotted along y-axis. Dashed lines connect same proton chemical shifts assigned to Arixtra™, dNSA, and NAcArixtra. Here we need to note that chemical shifts of protons in dNSA are especially sensitive to pH variation associated with the carboxylate and amino

Table 3.1. Chemical shifts of carbon-bound protons in Arixtra™ (measured at 295.2 K in solution with pD 7.0),[36] dNSA (measured at 298.2 K in solution with pD 7.5), and NAcArixtra (measured at 298.2 K in solution with pD 7.8)

Residue	Proton	^{1}H Chemical shift, ppm		
		Arixtra™	dNSA	NAcArixtra
GlcNS6S (I) /	1	5.02	4.971	4.75
GlcN6S (I)/	2	3.28	3.305	3.954
GlcNAc6S (I)	3	3.64	3.935	3.81
	4	3.77	3.756	3.73
	5	3.95	4.05	4.012
	6	4.34	4.28	4.30
	6’	4.40	4.37	4.36
	-CH_3	3.41	3.447	3.38
	amide -CH_3	-	-	2.023
IdoA2S (II)	1	5.16	5.250	5.196
	2	4.30	4.33	4.30
	3	4.15	4.33	4.25
	4	4.14	4.18	4.06
	5	4.72	4.869	4.846
GlcNS3S6S (III)/	1	5.52	5.433	5.184
GlcN3S6S (III)/	2	3.44	3.618	4.212
GlcNAc6S (III)	3	4.35	4.556	4.403
	4	3.97	4.013	3.983
	5	4.16	4.13	4.12
	6	4.26	4.27	4.27
	6’	4.48	4.507	4.486
	amide -CH_3	-	-	2.047
GlcA (IV)	1	4.61	4.595	4.602
	2	3.41	3.422	3.363
	3	3.83	3.736	3.690
	4	3.84	3.878	3.79
	5	3.76	3.794	3.85
GlcNS6S (V)/	1	5.62	5.692	5.423
GlcN6S (V)/	2	3.25	3.287	3.90
GlcNAc6S (V)	3	3.62	3.832	3.56
	4	3.57	3.583	3.72
	5	3.88	3.90	3.72
	6	4.15	4.18	4.36
	6’	4.37	4.38	4.73
	amide -CH_3	-	-	2.023

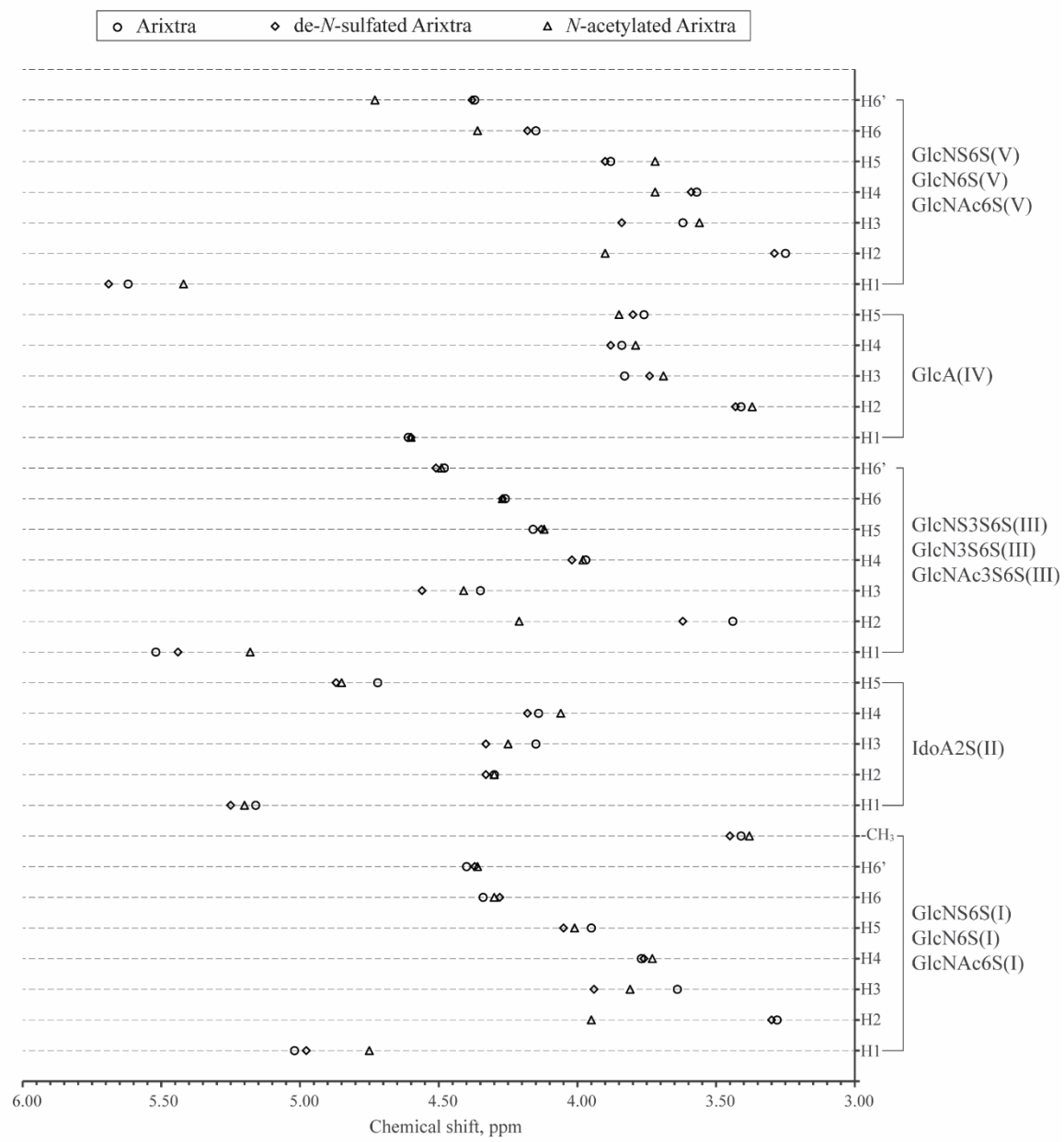

Figure 3.2. Graphical depiction of chemical shifts listed in Table 3.1. Chemical shifts of the Arixtra^{TM} carbon-bound protons for are marked by circles, those of dNSA are marked by diamonds, and for NAcArixtra are marked by triangles.

group ionization states (further discussed in Section 3.3.3). Consequently, it is possible that the reported dNSA chemical shifts will include small deviations when compared to relevant chemical shifts in Arixtra™ (measured at pD 7.0) and NAcArixtra (measured at pD 7.8).

Removal of the bulky *N*-sulfo groups from Arixtra™ caused the H3 resonances in all GlcN residues to be shifted downfield. An interesting observation is made for H2 in 3-*O*-sulfated GlcN3S6S(III) residue, the only H2 proton of the glucosamine residues significantly affected by de-*N*-sulfation. Its resonance is deshielded and appears downfield relative to the corresponding H2 of Arixtra™.

Introduction of the *N*-acetyl groups imparts large chemical shift changes in the H1, H2, and H3 proton resonances of the glucosamine residues relative to Arixtra™ and dNSA. The anomeric protons (H1) of the NAcArixtra glucosamine residues more shielded than in Arixtra™ or dNSA. The H2 proton resonances were downfield shifted as a result of strong deshielding effect exerted by the adjacent *N*-acetyl groups. The H3 chemical shifts were less affected by *N*-acetylation. The H3 chemical shifts of GlcNAc6S(I) and GlcNAc3S6S(III) are found between the H3 resonances of Arixtra™ and dNSA and the H3 of GlcNAc6S(V) is slightly shielded compared to Arixtra™ and dNSA. Only in the GlcNAc6S(V) residue, chemical shifts of even numbered protons are deshielded, while the odd numbered protons are more shielded compared to Arixtra™ and dNSA. This trend may be explained by sugar ring conformational changes of the GlcNAc6S(V) residue, perhaps due to steric crowding between the reducing end O-CH_3 and the *N*-acetyl group.

Variations of the *N*-substituents of Arixtra™ imparted small chemical shift changes in the H3, H4 and H5 resonances of uronic acid residues may be associated with their closer

spatial proximity to the *N*-substituents. A similar, but inverse dependence is observed for H4-6 in first and third glucosamine residues, for H1 in GlcA(IV) and for H2 in IdoA2S(II). However, the unaffected chemical shift of H2 in IdoA2S(IV) can be attributed to its special chemical and magnetic environment due to adjacent 2-*O*-sulfo group.

3.3.2. Temperature coefficients, $\Delta\delta/\Delta T$. Identification of hydrogen bonds in proteins, peptides, nuclei acids and carbohydrates is widely performed through NMR measurements of the temperature coefficients, $\Delta\delta/\Delta T$, of labile protons.[29, 50-58] Because of their prevalence in proteins, temperature coefficients have been widely characterized for amide protons in peptides and proteins, and in this work we apply the same principles to oligosaccharide amino groups. The chemical shifts of labile protons, like those of amide or amino groups, are strongly temperature dependent. Gradual increases in temperature cause an increase in the thermal motion of atoms, which in turn forces the hydrogen bond length to stretch. As the distance between the hydrogen bond acceptor and labile proton group donor increases, the deshielding effect exerted by the acceptor becomes less prominent. This effect can be observed in the ^{1}H NMR spectrum by an upfield shift of the labile proton resonance. This temperature dependence is perhaps most notable for the water (or HOD) ^{1}H NMR resonance. The reason that temperature coefficients can be used to identify labile protons involved in hydrogen bonds is that average lengthening of an intermolecular hydrogen bond distance, for example for an amide proton with bulk water, is greater than for an intramolecular hydrogen bond.[51] As a consequence, labile protons involved in an intramolecular hydrogen bond will have a significantly smaller change in chemical shift

with increasing temperature (a reduced temperature coefficient) than their non-hydrogen bonding counterparts.

Because a salt bridge involving the dNSA amino and 3-*O*-sulfo groups could behave similarly to a hydrogen bond, its presence was probed through the measurement of temperature coefficients. To examine possible electrostatic interactions between the positively charged amino and negatively charged carboxylate groups, as well as the possibility that the GlcA(IV) and IdoA2S(II) carboxylate groups could polarize the amino N–H bonds through their nearby negative charge, temperature coefficients and solvent exchange rate measurements for the dNSA amino protons were performed at two pH values, 1.6 and 4.1. It is expected that at pH 1.6, the carboxylate groups are mostly protonated and therefore largely uncharged, and that at pH 4.1, they are mostly deprotonated and hence carry a negative charge. In contrast, the 3-*O*-sulfo group should be consistently negatively charged over this pH range. Lower and higher pH conditions were avoided because lower pH can affect the stability of the sugar and higher pH promotes faster amino protons solvent exchange rates that would cause problems detecting the amino resonances.[34]

Figure 3.3A shows a portion of the ^{1}H NMR spectrum of dNSA highlighting the effect of gradual temperature increase on the amino protons resonance at pH 1.6 and 4.1. The magnitude of the chemical shift change with temperature for the GlcN3S6S(III) is significantly less than is observed for the other amino groups at both pH values, suggesting possible involvement in a hydrogen bond with the adjacent 3-*O*-sulfo group. Figure 3.3B highlights reduced intensity of the GlcN3S6S(III) amino resonance at pH 4.1 in result of

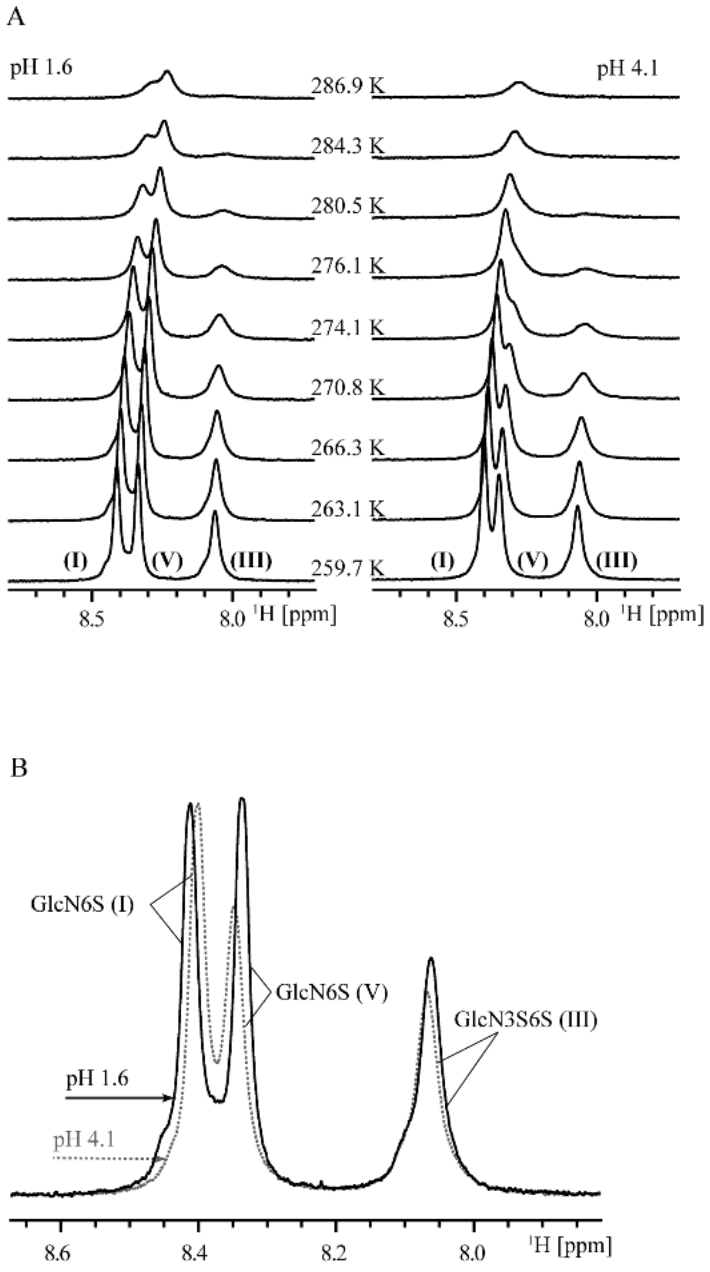

Figure 3.3. (A) The region of the ^{1}H NMR spectrum of dNSA showing the temperature dependence of the amino proton resonances at pH 1.6 and 4.1. Amino resonances are labeled according to residue number (Figure 3.1). (B) Comparison of the amino protons resonance linewidths at pH 1.6 and 4.1 and 259.7 K.

faster chemical exchange. Note that in Figure 3.3B the linewidth of amino proton in GlcN6S(I) is almost unaffected by the pH change, while resonance of amino proton in GlcN6S(V) broadens and shifts downfield at higher pH, suggesting dependence on the ionization state of the adjacent GlcA(II) carboxylate group.

Quantitatively, the effect of temperature on the chemical shifts of labile protons is represented by temperature coefficients ($\Delta\delta/\Delta T$) calculated from the absolute value of the slope of the line obtained by plotting amino group proton chemical shift as a function of temperature (Figure 3.4). Calculated $\Delta\delta/\Delta T$ values for the amino resonances of the de-*N*-sulfated oligosaccharides are provided in Table 3.2. Significantly smaller $\Delta\delta/\Delta T$ values were obtained for the dNSA amino resonance of GlcN3S6S(III) (1.22 ± 0.03 ppb/K and 1.92 ± 0.05 ppb/K at pH 1.6 and 4.1, respectively) compared to all other amino groups. This small temperature coefficient suggests the involvement of the GlcN3S6S(III) amino protons in a hydrogen bond.[29] Moreover, the small $\Delta\delta/\Delta T$ values obtained at the lower pH limits support the hydrogen bonding and possible salt bridge formation with the GlcN3S6S 3-*O*-sulfo group because at pH 1.6 the carboxylate groups are mostly protonated.

The large temperature coefficients measured for dNSt further support a hydrogen bond in dNSA involving the GlcN3S6S(III) amino group. The amino temperature coefficients of the internal GlcN6S(III) residue in dNSt are 4.01 ppb/K and 4.33 ppb/K at pH 1.6 and 4.1, respectively, and are comparable to non-hydrogen bonded amino protons in dNSA. Note, in contrast to dNSA, dNSt has its anomeric carbon at the reducing end residue GlcN6S(I) and consequently two anomers are present in solution. However, the

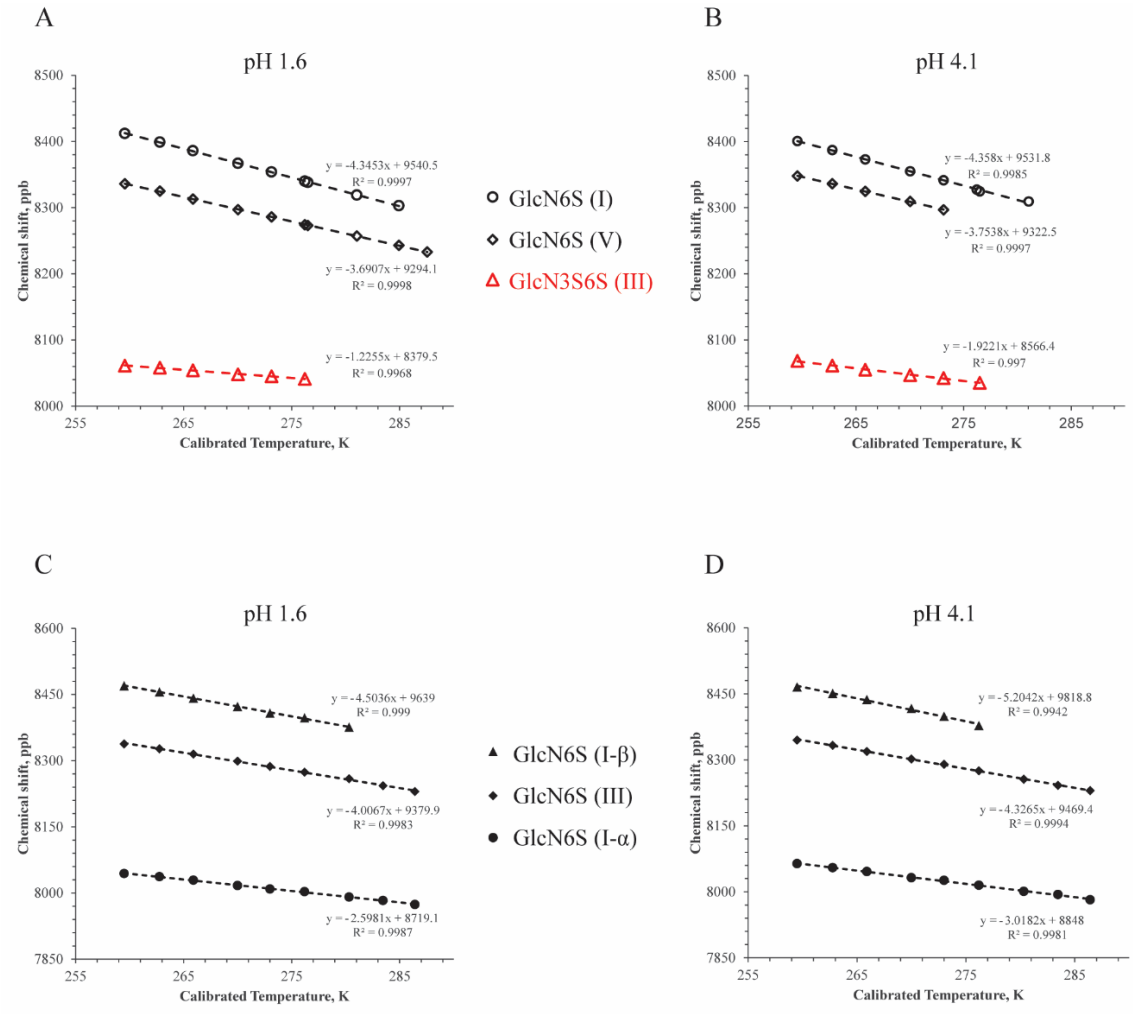

Figure 3.4. Temperature coefficient plots of amino proton chemical shifts measured at pH 1.6 and 4.1 for dNSA (A and B), and dNSt (C and D), respectively. Chemical shifts were plotted as a function of the calibrated temperature and the absolute value of the slope represents the temperature coefficient.

Table 3.2. Summary of the dNSA and dNSt temperature coefficients (Δδ/ΔT), exchange rate constants (k_{ex}) and pK_a values. Exchange rates were measured at 259.7 K. pK_a values were determined at 298.2 K. All pK_a values measured in D_2O are reported as their water equivalents.

Oligosaccharide	Δδ/ΔT, ppb/K		k_{ex}, s^{-1}		pK_a	
	pH 1.6	pH 4.1	pH 1.6	pH 4.1	de-*N*-sulfated	*N*-sulfated
dNSA						
GlcN6S(V)	3.69 ± 0.02	3.75 ± 0.04	4.1 ± 0.1	17.0 ± 0.1	8.36 ± 0.02	
GlcA(IV)					3.51 ± 0.02	3.49 ± 0.05[a]
GlcN3S6S(III)	1.22 ± 0.03	1.92 ± 0.05	25.4 ± 0.2	34.3 ± 0.2	8.17 ± 0.01	
IdoA2S(II)					2.81 ± 0.04	3.40 ± 0.05[a]
GlcN6 (I)	4.35 ± 0.03	4.36 ± 0.07	6.5 ± 0.1	8.8 ± 0.1	8.31 ± 0.02	
dNSt						
ΔUA2S(IV)					2.87 ± 0.02	2.98 ± 0.03
GlcN6S(III) α	4.01 ± 0.06	4.33 ± 0.04	4.0 ± 0.1	12.6 ± 0.1	8.30 ± 0.01	
GlcN6S(III) β			5.1 ± 0.1			
IdoA2S(II) α					3.03 ± 0.02	3.42 ± 0.02
IdoA2S(II) β					2.98 ± 0.02	3.46 ± 0.02
GlcN6S(I) α	2.60 ± 0.03	3.02 ± 0.05	4.2 ± 0.1	11.4 ± 0.1	8.59 ± 0.02	
GlcN6S(I) β	4.50 ± 0.06	5.20 ± 0.20	9.8 ± 0.1	17.4 ± 0.1	8.99 ± 0.02	

[a] pK_a values of the Arixtra™ carboxylates were determined previously.[36]

temperature coefficients measured for GlcN6S(I-α) and GlcN6S(I-β) are not relevant to the internal residue of the oligosaccharide and consequently will be omitted from further discussion.

In addition to reporting on the temperature dependence of the resonance chemical shift, Figure 3.3. also provides insights about the effects of temperature on resonance linewidths. As the temperature is increased, greater broadening is observed at both pH values for the amino resonance of GlcN3S6S(III) compared with the resonances of GlcN6S(V) and GlcN6S(I) residues. For labile protons, a greater resonance linewidth indicates faster chemical exchange with water. This result is strikingly different from the reduced linewidths, and therefore reduced exchange rates reported for amide, sulfamate, and hydroxyl protons involved in hydrogen bonds.[29, 37, 54, 57-60] This result suggests that amino protons in close spatial proximity to negatively charged groups might experience an acceleration of the exchange rates, perhaps due to the presence of a salt bridge.[61]

3.3.3. Measurements of solvent exchange rates. To verify the faster solvent exchange rates suggested by the greater degree of line broadening of the dNSA GlcN3S6S(III) amino resonance in Figure 3.3, exchange rates for the amino groups of dNSA and dNSt were measured using the EXSY pulse sequence.[34, 36, 37] Though only one of the three glucosamine residues of dNSA contains a 3-*O*-sulfo group, the position of this amino in the center of the pentasaccharide raises the possibility the glucosamine residues at the reducing and non-reducing ends experience less line broadening with temperature simply because of their position in the oligosaccharide sequence. Performing similar

measurements for the de-*N*-sulfated heparin tetrasaccharide allows us to test this hypothesis.

As shown in Figure 3.5, incrementally increasing the EXSY mixing time increases the intensities of the amino solvent exchange cross-peaks. Compared with the other dNSA and dNSt amino protons, the cross-peak intensity for the dNSA GlcN3S6S(III) amino (highlighted in red in Figure 3.5) appears to increase most rapidly with increased mixing time at both pH values studied. To quantitatively evaluate the differences between the amino groups, cross-peak intensities were extracted into one-dimensional spectra, integrated, and normalized to the intensity of the corresponding diagonal peak. The results were plotted as a function of mixing time generating the build-up curves shown in Figure 3.6. These build-up curves further support the accelerated exchange of the amino protons of GlcN3S6S(III) relative to the other amino groups of dNSA as well as the dNSt internal GlcN6S(III) residue. Faster build-up for the amino protons in GlcN3S6S(III) is observed at both pH values. In contrast, the build-up rates of the dNSA GlcN6S(V) amino protons were significantly accelerated at pH 4.1 likely due to the spatial proximity of the carboxylate group of the adjacent GlcA(II) residue. Note that build-up rates of the amino protons in GlcN6S(I), GlcN6S(III), and GlcN6S(I-α/β) were relatively unaffected by the change in the ionization state of carboxylate groups.

Exchange rates (k_{ex}) were quantitatively extracted from individual EXSY build-up curves by fitting with the nonlinear least squared equation derived earlier by Beecher et al. for the hydroxyl and amino protons (Eq. 3.1)[34, 36, 53] using Mathematica[61] and are summarized in Table 3.2.

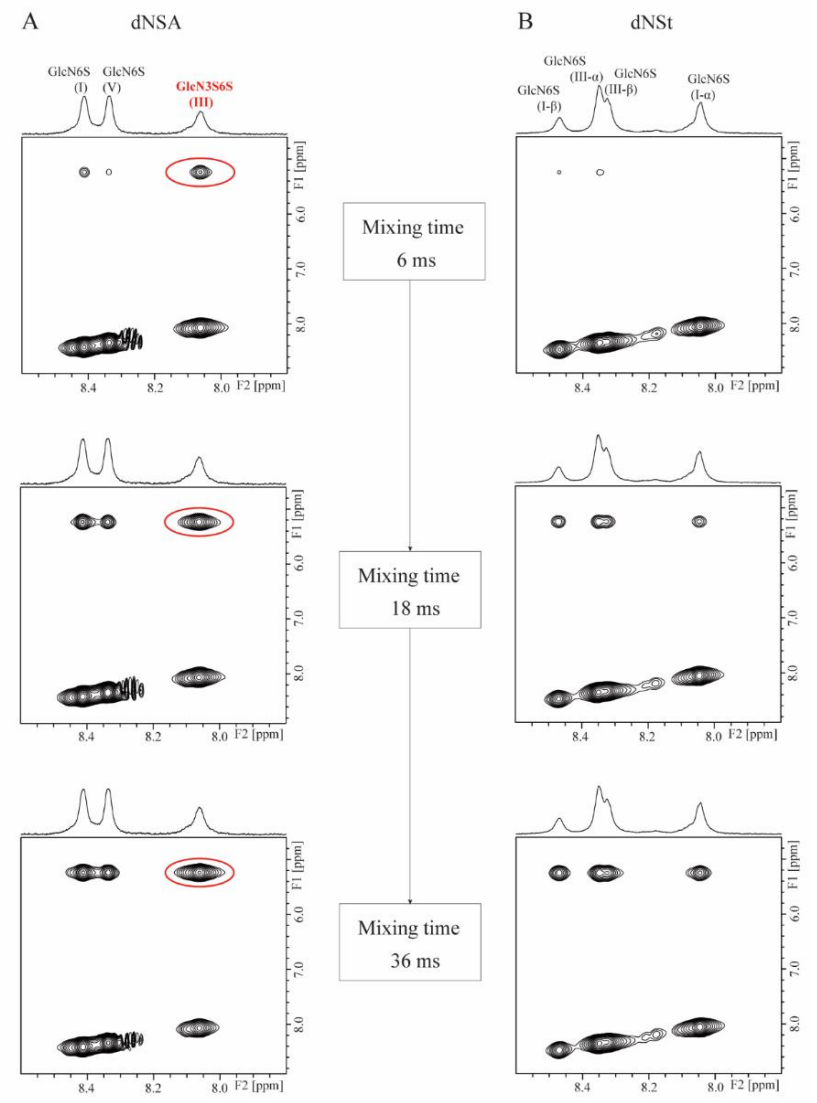

Figure 3.5. Example of EXSY spectra of (A) dNSA and (B) dNSt measured at pH 1.6. Selected spectra with mixing times 6 ms, 18 ms, and 36 ms show differences in the exchange cross-peak intensity for each amino group. Traces through the exchange cross-peaks at the water chemical shift (≈ 5.2 ppm along the F1 dimension) are plotted at the top of each contour map. Notably higher intensity is observed for the GlcN3S6S(III) amino group exchange cross-peak (highlighted in red) relative to other amino groups containing residues confined in the dNSA and dNSt oligosaccharides.

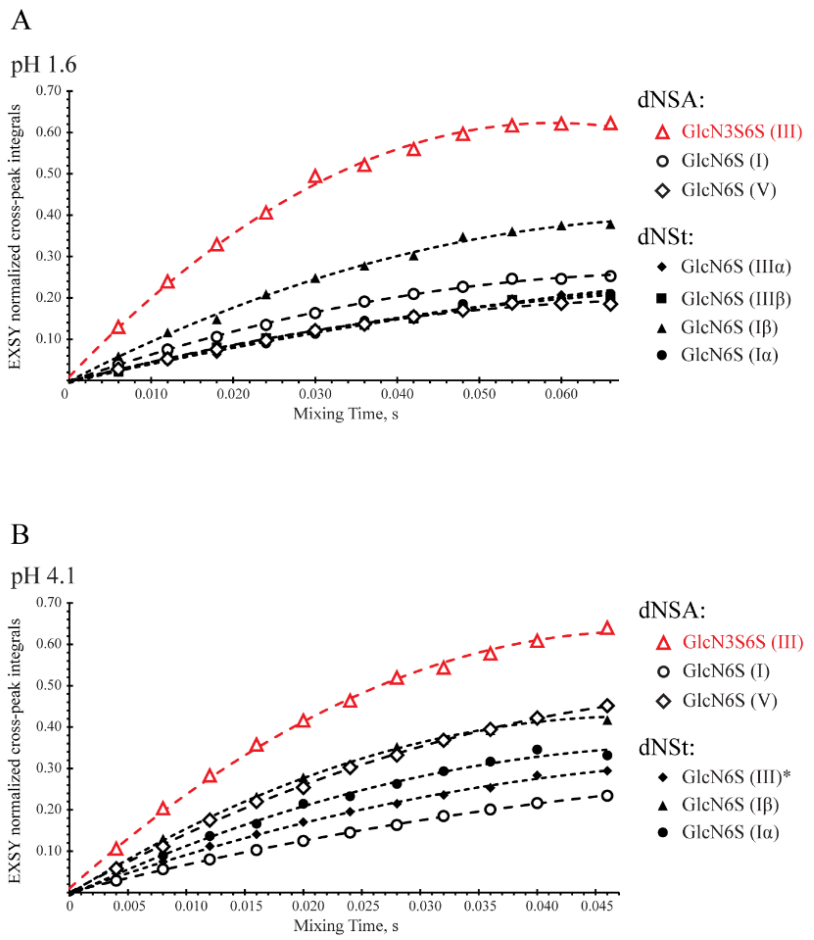

Figure 3.6. EXSY build-up curves for the solvent exchange of the amino protons of dNSA and dNSt measured at (A) pH 1.6 and (B) 4.1 in 85% H_2O/15% acetone-d_6.

* Measurement of individual exchange rates of the dNSt amino protons of the GlcN6S(III) α and β anomers at pH 4.1 was not possible because of resonance overlap, therefore, only the average exchange rate is reported.

$$\frac{M_{analyte,z}(t)}{M^{o}_{analyte,z}} = 1 - e^{-kt} + \\ + \frac{e^{2(t-t_0)/T_{RD}}k}{k+2/T_{RD}}\,{}_2F_1\left[1, \frac{2+kT_{RD}}{2}; \frac{4+kT_{RD}}{2}; -e^{2(t-t_0)/T_{RD}}\right] + \\ + \frac{e^{-kt-2t_0/T_{RD}}k}{k+2/T_{RD}}\,{}_2F_1\left[1, \frac{2+kT_{RD}}{2}; \frac{4+kT_{RD}}{2}; -e^{-2t_0/T_{RD}}\right] \quad \text{(Eq. 3.1)}$$

Notably, the amino proton exchange rates increase as the pH is raised from 1.6 to 4.1. For instance, the largest increase in exchange rates was observed for GlcN6S(V) in dNSA which changed from 4.08 s^{-1} to 17.04 s^{-1} (Δk_{ex} = 12.96 s^{-1}). Slightly lower increases in the exchange rate were observed for the dNSA GlcN3S6S(III) (Δk_{ex} = 8.90 s^{-1}), and the GlcN6S(III α/β) (average Δk_{ex} = 8.2 s^{-1}) and GlcN6S(I α/β) (average Δk_{ex} = 8.2 s^{-1}) in dNSt. The smallest increase in exchange rates was observed for the GlcN6S(I) residue (Δk_{ex} = 2.3 s^{-1}) of dNSA. However, the pH dependence of the exchange rates is expected accordingly to Eq. 1.2.[62] This equation dictates that solvent exchange reaction (Figure 1.8) can be acid or base catalyzed. The rate constants for the acid (k_{H^+}) and base (k_{OH^-}) catalyzed reactions are not equal and depend on the nature of the labile proton functional group and its local environment.

In terms of the overall magnitude of the exchange rate, the values of k_{ex} for dNSA GlcN3S6S(III) (k_{ex} = 25.4 s^{-1} at pH 1.6 and 34.4 s^{-1} at pH 4.1) are significantly larger than the values for other amino groups at both pH values, and is likely due the close proximity of the 3-*O*-sulfo group, which remains deprotonated even at pH 1.6. A possible explanation for this effect is that the exchange driven by general-base catalysis promoted by the neighboring negatively charged sulfate, a mechanism that was proposed previously for

amino-carboxylate salt bridges in proteins.[61] Another plausible explanation is the polarization of water molecules surrounding two oppositely charged groups, which in turn promotes accelerated exchange. In either case, the effect of nearby negatively charged moieties on the amino proton exchange rate should decrease as the distance separating the charged groups increases. Therefore, acceleration of exchange rates (in the absence of other factors, such as salt concentration, solution composition, temperature, etc.) indicates the possibility of charge-charge interaction and spatial proximity of the negatively charged group to the positively charged amino group. This also explains the observation made for the dNSA GlcN6S(V) that the exchange rate jumped from 4.08 s^{-1} to 17.04 s^{-1} (Δk_{ex} = 12.96 s^{-1}) as the nearby GlcA carboxylate group was deprotonated. The accelerated exchange rates promoted by the close spatial proximity of negatively charged groups and the possibility of electrostatic attraction with the positively charged amino group can be further evaluated through measurement of the pK_a values of ionizable groups.

3.3.4. Comparison of pK_a values. The identification of salt bridges in proteins has been established through comparison of the pK_a values of ionizable amine, guanidium and carboxylate groups of the amino acid side chains.[61, 63-67] In proteins, the formation of a salt bridge alters the pK_a values of the ionizable groups involved in the electrostatic interaction and a similar principle could be applied to GAG oligosaccharides. It is expected that if the amino group of a GlcN3S6S(III) residue is involved in a salt bridge with an adjacent 3-*O*-sulfo group, the pK_a of amino group would be altered relative to its normal values (e.g. in absence of a salt bridge). However, unlike proteins, where the difference in pK_a of ionizable groups can be measured by the folding and unfolding of the protein,[64] identification of pK_a

differences in GAG oligosaccharides requires another approach. In this section the pK_a values of the amino and carboxylate groups of dNSA and dNSt are compared based on the similarity of their residue composition, saccharide sequence order, and oligosaccharide length. The pK_a of the GlcN3S6S(III) amino was compared to the pK_a values for the aminos in 6-*O*-sulfated glucosamine residues lacking a 3-*O*-sulfo group, such as GlcN6S(I) and GlcN6S(V) in dNSA, and the internal GlcN6S(III) residue of dNSt.

Experimentally, pK_a values can be conveniently determined by monitoring the ^1H NMR spectrum over the course of a pH titration.[34, 36, 61, 63] The versatility of NMR spectra allows simultaneous determination of the pK_as of all ionizable groups within an oligosaccharide. Moreover, due to the capability of NMR to detect small changes in the magnetic and chemical environments of the spin systems, direct detection of the amino and carboxylate group protons is unnecessary. The pK_a can be determined by following the chemical shifts of the carbon-bound protons adjacent to the amino and carboxylate group, specifically (H2) for the amino containing glucosamine residues and (H5) for carboxylate containing uronic acid residues (numbering nomenclature is shown in Figure 3.1B). To reduce the interference from the water resonance, NMR spectra of the oligosaccharides were acquired in D_2O and the solution pD adjusted using DCl and NaOD.[68] The relationship between the pH meter reading (pH^*) of a D_2O solution and pD is established by Eq. 3.2:[36, 39]

$$pD = pH^* + 0.40 \qquad \text{(Eq. 3.2.)}$$

Figure 3.7 shows the effect of pD on the proton chemical shifts of dNSA. In large molecules such as proteins, a change in ionization states of one group involved in a salt bridge affects the chemical shift of the other group allowing identification of the salt bridging pairs. However, because dNSA is a small flexible molecule, changes in the ionization state of the carboxylate and amino groups propagate through the oligosaccharide affecting nearly all dNSA's protons and making identification of the potential salt bridge pairs by observation unfeasible. Though the one-dimensional ^{1}H NMR spectrum provides insights into the resonance chemical shift dependence on pD, it suffers from low dispersity within the 3.3 – 4.5 ppm spectral window, which interferes with observation of the H5 in GlcA(IV) and H2 in GlcN3S6S(III) resonances for pK_a determination. Consequently, chemical shifts were also determined using TOCSY spectra acquired in parallel with the one-dimensional spectra.

Figure 3.8 shows the pD titration curves of the five ionizable groups of dNSA, highlighting the effect of the protonation state of the GlcA(IV) and IdoA2S(II) carboxylate groups on the chemical shifts of H2 protons of the GlcN6S(V) and GlcN3S6S(III) residues at low pD. Similarly, the deprotonation of the amino groups affected the chemical shifts of the H5 protons of GlcA(IV) and IdoA2S(II) at higher pD. Notably, deprotonation of both carboxylates affected the chemical shifts of the GlcN6S(I) H2 resonance to a much smaller extent, but interestingly the exchange rates of the amino protons in the same residue experienced the smallest dependence on the ionization states of carboxylates (Δk_{ex}=2.3s^{-1}). These observations suggest that the carboxylate in IdoA2S(II) and the amino group in GlcN6S(I) are separated from each other.

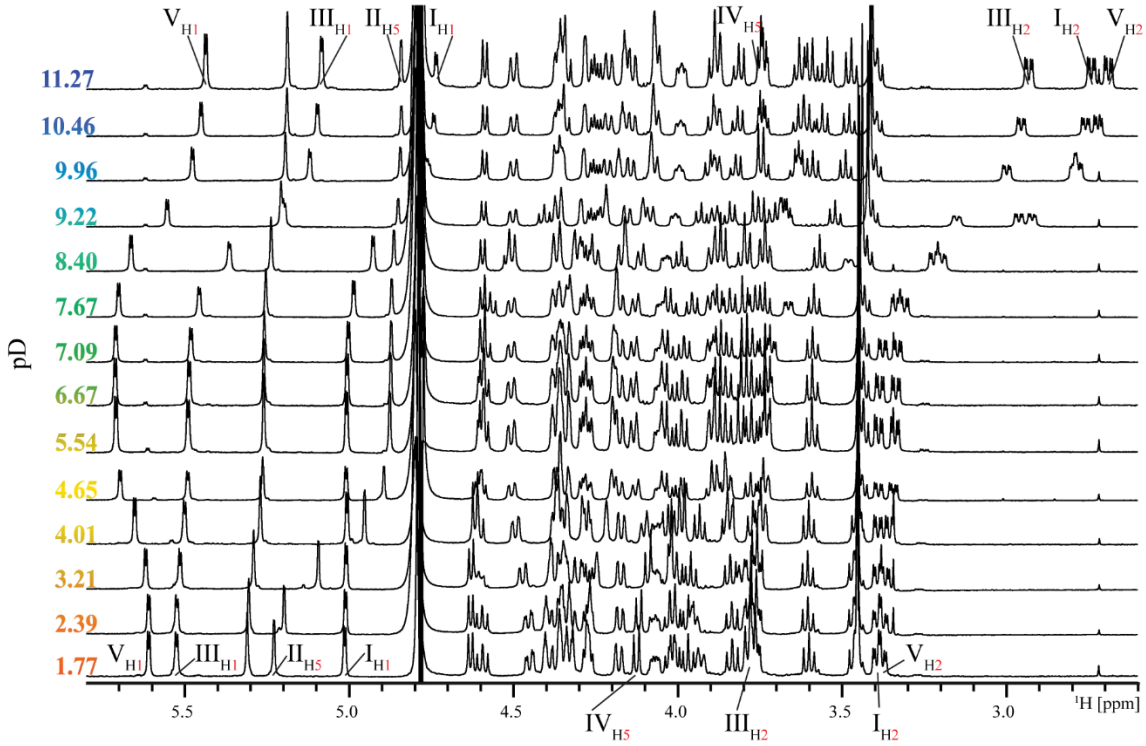

Figure 3.7. pD titration of the dNSA in deuterated 10 mM phosphate buffer. ^{1}H NMR spectra acquired as a function of pD reflect the effect of solution pD on the chemical shifts of carbon-bound protons in dNSA. Resonances are labeled according to the dNSA residue number with the subscript indicating the corresponding proton number within a given residue (see Figure 3.1B). The sequential deprotonation of ionizable groups induces chemical shifts changes. The most highly affected proton resonances were those in close spatial proximity to ionizable groups.

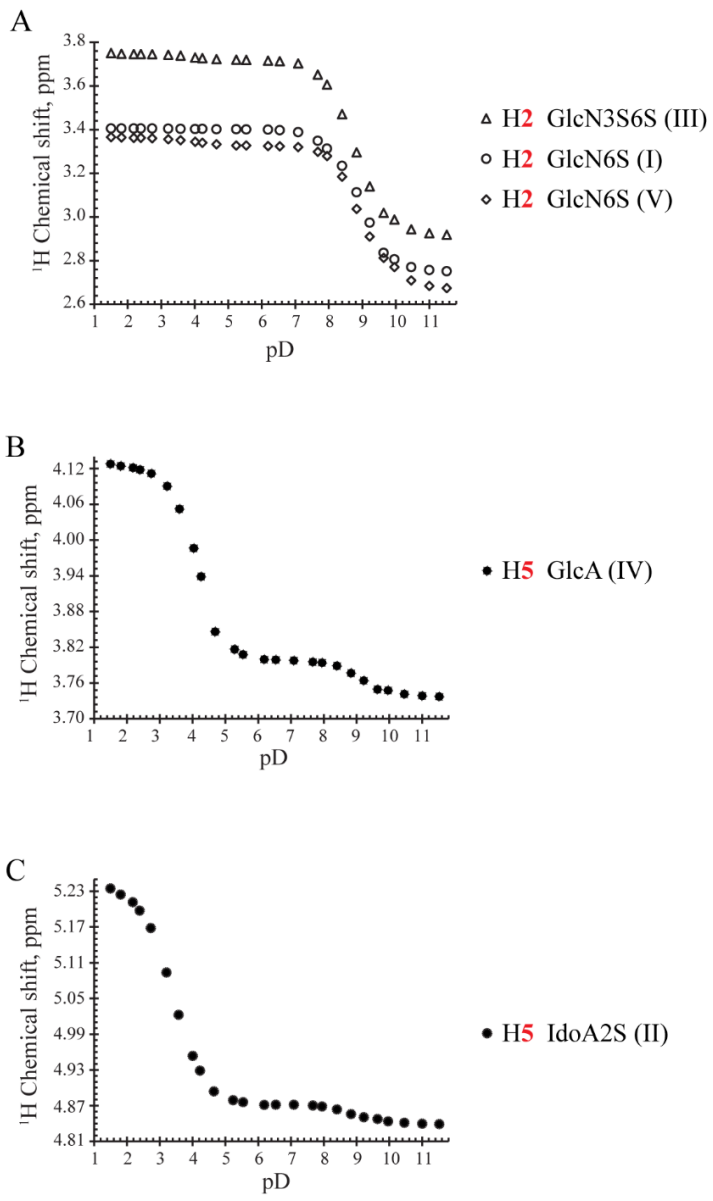

Figure 3.8. pD titration curves obtained through TOCSY experiments for (A) H2 protons in amino containing residues and (B and C) H5 protons for carboxylate containing residues. H2 protons in GlcN3S6S (III) and GlcN6S(V) residues showed sensitivity to changes in ionization state of carboxylates. Reciprocally, the H5 protons of GlcA(II) and IdoA2S(IV) were sensitive to changes in the ionization states of the amino groups.

The pK_a values in D_2O were determined by plotting the observed chemical shifts (δ_{obs}) of the carbon-bound protons H5 and H2 as a function of pD (Figure 3.7), followed by fitting with Eq. 3.3 using Mathematica:[69]

$$\delta_{obs} = \delta_u + \frac{\delta_p - \delta_u}{1 + 10^{n(pK_a - pH)}} \quad \text{(Eq. 3.3.)}$$

In Eq. 3.3, δ_p is the chemical shift of the protonated form (carboxylate -COOH or amino $-NH_3^+$), δ_u is the chemical shift of the deprotonated form (carboxylate $-COO^-$ and amine $-NH_2$), and *n* is the Hill coefficient, which in our case is equal to 1.[34, 70, 71] Conversion of the pK_a (D_2O) values to equivalent values in aqueous solution, pK_a (H_2O), was performed by using Eq. 3.4:[36, 40]

$$pK_a\,(H_2O) = pK_a\,(D_2O) - 0.6 \quad \text{(Eq. 3.4.)}$$

Table 3.2 lists the pK_a values determined for dNSA, dNSt, and heparin tetrasaccharide, as well as the literature pK_a values for the carboxylates of Arixtra™.[36] Comparison of the carboxylate group pK_as of the *N*-sulfated and de-*N*-sulfated forms of the same residue in dNSt reveals that the removal of *N*-sulfo group reduced the carboxylate pK_a of the IdoA2S(II) residues by approximately 0.4 pH units. In dNSA, the pK_a of the GlcA(IV) carboxylate was unaffected by de-*N*-sulfation, while carboxylate pK_a of the IdoA2S(II) was reduced by 0.6 units from its relative value in Arixtra™ and is 0.2 units lower than pK_a in IdoA2S(II) of the dNSt, suggesting its possible involvement in a salt bridge. Because the unsaturated uronic acid (ΔUA2A) in dNSt is introduced by the

enzymatic depolymerization reaction and is not found in intact GAGs, it will be omitted from further discussion.

Through the comparison of amino group pK_a values in Table 3.2, it is apparent that the pK_a (8.17) of dNSA GlcN3S6S(III) is smaller than the pK_a values of the other aminos in dNSA and dNSt, which are around 8.3. Normally, a higher amino group pK_a would be expected in the presence of a salt bridge, so at first glance this value is not consistent with the reduced temperature coefficient and enhanced exchange rates of the dNSA GlcN3S6S(III) amino protons, which both suggest salt bridge participation. However, because the reduced pK_a measured for IdoA2S(II) suggests its involvement in a salt bridge, we raised the question about its possible interaction with amino group in adjacent GlcN3S6S(III) residue.

Interpreting differences in the pK_a of a carboxylate or amino group in isolation neglects that fact that it is the overall stabilization produced by ion pairing that must be considered. Changes in the pK_a values of salt bridging pairs in proteins can be interpreted in terms of the free energy difference, $\Delta\Delta G_u$ (kJ/mol), which can predict the contribution of the charged site (*i*) to the stability of the protein by following Eq. 3.5:

$$\Delta\Delta G_u^{\,i} = 2.3RT(pK_a^{U,i} - pK_a^{F,i}) \qquad \text{(Eq. 3.5.)}$$

where $pK_a^{U,i}$ and $pK_a^{F,i}$ are pK_a values of *i* in unfolded and folded states, respectively.[64, 72] This equation can be adapted to GAG oligosaccharides as follows: $\Delta\Delta G_u^{\,i} = 2.3RT(pK_a^{\text{no salt bridge},i} - pK_a^{\text{salt bridge},i})$, where $pK_a^{\text{no salt bridge},i}$ and $pK_a^{\text{salt bridge},i}$ are values measured for *i* without and with the salt bridge, respectively. Consequently, if a carboxylate group

participates in a salt bridge and contributes to the stability of the oligosaccharide, then $\Delta\Delta G_u^{-COOH}$ will be positive; if the amino group participates in a salt bridge and contributes to the stability of GAG, then $\Delta\Delta G_u^{-NH3^+}$ is expected to be negative.[64] The approximate value for $\Delta\Delta G_u^{-COOH}$ for the carboxylate of IdoA2S(II) in dNSA was +1.37 kJ/mol (with $pK_a^{\text{no salt bridge}} = 3.00$, and $pK_a^{\text{salt bridge}} = 2.81$). Therefore, it is expected that this group stabilizes the GAG structure. However, an approximation of $\Delta\Delta G_u^{-NH3^+}$ for the amino group of GlcN3S6S(III) in dNSA in a salt bridge with the adjacent carboxylate group in IdoA2S(II) was +0.97 kJ/mol (with $pK_a^{\text{no salt bridge}} = 8.34$ (an average pK_a of GlcN6S(I) and GlcN6S(V)), and $pK_a^{\text{salt bridge}} = 8.17$), which destabilizes the dNSA. However, this unfavorable effect of the charged group on dNSA structure does not completely cancel out overall stabilization estimated from the existence of the salt bridge.

3.3.5. Comparison of coupling constants. Finally, one-dimensional spectra acquired at different pD values allow the measurement of three bond coupling constants which can reflect pH dependent conformational changes (Table 3.3). At low pD (1.77), the amino groups are positively charged and carboxylates mostly carry no charge; at intermediate pD (7.67), the amino groups and carboxylates are both charged; and at high pD (11.27), the amines are mostly neutral, and carboxylates are charged (Table 3.3). The three bond coupling constants for the dNSA GlcN3S6S(III) H1 and H2 ($^3J_{H1\text{-}H2}$) change consistently through these three molecular ionization states. At low pD, the $^3J_{H1\text{-}H2}$ is 3.9 Hz; at intermediate pD it is 3.7 Hz; and at high pD it is 3.5 Hz. Changes in the coupling constant of H1 are likely driven by changes in the molecular conformation associated with differences in charge-charge interactions resulting from deprotonation of the IdoA2S(II)

Table 3.3. $^{3}J_{H\text{-}H}$ constants of dNSA measured at 298.2 K

Residue	Proton	$^{3}J_{H\text{-}H}$	pD 1.77		pD 6.67		pD 11.27	
			δ, ppm	$^{3}J_{H\text{-}H}$, Hz	δ, ppm	$^{3}J_{H\text{-}H}$, Hz	δ, ppm	$^{3}J_{H\text{-}H}$, Hz
GlcN6S(V)								
	I_{H1}	$^{3}J_{1\text{-}2}$	5.610	3.7	5.701	3.7	5.436	3.7
	I_{H2}	$^{3}J_{1\text{-}2}$	3.377	3.7	3.336	3.7	2.690	3.8
		$^{3}J_{2\text{-}3}$		n/a[c]		10.7		10.1
GlcA(IV)								
	II_{H1}	$^{3}J_{1\text{-}2}$	4.631	7.9	4.594[a]	7.8[a]	4.587	8.0
GlcN3S6S(III)								
	III_{H1}	$^{3}J_{1\text{-}2}$	5.525	3.9	5.456[b]	3.7[b]	5.084	3.5
	III_{H2}	$^{3}J_{1\text{-}2}$	n/a[c]	n/a[c]	3.664[b]	3.7[b]	2.932	3.5
		$^{3}J_{2\text{-}3}$		n/a[c]		10.3[b]		10.2
IdoA2S(II)								
	IV_{H5}	$^{3}J_{4\text{-}5}$	5.228	1.7	4.873	1.7	4.842	2.0
GlcN6S(I)								
	V_{H1}	$^{3}J_{1\text{-}2}$	5.013	3.6	5.006	3.6	4.735	3.6
	V_{H2}	$^{3}J_{1\text{-}2}$	3.395	3.6	3.385	3.6	2.741	3.7
		$^{3}J_{2\text{-}3}$		n/a[c]		10.5		9.8

[a] Measured at pD 7.95.
[b] Measured at pD 7.67.
[c] Overlapped with other peak/peaks.

carboxylate group. For instance, $^{3}J_{H1\text{-}H2}$ of H1 in GlcN6S(V) and GlcN6S(I) residues remained constant, at 3.7 Hz and 3.6 Hz, respectively, as the pH was increased.

3.3.6. MD simulations. The experimentally identified hydrogen bond and possible two salt bridges in dNSA were reinforced by molecular dynamics (MD) simulations providing a molecular perspective. Examination of the structure of dNSA was initiated with Arixtra™ in the conformation it adopts when bound to AT-S195A factor Xa[29, 36, 41] by removal of *N*-sulfo groups, followed by charge adjustments. Figure 3.9 shows a perspective of the dNSA structure taken from one of the simulation frames with predicted hydrogen bonds and measured interatomic distances separating oppositely charged atoms. MD predicted a hydrogen bond (71%) involving GlcN3S6S(III) amino and 3-*O*-sulfo groups, which was experimentally confirmed by the reduced temperature coefficients determined for the amino group. Additionally, the simulation identified two other possible donor-acceptor pairs in dNSA: the 3-OH (a proton in the hydroxyl group bound to a third carbon) in GlcN6S(I) and the ring *O* in IdoA2S(II), and the 3-OH and 2-*O*-sulfo groups in IdoA2S(II). These hydrogen bonds were also previously predicted by MD for Arixtra™ and were further confirmed experimentally.[29, 36] Nevertheless, removal of the *N*-sulfo groups from Arixtra™ disrupted strong hydrogen bonding between the *N*-sulfo group and 3-OH,[36] resulting in an overall conformation change of the pentasaccharide described in terms differences in torsion angles between the Arixtra™ and dNSA (Figure 3.9 and Table 3.4).[73] Measured interatomic distance in 2.96 Å separating negatively charged oxygens in the 3-*O*-sulfo group with positively charged nitrogen of the amino group is favorable for the electrostatic attraction of a salt bridge pair and is consistent with the accelerated

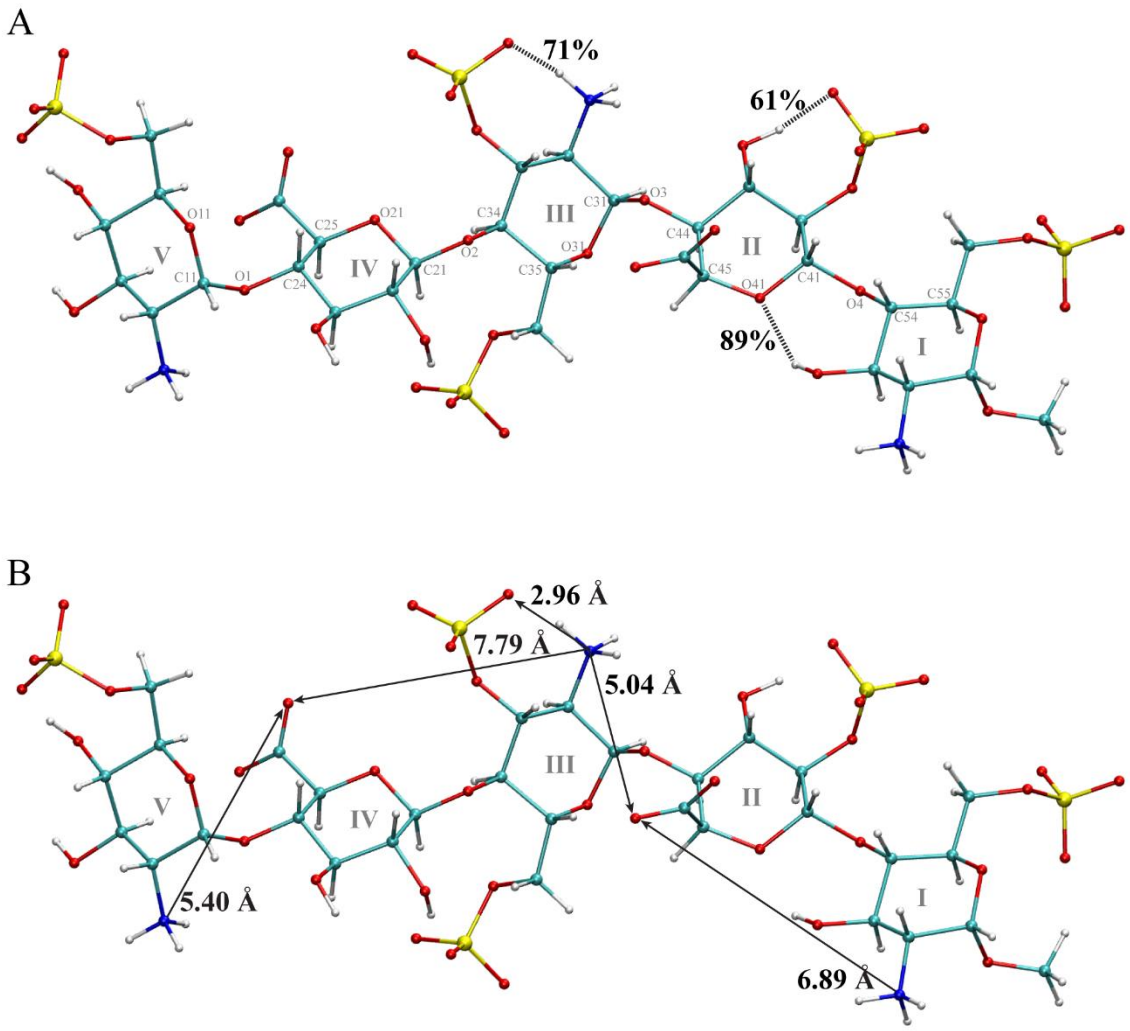

Figure 3.9. Representative structure of dNSA taken from one step of the 300 ns MD. (A) Intramolecular hydrogen bonds predicted from MD are labeled by black dashed lines. Only hydrogen bonds with occupancies greater than 20% are shown. (B) Interatomic distances were calculated by averaging the shortest distances separating oxygens from nitrogen atoms. Residues are labeled with corresponding residue numbers.

Table 3.4. Averaged torsion angles measured in dNSA. Atoms used to assign torsion angles in dNSA are shown in Figure 3.9A

Torsion Angles	Degrees, °
τ(O11-C11-O1-C24)	75.1
τ(C11-O1-C24-C25)	-143.3
τ(O21-C21-O2-C34)	-101.0
τ(C21-O2-C34-C35)	-128.5
τ(O31-C31-O3-C44)	71.6
τ(C31-O3-C44-C24)	-123.8
τ(O41-C41-O4-C54)	-83.4
τ(C41-O4-C54-C55)	-138.6

solvent exchange rate of the GlcN3S6S(III) amino protons. Moreover, estimated distances separating the carboxylate oxygens and the amino group nitrogen explains the reduced pK_a value of the IdoA2S(II) carboxylate and the acceleration of the amino proton exchange rates observed for the GlcN6S(V) and GlcN3S6S(III) residues as the solution pH is raised from 1.6 to 4.1. The 5.04 Å between the electrostatically interacting carboxylate of IdoA2S(II) and the amino of GlcN3S6S(III) places it within the range of weak salt bridge, consistent with our experimental observations. In contrast, the charge separation of 5.40 Å between the amino in GlcN6S (V) and carboxylate in GlcA (IV) was insufficient for salt bridge formation, however, it was sufficient to promote acceleration of the solvent exchange rate of the GlcN6S (V) amino group. Further, the 6.89 Å separation of the GlcN6S(I) amino from the nearby IdoA2S(II) carboxylate explains why the amino protons do not experience an observable influence from the negatively charged carboxylate group.

3.4. Conclusions

In this chapter, dNSA was synthesized from synthetic pentasaccharide Arixtra^{TM} for the purpose of mimicking rare 3-*O*-sulfated glucosamine residues found in HS. Through the comparison of exchange rates and pK_a values, an electrostatic interaction involving the GlcN3S6S positively charged amino group with possibly two negatively charged groups - the adjacent 3-*O*-sulfo group and the IdoA2S(II) carboxylate group - was identified for the first time. Furthermore, salt bridges accompanied by hydrogen bonds, as is the case for the amino group in the dNSA GlcN3S6S(III), are identifiable through small temperature coefficients. These results suggest that reduced temperature coefficients and highly accelerated amino group proton solvent exchange rates are potential markers for screening for salt bridge formation in aqueous solutions of GAGs. Taken together this new information related to structure further contributes to our knowledge of the possible function of 3-*O*-sulfo groups in HS, and to the ability of elements of primary structure to impact the secondary structure and, in turn, the spatial organization of functional groups involved in protein recognition and binding.

3.5. References

1. Rabenstein, D. L., Heparin and heparan sulfate: structure and function. *Nat. Prod. Rep.* **2002,** *19* (3), 312-31.

2. Meneghetti, M. C.; Hughes, A. J.; Rudd, T. R.; Nader, H. B.; Powell, A. K.; Yates, E. A.; Lima, M. A., Heparan sulfate and heparin interactions with proteins. *J. R. Soc. Interface* **2015,** *12* (110), 0589.

3. Gatti, G.; Casu, B.; Hamer, G. K.; Perlin, A. S., Studies on the Conformation of Heparin by 1H and 13C NMR Spectroscopy. *Macromolecules* **1979,** *12* (5), 1001-1007.

4. Gallagher, J. T.; Walker, A., Molecular Distinctions between Heparan-Sulfate and Heparin - Analysis of Sulfation Patterns Indicates That Heparan-Sulfate and Heparin Are Separate Families of N-Sulfated Polysaccharides. *Biochem. J.* **1985,** *230* (3), 665-674.

5. Gallagher, J. T.; Turnbull, J. E.; Lyon, M., Heparan sulphate proteoglycans: molecular organisation of membrane--associated species and an approach to polysaccharide sequence analysis. *Adv. Exp. Med. Biol.* **1992,** *313*, 49-57.

6. Sarrazin, S.; Lamanna, W. C.; Esko, J. D., Heparan sulfate proteoglycans. *Cold Spring Harb Perspect Biol* **2011,** *3* (7), a004952.

7. Carlsson, P.; Presto, J.; Spillmann, D.; Lindahl, U.; Kjellen, L., Heparin/heparan sulfate biosynthesis: processive formation of N-sulfated domains. *J. Biol. Chem.* **2008,** *283* (29), 20008-14.

8. Kreuger, J.; Kjellen, L., Heparan sulfate biosynthesis: regulation and variability. *J. Histochem. Cytochem.* **2012,** *60* (12), 898-907.

9. Whitelock, J. M.; Iozzo, R. V., Heparan sulfate: a complex polymer charged with biological activity. *Chem. Rev.* **2005,** *105* (7), 2745-64.

10. Dreyfuss, J. L.; Regatieri, C. V.; Jarrouge, T. R.; Cavalheiro, R. P.; Sampaio, L. O.; Nader, H. B., Heparan sulfate proteoglycans: structure, protein interactions and cell signaling. *An. Acad. Bras. Cienc.* **2009,** *81* (3), 409-29.

11. Powell, A. K.; Yates, E. A.; Fernig, D. G.; Turnbull, J. E., Interactions of heparin/heparan sulfate with proteins: appraisal of structural factors and experimental approaches. *Glycobiology* **2004,** *14* (4), 17R-30R.

12. Ori, A.; Wilkinson, M. C.; Fernig, D. G., The heparanome and regulation of cell function: structures, functions and challenges. *Front. Biosci.* **2008,** *13*, 4309-38.

13. Akhtar, J.; Shukla, D., Viral entry mechanisms: cellular and viral mediators of herpes simplex virus entry. *FEBS J.* **2009,** *276* (24), 7228-36.

14. Spear, P. G., Entry of Alphaherpesviruses into Cells. *Semin. Virol.* **1993,** *4* (3), 167-180.

15. Spear, P. G., Herpes simplex virus: receptors and ligands for cell entry. *Cell. Microbiol.* **2004,** *6* (5), 401-10.

16. Eisenstein, L. E.; Calio, A. J.; Cunha, B. A., Herpes simplex (HSV-1) aseptic meningitis. *Heart Lung* **2004,** *33* (3), 196-7.

17. Whitley, R. J.; Roizman, B., Herpes simplex virus infections. *Lancet* **2001,** *357* (9267), 1513-8.

18. Liu, J.; Shriver, Z.; Blaiklock, P.; Yoshida, K.; Sasisekharan, R.; Rosenberg, R. D., Heparan Sulfate d-Glucosaminyl 3-O-Sulfotransferase-3A SulfatesN-Unsubstituted Glucosamine Residues. *J. Biol. Chem.***1999,** *274* (53), 38155-38162.

19. Borjigin, J.; Deng, J.; Sun, X.; De Jesus, M.; Liu, T.; Wang, M. M., Diurnal pineal 3-O-sulphotransferase 2 expression controlled by beta-adrenergic repression. *J. Biol. Chem.* **2003,** *278* (18), 16315-9.

20. Pempe, E. H.; Xu, Y.; Gopalakrishnan, S.; Liu, J.; Harris, E. N., Probing structural selectivity of synthetic heparin binding to Stabilin protein receptors. *J. Biol. Chem.* **2012,** *287* (25), 20774-83.

21. Vanpouille, C.; Deligny, A.; Delehedde, M.; Denys, A.; Melchior, A.; Lienard, X.; Lyon, M.; Mazurier, J.; Fernig, D. G.; Allain, F., The heparin/heparan sulfate sequence that interacts with cyclophilin B contains a 3-O-sulfated N-unsubstituted glucosamine residue. *J. Biol. Chem.* **2007,** *282* (33), 24416-29.

22. McKeehan, W. L.; Wu, X.; Kan, M., Requirement for anticoagulant heparan sulfate in the fibroblast growth factor receptor complex. *J. Biol. Chem.* **1999,** *274* (31), 21511-4.

23. Samson, S. C.; Ferrer, T.; Jou, C. J.; Sachse, F. B.; Shankaran, S. S.; Shaw, R. M.; Chi, N. C.; Tristani-Firouzi, M.; Yost, H. J., 3-OST-7 regulates BMP-dependent cardiac contraction. *PLoS Biol.* **2013,** *11* (12), e1001727.

24. Thacker, B. E.; Xu, D.; Lawrence, R.; Esko, J. D., Heparan sulfate 3-O-sulfation: a rare modification in search of a function. *Matrix Biol.* **2014,** *35*, 60-72.

25. Bishop, J. R.; Schuksz, M.; Esko, J. D., Heparan sulphate proteoglycans fine-tune mammalian physiology. *Nature* **2007,** *446* (7139), 1030-7.

26. Petitou, M.; Casu, B.; Lindahl, U., 1976–1983, a critical period in the history of heparin: the discoveryof the antithrombin binding site. *Biochimie* **2003,** *85* (1), 83-89.

27. Lindahl, U.; Backstrom, G.; Thunberg, L.; Leder, I. G., Evidence for a 3-O-sulfated D-glucosamine residue in the antithrombin-binding sequence of heparin. *Proc. Natl. Acad. Sci. U.S.A.* **1980,** *77* (11), 6551-5.

28. Atha, D. H.; Lormeau, J. C.; Petitou, M.; Rosenberg, R. D.; Choay, J., Contribution of monosaccharide residues in heparin binding to antithrombin III. *Biochem.* **1985,** *24* (23), 6723-9.

29. Langeslay, D. J.; Young, R. P.; Beni, S.; Beecher, C. N.; Mueller, L. J.; Larive, C. K., Sulfamate proton solvent exchange in heparin oligosaccharides: evidence for a persistent hydrogen bond in the antithrombin-binding pentasaccharide ArixtraTM. *Glycobiology* **2012,** *22* (9), 1173-82.

30. Xu, Y.; Masuko, S.; Takieddin, M.; Xu, H.; Liu, R.; Jing, J.; Mousa, S. A.; Linhardt, R. J.; Liu, J., Chemoenzymatic synthesis of homogeneous ultralow molecular weight heparins. *Science* **2011,** *334* (6055), 498-501.

31. Fernandez-Tejada, A.; Haynes, B. F.; Danishefsky, S. J., Designing synthetic vaccines for HIV. *Expert. Rev. Vaccines* **2015,** *14* (6), 815-31.

32. Fera, D.; Lee, M. S.; Wiehe, K.; Meyerhoff, R. R.; Piai, A.; Bonsignori, M.; Aussedat, B.; Walkowicz, W. E.; Ton, T.; Zhou, J. O.; Danishefsky, S.; Haynes, B. F.; Harrison, S. C., HIV envelope V3 region mimic embodies key features of a broadly neutralizing antibody lineage epitope. *Nat. Commun.* **2018,** *9* (1), 1111.

33. Seeberger, P. H.; Werz, D. B., Synthesis and medical applications of oligosaccharides. *Nature* **2007,** *446* (7139), 1046-51.

34. Beecher, C. N.; Larive, C. K., (1)H and (15)N NMR Characterization of the Amine Groups of Heparan Sulfate Related Glucosamine Monosaccharides in Aqueous Solution. *Anal. Chem.* **2015,** *87* (13), 6842-8.

35. Van Geet, A. L., Calibration of the methanol and glycol nuclear magnetic resonance thermometers with a static thermistor probe. *Anal. Chem.* **1968,** *40* (14), 2227-2229.

36. Mazak, K.; Beecher, C. N.; Kraszni, M.; Larive, C. K., The interaction of enoxaparin and fondaparinux with calcium. *Carbohydr. Res.* **2014,** *384*, 13-9.

37. Sandstrom, C.; Baumann, H.; Kenne, L., NMR spectroscopy of hydroxy protons of 3,4-disubstituted methyl [small alpha]-D-galactopyranosides in aqueous solution. *J.C.S. Perkin 2* **1998,** (4), 809-816.

38. Hwang, T. L.; Shaka, A. J., Water Suppression That Works - Excitation Sculpting Using Arbitrary Wave-Forms and Pulsed-Field Gradients. *J. Magn. Reson. A* **1995,** *112* (2), 275-279.

39. Glasoe, P. K.; Long, F. A., USE OF GLASS ELECTRODES TO MEASURE ACIDITIES IN DEUTERIUM OXIDE1,2. *J. Phys. Chem.* **1960,** *64* (1), 188-190.

40. Wang, H. M.; Loganathan, D.; Linhardt, R. J., Determination of the pKa of glucuronic acid and the carboxy groups of heparin by 13C-nuclear-magnetic-resonance spectroscopy. *Biochem. J.* **1991,** *278 (Pt 3)* (Pt 3), 689-95.

41. Hricovini, M.; Guerrini, M.; Bisio, A.; Torri, G.; Petitou, M.; Casu, B., Conformation of heparin pentasaccharide bound to antithrombin III. *Biochem. J.* **2001,** *359* (Pt 2), 265-272.

42. Case D.A., B. R. M., Cerutti D.S., Cheatham T.E., III, Darden T.A., Duke R.E., Giese T.J., Gohlke H., Goetz A.W., Homeyer N., Izadi S., Janowski P., Kaus J., Kovalenko A., Lee T.S., LeGrand S., Li S., Lin C., Luchko T., Luo R., Madej B., Mermelstein D., Merz K.M., Monard G., Nguyen H., Nguyen H.T., Omelyan I., Onufriev A., Roe D.R., Roitberg A., Sagui C., Simmerling C.L., Botello-Smith W.M., Swails J., Walker R.C., Wang J., Wolf R.M., Wu X., Xiao L., Kollman P.A. AMBER 16. University of California; San Francisco.

43. Kirschner, K. N.; Yongye, A. B.; Tschampel, S. M.; Gonzalez-Outeirino, J.; Daniels, C. R.; Foley, B. L.; Woods, R. J., GLYCAM06: a generalizable biomolecular force field. Carbohydrates. *J. Comput. Chem.* **2008,** *29* (4), 622-55.

44. Hornak, V.; Abel, R.; Okur, A.; Strockbine, B.; Roitberg, A.; Simmerling, C., Comparison of multiple Amber force fields and development of improved protein backbone parameters. *Proteins* **2006,** *65* (3), 712-25.

45. Jorgensen, W. L.; Chandrasekhar, J.; Madura, J. D.; Impey, R. W.; Klein, M. L., Comparison of Simple Potential Functions for Simulating Liquid Water. *J. Chem. Phys.* **1983,** *79* (2), 926-935.

46. Phillips, J. C.; Braun, R.; Wang, W.; Gumbart, J.; Tajkhorshid, E.; Villa, E.; Chipot, C.; Skeel, R. D.; Kale, L.; Schulten, K., Scalable molecular dynamics with NAMD. *J. Comput. Chem.* **2005,** *26* (16), 1781-802.

47. Darden, T.; York, D.; Pedersen, L., Particle Mesh Ewald - an N.Log(N) Method for Ewald Sums in Large Systems. *J. Chem. Phys.* **1993,** *98* (12), 10089-10092.

48. Miyamoto, S.; Kollman, P. A., Settle - an Analytical Version of the Shake and Rattle Algorithm for Rigid Water Models. *J. Comp. Chem.* **1992,** *13* (8), 952-962.

49. Humphrey, W.; Dalke, A.; Schulten, K., VMD: visual molecular dynamics. *J. Mol. Graph.* **1996,** *14* (1), 33-8, 27-8.

50. Adams, B.; Lerner, L., Observation of Hydroxyl Protons of Sucrose in Aqueous-Solution - No Evidence for Persistent Intramolecular Hydrogen-Bonds. *J. Am. Chem. Soc.* **1992,** *114* (12), 4827-4829.

51. Baxter, N. J.; Williamson, M. P., Temperature dependence of H-1 chemical shifts in proteins. *J. Biomol. NMR* **1997,** *9* (4), 359-369.

52. Kindahl, L.; Sandstrom, C.; Norberg, T.; Kenne, L., H-1 NMR studies of hydroxy protons of Asn- and Ser-linked disaccharides in aqueous solution. *J. Carbohydr. Chem.* **2000,** *19* (9), 1291-1303.

53. Kindahl, L.; Sandstrom, C.; Norberg, T.; Kenne, L., H-1 NMR studies of hydroxy protons of the V[beta-Gal(1 -> 3)-alpha-GalNAc(1 -> O)THPGY glycopeptide. *Carbohydr. Res.* **2001,** *336* (4), 319-323.

54. Beecher, C. N.; Young, R. P.; Langeslay, D. J.; Mueller, L. J.; Larive, C. K., Hydroxyl-proton hydrogen bonding in the heparin oligosaccharide ArixtraTM in aqueous solution. *J. Phys. Chem. B* **2014,** *118* (2), 482-91.

55. Cierpicki, T.; Otlewski, J., Amide proton temperature coefficients as hydrogen bond indicators in proteins. *J. Biomol. NMR* **2001,** *21* (3), 249-261.

56. Andersen, N. H.; Neidigh, J. W.; Harris, S. M.; Lee, G. M.; Liu, Z. H.; Tong, H., Extracting information from the temperature gradients of polypeptide NH chemical shifts .1. The importance of conformational averaging. *J. Am. Chem. Soc.* **1997,** *119* (36), 8547-8561.

57. Blundell, C. D.; Almond, A., Temperature dependencies of amide 1H- and 15N-chemical shifts in hyaluronan oligosaccharides. *Magn. Reson. Chem. MRC* **2007,** *45* (5), 430-3.

58. Blundell, C. D.; Deangelis, P. L.; Almond, A., Hyaluronan: the absence of amide-carboxylate hydrogen bonds and the chain conformation in aqueous solution are incompatible with stable secondary and tertiary structure models. *Biochem. J.* **2006,** *396* (3), 487-98.

59. Battistel, M. D.; Shangold, M.; Trinh, L.; Shiloach, J.; Freedberg, D. I., Evidence for helical structure in a tetramer of alpha2-8 sialic acid: unveiling a structural antigen. *J. Am. Chem. Soc.* **2012,** *134* (26), 10717-20.

60. Battistel, M. D.; Pendrill, R.; Widmalm, G.; Freedberg, D. I., Direct evidence for hydrogen bonding in glycans: a combined NMR and molecular dynamics study. *J. Phys. Chem. B* **2013,** *117* (17), 4860-9.

61. Tomlinson, J. H.; Ullah, S.; Hansen, P. E.; Williamson, M. P., Characterization of salt bridges to lysines in the protein G B1 domain. *J. Am. Chem. Soc.* **2009,** *131* (13), 4674-84.

62. Englander, S. W.; Kallenbach, N. R., Hydrogen exchange and structural dynamics of proteins and nucleic acids. *Q. Rev. Biophys.* **1983,** *16* (4), 521-655.

63. Anderson, D. E.; Becktel, W. J.; Dahlquist, F. W., pH-induced denaturation of proteins: a single salt bridge contributes 3-5 kcal/mol to the free energy of folding of T4 lysozyme. *Biochem.* **1990,** *29* (9), 2403-8.

64. Bosshard, H. R.; Marti, D. N.; Jelesarov, I., Protein stabilization by salt bridges: concepts, experimental approaches and clarification of some misunderstandings. *J. Mol. Recognit.* **2004,** *17* (1), 1-16.

65. Clark, A. T.; Smith, K.; Muhandiram, R.; Edmondson, S. P.; Shriver, J. W., Carboxyl pK(a) values, ion pairs, hydrogen bonding, and the pH-dependence of folding the hyperthermophile proteins Sac7d and Sso7d. *J. Mol. Biol.* **2007,** *372* (4), 992-1008.

66. Forsyth, W. R.; Antosiewicz, J. M.; Robertson, A. D., Empirical relationships between protein structure and carboxyl pKa values in proteins. *Proteins* **2002,** *48* (2), 388-403.

67. Williamson, M. P.; Hounslow, A. M.; Ford, J.; Fowler, K.; Hebditch, M.; Hansen, P. E., Detection of salt bridges to lysines in solution in barnase. *Chem. Commun. (Camb)* **2013,** *49* (84), 9824-6.

68. Kohda, D.; Inagaki, F., Three-dimensional nuclear magnetic resonance structures of mouse epidermal growth factor in acidic and physiological pH solutions. *Biochem.* **1992,** *31* (47), 11928-39.

69. Wolfram, S., *Mathematica: a system for doing mathematics by computer (2nd ed.)*. Addison Wesley Longman Publishing Co., Inc.: **1991**; p 961.

70. Gao, G.; DeRose, E. F.; Kirby, T. W.; London, R. E., NMR determination of lysine pKa values in the Pol lambda lyase domain: mechanistic implications. *Biochem* **2006,** *45* (6), 1785-94.

71. Gao, G.; Prasad, R.; Lodwig, S. N.; Unkefer, C. J.; Beard, W. A.; Wilson, S. H.; London, R. E., Determination of lysine pK values using [5-13C]lysine: application to the lyase domain of DNA Pol beta. *J. Am. Chem. Soc.* **2006,** *128* (25), 8104-5.

72. Biedermann, F.; Schneider, H. J., Experimental Binding Energies in Supramolecular Complexes. *Chem. Rev.* **2016,** *116* (9), 5216-300.

73. Wildt, W.; Kooijman, H.; Funke, C.; Ustun, B.; Leika, A.; Lunenburg, M.; Kaspersen, F.; Kellenbach, E., Extended Physicochemical Characterization of the Synthetic Anticoagulant Pentasaccharide Fondaparinux Sodium by Quantitative NMR and Single Crystal X-ray Analysis. *Molecules* **2017,** *22* (8).

CHAPTER FOUR

Investigation of Amide Proton Solvent Exchange Properties in GAG Oligosaccharides

Acknowledgements: I would like to thank the following people for their contributions to this research: Blake Lockard, undergraduate student researcher, for his help in the chemical modification and structure elucidation of oligosaccharides; Dr. Kecheng Li, visiting professor from China, for his help with the pH titrations of monosaccharides with sulfamate containing groups; Dr. Leonard Mueller for our discussions on proton exchange and for providing the Mathematica program for activation energy barrier calculations; Dr. Robert Young, a former graduate student in Mueller's research lab, for teaching me the basics of Linux and MD; and Dr. Dan Borchardt, the NMR facility manager, for training me to properly operate 400 MHz, 600 MHz, and 700 MHz Bruker NMR instruments and for his guidance on improving the quality of the acquired data.

Abstract: In this chapter, we conducted one-dimensional proton NMR experiments for the determination of temperature coefficients and activation energy barriers, and to evaluate the effect of pH on the solvent exchange properties of the amide protons of GAG oligosaccharides. A library of saccharides was prepared by enzymatic depolymerization of amide-containing polysaccharides and by chemical modification of heparin and heparan sulfate (HS) saccharides including members that contain a 3-*O*-sulfated glucosamine residue. The systematic evaluation of this saccharide library facilitated the assessment of

the effects of structural characteristics, such as size, sulfation number and site, and glycosidic linkage, on amide proton solvent exchange. Charge repulsion by neighboring negatively charged sulfate and carboxylate groups was found to have a significant impact on the catalysis of amide proton solvent exchange by hydroxyl ions. This observation led to the conclusion that significantly reduced solvent exchange rates do not conclusively establish the involvement of a labile proton in a hydrogen bond, as previously proposed, and additional supporting experimental evidence, for example reduced temperature coefficients, is required.

4.1. Introduction

In Chapter 1 it was noted that hydrogen bonds play an important role in many chemical and biological processes, therefore, the development of reliable methods for the identification of hydrogen bonds in saccharides is critically important. Variable temperature experiments have been used in studies of GAG oligosaccharides to probe the involvement of labile protons in hydrogen bonds and to the investigate kinetics and thermodynamics of solvent exchange in aqueous solutions.[1-4] As discussed in Chapter 3, reduced temperature coefficients ($\Delta\delta/\Delta T$) in the range of 2 - 4 ppb/K can identify labile protons involved in hydrogen bonds.[1-4] In addition, the in-depth analysis of NMR spectra acquired at different temperatures can provide additional insights into the solvent exchange properties of labile protons. For example, Langeslay et al. used line-shape analysis of the sulfamate (*N*-sulfo group) ^{1}H NMR resonances to complement temperature coefficient

results and identify a hydrogen bond between the sulfamate group and the adjacent 3-*O*-sulfo group of the internal GlcNS3S6S residue of Arixtra™.[1]

For the more slowly exchanging sulfamate and amide protons, ^{1}H NMR resonance line widths are related to the rate constant (k_{ex}) of the solvent exchange reaction. Consequently, resonance line widths measured as a function of temperature can be fit with the Eyring-Polanyi equation (Eq. 1.1, Chapter 1), followed by calculation of the energy barrier ($\Delta G^{\ddagger}$ in kcal/mol) associated with solvent exchange.[5-7] In prior work, protons with a comparatively high energy barrier (2 - 3 kcal/mol or more) were proposed to be protected from exchange through involvement in a hydrogen bond. For example, Langeslay et al. used the $\Delta G^{\ddagger}$ of the Arixtra™ GlcNS3S6A(III) sulfamate proton ($\Delta G^{\ddagger}$ = 18.1 kcal/mol) as evidence for participation in the hydrogen bond as it is about 3.0 kcal/mol larger than the values of the other Arixtra™ sulfamate protons ($\Delta G^{\ddagger}$ = 15.1 – 15.7 kcal/mol).[1]

Though line-shape analysis is suitable for the sulfamate and amide protons, it is not feasible for the characterization of the hydroxyl and amino protons under the conditions of our experiments because their faster rates of solvent exchange and the freezing point of the solution limit the temperature range over which measurements can be performed. Fortunately, there is another approach to access exchange rates and test susceptibility to exchange: the 2D ^{1}H NMR exchange spectroscopy (EXSY) experiment.[2, 3, 8, 9] The EXSY experiment, which uses the NOESY pulse sequence, is well-suited to characterize more rapidly exchanging protons and is one of the most popular NMR methods for measuring exchanging rates. The EXSY cross-peak intensity depends on the exchange rates and spin relaxation properties of the detected nuclei. Therefore, by integrating the cross-peak

volumes or, as demonstrated in Chapter 3, using the areas from 1D spectra extracted from the EXSY contour plots, a build-up curve can be generated by plotting cross peak intensity as a function of the EXSY mixing time. Exchange rates are extracted by fitting the build-up curve with the Bloch equation modified to account for contributions from radiation damping to the longitudinal relaxation rate (Section 3.3.3.).[1, 10, 11]

Using EXSY results, Beecher et al. reported three hydrogen bonds involving the Arixtra™ hydroxyl protons.[2] Importantly, there was agreement between the reduced temperature coefficients and decreased exchange rates for only of the two hydroxyl protons. The protons of the hydroxyl group attached to the third carbon of IdoA2S residue (OH3) behaved inconsistently, having a reduced exchange rate but large temperature coefficients. In other words, the exchange rate suggested a hydrogen bond involving the IdoA2S OH3, but the temperature coefficient did not support its presence.

Because temperature coefficients are a well-established indicator of hydrogen bonds in carbohydrates, proteins and peptides,[1, 2, 12-15] we questioned the identification of a hydrogen bond by faster exchange rates alone without support from the temperature coefficient results. This work also raised questions about the factors affecting the solvent exchange rate including the size, sulfo group position, type of glycosidic linkage, and other elements of the structure of the monosaccharide residue. As discussed in Chapter 3, in addition to the expected exchange rate dependence on general acid-base catalysis (Eq. 1.2), the spatial proximity of negatively charged groups can catalyze the solvent exchange of amino protons.

In this Chapter, the solvent exchange properties of the labile amide protons in a variety of GAG oligosaccharides are examined and discussed as they relate to hydrogen bond participation. Additionally, the polyelectrolyte character of selected oligosaccharides is explored at physiological pH.

4.2. Experimental Section

4.2.1. Materials and Reagents. Arixtra™ (Fondaparinux sodium), formulated as prefilled syringes for clinical use, was obtained from the University Pharmacy and Department of Pharmacy Administration of Semmelweis University (Budapest, Hungary). The cation exchange resin Dowex 50WX8 hydrogen form (50 - 100 mesh); 3-(trimethylsilyl)-1-propanesulfonic acid-d_6 sodium salt (DSS-d_6, 98% D); 99.5% acetic anhydride; chondroitin sulfate A sodium salt from bovine trachea; enzymes Chondroitinase ABC from *Proteus vulgaris* and Hyaluronidase from *Streptomyces hyalurolyticus*; monosaccharides *N*-acetyl-D-glucosamine (GlcNAc), *N*-acetyl-D-glucosamine-6-*O*-sulfate (GlcNAc6S), *N*-acetyl-D-galactosamine (GalNAc), D-glucosamine-3-*O*-sulfate (GlcN3S), and D-glucosamine-2-*N*-sulfate (GlcNS); ammonium bicarbonate (NH_4HCO_3); Tris-HCl; and 35 wt% deuterated hydrochloric acid (DCl, 99% D) were purchased from Sigma-Aldrich (St. Louis, MO). HPLC grade methanol, 12.1 *N* hydrochloric acid (HCl), 50% w/w sodium hydroxide solution (NaOH), glacial acetic acid, sodium borohydride ($NaBH_4$), disodium orthophosphate heptahydrate ($Na_2HPO_4 \cdot 7H_2O$), monobasic sodium phosphate ACS grade ($NaH_2PO_4 \cdot H_2O$), sodium chloride (NaCl), bovine serum albumin (BSA) lyophilized powder, and sodium acetate trihydrate ($CH_3COONa \cdot 3H_2O$) were

purchased from Thermo Fisher Scientific (Bellefonte, PA). The disaccharides ΔUA-GalNAc, ΔUA-GalNAc6S, and ΔUA-GalNAc4S were purchased from Iduron Ltd. (Manchester, UK). The disaccharides ΔUA2S-GlcNAc; ΔUA2S-GlcNAc6S; ΔUA-GlcNAc6S; and ΔUA-GlcNAc and monosaccharides D-glucosamine-2-*N*, 3-*O*-disulfate (GlcNS3S); D-glucosamine-2-*N*, 6-*O*-disulfate (GlcNS6S); and D-glucoamine-2-*N*, 3-*O*, 6-*O*-trisulfate (GlcNS3S6S) were purchased from Dextra Laboratories Ltd. (Reading, UK). Sodium hyaluronate was purchased from Spectrum Chemical MFG Corp. (New Brunswick, NJ). Chitin disaccharide (*N*-acetyl-glucosamine)$_2$ was purchased from Qingdao BZ Oligos Biotech Co., LTD (Qingdao, China). Koptec Pure Ethanol (200 proof) was purchased from Decon Labs, Inc. (King of Prussia, PA). Deuterium oxide (D_2O, 99.9% D), 40% w/w sodium deuteroxide (NaOD, 99.5% D), and the low temperature methanol standard were purchased from Cambridge Isotope Laboratories (Andover, MA). The pH meter calibration buffers 2.00, 4.00, 7.00, and 10.00 were purchased from Fisher Scientific (Nazareth, PA). Ultrapure deionized water (18 MΩ/cm) was prepared by Simplicity UV water purification system from Millipore (Billerica, MA). All pH measurements were performed at room temperature using an AB 15 Accumet Basic pH meter and a 9110DJWP double-junction Ag/AgCl micro pH electrode, both from Thermo Scientific (Chelmsford, MA). All pH values measured in deuterated solutions were reported with correction for the deuterium isotope effect (pD). NMR NE-H5/3-Br tubes were purchased from New Era Enterprises (Vineland, NJ).

4.2.2. Partial digestion of bovine trachea chondroitin sulfate A with Chondroitinase ABC from *Proteus vulgaris*.[16] A 0.90 g sample of bovine trachea

chondroitin sulfate A sodium salt was dissolved in 35 mL of 50 mM Tris buffer pH 8.0 with 150 mM sodium acetate and 5 mg of BSA was added. Chondroitinase ABC equivalent to 2.5 IU was added to the room temperature solution and carefully mixed. An aliquot of 524 µL taken from the digestion mixture was combined with 60 µL of D_2O and 16 µL of a 100 mM DSS-d_6 solution and transferred to a 5 mm NMR tube to monitor digestion progress as described in Chapter 1, Section 1.2.1.1. Both samples were incubated at 37 °C for 2 h 50 min at which point both solutions were combined and the reaction quenched by placing the solution in boiling water for 15 min.

4.2.3. Digestion of hyaluronic acid with Hyaluronidase from *Streptomyces hyalurolyticus*.[17-19] Two batches of hyaluronic acid oligosaccharides were prepared at different times using the same amounts, concentrations, and proportions of the starting reagents. Vials of Hyaluronidase from *Streptomyces hyalurolyticus* were received at different times and came from different lots. The digestions were carried out using a 50 mg sample of sodium hyaluronate dissolved in 15 mL of 200 mM sodium acetate buffer at pH 5.1 with 0.15 M sodium chloride stored overnight in a refrigerator at 4 °C. Hyaluronidase equivalent to 900 IU was dissolved in 1 mL of 200 mM acetate buffer at pH 5.1 containing 0.15 M sodium chloride and added to the hyaluronic acid solution pre-equilibrated to 37 °C. The resulting digestion mixture was carefully but thoroughly agitated and an aliquot of 540 µL was combined with 60 µL D_2O and 10 µL of 100 mM DSS-d_6 solution and transferred to a 5 mm NMR for reaction progress monitoring. Both samples were incubated for 10 h 5 min at 37 °C after which the samples were recombined and the reaction quenched by placing the solution in boiling water for 10 min.

4.2.4. Size-exclusion chromatography of chondroitin sulfate A digested oligosaccharides.[16] The mixture of chondroitin sulfate A oligosaccharides prepared by enzymatic depolymerization was separated by size-exclusion chromatography using a mobile phase of 1 M sodium chloride with 10% of ethanol at a flow rate of 0.07 mL/min and a 3.0 x 200 cm atmospheric pressure chromatographic column packed with Bio-Rad Bio-Gel P-10 fine polyacrylamide resin (Bio-Rad Laboratories Hercules, CA). The eluted oligosaccharides were collected in separate 4.5 mL fractions and the separation monitored offline at 232 nm using a Thermo Scientific NanoDrop 2000 UV-Vis spectrophotometer (Wilmington, DE). The size-uniform fractions were pooled, lyophilized and desalted using deionized water on a 1.6 x 70 cm column packed with Sephadex G10 resin (GE Healthcare, Pittsburgh, PA). After desalting, the isolated oligosaccharide samples were lyophilized and stored at -80 °C for future use. A representative size-exclusion chromatogram is shown in Figure 1.5A of Chapter 1.

4.2.5. Size-exclusion chromatography of hyaluronic acid digested oligosaccharides.[18] **Batch #1.** A mixture of hyaluronic acid oligosaccharides prepared by enzymatic depolymerization was separated by size-exclusion chromatography using a 50 mM ammonium bicarbonate solution at an average flow rate of 0.124 mL/min using a 3.0 x 200 cm atmospheric pressure chromatographic column packed with Bio-Rad Bio-Gel P-10 fine polyacrylamide resin. Eluted oligosaccharides were collected in separate 3.5 mL fractions. The separation was monitored offline at 232 nm using a Thermo Scientific NanoDrop 2000 UV-Vis spectrophotometer. The resulting size-exclusion chromatogram is shown in Figure 4.1A.

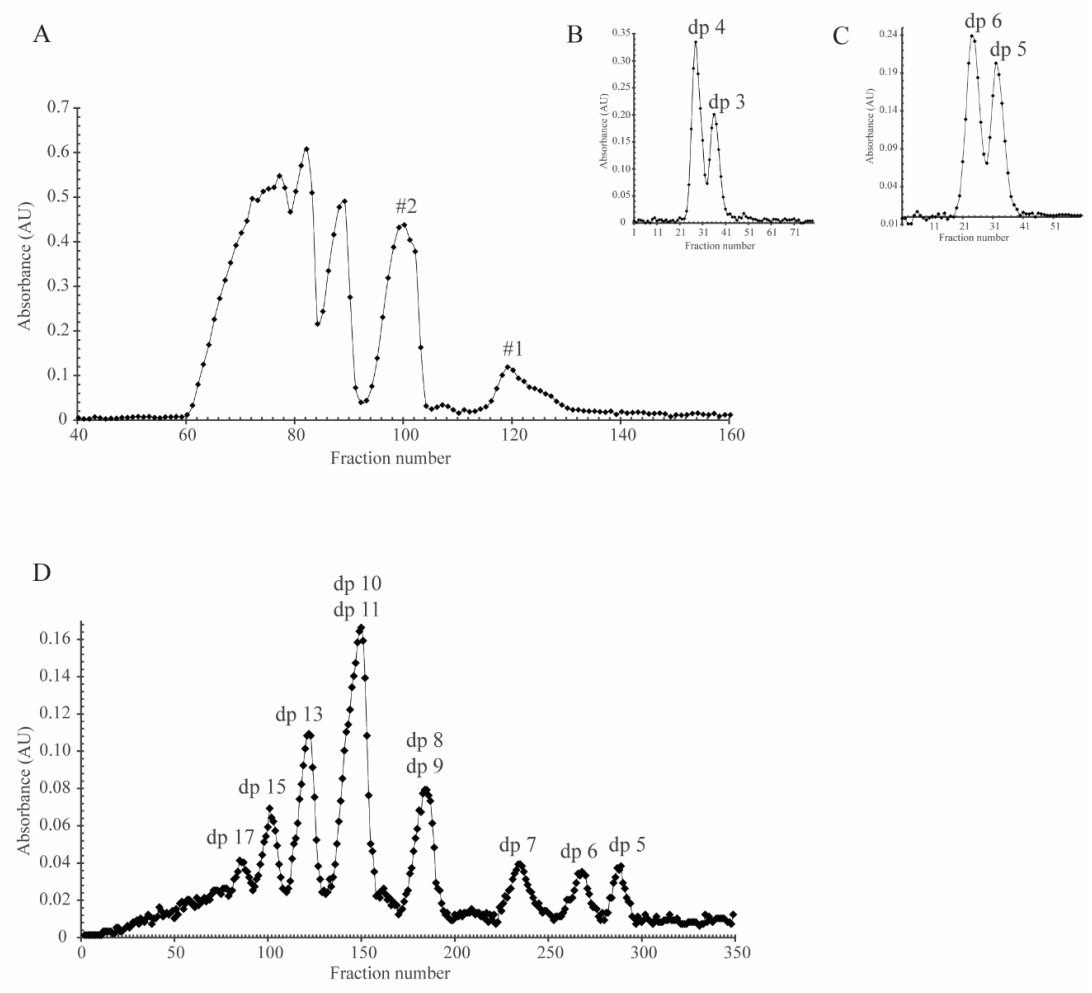

Figure 4.1. Size-exclusion chromatograms of hyaluronic acid digested by Hyaluronidase from *Streptomyces hyalurolyticus* in batch #1. (A) The poor separation of the mixture of hyaluronic acid oligosaccharides was due to column performance. Peaks labeled #1 and #2 were further separated at atmospheric pressure on a 1.6 x 70 cm column packed with Bio-Rad Bio-Gel P-6 fine polyacrylamide resin. (B) Peak #1 contains tri- and tetrasaccharides. (C) Peak #2 contains penta- and hexasaccharides. (D) Unresolved peaks from (A) were combined and separated again on a 3.0 x 200 cm column repacked with Bio-Gel P-10 fine resin and yielding improved chromatographic resolution.

An unstable flow rate and poor column packing resulted in suboptimal resolution of different sized hyaluronic acid oligosaccharides in the chromatogram in Figure 4.1A. Screening of isolated fractions by ESI-MS revealed the presence of odd-numbered oligosaccharides, which was inconsistent with the expected specificity of the enzyme used in this digestion. Major products of enzymatic depolymerization of hyaluronic acid by Hyaluronidase from *Streptomyces hyalurolyticus* are expected to be even-numbered oligosaccharides.[19] The fractions constituting the chromatographic peak labeled #1 in Figure 4.1A were pooled and lyophilized before being subjected to an additional size-exclusion chromatography using the same mobile phase at a flow rate of 0.15 mL/min on a 1.6 x 70 cm atmospheric pressure column packed with Bio-Rad Bio-Gel P-6 fine polyacrylamide resin (Bio-Rad Laboratories Hercules, CA). Eluents were collected in separate 0.85 mL tubes and monitored offline at 232 nm by using a Thermo Scientific NanoDrop 2000 UV-Vis spectrophotometer. A size-exclusion chromatogram of this separation is shown in Figure 4.1B, where it can be observed that peak #1 was indeed composed of two unresolved tri- and tetrasaccharides (labeled as dp 3 and dp 4, respectively). Similarly, but only part of peak #2 was resolved on a 1.6 x 70 cm size-exclusion chromatography column, yielding the penta- and hexasaccharides labeled dp 5 and dp 6, respectively, shown in Figure 4.1C.

Because of the poor separation achieved in Figure 4.1A, the 3.0 x 200 cm atmospheric pressure chromatographic column was repacked with Bio-Rad Bio-Gel P-10 fine polyacrylamide resin and the collected fractions including the second part of peak #2, were pooled, lyophilized and reconstituted in 15 mL of 50 mM ammonium bicarbonate

buffer and the size-exclusion chromatography carried out at a stable flow rate of 0.08 mL/min. The result of this separation is shown in Figure 4.1D. As with before, the isolated fractions were identified by ESI-MS, which clearly indicated that the digestion mixture was composed of even- and odd-numbered oligosaccharides. Fractions constituting each peak were combined, lyophilized, and stored at -80 °C for future use.

Batch #2. A second batch of hyaluronic acid oligosaccharides were prepared by enzymatic depolymerization with Hyaluronidase (from a different lot) and separated by size using a 50 mM ammonium bicarbonate solution at a flow rate of 0.07 mL/min on a 3.0 x 200 cm atmospheric pressure chromatographic column packed with Bio-Rad Bio-Gel P-10 fine polyacrylamide resin. The eluted oligosaccharides were collected in separate 3.5 mL fractions and the separation monitored offline at 232 nm by using a Thermo Scientific NanoDrop 2000 UV-Vis spectrophotometer. The chromatogram for this separation is shown in Figure 1.5B (Chapter 1) and revealed good resolution of the depolymerization products. This digestion with Hyaluronidase from *Streptomyces hyalurolyticus* yielded even-numbered oligosaccharides, as expected. Size-uniform fractions were pooled, lyophilized, desalted using deionized water on a 1.6 x 70 cm column packed with Sephadex G10 resin (GE Healthcare, Pittsburgh, PA), lyophilized again and stored at -80 °C for future use.

4.2.6. Reduction of oligosaccharides with sodium borohydride.[20] About 77.0 mg of chondroitin sulfate A tetrasaccharide, 74.4 mg of chondroitin sulfate A hexasaccharide, and 2 mg of hyaluronic acid hexasaccharide were converted to alditols by reaction of the reducing end residues with sodium borohydride as discussed in Chapter 2, Section 2.3.3.

Due to the problems encountered with degradation of the unsulfated hyaluronic acid hexasaccharides, all steps of the hyaluronic acid hexasaccharide reduction reaction were performed in the presence of 10 mM phosphate buffer, which improved the stability of the reaction products. After desalting, the size-uniform fractions containing the hyaluronic acid hexasaccharides were combined and buffered with 10 mM phosphate, followed by lyophilization and storage at -80 °C.

4.2.7. Strong anion-exchange high-performance liquid chromatography. The fractions of the bovine trachea chondroitin sulfate A digestion labeled dp 4 (tetrasaccharide) and dp 6 (hexasaccharide) in the size-exclusion chromatogram shown Figure 1.5A (Chapter 1) were reduced according to the procedure previously described in Chapter 2, Section 2.2.4. and separated by strong anion-exchange high-performance liquid chromatography using a Waters Spherisorb 5 µm (Milford, MA) semi-preparative column (10 x 250 mm) on a Dionex 500 ion chromatography system equipped with a GP40 gradient pump and AD20 UV-Vis detector. The size-exclusion chromatography fractions of the reduced tetra- and hexasaccharides were individually dissolved in purified deionized degassed water and introduced onto the strong-anion exchange column in 500 µL injections at a flow rate of 3.0 mL/min. The oligosaccharides were separated using a 20 mM sodium acetate buffer at pH 3.9 as mobile phase A, and 1.0 M sodium chloride in a 20 mM sodium acetate buffer at pH 3.9, as mobile phase B. The following gradient profile was employed to separate the tetrasaccharides: 0 min, 100% A and 0% B; 1 min, 89% A and 11% B; and 23 min, 70% A and 30% B. The following gradient profile was used for the hexasaccharide separation: 0 min, 100% A and 0% B; 3 min, 85% A and 15% B; and 27 min, 65% A and

35% B. Each run was followed by a washing step of 100% B for 10 min and column equilibration with 100% A for 20 min. The eluted chromatographic peaks were collected separately over multiple consecutive injections. Each sample was lyophilized and reconstituted in the minimum amount of degassed deionized water for desalting on a 1.6 x 70 cm column packed with Sephadex G10 resin. Deionized water sonicated for 25 min was used as the mobile phase at a flow rate of 0.14 mL/min with the eluent collected in 1.0 mL fractions. The collected fractions were monitored offline using a NanoDrop 2000 UV-Vis spectrophotometer at 232 nm. Fractions containing the desalted oligosaccharides were combined, lyophilized, and stored at -80 °C for future use.

4.2.8. Chemoselective *N*-acetylation of dNSA and 3-*O*-sulfated glucosamine. The chemoselective *N*-acetylation reaction of dNSA and 3-*O*-sulfated glucosamine (GlcN3S) are discussed in detail in Section 2.2.3, Chapter 2.

4.2.9. ESI-MS measurements. About 1.0 mg of each desalted oligosaccharide: *N*-acetylated Arixtra^{TM} (NAcArixtra), reduced chondroitin sulfate A tetra- and hexasaccharides after strong anion-exchange chromatography, and size-exclusion chromatography separated tri-, tetra-, penta-, and hexasaccharides of hyaluronic acid - were individually dissolved in separate 500 µL aliquots of deionized water. An aliquot of 30 µL of each solution was transferred to a 1.5 mL Eppendorf safe-lock tube and diluted with 200 µL of solution composed of 30% methanol and 70% water. These samples were infused into a Micromass/Waters ESI quadrupole time-of-flight (Q-Tof micro) mass spectrometer (Waters Corporation, Millford, MA) at a flow rate of 10 µL/min. Data acquisition was performed using Masslynx 4.1 software. The mass spectrum was obtained in negative

mode using the following instrumental parameters: capillary voltage, 2800-3000 kV; cone voltage, 25-35 V; extractor voltage, 1-3 V; source temperature, 120 °C; desolvation temperature, 275 °C; interscan delay, 0.1 s; and m/z range, 200 – 1500. A representative mass spectrum for NAcArixtra with assigned ion peaks is shown in Figure A2 of the Appendix.

4.2.10. NMR measurements.

4.2.10.1 Carbon-bound proton resonance assignments. About 1.1 mg of reduced chondroitin sulfate A (unsaturated reduced CS-A) tetrasaccharide and 2.0 mg of reduced chondroitin sulfate A (unsaturated reduced CS-A) hexasaccharide were dissolved in 700 µL of 10 mM phosphate buffer, pH 7.40, containing 0.5 mM DSS-d_6 and lyophilized. To reduce the intensity of the residual HOD peak, the freeze-dried samples were dissolved in 300 µL of 99.9% D_2O, lyophilized again, and reconstituted in 700 µL of 99.9% D_2O. The unsaturated reduced CS-A tetrasaccharide solution was adjusted to pD 9.10 and the unsaturated reduced CS-A hexasaccharide solution was adjusted to pD 9.00 using NaOD and DCl prepared from concentrated solutions by dilution with the appropriate volume of 99.9% D_2O). Both solutions were lyophilized and stored at -80 °C. Prior to NMR measurements, the solutions were reconstituted in 700 µL of 99.9% D_2O and 600 µL aliquots transferred to individual 5 mm NMR tubes.

Similarly, 1.9 mg of NAcArixtra was dissolved in 300 µL of 10 mM phosphate buffer, pH 7.40, containing 0.5 mM DSS-d_6 and lyophilized. The sample was reconstituted in 300 µL of 99.9% D_2O, adjusted to pD 7.80 with NaOD and DCl, and lyophilized again.

The solid sample was stored at -80 °C and reconstituted for NMR measurements in 300 µL of 99.9% D_2O before transferring 200 µL to a NE-H5/3-Br NMR tube.

The 1D ^1H, and 2D COSY, TOCSY, and ROESY spectra of the unsaturated reduced CS-A tetra- and hexasaccharides were acquired at 316.2 K using a Bruker Avance 600 MHz spectrometer operating at 599.58 MHz and equipped with a BBI probe. The 90° pulse lengths ranged between 9.25 - 9.27 µs with solvent suppression of the HOD resonance provided by presaturation at a power of 59 dB during the 2.0 s relaxation delay. All spectra were referenced to the ^1H resonance of DSS-d_6 (0.00 ppm).

The 1D ^1H NMR spectra were acquired using a spectral window of 7002 Hz and 256 scans coadded into 42,014 complex points. Spectra were zero-filled to 65,536 points and apodized using an exponential multiplication window function equivalent 0.3 Hz line broadening. The phase-sensitive 2D COSY, TOCSY, and ROESY spectra were acquired using States-TPPI with a spectral window of 7002 Hz in both dimensions. COSY spectra were acquired into 2048 complex points with 64 coadded scans and 416 t_1 increments. TOCSY spectra were acquired using a mixing time of 120 ms with a 41 µs spinlock pulse at a power of 8.20 dB into 2048 complex points using 48 coadded scans and 416 experiments. Finally, ROESY spectra were acquired using a 350 ms spinlock pulse at a power of 59 dB into 2048 complex points using 48 coadded scans, and 512 experiments. The 2D spectra were zero filled to 4096 × 1024 data points and apodized using a $\cos^2$ window function. All spectra were analyzed using TopSpin 3.2.

The 1D ^1H, COSY, TOCSY, and ROESY spectra for NAcArixtra were acquired using a Bruker Avance 600 MHz spectrometer operating at 599.88 MHz and equipped with

a TBI probe at 298.2 K. A 90° pulse length of 10.12 µs was used with solvent suppression of the HOD resonance provided by presaturation at a power of 59 dB during the 2.0 s relaxation delay. The 1D ^{1}H NMR spectra were acquired using a spectral window of 6361 Hz with 120 scans coadded into 42,014 complex points. The spectra were processed by zero filling to 65,536 points and apodized with an exponential multiplication window function equivalent to 0.3 Hz line broadening. Phase-sensitive 2D COSY, TOCSY, and ROESY spectra were acquired using States-TPPI with a spectral window of 7002 Hz in both dimensions. The COSY and TOCSY spectra were acquired into 2048 complex points using 40 coadded scans and 416 experiments. The TOCSY were measured using a 120 ms mixing time with a 35 µs spinlock pulse at a power of 8.20 dB. Finally, ROESY spectra were acquired into 2048 complex points using 48 experiments, each with 512 coadded scans using a 350 ms spinlock pulse at a power of 53 dB. All two-dimensional spectra were zero filled to 4096 × 1024 data points and apodized using a $\cos^2$ window function. All spectra were analyzed using the TopSpin 3.2. Chemical shifts assignments for the unsaturated reduced CS-A tetra- and hexasaccharides are provided in Tables A4 and A5 (Appendix), respectively. The NAcArixtra carbon-bound proton assignments are provided in Table 3.1, Chapter 3.

4.2.10.2. Amide proton resonance assignments. Following completion of the carbon-bound proton resonance assignments, the samples of the unsaturated reduced CS-A tetra- and hexasaccharides were lyophilized, reconstituted in 630 µL of H_2O and adjusted to pH 7.40 with NaOH and HCl solutions. After pH adjustment, 70 µL of D_2O was added and 600 µL transferred to individual 5 mm NMR tubes. Similarly, the lyophilized

NAcArixtra sample was reconstituted in 270 µL of H_2O and adjusted to pH 7.40 before adding 30 µL of D_2O. A 200 µL aliquot was transferred to the NE-H5/3-Br NMR tube. The assignment of the carbon-bound protons and the amide protons of the GlcNAc3S monosaccharide was performed using a solution prepared for temperature experiments (Section 4.2.10.3).

The 1D ^{1}H, COSY and TOCSY spectra of the unsaturated reduced CS-A tetra- and hexasaccharide solutions were acquired at 316.2 K and 308.2 K, respectively, using a Bruker Avance spectrometer operating at 599.58 MHz and equipped with a 5 mm BBI probe. A 90° pulse length of 8.73 µs (tetrasaccharide) or 8.82 µs (hexasaccharide) were used at a power level of -4.00 dB with solvent suppression provided by excitation sculpting. The one-dimensional ^{1}H NMR spectrum was recorded using a spectral window of 6887 Hz and a relaxation delay of 2.0 s with 280 scans coadded into 32,768 complex points. Free induction decays (FIDs) were zero-filled to 65,536 points and apodized by multiplication with an exponential function equivalent to 0.3 Hz line broadening prior to Fourier transformation. The phase-sensitive COSY and TOCSY spectra were acquired into 2048 complex points over 256 increments using States-TPPI with a 2.0 s relaxation delay and a spectral window of 7003 Hz in both dimensions. The COSY spectra were recorded by coaddition of 96 and 160 scans for the tetra- and hexasaccharide, respectively, while 72 (tetrasaccharide) and 96 scans (hexasaccharide) were coadded for the TOCSY spectra. The TOCSY spectra were acquired using a mixing time of 120 ms with a 43 µs spinlock pulse. The COSY and TOCSY spectra were zero-filled to 4096 × 1024 data points and apodized using a $\cos^2$ window function.

^{1}H, COSY, and TOCSY spectra of GlcNAc3S and NAcArixtra were acquired using a Bruker Avance spectrometer operating at 599.88 MHz equipped with a 5 mm TBI probe. All spectra were acquired at 298.2 K using a 90° pulse of 10.4 μs (GlcNAc3S) and 9.83 μs (NAcArixtra) at a power level of -4.00 dB with solvent suppression provided by excitation sculpting. The 1D ^{1}H NMR spectrum was recorded using a spectral window of 6887 Hz and a relaxation delay of 2.0 s with 128 scans coadded into 32,768 complex points. FIDs were zero filled to 65,536 points and apodized by multiplication with an exponential function equivalent to 0.3 Hz line broadening prior to Fourier transformation. Phase-sensitive COSY and TOCSY spectra were acquired using States-TPPI into 2048 complex points over 256 increments using a 2.0 s relaxation delay and a spectral window of 6614 Hz in both dimensions. The COSY spectrum was recorded by coaddition of 48 scans while 40 scans were coadded for the TOCSY spectrum. The TOCSY spectrum was acquired using a mixing time of 120 ms with a 41 μs (GlcNAc3S) or a 39 μs (NAcArixtra) spinlock pulse. The COSY and TOCSY spectra were zero filled to 4096 × 1024 data points and apodized using a $\cos^2$ window function. Amide protons assignments for the unsaturated reduced CS-A tetrasaccharide (Table A6A), unsaturated reduced CS-A hexasaccharide (Table A6B), NAcArixtra (Table A6C), and GlcNAc3S (Table A6B) are provided in Appendix.

4.2.10.3. Temperature experiments. Samples of 1.75 mg GlcNAc3S, 0.77 mg GalNAc, 0.67 mg GlcNAc, 1.02 mg GlcNAc6S, 1.0 mg ΔUA-GlcNAc, 1.0 mg ΔUA-GlcNAc6S, 1.0 mg ΔUA2S-GlcNAc, 1.33 mg ΔUA2S-GlcNAc6S, 1.0 mg ΔUA-GalNAc, 1.14 mg ΔUA-GalNAc4S, 1.0 mg ΔUA-GalNAc6S, 0.97 mg unsaturated reduced CS-A

hexasaccharide, 1.80 mg unsaturated reduced CS-A tetrasaccharide, 1.90 mg NAcArixtra, 1.2 mg unsaturated reduced hyaluronic acid (HA) hexasaccharide, 0.90 mg unsaturated HA trisaccharide, 1.05 mg unsaturated HA pentasaccharide, 1.26 mg unsaturated HA tetrasaccharide, 3.0 mg unsaturated HA hexasaccharide, and 1.12 mg chitin disaccharide (GlcNAc-GlcNAc) were each dissolved in 300 µL of an aqueous 10 mM phosphate buffer at pH 7.48 containing 0.5 mM DSS-d_6. The pH of each solution was adjusted to 7.40 with NaOH and HCl, lyophilized and stored frozen. Prior to the NMR experiments, the solid samples were reconstituted in 270 µL of H_2O and, if necessary, the pH was re-adjusted to 7.40. Then, 30 µL of D_2O was added to provide a lock signal and 200 µL aliquots were transferred to NE-H5/3-Br NMR tubes.

Solutions of GlcNAc and GalNAc were also prepared containing various concentrations of the monosaccharides and buffers. For instance, 6.55 mg GlcNAc and 6.40 mg GalNAc were dissolved in 300 µL of 10 mM phosphate buffer pH 7.48 containing 0.5 mM DSS-d_6. Alternatively, 0.74 mg GlcNAc and 0.62 mg GalNAc were dissolved in 300 µL of 50 mM phosphate buffer at pH 7.48 containing 0.5 mM DSS-d_6. The pH of each solution was adjusted to pH 7.40 with NaOH and HCl, followed by lyophilization. Prior to NMR experiments, the solid samples were dissolved in 270 µL of H_2O and the pH, if needed, was re-adjusted to 7.40. Then, 30 µL of D_2O was added and 200 µL aliquots were transferred to NE-H5/3-Br NMR tubes.

Variable temperature experiments were performed over the range 283.2 K to 338.2 K using a Bruker Avance spectrometer operating at 599.88 MHz and equipped with a 5 mm TBI probe. One-dimensional spectra were acquired using a 90° pulse length between

9.5 and 10.6 µs at a power level of -4.00 dB with solvent suppression provided by excitation sculpting. A total of 128 scans were coadded into 32,768 complex points. A spectral window of 6887 Hz and a relaxation delay of 2.0 s were used. FIDs were zero filled to 65,536 points and apodized by multiplication with an exponential function equivalent to a 0.3 Hz line broadening prior to Fourier transformation. At least 7 min was allowed for sample thermal equilibration at each temperature. Sample temperatures were calibrated using an external low temperature methanol standard obtained from Cambridge Isotope Labs (Andover, MA) and calculated using the Van Geet equation.[21] The spectra were referenced to the ^{1}H resonance of DSS-d_6 (0.00 ppm) and all spectra were analyzed using MestReNova-12.0.1.

4.2.10.4. pH titrations. Samples of GlcNAc, GlcNAc3S, GlcNAc6S, chitin disaccharide, NAcArixtra, and GalNAc used for the temperature experiments were titrated with NaOH and HCl solutions prepared in 90% H_2O/10% D_2O. After adjustment to the desired pH, the solutions were transferred to NE-H5/3-Br NMR tubes and the spectra measured at 298.2 K using a Bruker Avance spectrometer operating at 599.88 MHz and equipped with a 5 mm TBI probe. Spectra were acquired as a function of pH using a 90° pulse length between 9.8 and 10.2 µs at a power level of -4.00 dB with solvent suppression by excitation sculpting. A total of 128 scans were coadded into 32,768 complex points using a spectral window of 6887 Hz and a relaxation delay of 2.0 s. FIDs were zero filled to 65,536 points and apodized by multiplication with an exponential function equivalent to a 0.3 Hz line broadening prior to Fourier transformation. Spectra were referenced to the ^{1}H resonance of DSS-d_6 (0.00 ppm) and analyzed using MestReNova-12.0.1.

For experiments with *N*-sulfo-glucosamines, 1.5 mg GlcNS3S6S, 0.9 mg GlcNS, 1.3 mg GlcNS3S, and 0.9 mg GlcNS were each dissolved in 800 µL of a 90% H_2O/10% D_2O 25 mM phosphate buffer at pH 6.09 containing mM DSS-d_6. The samples were titrated with NaOH and HCl in 90% H_2O/10% D_2O and aliquots of the solution at each pH were transferred to NE-H5/3-Br NMR tubes. ^{1}H NMR spectra were acquired as a function of pH using a Bruker Avance spectrometer operating at ^{1}H frequency of 599.52 MHz and equipped with a 5 mm BBI probe. NMR spectra were at 298.2 K using WATERGATE-W5 solvent suppression.[22] A total of 128 scans were coadded into 32,768 complex points using a 6887 Hz spectral window and a relaxation delay of 2.0 s. FIDs were zero filled to 65,536 points and apodized by multiplication with an exponential function equivalent to 0.3 Hz line broadening prior to Fourier transformation. All spectra were analyzed using the MestReNova-12.0.1.

4.2.11. Molecular dynamics simulations. The AmberTools 16 module *xleap*[23] was used to model the structures of the following saccharides in α conformation: GlcNAc, GlcNAc3S, GlcNAc6S, GlcNS3S6S, ΔUA-GalNAc4S, ΔUA-GalNAc6S, unsaturated HA hexasaccharide, unsaturated CS-A hexasaccharide, and NAcArixtra. These saccharides were modeled to generate the parameter, topology, and coordinate files for molecular dynamics simulations using a GLYCAM 06g force field.[24] The *xleap* module was used to add sodium ions (ff99SB parameters) to oligosaccharide structures to make the system's overall charge neutral (*addions* function) and to construct a cubic water box with each face a distance 12 Å from the solute.[23-26] Minimization, heating, equilibration, and molecular dynamics simulation production runs were performed using NAMD 2.11.[27] To remove

possible bad contacts, conjugate-gradient minimization was performed separately in the following order: solute, solvent, and the entire system. Periodic boundary conditions were applied throughout. The particle mesh Ewald algorithm was used to treat long range electrostatic interactions with the grid spacing set to 1 Å.[28] Non-bonded interactions were cut off at 12 Å and a smooth switching function was applied to 10 Å. The VDW and electrostatic 1-4 scaling factors (*SCNB* and *SCEE*, respectively) were set to unity for consistency with the GLYCAM 06g parameters.[24] The SETTLE algorithm was used to hold rigid hydrogen-oxygen bonds within water molecules.[29] Slow system heating from 0 K to 298 K was performed in 398 ps, including a 100 ps hold at 298 K using a constant-*NVE* ensemble. A constant-*NPT* ensemble with a pressure of 1 atm and a temperature of 298 K was used for system equilibration and the production run. Temperature control was performed using the Langevin thermostat with a damping coefficient of 5 ps^{-1}, while control over pressure was performed by using NAMD's Nosé-Hoover Langevin piston method.[27] Trajectory outputs of 11 ns simulations were saved every 500 fs with a time step of simulation integration in 1 fs. Monitoring of temperature, pressure, and energy, in addition to trajectories visualization, was performed in VMD 1.9.2.[30] The hydrogen bonding analysis, including a 3.5 Å heavy-atom cutoff distance and a 120° angle cutoff, was performed using the AmberTools 16 module *cpptraj*.[23]

4.3. Results and Discussion

To experimentally explore amide proton solvent exchange properties, we generated a library of amide-containing saccharides found in GAG polysaccharides, structures shown

in Figure 4.2 with descriptions provided in Table 4.1. Figure 4.2 C and Q also shows two chemically modified structures that do not occur naturally: 3-*O*-sulfo-*N*-acetyl-glucosamine (GlcNAc3S) and *N*-acetylated Arixtra™ (NAcArixtra). The variations in size, composition, sulfation position and extent, overall oligosaccharide charge, and glycosidic linkage of the compounds listed in Figure 4.2 allow the evaluation of the effect of these structural features on amide solvent exchange rates.

4.3.1. Amide proton temperature coefficients. To characterize the temperature dependence of the amide proton chemical shifts and explore the possibility of hydrogen bonds involving the amide protons, ^{1}H NMR spectra of each oligosaccharide shown in Figure 4.2 were acquired at pH 7.40 over the temperature range 283.2 - 338.2 K. Temperature coefficients were calculated by taking the absolute value of the slopes of the lines obtained by plotting amide proton chemical shifts as a function of calibrated temperatures as previously shown in Figure 3.4. Calculated $\Delta\delta/\Delta T$ values for the oligosaccharide amide protons are presented in Table 4.2. None of the investigated structures produced a temperature coefficient that would suggest formation of an intramolecular hydrogen bond involving an amide proton. To help visualize the data shown in Table 4.2, it is also depicted in a graphical form in Figure 4.3 with the $\Delta\delta/\Delta T$ values plotted as a function of the corresponding residue. In Figure 4.3, oligosaccharides are arranged in the order of decreasing $\Delta\delta/\Delta T$. Also, because the α conformers are more energetically favorable and dominate in aqueous solutions, they are of greater interest. As such, in the following discussion, the β conformers are omitted.

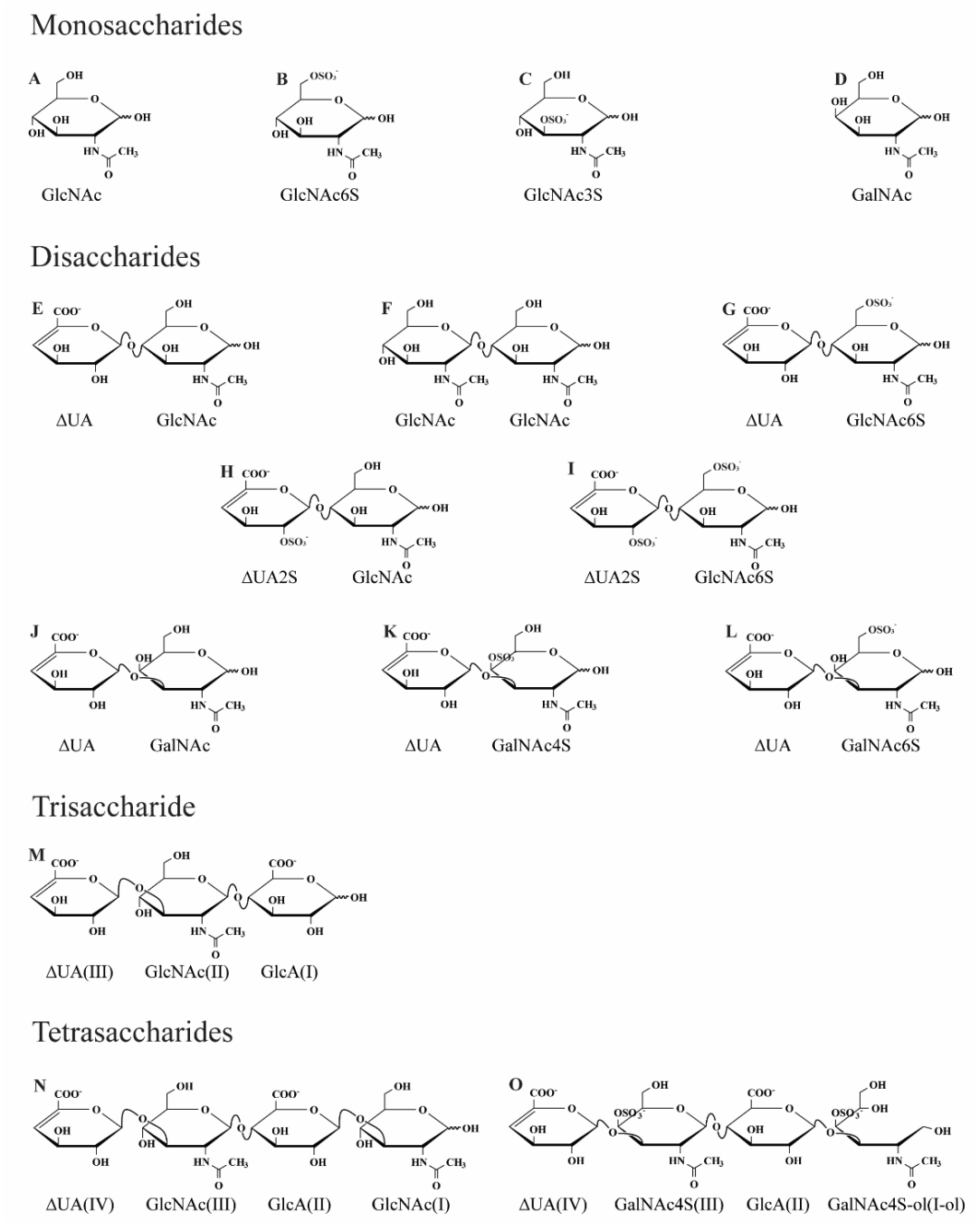

Figure 4.2. Library of amide-containing saccharides. For oligosaccharide descriptions refer to Table 4.1. Oligosaccharide residue numbering order is from right to the left. The corresponding residue number is indicated in brackets by Roman numerals.

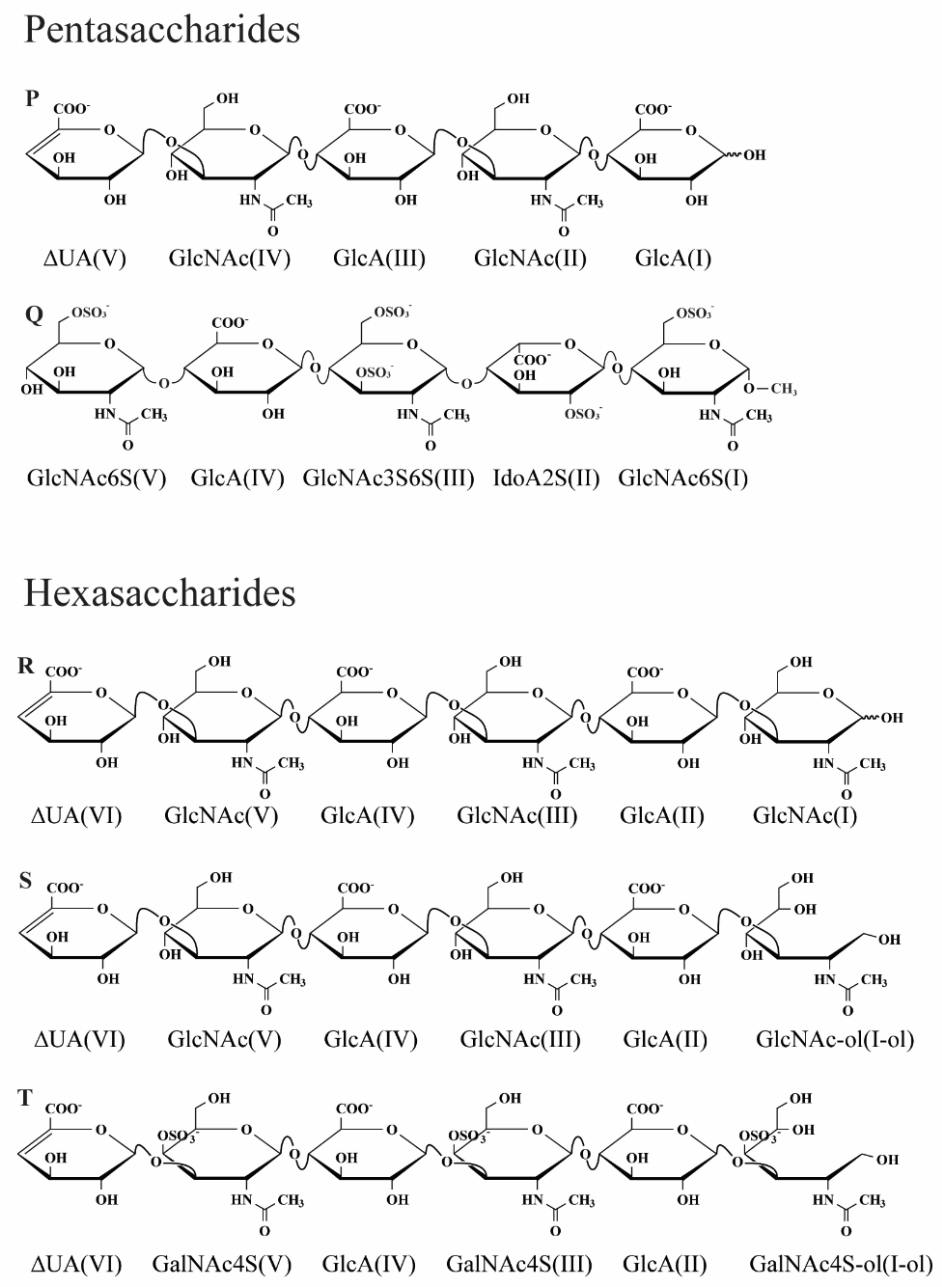

Figure 4.2. Cont'd

Table 4.1. Description of oligosaccharide structures shown in Figure 4.2.

Letter code	Name	Oligosaccharide sequence and abbreviation
A	*N*-acetyl-D-glucosamine	GlcNAc
B	*N*-acetyl-D-glucosamine-6-*O*-sulfate	GlcNAc6S
C	*N*-acetyl-D-glucosamine-3-*O*-sulfate	GlcNAc3S
D	*N*-acetyl-D-galactosamine	GalNAc
E	HEP disaccharide IVA	ΔUA(II)(β1→4)GlcNAc(I)
F	Chitin disaccharide	GlcNAc(II)(β1→4)GlcNAc(I)
G	HEP disaccharide IIA	ΔUA(II)(β1→4)GlcNAc6S(I)
H	HEP disaccharide IIIA	ΔUA2S(II)(β1→4)GlcNAc(I)
I	HEP disaccharide IA	ΔUA2S(II)(β1→4)GlcNAc6S(I)
J	CS/DS disaccharide	ΔUA(II)(β1→3)GalNAc(I)
K	CS-A disaccharide	ΔUA(II)(β1→3)GalNAc4S(I)
L	CS-C disaccharide	ΔUA(II)(β1→3)GalNAc6S(I)
M	unsaturated HA trisaccharide	ΔUA(III)(β1→3)GlcNAc(II)(β1→4)GlcA(I)
N	unsaturated HA tetrasaccharide	ΔUA(IV)(β1→3)GlcNAc(III)(β1→4)GlcA(II)(β1→3)GlcNAc(I)
O	unsaturated reduced CS-A tetrasaccharide	ΔUA(IV)(β1→3)GalNAc4S(III)(β1→4)GlcA(II)(β1→3)GalNAc 4S(I-ol)
P	unsaturated HA pentasaccharide	ΔUA(V)(β1→3)GlcNAc(IV)(β1→4)GlcA(III)(β1→3)GlcNAc(II) (β1→4)GlcA(I)

Q	*N*-acetylated Arixtra™	GlcNAc6S(V)(α1→4)GlcA(IV)(β1→4)GlcNAc3S6S(III)(α1→4)IdoA2S(II)(α1→4)GlcNAc6S(I)-CH_3
R	unsaturated HA hexasaccharide	ΔUA(VI)(β1→3)GlcNAc(V)(β1→4)GlcA(IV)(β1→3)GlcNAc(III)(β1→4)GlcA(II)(β1→3)GlcNAc(I)
S	unsaturated reduced HA hexasaccharide	ΔUA(VI)(β1→3)GlcNAc(V)(β1→4)GlcA(IV)(β1→3)GlcNAc(III)(β1→4)GlcA(II)(β1→3)GlcNAc(I-ol)
T	unsaturated reduced CS-A hexasaccharide	ΔUA(VI)(β1→3)GalNAc4S(V)(β1→4)GlcA(IV)(β1→3)GalNAc4S(III)(β1→4)GlcA(II)(β1→3)GalNAc4S(I-ol)

Table 4.2. Amide proton temperature coefficients in ppb/K measured at pH 7.40. Subdivision of the residues in column I distinguishes temperature coefficients measured for the reducing end sugar in the α (I-α) or β (I-β) conformation, or in a single conformation such as NAcArixtra, unsaturated reduced CS-A tetra- and hexasaccharides, and unsaturated reduced HA hexasaccharide (I)

Saccharide name / Residue number	I			II	III	IV	V
	I-α	I-β	I				
Chitin disaccharide, GlcNAc-GlcNAc	9.0	7.8		8.3			
Monosaccharide, GlcNAc6S	8.6	7.6					
Monosaccharide, GlcNAc	8.7	7.8					
Disaccharide, ΔUA2S-GlcNAc	8.3	7.4					
Monosaccharide, GalNAc	8.6	7.5					
Disaccharide, ΔUA-GlcNAc6S	8.4	7.5					
Disaccharide, ΔUA-GlcNAc	8.7	7.6					
Disaccharide, ΔUA2S-GlcNAc6S	8.3	7.5					
Disaccharide, ΔUA-GalNAc	8.1	7.2					
Disaccharide, ΔUA-GalNAc6S	8.2	7.4					
Disaccharide, ΔUA-GalNAc4S	7.4	7.2					
Monosaccharide, GlcNAc3S	7.1	8.1					
Unsaturated HA trisaccharide				6.7			
Unsaturated HA tetrasaccharide	8.9	7.6			6.7		
Unsaturated HA pentasaccharide				6.7		6.6	
Unsaturated HA hexasaccharide	8.9	7.5			6.6		6.5
Unsaturated reduced HA hexasaccharide			8.4		6.1		6.7
Unsaturated reduced CS-A tetrasaccharide			5.8		6.1		
Unsaturated reduced CS-A hexasaccharide			6.2		6.1		6.1
NAcArixtra			7.8		7.4		7.8

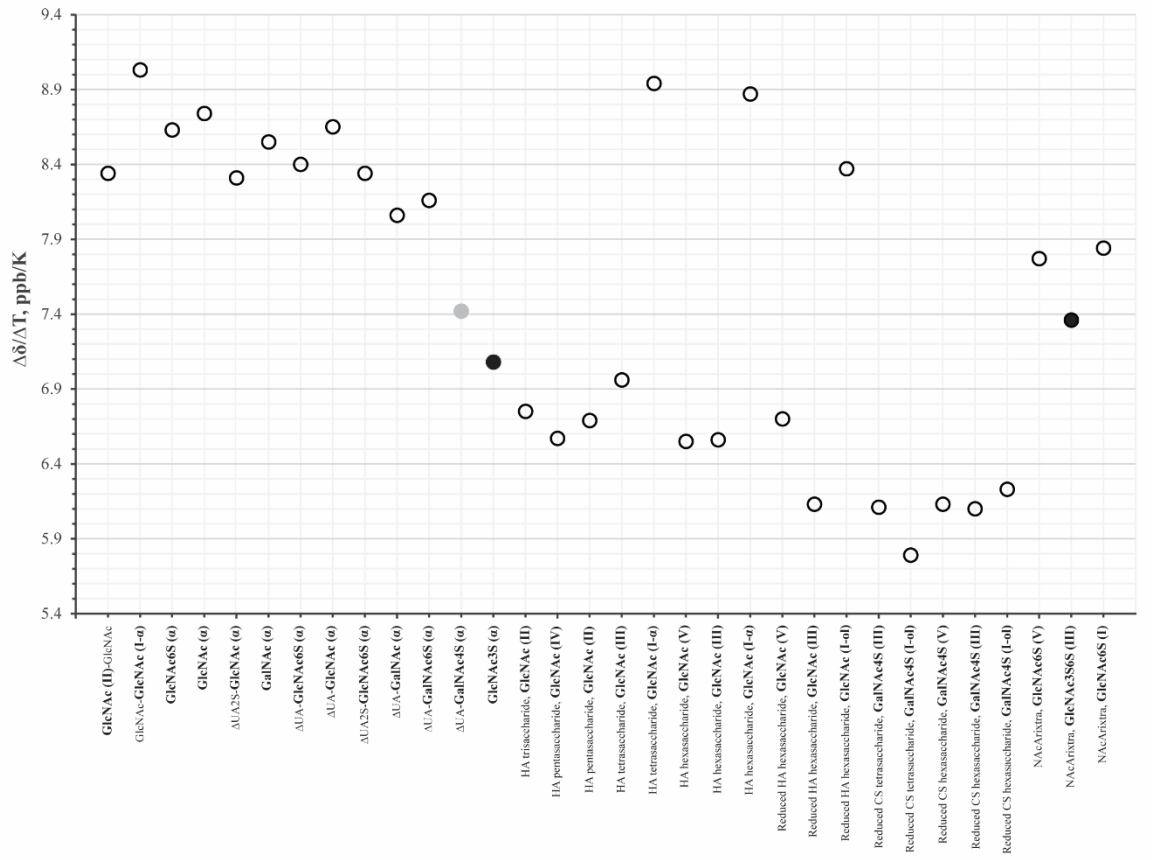

Figure 4.3. Graphical depiction of the data of the amide proton temperature coefficients presented in Table 4.2. The graph does not include the temperature coefficient of β conformers. The 3-*O*-sulfated residues are indicated by solid black circles and 4-*O*-sulfated GalNAc residue is highlighted by a solid grey circle.

The GlcNAc3S monosaccharide and NAcArixtra pentasaccharide are structurally unique and were prepared to facilitate evaluation the effect of a 3-*O*-sulfo group on an adjacent amide moiety. Previously, in Chapter 3, it was shown that the 3-*O*-sulfo group of the internal residue of de-*N*-sulfated Arixtra™ (dNSA) formed a hydrogen bond with amino protons stabilized by a salt bridge. The earlier work of Langeslay et al.[1] identified that the same 3-*O*-sulfo group in Arixtra™ was involved in a hydrogen bond with the adjacent sulfamate group proton. In this work, the *N*-sulfo groups of Arixtra™ were replaced by *N*-acetyl groups to evaluate possible hydrogen bond formation involving an amide proton and an adjacent 3-*O*-sulfo group. To our surprise, all three amide groups of NAcArixtra gave virtually identical $\Delta\delta/\Delta T$ values, a result that does not support the formation of a persistent hydrogen bond between the 3-*O*-sulfo group and the adjacent amide group of the internal glucosamine residue. This is in contrast to what was reported for the *N*-sulfated glucosamine of Arixtra™,[1] or observed for the unmodified amine group of dNSA in Chapter 2. Moreover, the $\Delta\delta/\Delta T$ values of NAcArixtra were slightly higher than those of the GlcNAc3S monosaccharide and opposed to the general trend formed by the other larger oligosaccharides.

Interestingly, the 3-*O*-sulfo group of the GlcNAc3S monosaccharide showed the most reduced $\Delta\delta/\Delta T$ value of all mono- and disaccharides. A slightly higher $\Delta\delta/\Delta T$ value was observed for ΔUA(II) (β1→3) GalNAc4S(I). This disaccharide has three distinctive features that distinguishes it from the GlcNAc3S monosaccharide, including a 4-*O*-sulfated GalNAc residue (GalNAc4S), and an unsulfated unsaturated uronic acid residue (ΔUA) connected to GalNAc4S by a β1→3 glycosidic linkage. The temperature coefficients for

GalNAc and GlcNAc are not significantly different, so the effect of sugar type can be excluded. Replacement of the GalNAc 4-*O*-sulfo group with a 6-*O*-sulfo group in ΔUA(II) (β1→3) GalNAc6S(I) led to increased Δδ/ΔT relative to ΔUA(II) (β1→3) GalNAc6S(I). Also, there is no difference in the Δδ/ΔT values for ΔUA(II) (β1→3) GalNAc6S(I) and the unsubstituted ΔUA(II) (β1→3) GalNAc(I), indicating that the 6-*O*-sulfo substituent is too distant to affect the amide proton.

Comparison of the effect of different glycosidic linkages for ΔUA(II) (β1→3) GalNAc(I) and ΔUA(II) (β1→4) GlcNAc(I) indicates a slightly higher Δδ/ΔT associated with the β1→4 linkage. Insertion of the 2-*O*-sulfo group in the unsaturated uronic acid residue of ΔUA2S(II) (β1→4) GlcNAc(I) and produced a slight decrease in Δδ/ΔT compared with ΔUA(II) (β1→4) GlcNAc(I). Identical results were obtained for ΔUA2S(II) (β1→4) GlcNAc(I) and ΔUA2S(II) (β1→4) GlcNAc6S(I) and, as with GalNAc, no effect was observed between the unsulfated and 6-*O*-sulfated GlcNAc monosaccharides. Interestingly, however, replacement of the ΔUA with a GlcNAc residue produced a larger Δδ/ΔT for GlcNAc(II) (β1→4) GlcNAc(I).

Comparison of the amide proton's Δδ/ΔT within monosaccharides and disaccharides revealed the following trends: (1) no difference is observed between types of unsulfated amino sugars; (2) the amide protons in disaccharides with a β1→3 glycosidic linkage have slightly reduced Δδ/ΔT values relative to the β1→4 linkage; (3) 6-*O*-sulfation had no or a very little effect on Δδ/ΔT; (4) negatively charged unsaturated uronic acid residues decreased Δδ/ΔT, while 2-*O*-sulfo substituted ΔUA residues contributed to further

decreases in Δδ/ΔT; and (5) 4-*O*-sulfated and 3-*O*-sulfated amino sugars had significantly reduced Δδ/ΔT compared to other mono- and disaccharides.

The monosaccharide GlcNAc3S gave Δδ/ΔT values comparable to the larger oligosaccharides. Across the large oligosaccharides, the most reduced Δδ/ΔT values were observed for the unsaturated tetra- and hexasaccharides derived from CS-A, and unsaturated HA hexasaccharide. The Δδ/ΔT values of amide protons of the reducing end residues were consistent with the Δδ/ΔT's of mono- and disaccharides. The amides of the CS-A oligosaccharides had lower Δδ/ΔT values compared to the unsulfated HA oligosaccharides, further supporting the effect of 4-*O*-sulfation on reduction of Δδ/ΔT values.

Another important observation is that the presence of glucuronic acid (GlcA) in reduces the Δδ/ΔT of adjacent amide-containing residues, especially when the amide-containing residue is situated between two GlcA residues. For disaccharides with an unsaturated uronic acid at the non-reducing end, the presence of the ΔUA residue appears to slightly reduce the Δδ/ΔT of the preceding *N*-acetylated amine group. In larger oligosaccharides, when the *N*-acetylated amine group is preceded by a GlcA residue and followed by an unsaturated uronic acid, the amide proton Δδ/ΔT value is reduced more substantially, as can be observed for the unsaturated HA trisaccharide. Furthermore, the GlcNAc6S(I) and GlcNAc6S(V) residues of NAcArixtra, which are linked to only one uronic acid, showed higher values of Δδ/ΔT than the amide of GlcNAc3S6S(III) which is situated between GlcA(IV) and IdoA2S(II) residues.

Because the concentrations of the saccharide samples studied varied due to the limited availability of some compounds, we evaluated the effect of sugar and phosphate buffer concentrations on our measurements. Temperature coefficients of 10 mM GlcNAc in 10 mM phosphate buffer (α = 8.7 ppb/K, β = 7.8 ppb/K), 100 mM GlcNAc in 10 mM phosphate buffer (α = 8.6 ppb/K, β = 7.6 ppb/K), and 10 mM GlcNAc in 50 mM phosphate buffer (α = 8.6 ppb/K, β = 7.5 ppb/K) showed no large deviations that can be ascribed to either the saccharide or buffer concentration. Similarly, 10 mM GalNAc in 10 mM phosphate buffer (α = 8.6 ppb/K, β = 7.5 ppb/K), 100 mM GalNAc in 10 mM phosphate buffer (α = 8.5 ppb/K, β = 7.5 ppb/K), and 10 mM GalNAc in 50 mM phosphate buffer (α = 8.7 ppb/K, β = 7.6 ppb/K) also showed no large deviations. Errors in the experimental values of $\Delta\delta/\Delta T$ are estimated to be around ± 0.1 ppb/K due to differences in sample preparation, shimming, temperature fluctuations and error in the temperature calibration using the external methanol standard.

4.3.2. Line-shape analysis and energy barriers. The variable temperature experiments used for the calculation of temperature coefficients can also provide information about the solvent exchange of the labile protons. Resonance line widths are related to the rate constant (k_{ex}) of the solvent exchange reaction and were measured for the amide protons by nonlinear least squares fitting of a Lorentzian peak shape to the experimental spectra using MestReNova-12.0.1 as shown in Figure 4.4A. The extracted line widths at half height were plotted as a function of the calibrated temperatures as shown in Figure 4.4B, followed by fitting into the Eyring-Polanyi equation (Eq. 1.1) to calculate the energy barrier, $\Delta G^{\ddagger}$, associated with amide proton solvent exchange. Example with

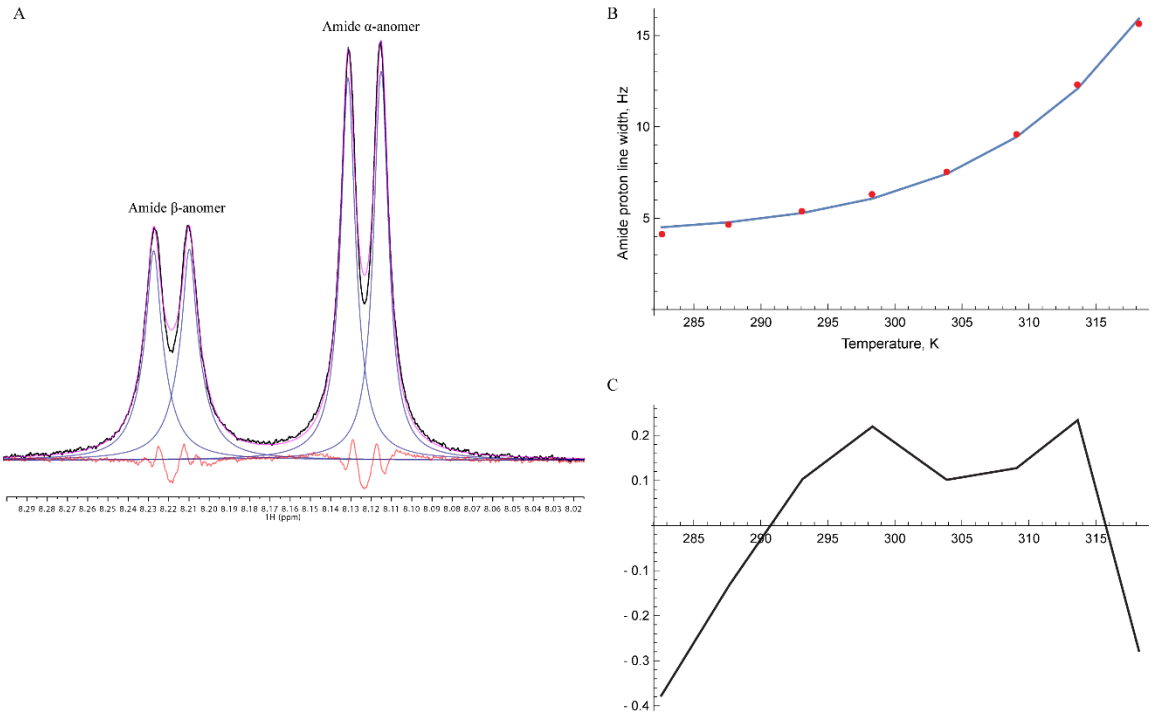

Figure 4.4. (A) Example of amide proton resonance peak fitting to extract the line widths at half height for a GlcNAc α and β anomer measured at 293.2 K using MestReNova-12.0.1 software. Experimentally measured spectrum is plotted in black, simulated spectrum in blue, fitted spectrum in purple with residuals shown in red. (B) Example plot for the determination of activation energy barriers, $\Delta G^{\ddagger}$, for GlcNAc α anomer. Each red data point corresponds to amide proton resonance line width measured at half height as function of calibrated temperature. Blue line is an exponential fit of the data to the Eyring-Polanyi equation (Eq. 1.1.). (C) Residual line widths (difference between measured and fitted line widths) for plot shown in (B).

detailed $\Delta G^{\ddagger}$ calculation can be found in Figure A3 (Appendix). The calculated values of $\Delta G^{\ddagger}$ are summarized in Table 4.3.

Again, the data presented in Table 4.3 can be more easily visualized as a graph of $\Delta G^{\ddagger}$ plotted as a function of the corresponding amide-containing residue. Figure 4.5 plots the measured $\Delta G^{\ddagger}$ values using the same saccharide order as in Figure 4.3. Comparison of Figures 4.3 and 4.5 reveals that the trend of the $\Delta G^{\ddagger}$ values is reciprocal to that for the $\Delta\delta/\Delta T$ values. In other words, amide protons with reduced values of $\Delta\delta/\Delta T$ have generally higher activation energy barriers, meaning that their rate of exchange with water molecules is slower. This is in contrast to the reduced $\Delta\delta/\Delta T$ value and accelerated solvent exchange rates observed for the dNSA GlcN3S6S(III) amine protons in Chapter 3.

Most interesting is the high energy barrier calculated for the internal GlcNAc3S6S(III) residue of NAcArixtra. The hydrogen bond identified by Langeslay et al. involving the internal Arixtra™ GlcNS3S6S(III) sulfamate proton was supported by both a reduced temperature coefficient and a high energy barrier for solvent exchange.[1] In contrast, despite its higher $\Delta G^{\ddagger}$ value, the absence of a reduced temperature coefficient does not support the participation of the NAcArixtra GlcNAc3S6S(III) amide proton in a hydrogen bond.

Distinctively different $\Delta G^{\ddagger}$ values were observed for the 3-*O*- and 4-*O*-sulfated residues of GlcNAc3S and ΔUA(II) (β1→3) GalNAc4S(I), respectively. Their $\Delta G^{\ddagger}$ values are comparable to those measured for the larger oligosaccharides. Furthermore, the energy barrier for amide proton solvent exchange in the chitin disaccharide, which lacks a linkage to a uronic acid residue, was the lowest value of all the saccharides examined.

Table 4.3. Calculated activation energy barriers, $\Delta G^{\ddagger}$ (in kcal/mol) associated with amide proton solvent exchange. Errors were calculated through a numerical estimate of the covariance matrix and corresponded to ± 2.48 times the standard error for each parameter in this two-parameter fit. To compensate for systematic errors, the calculated errors for each measurement were rounded up to ± 0.1 kcal/mol.

Saccharide name / Residue number	I			II	III	IV	V
	I-α	I-β	I				
Chitin disaccharide, GlcNAc-GlcNAc	16.2	15.6		15.8			
Monosaccharide, GlcNAc6S	16.2	15.7					
Monosaccharide, GlcNAc	16.4	15.8					
Disaccharide, ΔUA2S-GlcNAc	16.4	15.9					
Monosaccharide, GalNAc	16.5	15.9					
Disaccharide, ΔUA-GlcNAc6S	16.5	15.7					
Disaccharide, ΔUA-GlcNAc	16.5	15.5					
Disaccharide, ΔUA2S-GlcNAc6S	16.6	16.0					
Disaccharide, ΔUA-GalNAc	16.8	16.0					
Disaccharide, ΔUA-GalNAc6S	16.9	15.9					
Disaccharide, ΔUA-GalNAc4S	17.7	16.2					
Monosaccharide, GlcNAc3S	17.8	17.7					
Unsaturated HA trisaccharide				17.6			
Unsaturated HA tetrasaccharide	16.6	16.0			17.5		
Unsaturated HA pentasaccharide				18.0		17.8	
Unsaturated HA hexasaccharide	16.9	16.0			17.7		17.6
Unsaturated reduced HA hexasaccharide			16.9		17.7		17.6
Unsaturated reduced CS-A tetrasaccharide			17.7		17.6		
Unsaturated reduced CS-A hexasaccharide			18.4		17.8		17.6
NAcArixtra			17.4		19.5		17.4

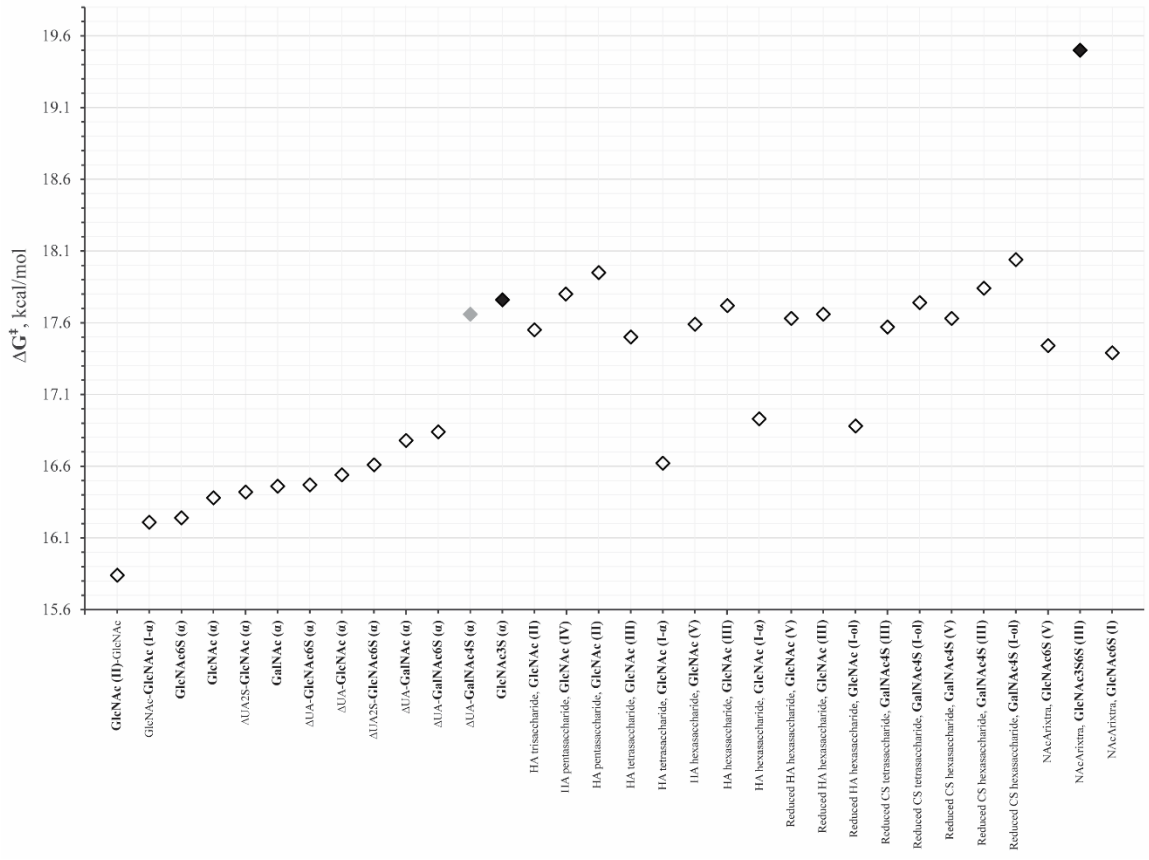

Figure 4.5. Graphical depiction of the amide proton $\Delta G^{\ddagger}$ results from Table 4.3 with the β conformers omitted. The saccharide order is the same as in Figure 4.3. 3-*O*-sulfated GlcNAc residues are highlighted with solid black diamonds and the 4-*O*-sulfated GalNAc residue is indicated with a solid grey diamond.

These observations suggest that charge plays an important role in the energy barriers for amide proton exchange with water. Given the role of H^+ and OH^- ions in catalyzing the solvent exchange of labile protons, as described by Eq. 1.2 ($k_{ex} = k_{H^+}[H^+] + k_{OH^-}[OH^-]$), the proximity of centers of negative charge nearby an amide proton would be expected to slow exchange by repulsing OH^- ions, which would be reflected by higher values of $\Delta G^{\ddagger}$. To examine the effects of negatively charged groups on amide proton exchange, pH titrations were performed for a set of saccharides with unique structural differences as described in the following section.

4.3.3. Effects of pH on labile proton resonance linewidths. ^{1}H NMR spectra were acquired as a function of pH for GalNAc, GlcNAc, GlcNAc6S, GlcNAc3S, the chitin disaccharide and NAcArixtra. The linewidths of the amide proton resonances of these saccharides are plotted in Figure 4.6 as a function of pH. It was previously reported that amide proton exchange with water occurs through an acid-base catalysis mechanism.[31, 32] As noted in Section 1.4.2, rate constants for the acid and base catalyzed exchange reactions are not equal and depend on the chemical system. From Figure 4.6, it is apparent that in the acidic region there are no changes in the amide proton line widths even at the lowest pH tested (~2.5). In the resonance structure of amide groups, the carbonyl oxygen atom is partially negatively charged, while the amide nitrogen carries partial positive charge. Consequently, charge repulsion between the partially positively charged nitrogen and hydronium ions at low pH prevents acid catalyzed exchange. As the pH is raised, the concentration of hydroxyl ions increases and base catalyzed exchange rates increase resulting in line broadening.

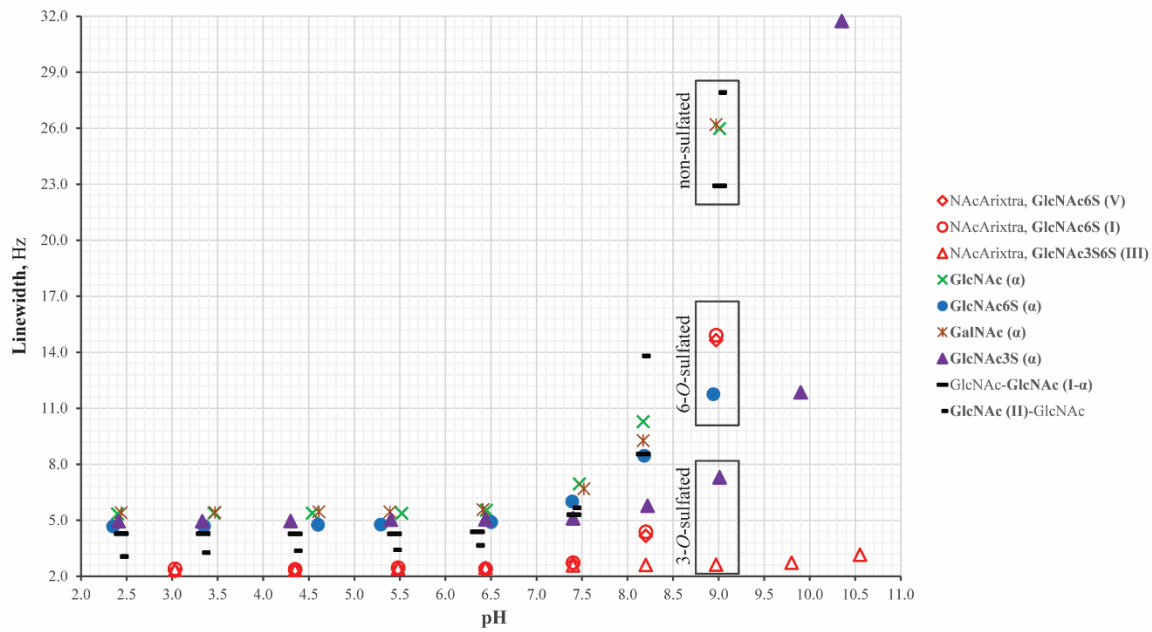

Figure 4.6. pH titration of GalNAc, GlcNAc, chitin disaccharide, GlcNAc6S, GlcNAc3S, and NAcArixtra. Line widths of the amide resonances were measured as function of solution pH at 298.2 K.

Closer examination of the basic region of Figure 4.6 reveals interesting trends correlated to the saccharide structures. At pH 9, the uncharged saccharides have the broadest resonances reflecting faster solvent exchange. In contrast, for the sulfated sugars, the bulky negatively charged sulfate groups repel the negatively charged hydroxyl ions, reducing the extent of base catalyzed solvent exchange and producing less line broadening. Because of the close spatial proximity of the 3-*O*-sulfo and amide groups, base catalyzed exchange is least effective for the 3-*O*-sulfated saccharide residues. Though increased line broadening is observed for the GlcNAc3S monosaccharide above pH 9, the NAcArixtra GlcNAc3S6S(III) amide proton is unaffected by increases in pH. In addition to the 3-*O* and 6-*O* sulfo groups of this residue, the additional negative charges from the adjacent GlcA and IdoA2S residues contribute to the negative charge density in the neighborhood of the amide proton, essentially shutting down the base catalyzed exchange mechanism.

To further evaluate the effect of structure and charge repulsion on the solvent exchange rates of labile protons, we performed a similar NMR pH titration for the *N*-sulfated monosaccharides GlcNS, GlcNS3S, GlcNS6S, and GlcNS3S6S. Because the sulfamate nitrogen does not have a resonance structure and the charge on nitrogen is neutral, acid and base catalysis of the sulfamate proton exchange is observed in Figure 4.7 as expected. However, based on the results for the *N*-acetylated saccharides (Figure 4.6), monosaccharides containing a 3-*O*-sulfo group should repel hydroxide ions and reduce the contributions from base catalyzed exchange. Among the monosaccharides examined, only GlcNS has no *O*-sulfo groups and therefore it should experience the greatest base catalyzed exchange as observed in Figure 4.7. The pH dependent line broadening experienced by the

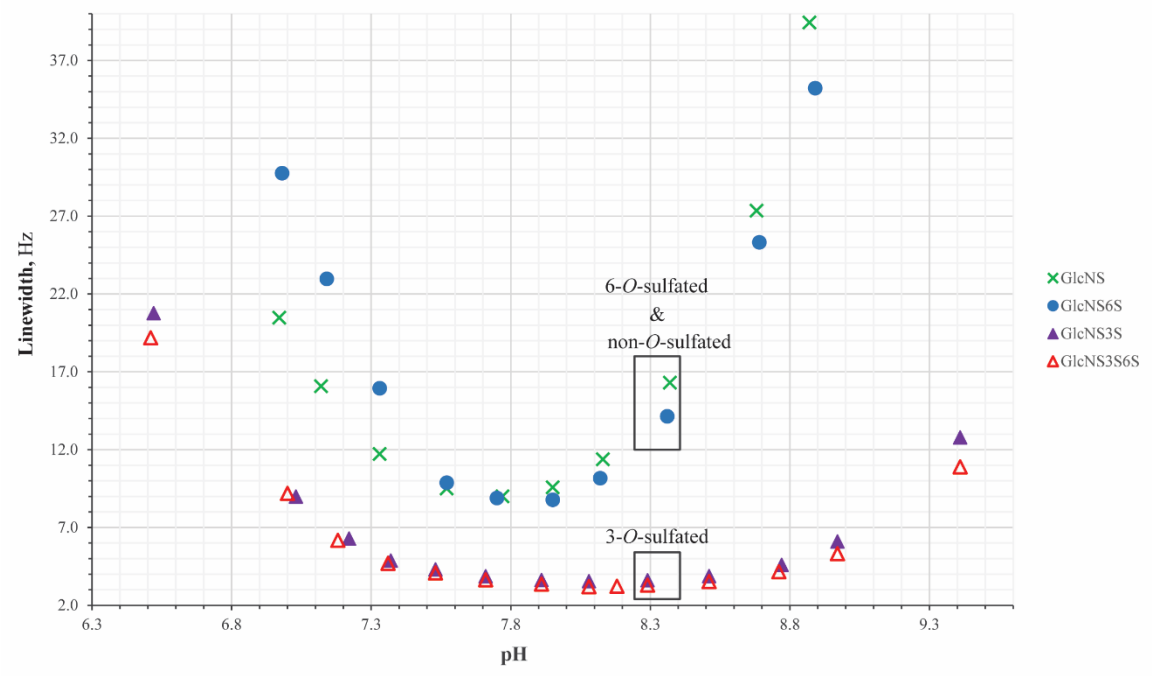

Figure 4.7. pH titration of *N*-sulfo glucosamine monosaccharides: D-glucosamine-2-*N*-sulfate (GlcNS), D-glucoamine-2-*N*,3-*O*-disulfate (GlcNS3S), D-glucosamine-2-*N*,3-*O*- and 6-*O*-trisulfate (GlcNS3S6S), and D-glucosamine-2-*N*,6-*O*-disulfate (GlcNS3S6S). Line widths of the sulfamate resonances were measured as function of solution pH at 298.2 K.

6-*O*-sulfated GlcNS sulfamate proton is only slightly less than that of GlcNS because the 6-*O*-sulfo group is located far from the sulfamate and only weakly repels the hydroxyl ions. Finally, the sulfamate line widths of the GlcNS3S and GlcNS3S6S monosaccharides are least affected by increasing pH because the adjacent bulky negatively charged 3-*O*-sulfate group effectively repels hydroxyl ions. A similar pH titration curve was reported for the sulfamate group of the Arixtra™ GlcNS3S6S(III) residue by Langeslay et al. with narrow line widths observed even at pH values near 11.[1] Though Langeslay et al. attributed this unusual pH stability to the participation of the sulfamate proton in a hydrogen bond with the 3-*O*-sulfo group, based on the results obtained for the *N*-sulfo glucosamine monosaccharides in Figure 4.7 and the similar pH dependence of the NAcArixtra titration curve (Figure 4.6) it is clear that the lack of line broadening of the Arixtra™ GlcNS3S6S(III) sulfamate proton in basic solution is due to charge repulsion of the hydroxide ions and less effective base catalysis.

In another study, Beecher et al. identified three hydrogen bonds involving the hydroxyl protons of Arixtra™ by measurements of the hydroxyl proton solvent exchange rates and temperature coefficients.[2] The reduced exchange rates measured for two of the hydroxyl protons involved in hydrogen bonds were supported by reduced temperature coefficients. However, there was a discrepancy between the lower solvent exchange rate of the IdoA2S hydroxyl proton (OH3) and its large temperature coefficient. Because of the proximity of the IdoA2S 2-*O*-sulfo group, the reduced exchange rate observed for OH3 likely reflects charge repulsion of hydroxide ions and a reduction in base catalyzed solvent exchange rate. This information, together with the results presented in Chapter 3 confirm

that temperature coefficients are the most reliable indicators of hydrogen bonding, and that while exchange rates can provide important insights, their interpretation must include an understanding of the effects of local structure on the acid-base catalyzed solvent exchange mechanism.

4.4. Molecular dynamics simulations. To visualize the oligosaccharide structures and estimate the distances separating amide protons from the oxygens of *O*-sulfo groups and uronic acid carboxylates, we selected saccharides with variable sulfation patterns and size. The structures of mono- and disaccharides shown in Figure 4.8 were prepared as described in the experimental section. Figures 4.8 A, B, and C show monosaccharides of *N*-acetylated glucosamines that differ in the sulfation position. We can see that the GlcNAc3S 3-*O*-sulfo group is indeed closest to the amide group. Furthermore, the distance for the 4-*O*-sulfo group of the GalNAc4S residue (Figure 4.8E) is only 2.30 Å longer than that of the 3-*O*-sulfo group, which explains why the amide proton had the second highest activation energy of the measured mono- and disaccharides (Table 4.3). A shorter distance (4.3 Å) between the sulfamate proton and 3-*O* sulfo group was also measured for the GlcNS3S6S monosaccharide shown in Figure 4.9D. However, because the GlcNS3S6S monosaccharide needs to accommodate three negatively charged sulfate groups, the distance separating the sulfamate proton and 3-*O*-sulfo group is slightly longer (by 0.20 Å) than in GlcNAc3S. Therefore, all measured distances support charge repulsion of hydroxyl ions by neighboring negatively charged groups.

Interesting results were also obtained from the MD simulations for NAcArixtra, the unsaturated HA hexasaccharide, and the unsaturated CS-A hexasaccharide. Representative

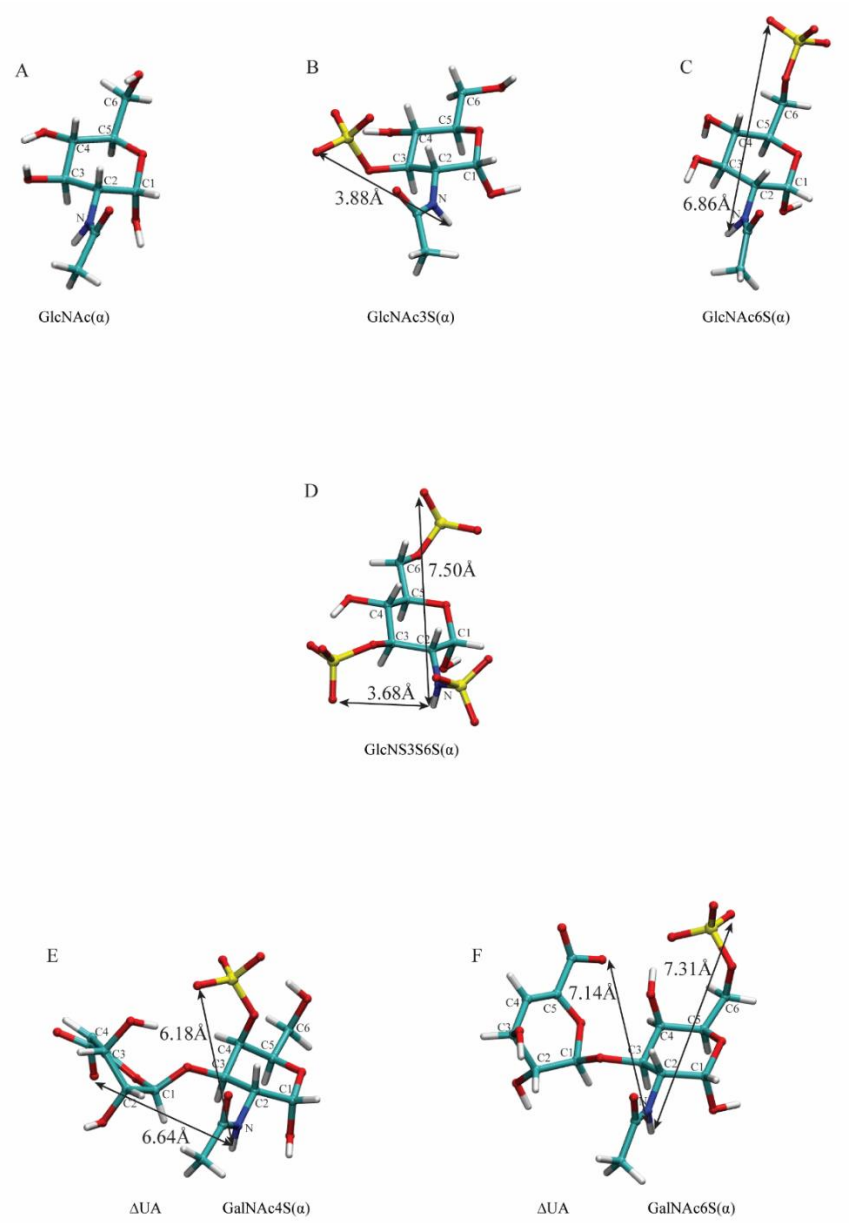

Figure 4.8. 3D representations of the mono- and disaccharides in the α conformation. (A) GlcNAc, (B) GlcNAc3S, (C) GlcNAc6S, (D) GlcNS3S6S, (E) ΔUA-GalNAc4S, and (F) ΔUA-GalNAc6S. For convenience, each carbon of the sugar ring is labeled according to its position relative to anomeric carbon (C1). Measured average distances separating amide/sulfamate proton and the *O*-sulfo groups are shown.

structures of each oligosaccharide taken from one of the simulation frames are shown in Figure 4.9. The experimentally observed effect of glucuronic acid on the adjacent amide-containing residue is reflected by the proximity of the negatively charged carboxylate oxygens to the amide protons. Consider, for example, the HA hexasaccharide, shown in Figure 4.9B. The amide proton of the GlcNAc(V) residue is only 3.16Å away from the GlcA(IV) carboxylate oxygens. Similarly, the amide proton of the GlcNAc(III) residue is only 3.01Å from the carboxylate oxygens of the GlcA(II) residue. In contrast, the distance between the amide proton in GlcNAc(III) and carboxylate oxygens of GlcA(IV) was almost two times greater, approaching 7.55Å. Also, the longer distance separating the carboxylate of the ΔUA(VI) residue and the amide proton of GlcNAc(V) residue (~ 6.71Å) explains the small effect of the ΔUA residue on solvent exchange rates. These observations are also applicable to the GlcA residues of the CS hexasaccharide and NAcArixtra, shown in Figure 4.9 C and D, respectively.

Finally, analysis of the trajectories of the MD simulations for the structures shown in Figure 4.9 predicted hydrogen bonds, however, none of the amide protons are involved in hydrogen bonds, consistent with experimental data. Hydrogen bond donor-acceptor pairs predicted by MD with occupancies greater than 25% lifetime of frames are highlighted with black dashed lines. The hydrogen bond that was predicted between the 2-*O*-sulfo group and OH3 hydroxyl proton in IdoA2S(II) (39%) was consistent with what was previously reported in Arixtra^{TM} (32%) when IdoA2S residue adopts a $^{2}S_{0}$ chair conformation. Another hydrogen bond between hydroxyl proton OH3 in GlcNAc6S(I) and ring oxygen of IdoA2S(II) (45%) was also previously reported for Arixtra^{TM} (32% when

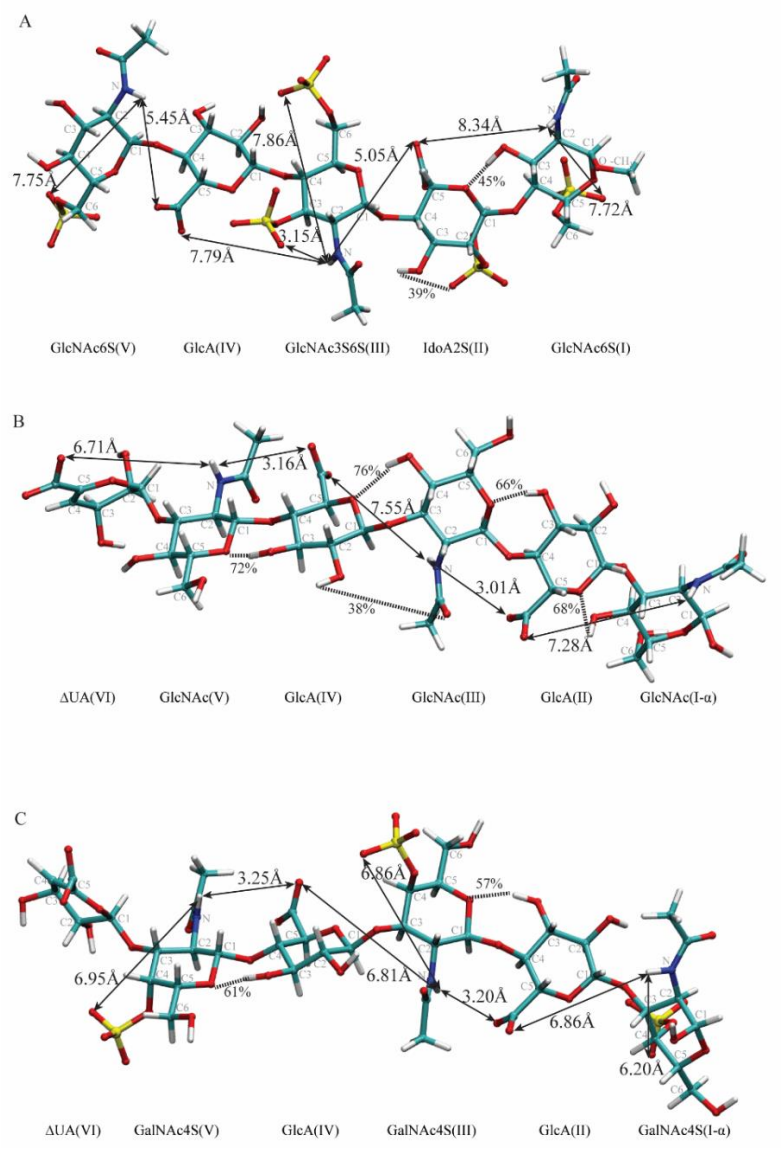

Figure 4.9. 3D representation of the penta- and hexasaccharides (A) *N*-acetylated Arixtra™ (NAcArixtra), (B) unsaturated HA hexasaccharide, and (C) unsaturated 4-*O*-sulfated chondroitin sulfate hexasaccharide. In addition to the shortest averaged distances separating the amide protons from oxygens of the *O*-sulfo groups, the distances separating amide protons from the uronic acid carboxylate oxygens are also reported, and hydrogen bonds, shown by striped bars, with occupancies greater than 25% are indicated.

IdoA2S residue adopts $^{2}S_{0}$, 60% when IdoA2S residue adopts $^{1}C_{4}$, and 43% overall). For the HA hexasaccharide, MD predicted hydrogen bonds involving all ring oxygens in internal residues with hydroxyl protons in adjacent residues. However, as can be seen from Figure 4.9C for the CS hexasaccharide, disruption of hydrogen bonds was observed between GalNAc4S(I) and GlcA(II) and between GalNAc4S(III) and GlcA(IV) when the 4-*O*-sulfo group was present in GalNAc residues.

4.4 Conclusions

By generating a library of *N*-acetylated saccharides, we evaluated the effect of structural features, including size, sulfation, and glycosidic linkage, on amide proton solvent exchange. Through the temperature experiment carried out at solution pH 7.4, we acquired one-dimensional NMR spectra from which amide proton temperature coefficients and energy barriers for solvent exchange were calculated. None of the structures were identified to be involved in hydrogen bonds, however, 3-*O*-sulfated amide-containing residues showed very distinctive and high energy barriers associated with reduced exchange rates. By comparison of the activation energy barriers for all the saccharides studied, we identified certain elements of saccharide structure that slow exchange by charge repulsion of hydroxyl ions reducing based catalyzed exchange. Negatively charged sulfate and carboxylate groups in close spatial proximity to amide protons reduce the exchange rate. The experimental observations were supported by distances calculated from MD simulations. Reduced exchange rates or very high activation energies cannot alone be used to identify hydrogen bonds involving the labile protons of GAG oligosaccharides and

should be interpreted in concert with additional evidence supporting hydrogen bond participation, such as a reduced temperature coefficient.

4.5. References

1. Langeslay, D. J.; Young, R. P.; Beni, S.; Beecher, C. N.; Mueller, L. J.; Larive, C. K., Sulfamate proton solvent exchange in heparin oligosaccharides: evidence for a persistent hydrogen bond in the antithrombin-binding pentasaccharide Arixtra. *Glycobiology* **2012,** *22* (9), 1173-82.

2. Beecher, C. N.; Young, R. P.; Langeslay, D. J.; Mueller, L. J.; Larive, C. K., Hydroxyl-proton hydrogen bonding in the heparin oligosaccharide Arixtra in aqueous solution. *J. Phys. Chem. B* **2014,** *118* (2), 482-91.

3. Beecher, C. N.; Larive, C. K., (1)H and (15)N NMR Characterization of the Amine Groups of Heparan Sulfate Related Glucosamine Monosaccharides in Aqueous Solution. *Anal. Chem.* **2015,** *87* (13), 6842-8.

4. Battistel, M. D.; Pendrill, R.; Widmalm, G.; Freedberg, D. I., Direct evidence for hydrogen bonding in glycans: a combined NMR and molecular dynamics study. *J. Phys. Chem. B* **2013,** *117* (17), 4860-9.

5. Eyring, H., The activated complex in chemical reactions. *J. Chem. Phys.* **1935,** *3* (2), 107-115.

6. Pechukas, P., Transition-State Theory. *Annu. Rev. Phys. Chem.* **1981,** *32*, 159-177.

7. Bain, A. D., Chemical exchange in NMR. *Prog. Nucl. Mag. Res. Sp.* **2003,** *43* (3-4), 63-103.

8. Sandstrom, C.; Baumann, H.; Kenne, L., NMR spectroscopy of hydroxy protons of 3,4-disubstituted methyl alpha-D-galactopyranosides in aqueous solution. *J. Chem. Soc. Perk. T 2* **1998,** (4), 809-815.

9. Dobson, C. M.; Lian, L. Y.; Redfield, C.; Topping, K. D., Measurement of Hydrogen-Exchange Rates Using 2d Nmr-Spectroscopy. *J. Magn. Reson.* **1986,** *69* (2), 201-209.

10. Chen, J. H.; Mao, X. A., Measurement of chemical exchange rate constants with solvent protons using radiation damping. *J. Magn. Reson.* **1998,** *131* (2), 358-361.

11. Chen, J. H.; Mao, X. A., Radiation damping transfer in nuclear magnetic resonance experiments via chemical exchange. *J. Chem. Phys.* **1997,** *107* (18), 7120-7126.

12. Baxter, N. J.; Williamson, M. P., Temperature dependence of H-1 chemical shifts in proteins. *J. Biomol. Nmr* **1997,** *9* (4), 359-369.

13. Adams, B.; Lerner, L., Observation of Hydroxyl Protons of Sucrose in Aqueous-Solution - No Evidence for Persistent Intramolecular Hydrogen-Bonds. *J. Am. Chem. Soc.* **1992,** *114* (12), 4827-4829.

14. Kindahl, L.; Sandstrom, C.; Norberg, T.; Kenne, L., H-1 NMR studies of hydroxy protons of the V[beta-Gal(1 -> 3)-alpha-GalNAc(1 -> O)THPGY glycopeptide. *Carbohyd. Res.* **2001,** *336* (4), 319-323.

15. Kindahl, L.; Sandstrom, C.; Norberg, T.; Kenne, L., H-1 NMR studies of hydroxy protons of Asn- and Ser-linked disaccharides in aqueous solution. *J. Carbohyd. Chem.* **2000,** *19* (9), 1291-1303.

16. Pomin, V. H.; Park, Y.; Huang, R.; Heiss, C.; Sharp, J. S.; Azadi, P.; Prestegard, J. H., Exploiting enzyme specificities in digestions of chondroitin sulfates A and C: production of well-defined hexasaccharides. *Glycobiology* **2012,** *22* (6), 826-38.

17. Ruhela, D.; Riviere, K.; Szoka, F. C., Jr., Efficient synthesis of an aldehyde functionalized hyaluronic acid and its application in the preparation of hyaluronan-lipid conjugates. *Bioconjug. Chem.* **2006,** *17* (5), 1360-3.

18. Price, K. N.; Tuinman, A.; Baker, D. C.; Chisena, C.; Cysyk, R. L., Isolation and characterization by electrospray-ionization mass spectrometry and high-performance anion-exchange chromatography of oligosaccharides derived from hyaluronic acid by hyaluronate lyase digestion: Observation of some heretofore unobserved oligosaccharides that contain an odd number of units. *Carbohyd. Res.* **1997,** *303* (3), 303-311.

19. Ohya, T.; Kaneko, Y., Novel hyaluronidase from streptomyces. *Biochim. Biophys. Acta.* **1970,** *198* (3), 607-9.

20. Nowotny, A., Reduction of Carbohydrates With NaBH4. In *Basic Exercises in Immunochemistry: A Laboratory Manual*, Nowotny, A., Ed. Springer Berlin Heidelberg: Berlin, Heidelberg, **1979**; pp 196-203.

21. Van Geet, A. L., Calibration of the methanol and glycol nuclear magnetic resonance thermometers with a static thermistor probe. *Anal. Chem.* **1968,** *40* (14), 2227-2229.

22. Liu, M. L.; Mao, X. A.; Ye, C. H.; Huang, H.; Nicholson, J. K.; Lindon, J. C., Improved WATERGATE pulse sequences for solvent suppression in NMR spectroscopy. *J. Magn. Reson.* **1998,** *132* (1), 125-129.

23. Case D.A., B. R. M., Cerutti D.S., Cheatham T.E., III, Darden T.A., Duke R.E., Giese T.J., Gohlke H., Goetz A.W., Homeyer N., Izadi S., Janowski P., Kaus J., Kovalenko A., Lee T.S., LeGrand S., Li S., Lin C., Luchko T., Luo R., Madej B., Mermelstein D., Merz K.M., Monard G., Nguyen H., Nguyen H.T., Omelyan I., Onufriev A., Roe D.R., Roitberg A., Sagui C., Simmerling C.L., Botello-Smith W.M., Swails J., Walker R.C.,

Wang J., Wolf R.M., Wu X., Xiao L., Kollman P.A. AMBER 16. University of California; San Francisco.

24. Kirschner, K. N.; Yongye, A. B.; Tschampel, S. M.; Gonzalez-Outeirino, J.; Daniels, C. R.; Foley, B. L.; Woods, R. J., GLYCAM06: a generalizable biomolecular force field. Carbohydrates. *J. Comput. Chem.* **2008,** *29* (4), 622-55.

25. Hornak, V.; Abel, R.; Okur, A.; Strockbine, B.; Roitberg, A.; Simmerling, C., Comparison of multiple Amber force fields and development of improved protein backbone parameters. *Proteins* **2006,** *65* (3), 712-25.

26. Jorgensen, W. L.; Chandrasekhar, J.; Madura, J. D.; Impey, R. W.; Klein, M. L., Comparison of Simple Potential Functions for Simulating Liquid Water. *J. Chem. Phys.* **1983,** *79* (2), 926-935.

27. Phillips, J. C.; Braun, R.; Wang, W.; Gumbart, J.; Tajkhorshid, E.; Villa, E.; Chipot, C.; Skeel, R. D.; Kale, L.; Schulten, K., Scalable molecular dynamics with NAMD. *J. Comput. Chem.* **2005,** *26* (16), 1781-802.

28. Darden, T.; York, D.; Pedersen, L., Particle Mesh Ewald - an N.Log(N) Method for Ewald Sums in Large Systems. *J. Chem. Phys.* **1993,** *98* (12), 10089-10092.

29. Miyamoto, S.; Kollman, P. A., Settle - an Analytical Version of the Shake and Rattle Algorithm for Rigid Water Models. *J. Comput. Chem.* **1992**, 13 (8), 952-962.

30. Humphrey, W.; Dalke, A.; Schulten, K., VMD: visual molecular dynamics. *J. Mol. Graph.* **1996**, 14 (1), 33-8, 27-8.

31. Englander, S. W.; Kallenbach, N. R., Hydrogen exchange and structural dynamics of proteins and nucleic acids. *Q. Rev. Biophys.***1983,** 16 (4), 521-655.

32. Woodward, C. K.; Hilton, B. D., Hydrogen isotope exchange kinetics of single protons in bovine pancreatic trypsin inhibitor. *Biophys. J.* **1980**, 32 (1), 561-75.

CHAPTER FIVE

Conclusions and Future Directions

5.1. Conclusions

Glycosaminoglycans (GAGs) are important biological players. They are involved in a range of life-essential processes, from lubrication of the human joints to modulating complex signaling pathways. The family of GAGs, composed of heparin, heparan sulfate, chondroitin sulfate, dermatan sulfate, keratan sulfate, and hyaluronic acid, is synthesized by non-template driven biosynthetic pathways. Complications in GAG studies arise from their structural complexity introduced by post-biosynthetic backbone modifications produced by a variety of enzymatic complexes capable of encoding certain specificities into their final structures. Some of these elements of structure are required for specific binding to proteins or other regulators of biological processes. Additional factors that complicate research on GAGs include the structural polydispersity and heterogeneity of these linear unbranched polysaccharides, where the molecular weight of some members (hyaluronic acid) approach several million Daltons.[1]

Many GAG-protein interactions occur through non-specific binding of negatively charged polysaccharides with positively charged amino acids in proteins. However, some interactions require specific recognition by proteins through different structural motifs and elements localized within the polysaccharide chains. Furthermore, some of the interactions are highly dependent on particular arrangements of saccharide residues within the polysaccharide sequences, aptly illustrated by the well-studied heparin-antithrombin-III

interactions. Moreover, certain structural elements present in GAGs may play key roles in the pre-organization of the secondary structure of regions found within the polysaccharide chains in a manner that facilitates high affinity binding. In the case of heparin-antithrombin-III, it requires a pentasaccharide sequence that includes a GlcA-GlcNS3S6S-IdoA2A structural motif as the minimum sequence for high affinity binding.[2] Removal of the 3-*O*-sulfo group from GlcNS3S6S residue decreases the antithrombin-III binding affinity of an oligosaccharide 1000-fold.[3]

Langeslay et al. identified an additional unique feature of the same 3-*O*-sulfo group - its involvement in a persistent hydrogen bond with the adjacent *N*-sulfo proton of GlcNS3S6S in Arixtra™.[4] More recently, Beecher et al. complemented the findings of Langeslay et al. with two additional identified hydrogen bonds involving hydroxyl protons of Arixtra™.[5] These discoveries suggest that certain structural elements may be responsible for the pre-organization of regions of secondary structure that promote specific GAG-protein recognition. The motivation underlying my dissertation research has been the deeper exploration of the properties of GAG oligosaccharides in aqueous solution with the aim of advancing our understanding of the relationship between elements of primary structure and how they can stabilize secondary structure. Knowledge of these aspects can in turn enhance our understanding of GAG-protein interactions.

Investigation of the structures and physico-chemical properties of GAGs by NMR requires sufficient amounts of relatively pure materials, typically about 1 mg of each compound. Because of the heterogeneity and polydispersity of GAGs, structural studies typically rely on oligosaccharides derived from polysaccharides. The desired

oligosaccharide structures can often be obtained through chemical or enzymatic depolymerization of suitable polysaccharide substrates followed by chromatographic isolation. However, for rare but biologically important motifs, isolation from GAG digests can be quite challenging given the labor-intensive nature of this process. In vitro chemoenzymatic and organic synthesis approaches under development show promise for the preparation of tailor-made heparin and heparan sulfate oligosaccharides but these methods are not yet robust or routine[6, 7]. The approach described in Chapter 2 relies on chemical modification of more abundant oligosaccharides to prepare novel oligosaccharides with desired structural elements. These oligosaccharides then were used in studies to explore their solution properties as discussed in Chapters 3 and 4. For example, to obtain access to heparan sulfate-like oligosaccharides containing the rare 3-*O*-sulfated glucosamine residue, the synthetic pentasaccharide Arixtra™ was modified by the chemical removal of the *N*-sulfo groups. As a result of the solvolytic de-*N*-sulfation reaction, we obtained the zwitterionic structure of de-*N*-sulfated Arixtra™ (dNSA) which provides an excellent substrate to examine the potential for salt bridge formation in heparan sulfate. Then, dNSA was further transformed by chemoselective *N*-acetylation into *N*-acetylated Arixtra™ (NAcArixtra). This unique semi-synthetic oligosaccharide provided an excellent substrate for the study of the solvent exchange properties of oligosaccharide amide protons, discussed in Chapter 4. Another important chemical modification of GAGs was the conversion of the reducing end aldose to an alditol through the reduction reaction with sodium borohydride. The isolation and structure elucidation of reduced oligosaccharides is simplified because the complexity introduced by the presence of α and

β anomers is removed. Finally, because these structural modifications involve chemical reactions that can potentially alter or degrade the targeted structures, all prepared oligosaccharides were structurally elucidated and confirmed by MS and NMR.

The hydrogen bond identified by Langeslay et al. in Arixtra^{TM} between the 3-*O*-sulfo group and the adjacent *N*-sulfamate proton suggests that a hydrogen bond or salt bridge could also be structurally important in the 3-*O*-sulfated glucosamine residues prevalent in heparan sulfate. In Chapter 3, the amino proton solvent exchange properties of dNSA and a structurally similar de-*N*-sulfated heparin tetrasaccharide (dNSt) are explored through measurements of temperature coefficients, exchange rates, and pK_a values. Reduced temperature coefficients, highly accelerated exchange rates promoted by neighboring negatively charged groups and altered the pK_a values of amino and carboxylate groups served as indicators of potential electrostatic interactions involving an amino group of the internal dNSA residue (GlcN3S6S(III)) and two negatively charged groups—the adjacent 3-*O*-sulfo group and the carboxylate group of the IdoA2S residue. To complement the experimental findings and visualize the trajectories of dNSA in water, we performed a 300 ns MD simulation using the GLYCAM 06g force field with custom adjusted partial charges on nitrogen and hydrogens of amino groups using GAUSSIAN B3LYP/6-31G.

In Chapter 4, a library of 20 saccharide structures was assembled differing in size, extent of sulfation, position of sulfation, glycosidic linkage, and type of amino sugar and uronic acid residue. Using this library, the effects of saccharide structure on amide proton solvent exchange were evaluated using temperature coefficients, the calculation of energy

barriers for exchange ($\Delta G^{\ddagger}$) obtained by line-shape analysis of NMR spectra acquired as a function of temperature, and pH titration to examine the role of structural elements, in particular sulfate and carboxylate groups, on the acid-base catalysis of amide proton-solvent exchange. We identified that charge repulsion of negatively charged hydroxyl ions takes place when negatively charged sulfates and carboxylates are in close spatial proximity to the amide protons. The strongest charge repulsion of hydroxyl ions is caused by the proximate 3-*O*-sulfo group, and as result the labile amide protons adjacent to the 3-*O*-sulfo group experience the highest energy barriers for solvent exchange and consequently the slowest exchange rates. The effects of charge repulsion on sulfamate proton exchange was also examined a for series of *N*-sulfated saccharides yielding similar observations and clarifying previous studies identifying hydrogen bonds involving the Arixtra™ sulfamate and hydroxyl protons. Although charge repulsion by the 4-*O*-sulfo group is less, its effect on amide proton exchange can be observed. In contrast the 6-*O*-sulfo group, which is much further away, has little to no effect on amide proton solvent exchange. Surprisingly, adjacent GlcA residues, especially those on the reducing end side of a GlcNAc residue exhibit a charge repulsion effect, reducing the magnitude of base-catalyzed amide exchange. The MD simulations revealed that the distance separating carboxylate oxygens of GlcA the adjacent residue (on the reducing end side) of the GlcNAc amide group proton is comparable to the distance separating the 3-*O*- and 4-*O*-sulfo groups from amide protons.

5.2. Future directions

Future research should be focused in two directions. One aspect would continue exploration of the properties of GAG oligosaccharides in aqueous solution with the aim of advancing our understanding of the relationship between elements of primary structure and how they stabilize secondary structure. The second direction is exploration of the biological properties of the novel dNSA and NAcArixtra oligosaccharides reported for the first time in this dissertation research.

The structure of Arixtra^{TM}, which contains the key structural elements required for high affinity binding to antithrombin-III, also provided an excellent substrate for further chemical modification to produce a model oligosaccharide with a 3-*O*-sulfated glucosamine residue mimicking a saccharide sequence occurring rarely in natural heparan sulfate. This modification led us to identify salt bridge involving amino group of the internal residue GlcN3S6S residue with the adjacent 3-*O*-sulfo group. Though this work suggested an additional electrostatic interaction between the GlcN3S6S(III) amino group and the adjacent IdoA2S residue carboxylate moiety, the evidence supporting this interaction was not conclusive. Therefore, we propose to measure and compare solvent exchange rates and pK_a values for the dNSA amino groups in the presence and absence of carboxylates. For this purpose, carboxylate groups will be replaced by neutral groups such as alcohols. This chemical modification can potentially be performed by using lithium aluminum hydride ($LiAlH_4$) which reduces the carboxylates to 1° alcohols. The chemical modification by the strong reducing agent $LiAlH_4$ will require preliminary optimization of the reaction followed by structural elucidation of resultant product. For example, because

the reduction reaction is typically performed in diethyl ether or tetrahydrofuran, it may be necessary to form the pyridinium salt of sulfated oligosaccharides to increase their solubility. Should this reaction prove difficult to execute, we will attempt to react the oligosaccharide carboxylate groups to generate the methyl ester.

In Chapter 4, the structures produced by chemical modification of NAcArixtra and GlcNAc3S were used to evaluate the effect of neighboring negatively charged groups on the catalysis of amide proton exchange with water. The effects of charge repulsion of the hydroxyl ions exerted by the negatively charged 3-*O*- and 4-*O*-sulfo groups was clear, however the strong dependence of neighboring negatively charged groups on exchange catalysis, rather than on overall oligosaccharide charge, was only postulated. Here we propose to selectively de-6-*O*-sulfate NAcArixtra using a solution composed of 90% DMSO and 10% methanol.[8] By comparison of the energy barriers for amide exchange in NAcArixtra and de-6-*O*-sulfated NAcArixtra, the effect of overall oligosaccharide charge on hydroxyl ions repulsion will be ascertained.

Perhaps the most exciting potential of this future work is the exploration of the biological properties of the novel dNSA and NAcArixtra oligosaccharides prepared in Chapter 2. Multiple research groups are pioneering novel methods of oligosaccharide preparation to explore the biological functions of 3-*O*-sulfated oligosaccharides.[7, 9] As mentioned in Chapter 3, specific 3-*O*-sulfated residues in heparan sulfate are believed to be responsible for assistance of herpes simplex virus 1 entry into the cells through their interactions with glycoprotein gD. Moreover, some reports link the specific binding of viral glycoprotein gD to polysaccharide chains of heparan sulfate containing -IdoA2S-

GlcN3S- and -IdoA2S-GlcN3S6S- residues in their sequences.[9-11] There are seven different types of heparan sulfate 3-*O*-sulfotransferases acting at the last stages of polysaccharide biosynthesis to insert 3-*O*-sulfo groups in the heparan sulfate polysaccharide.[12-15] Considering the other modifications incorporated by sulfotransferases and epimerases into the heparan sulfate polysaccharide chain at earlier steps of biosynthesis, the diversity of 3-*O*-sulfated structural variations is great. As a result, the precise 3-*O*-sulfated heparan sulfate oligosaccharide sequence required for gD binding is largely unknown.

To advance our current knowledge of the interactions of 3-*O*-sulfated residues of heparan sulfate with proteins and to better understand the biosynthetic mechanism of heparan sulfate, we propose to use our new compounds in biological studies designed to explore a structural role for 3-*O*-sulfated heparan sulfate. dNSA and NAcArixtra expand the library of available 3-*O*-sulfated oligosaccharides and provide another opportunity to investigate the relationships between 3-*O*-sulfated saccharides and biological function. Additionally, dNSA and NAcArixtra, can also be used for the discovery of novel proteins whose binding to heparan sulfate depends on 3-*O*-sulfation (expansion of the "3-*O*-sulfate proteome").[16] Recently, Thaker et al. reported utilization of the affinity matrices containing immobilized 3-*O*-sulfated heparan sulfate oligosaccharides on CNBr-activated Sepharose for screening potential proteins binding of whose influenced by 3-*O*-sulfation.[16] Through this work, they identified several proteins not previously known for preferential binding to 3-*O*-sulfated heparan sulfate. This approach is particularly well-suited for dNSA and NAcArixtra because it requires low quantities of the oligosaccharide (about 0.6 mg).

5.3. References

1. Almond, A., Hyaluronan. *Cell. Mol. Life Sci.* **2007,** *64* (13), 1591-6.

2. Lindahl, U.; Backstrom, G.; Hook, M.; Thunberg, L.; Fransson, L. A.; Linker, A., Structure of the antithrombin-binding site in heparin. *Proc. Natl. Acad. Sci. U. S. A.* **1979,** *76* (7), 3198-202.

3. Atha, D. H.; Lormeau, J. C.; Petitou, M.; Rosenberg, R. D.; Choay, J., Contribution of monosaccharide residues in heparin binding to antithrombin III. *Biochem.* **1985,** *24* (23), 6723-9.

4. Langeslay, D. J.; Young, R. P.; Beni, S.; Beecher, C. N.; Mueller, L. J.; Larive, C. K., Sulfamate proton solvent exchange in heparin oligosaccharides: evidence for a persistent hydrogen bond in the antithrombin-binding pentasaccharide Arixtra. *Glycobiology* **2012,** *22* (9), 1173-82.

5. Beecher, C. N.; Young, R. P.; Langeslay, D. J.; Mueller, L. J.; Larive, C. K., Hydroxyl-proton hydrogen bonding in the heparin oligosaccharide Arixtra in aqueous solution. *J. Phys. Chem. B* **2014,** *118* (2), 482-91.

6. Yang, W.; Yang, B.; Ramadan, S.; Huang, X., Preactivation-based chemoselective glycosylations: A powerful strategy for oligosaccharide assembly. *Beilstein. J. Org. Chem.* **2017,** *13*, 2094-2114.

7. Wang, Z.; Hsieh, P. H.; Xu, Y.; Thieker, D.; Chai, E. J.; Xie, S.; Cooley, B.; Woods, R. J.; Chi, L.; Liu, J., Synthesis of 3-O-Sulfated Oligosaccharides to Understand the Relationship between Structures and Functions of Heparan Sulfate. *J. Am. Chem. Soc.* **2017**.

8. Nagasawa, K.; Inoue, Y.; Kamata, T., Solvolytic desulfation of glycosaminoglycuronan sulfates with dimethyl sulfoxide containing water or methanol. *Carbohydr. Res.* **1977,** *58* (1), 47-55.

9. Liu, J.; Shriver, Z.; Pope, R. M.; Thorp, S. C.; Duncan, M. B.; Copeland, R. J.; Raska, C. S.; Yoshida, K.; Eisenberg, R. J.; Cohen, G.; Linhardt, R. J.; Sasisekharan, R., Characterization of a heparan sulfate octasaccharide that binds to herpes simplex virus type 1 glycoprotein D. *J. Biol. Chem.* **2002,** *277* (36), 33456-67.

10. Liu, J.; Shriver, Z.; Blaiklock, P.; Yoshida, K.; Sasisekharan, R.; Rosenberg, R. D., Heparan Sulfate d-Glucosaminyl 3-O-Sulfotransferase-3A SulfatesN-Unsubstituted Glucosamine Residues. *J. Biol. Chem.* **1999,** *274* (53), 38155-38162.

11. Shukla, D.; Liu, J.; Blaiklock, P.; Shworak, N. W.; Bai, X.; Esko, J. D.; Cohen, G. H.; Eisenberg, R. J.; Rosenberg, R. D.; Spear, P. G., A novel role for 3-O-sulfated heparan sulfate in herpes simplex virus 1 entry. *Cell* **1999,** *99* (1), 13-22.

12. Sarrazin, S.; Lamanna, W. C.; Esko, J. D., Heparan sulfate proteoglycans. *Cold Spring Harb. Perspect. Biol.* **2011,** *3* (7), a004952.

13. Kreuger, J.; Kjellen, L., Heparan sulfate biosynthesis: regulation and variability. *J. Histochem. Cytochem.* **2012,** *60* (12), 898-907.

14. Whitelock, J. M.; Iozzo, R. V., Heparan sulfate: a complex polymer charged with biological activity. *Chem. Rev.* **2005,** *105* (7), 2745-64.

15. Bishop, J. R.; Schuksz, M.; Esko, J. D., Heparan sulphate proteoglycans fine-tune mammalian physiology. *Nature* **2007,** *446* (7139), 1030-7.

16. Thacker, B. E.; Seamen, E.; Lawrence, R.; Parker, M. W.; Xu, Y.; Liu, J.; Vander Kooi, C. W.; Esko, J. D., Expanding the 3-O-Sulfate Proteome--Enhanced Binding of Neuropilin-1 to 3-O-Sulfated Heparan Sulfate Modulates Its Activity. *ACS Chem. Biol.* **2016,** *11* (4), 971-80.

APPENDIX

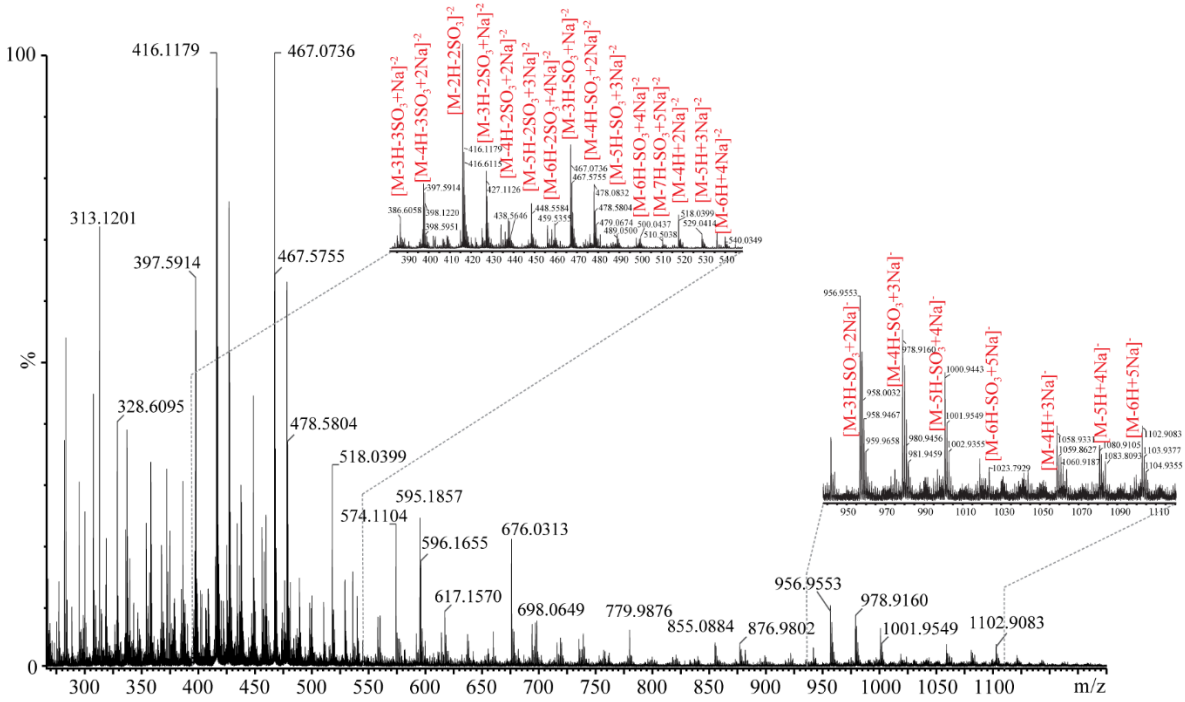

Figure A1. Mass spectrum of dNSt measured using an ESI Q-TOF mass spectrometer operating in negative ionization mode. The expected mass of dNSt, 993.54 U, was confirmed.

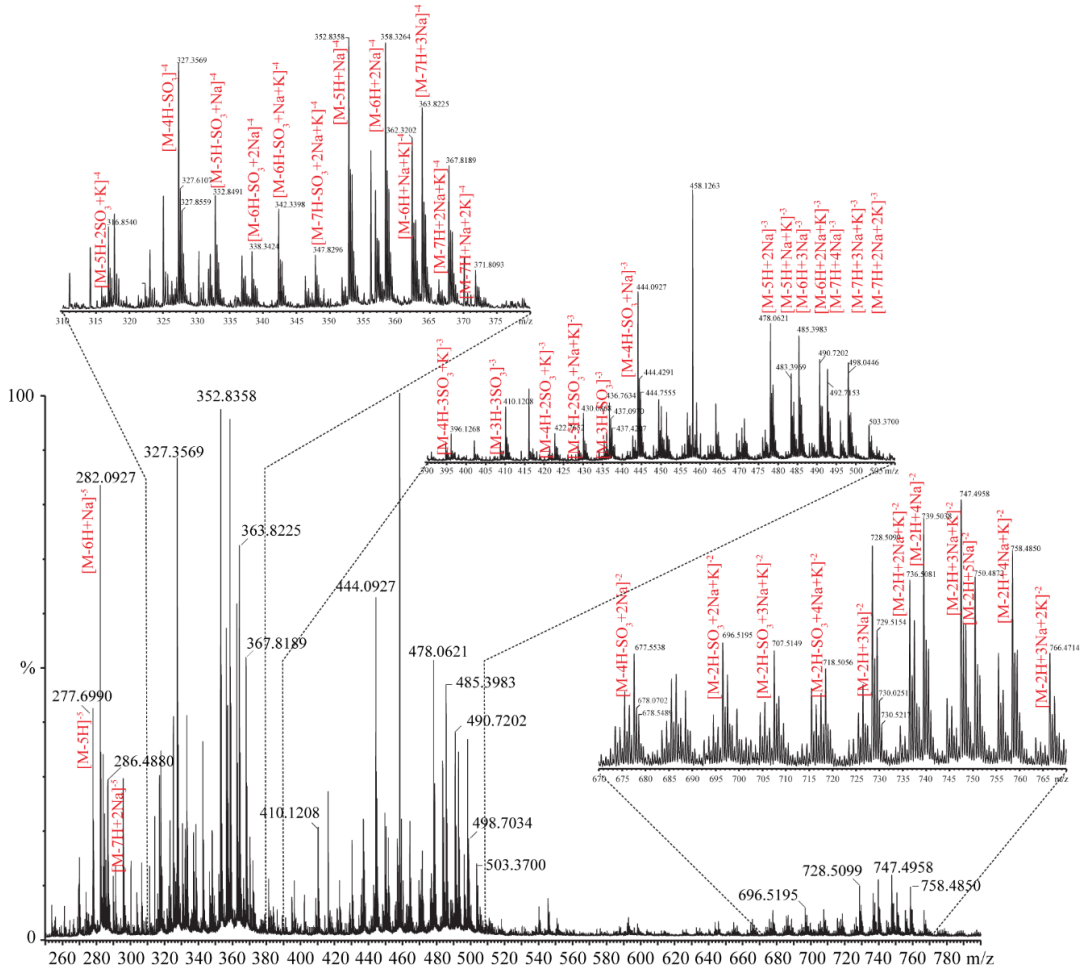

Figure A2. Mass spectrum of *N*-acetylated Arixtra (NAcArixtra) obtained using an ESI Q-TOF mass spectrometer operating in negative ionization mode. The expected mass of NAcArixtra, 1393.11 U, was confirmed. In contrast to the results for dNSA and dNSt, the NAcArixtra molecular ions were also accompanied by potassium adducts introduced during pH measurement due to a leaky pH electrode. Even though sample was desalted it still retained potassium ions. The spectrum also indicates that the sample contains other trace impurities possibly arising from unreacted or partially reacted reaction mixture components.

Table A1. Assignment of the carbon-bound protons of dNSt at pD 11.5 in 10 mM phosphate buffer acquired at 298.2 K. Chemical shift values from COSY spectra are reported to two decimal places while those extracted from the 1D spectra are reported to three decimal places.

Residue	Proton	^{1}H Chemical shift, ppm
		dNSt, pD 11.5
GlcN6S (I)	1 (α)	5.052
	1 (β)	5.024
	2 (α)	2.73
	2 (β)	2.71
	3	3.58
	4	3.74
	5	3.97
	6	4.20
	6’	4.35
IdoA2S (II)	1 (α)	5.145
	1 (β)	5.174
	2 (α)	4.26
	2 (β)	4.29
	3 (α)	4.18
	3 (β)	4.20
	4 (α)	4.05
	4 (β)	4.06
	5 (α)	4.844
	5 (β)	4.829
GlcN6S (III)	1	5.365
	2 (α)	2.75
	2 (β)	2.73
	3	3.57
	4	3.72
	5	3.99
	6	4.18
	6’	4.33
ΔUA2S (IV)	1	5.477
	2	4.621
	3	4.31
	4	5.982

Table A2. Comparison table of carbon-bound chemical shifts for heparin tetrasaccharide[1] and dNSt, structures shown in Figure 3.1D and E. Chemical shifts of heparin tetrasaccharide were measured at 293.2 K in 10 mM phosphate buffer, pD 7.0. Chemical shifts of dNSt were measured at 298.2 K in 10 mM phosphate buffer, pD 8.7. Chemical shift values from COSY spectra are reported to two decimal places while those extracted from the 1D spectra are reported to three decimal places.

Residue	Proton	^{1}H Chemical shift, ppm	
		Heparin tetrasaccharide	dNSt, pD 8.7
GlcN6S (I)	1	5.43	5.303 (α) / 5.367 (β)
	2	3.251	3.186 (α) / 3.084 (β)
	3	3.69	3.84
	4	3.74	3.71
	5	4.12	3.94
	6	4.30	4.16
	6’	4.36	4.29
IdoA2S (II)	1	5.209	5.21
	2	4.31	4.31
	3	4.20	4.27
	4	4.10	4.12
	5	4.75	4.86
GlcN6S (III)	1	5.414	5.530
	2	3.292	3.142
	3	3.64	3.79
	4	3.83	3.75
	5	4.03	3.99
	6	4.25	4.20
	6’	4.35	4.34
ΔUA2S (IV)	1	5.496	5.487
	2	4.62	4.623
	3	4.31	4.306
	4	5.991	6.000

Table A3. Amino proton assignment in dNSt acquired in 85% H_2O/15% acetone-d_6 solution

Residue	^{1}H Chemical shift, ppm	Solution conditions	
		pH	T, K
GlcN6S (I) α	8.044	1.6	259.5
GlcN6S (I) β	8.471		
GlcN6S (III) α	8.351		
GlcN6S (III) β	8.327		

Table A4. Assignment of the carbon-bound proton of the reduced chondroitin sulfate tetrasaccharide at pD 9.10 in 10 mM phosphate buffer acquired at 316.2 K. Chemical shift values from COSY spectra are reported to two decimal places while those extracted from the 1D spectra are reported to three decimal places.

Residue	Proton	^{1}H Chemical shift, ppm
		pD 9.1
GalNAc4S-ol (I)	1	3.69
	1’	3.70
	2	4.27
	3	4.24
	4	4.484
	5	4.13
	6	3.68
	6’	3.70
	amide -CH_3	2.089
GlcA (II)	1	4.62
	2	3.456
	3	3.632
	4	3.86
	5	3.77
GalNAc4S (III)	1	4.655
	2	4.071
	3	4.15
	4	4.62
	5	3.86
	6	3.76
	6’	3.80
	amide -CH_3	2.004
ΔUA (IV)	1	5.262
	2	3.83
	3	3.936
	4	5.952

Table A5. Assignments of the carbon-bound protons of the reduced chondroitin sulfate hexasaccharide at pD 9.0 in 10 mM phosphate buffer acquired at 316.2 K. Chemical shift values from COSY spectra are reported to two decimal places while those extracted from the 1D spectra are reported to three decimal places.

Residue	Proton	^{1}H Chemical shift, ppm
		pD 9.0
GalNAc4S-ol (I)	1	3.67
	1’	3.71
	2	4.271
	3	4.239
	4	4.476
	5	4.12
	6	3.67
	6’	3.69
	amide -CH_3	2.091
GlcA (II)	1	4.62
	2	3.450
	3	3.631
	4	3.86
	5	3.77
GalNAc4S (III)	1	4.74
	2	4.02
	3	4.04
	4	4.60
	5	3.99
	6	3.78
	6’	3.80
	amide -CH_3	2.027
GlcA (IV)	1	4.47
	2	3.377
	3	3.571
	4	3.80
	5	3.70

Table A5. Cont'd

Residue	Proton	^{1}H Chemical shift, ppm
		pD 9.0
GalNAc4S (V)	1	4.64
	2	4.07
	3	4.14
	4	4.62
	5	3.85
	6	3.74
	6'	3.76
	amide -CH_3	2.003
ΔUA (VI)	1	5.254
	2	3.82
	3	3.937
	4	5.948

Table A6. Amide proton chemical shifts assignments. (A) Reduced CS-A tetrasaccharide (ΔUA-GalNAc4S-GlcA-GalNAc4S-ol), (B) reduced CS-A hexasaccharide (ΔUA-GalNAc4S-GlcA-GalNAc4S-GlcA-GalNAc4S-ol), (C) *N*-acetylated Arixtra (NAcArixtra), (D) *N*-acetylated GlcN3S (GlcNAc3S).

A

Residue	^{1}H Chemical shift, ppm	Solution conditions	
		pH	T, K
GalNAc4s-ol (I)	8.008	7.4	316.2
GalNAc4S (III)	7.652		

B

Residue	^{1}H Chemical shift, ppm	Solution conditions	
		pH	T, K
GalNAc4s-ol (I)	8.042		
GalNAc4S (III)	7.926	7.4	308.2
GalNAc4S (V)	7.702		

C

Residue	^{1}H Chemical shift, ppm	Solution conditions	
		pH	T, K
GlcNAc6S (I)	8.085		
GlcNAc3S6S (III)	7.912	7.4	298.2
GlcNAc6S (V)	8.289		

D

Residue	^{1}H Chemical shift, ppm	Solution conditions	
		pH	T, K
GlcNAc3S (α)	7.825	7.4	289.2
GlcNAc3S (β)	8.135		

Table A7. *N*-acetylated GlcN3S (GlcNAc3S) carbon-bound proton chemical shifts assignments made in 90% H_2O/10% D_2O solution at 298.2K. Chemical shift values from COSY spectra are reported to two decimal places while those extracted from the 1D spectra are reported to three decimal places.

Residue	Proton	^{1}H Chemical shift, ppm
		pH 7.4
GlcNAc3S (α)	1	5.235
	2	4.044
	3	4.493
	4	3.663
	5	3.92
	6	3.82
	6’	3.86
	amide -CH_3	2.029
GlcNAc3S (β)	1	4.84
	2	3.79
	3	4.351
	4	3.628
	5	3.92
	6	3.78
	6’	3.80
	amide -CH_3	2.016

Fit for GlcNAc NH resonance alpha @ pH7.4 as function of T

Directories & settings

```
In[1]:= TOOLS = "C:\\Users\\andrew\\Desktop\\Paper_Amide
            exchange\\Temperature experiments\\SET 2_pH7.4\\";
        DATA = "C:\\Users\\andrew\\Desktop\\Paper_Amide exchange\\Temperature
            experiments\\SET 2_pH7.4\\";
```

Get tools

```
In[3]:= << "NonlinearRegression`";
        Get[ TOOLS <> "stat60.m"] ;
        (* Get[ TOOLS<>"SpecTools.m"] ;*)
```

... General: NonlinearRegression` is now obsolete. The legacy version being loaded may conflict with current functionality. See the Compatibility Guide for updating information.

```
In[5]:= cut[ data_, list_] :=
         Flatten[ Table[ Take[ data, { list[[ i]] , list[[ i + 1]]}]   , { i, 1, Length[ list] , 2}] , 1]

In[6]:= spline3[ a_, b_, c_, d_, x_] := a + b x + c x^2 + d x^3
```

Figure A3. Example of fit for activation energy barriers, $\Delta G^{\ddagger}$ for GlcNAc α anomer.

```
In[7]:= readjcamp[ filename_, pointstartin_, pointendin_] :=
         Module[ {datalist}, findstring = "$$ End of Bruker specific parameters";

          datafile = OpenRead[ filename] ;
          While[ Read[ datafile, Record] ≠ findstring] ;
          Read[ datafile, Record] ;
          Read[ datafile, Record] ;
          Read[ datafile, Record] ;
          Read[ datafile, Word] ;
          xfactor = Read[ datafile, Number] ;
          Read[ datafile, Record] ;
          Read[ datafile, Word] ;
          firstx = Read[ datafile, Number] ;
          Read[ datafile, Record] ;
          Read[ datafile, Record] ;
          Read[ datafile, Word] ;
          maxy = Read[ datafile, Number] ;
          maxy = 10^8;
          Read[ datafile, Record] ;
          Read[ datafile, Word] ;
          npoints = Read[ datafile, Number] ;
          Read[ datafile, Record] ;
          Read[ datafile, Record] ;
          linestart = Floor[ pointstartin / 4 + 3 / 4] ;
          lineend = Floor[ pointendin / 4 + 3 / 4] ;
          pointstart = 4 * linestart - 3;
          pointend = 4 * lineend;
          refstart = - firstx + xfactor ( pointstart - 1) + 60 000;
          Do[ Read[ datafile, Record] , { i, 1, linestart - 1}] ;
          temp = Table[ Table[ Read[ datafile, { Number, Number, Number, Number, Number}]] ,
            { j, linestart, lineend}] ;
          datalist = {} ;
          Do[ datalist = Join[ datalist,
              Table[{ refstart + ( 4 ( i - 1) + j - 2) * xfactor, temp[[ i, j]] / maxy} // N, { j, 2, 5} ]] ,
           { i, 1, lineend - linestart + 1} ] ;
          Close[ filename] ;
          datalist]

In[8]:= (* GlcNAc alpha*)

In[9]:= Tlist = { 282.58, 287.68, 293.11, 298.33, 303.87, 309.08, 313.64, 318.20}

Out[9]= { 282.58, 287.68, 293.11, 298.33, 303.87, 309.08, 313.64, 318.2}

In[10]:= Alist = { 4.125, 4.655, 5.39, 6.295, 7.53, 9.575, 12.33, 15.645}

Out[10]= { 4.125, 4.655, 5.39, 6.295, 7.53, 9.575, 12.33, 15.645}

In[11]:= fitA = Table[{ Tlist[[ i]] , Alist[[ i]]} , { i, Length[ Alist] - 0}]

Out[11]= {{ 282.58, 4.125} , { 287.68, 4.655} , { 293.11, 5.39} , { 298.33, 6.295} ,
          { 303.87, 7.53} , { 309.08, 9.575} , { 313.64, 12.33} , { 318.2, 15.645}}
```

Figure A3. Cont'd

In[12]:=
```
ListPlot[ fitA]
```

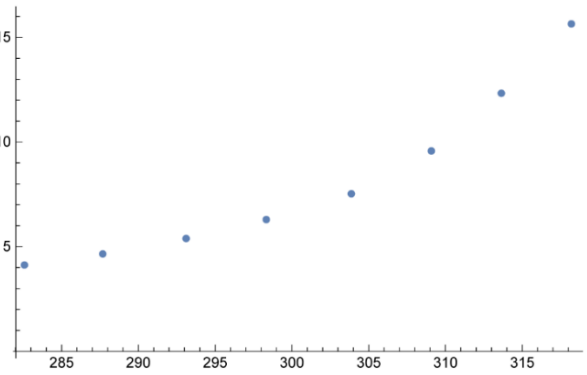

Out[12]=

In[13]:=
```
datapairs = fitA;
ps1 = ListPlot[ datapairs, Joined →True, PlotRange →All, Frame →True]
```

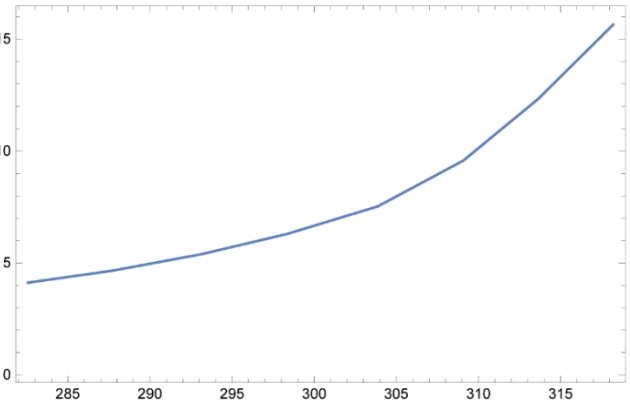

Out[14]=

In[15]:=
```
kb = 1.38 × 10^-23
h = 6.626 × 10^-34
R = 1.9872
```

Out[15]= 1.38×10^{-23}

Out[16]= 6.626×10^{-34}

Out[17]= 1.9872

In[18]:=
```
rate[ dg_, T_] := 1 / π  kb / h T Exp[ - dg / R / T]
```

In[19]:=
```
const[ a_, T_] := a
```

In[20]:=
```
startparams = {{ rate, { 16382.091536767006`}} , { const, { 4.1017165370152995`}}}
```

Out[20]= {{ rate, { 16 382.1}} , { const, { 4.10172}}}

Figure A3. Cont'd

In[21]:=
```
data$sim = gensim[ datapairs, startparams] ;
plot$sim = ListPlot[ data$sim, PlotRange→All, Joined→True, DisplayFunction→Identity] ;
plot$data =
  ListPlot[ datapairs, PlotRange→All, Joined→True, DisplayFunction→Identity, PlotStyle→Red] ;
Show[ plot$data, plot$sim, DisplayFunction→$DisplayFunction]
```

Out[24]=

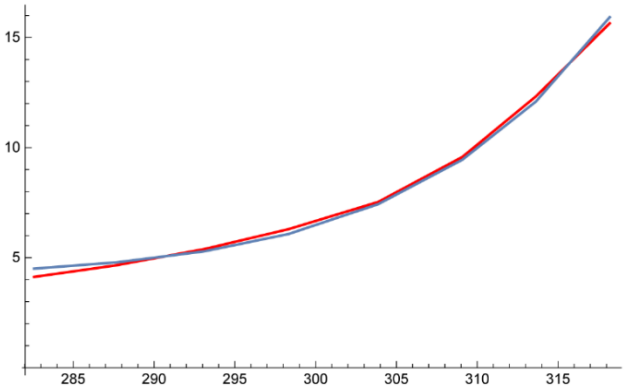

In[25]:=
```
fitresults = fitdatatight[ datapairs, startparams]
```

Out[25]=
```
{{ rate, { 16 382.1}} , { const, { 4.10172}}}
```

In[26]:=
```
fitdataerr[ datapairs, fitresults]
```

Out[26]=
```
{ BestFitParameters →{ a$$111 →16 382.1, a$$211 →4.10172} ,

 ParameterCITable →
                  |  Estimate    Asymptotic SE    CI
  a$$111          |  16 382.1    14.8142          { 16 345.8, 16 418.3} ,
  a$$211          |  4.10172     0.132218         { 3.77819, 4.42524}

                                                  DF    SumOfSq     MeanSq
 EstimatedVariance →0.0627715, ANOVATable →  Model                2     652.164     326.082
                                             Error                6     0.376629    0.0627715,
                                             Uncorrected Total    8     652.54
                                             Corrected Total      7     115.522

 AsymptoticCorrelationMatrix → ( 1.      0.7424 )
                               ( 0.7424  1.     ) ,

                                                  | Curvature
 FitCurvatureTable →  Max Intrinsic               | 0.000434075 }
                      Max Parameter-Effects       | 0.0500315   }
                      95. % Confidence Region     | 0.440942
```

Out[26]=
```
{{ rate, { 16 382.1}} , { const, { 4.10172}}}
```

Figure A3. Cont'd

In[27]:=
```
data$sim = gensim[ datapairs, fitresults] ;
plot$sim = ListPlot[ data$sim, PlotRange →All, Joined →True, DisplayFunction →Identity] ;
plot$data =
  ListPlot[ datapairs, PlotRange →All, Joined →True, DisplayFunction →Identity, PlotStyle →Red] ;
Show[ plot$data, plot$sim, DisplayFunction  $DisplayFunction]
```

Out[30]=

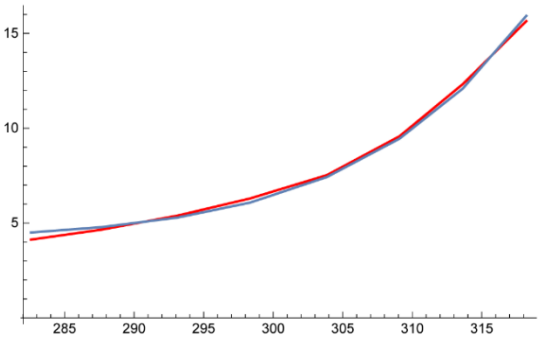

In[31]:=
```
data$res = Table[{ datapairs[[ i, 1]] , datapairs[[ i, 2]] - data$sim[[ i, 2]] } , { i, Length[ datapairs]}]  ;
plot$res = ListPlot[ data$res, PlotRange →All, Joined →True, DisplayFunction →Identity] ;
Show[ plot$res, DisplayFunction →$DisplayFunction]
```

Out[33]=

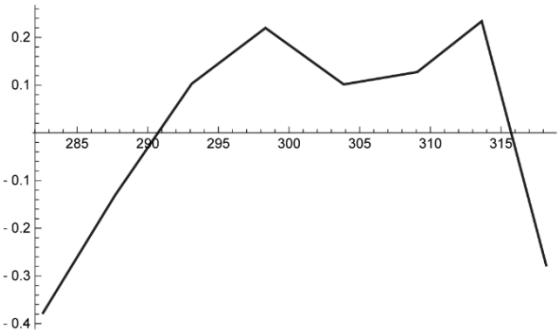

Figure A3. Cont'd

References

1. Beecher, C. N.; Manighalam, M. S.; Nwachuku, A. F.; Larive, C. K., Screening enoxaparin tetrasaccharide SEC fractions for 3-O-sulfo-N-sulfoglucosamine residues using [(1)H,(15)N] HSQC NMR. *Anal. Bioanal. Chem.* **2016,** *408* (6), 1545-55.